

Application of Microfluidics System for Evaluating the Biology of Glioblastoma Tissue and Testing Response to Chemotherapy

FAROUK OLUBANKOLE OLUBAJO

Thesis submitted for the degree of Doctor of Medicine

University of Hull and University of York

Hull York Medical School

April 2019

Abstract

The genetic and molecular variations that exist within Glioblastoma (GBM) tumours determine treatment responses. One way to improve patient outcomes is to optimise treatment(s) pre-clinically by studying each tumour on an individual basis.

Presented here are the results of an observational study on the maintenance of human GBM tissue on a microfluidic platform. The device, fabricated using photolithography processes, was composed of two layers of glass bonded together to contain a tissue chamber and a network of microchannels. A thin mesh layer was inserted to separate the tissue chamber from the microchannels and prevented blockage of the chip.

Over an 18-month period, 33 patients were recruited, and 128 tissue sections were maintained in the microfluidic device for an average of 72 hours (h). Tissue viability as measured by Annexin V and Propidium Iodide assays showed viability was 61.1 % in tissue maintained on chip after 72 h, compared with 68.9 % for fresh tissue analysed at the commencement of the experiment ($P < 0.05$). Other biomarkers, including LDH and Trypan Blue assays, supported the viability of the tissue maintained on chip. Histological appearances of the tissue remained unchanged during the maintenance period and immunohistochemical analysis of Ki67 and Caspase 3 also showed no statistically significant differences.

Drug testing with Temozolomide (n=6) and the experimental drug ExoPr0 (n=6) failed to show any cytotoxic effect on the tissues maintained. Preliminary analysis also failed to show any significant correlation between the tumour behaviour on chip and patient prognosis.

This work has demonstrated for the first time that human GBM tissue can be maintained *ex vivo* within a microfluidic device. The model has the potential to be developed as a new platform for studying the biology of brain tumours, with the long-term aim of facilitating personalised treatments.

List of Contents

<u>LIST OF FIGURES</u>	<u>5</u>
<u>LIST OF TABLES</u>	<u>7</u>
<u>PREFACE</u>	<u>8</u>
<u>ACKNOWLEDGEMENTS</u>	<u>9</u>
<u>DECLARATION</u>	<u>10</u>
1.1.1 GLIOBLASTOMA – WHAT’S IN A NAME?	11
1.1.2 GBM BY NUMBERS	12
1.1.3 UNDERSTANDING GBM	14
1.1.4 AN APPROACH TO THE GORDIAN KNOT	19
<u>1.2 MICROFLUIDICS</u>	<u>22</u>
1.2.1 OVERVIEW	22
1.2.2 APPLICATION	28
1.2.2.1 EMBRYOS AND CELLS	28
1.2.2.2 TISSUE CHIPS	31
1.2.3 BRAIN SLICE ON A CHIP	36
1.2.3.1 INTERFACE CHAMBER	36
1.2.3.2 SUBMERGED CHAMBER	37
1.2.3.3 ORGANOTYPIC SLICES	42
1.2.4 NON-CNS TISSUES ON CHIP	43
1.2.5 GLIOMA ON CHIP	45
1.2.6 HUMAN GBM TISSUE CULTURE	53
<u>1.3 STUDY AIMS</u>	<u>56</u>
<u>2.1 MATERIALS</u>	<u>58</u>
2.1.1 MATERIALS, REAGENTS AND EQUIPMENT	58
2.1.1.1 MICROFLUIDIC DEVICE	58
2.1.1.2 REAGENTS	58
2.1.1.3 HISTOLOGY/IMMUNOHISTOCHEMISTRY	59
2.1.1.4 DRUGS	59
2.1.1.5 EQUIPMENT	60
2.1.1.6 SOLUTIONS	60
<u>2.2 METHODS</u>	<u>62</u>
2.2.1 FABRICATION AND ASSEMBLING THE CHIP	62
2.2.2 TUMOUR SAMPLES	64

2.2.3	EXPERIMENTAL SET UP	65
2.2.3.1	CULTURE MEDIUM	65
2.2.3.2	TISSUE MAINTENANCE	65
2.2.3.3	PROTOCOL	67
2.2.3.4	STATIC TISSUE	68
2.2.4	POST CHIP ANALYSIS	68
2.2.4.1	HISTOLOGICAL PREPARATIONS	69
2.2.4.2	FLOW CYTOMETRY	73
2.2.4.3	LDH ANALYSIS	76
2.2.4.4	TRYPAN BLUE STAINING AND CELL COUNTS	78
2.2.4.5	DRUG TREATMENTS	79
2.2.5	STATISTICAL ANALYSIS	81
3.1	<u>OPTIMISATION AND RESULTS</u>	<u>82</u>
3.1.1	OVERVIEW	82
3.1.2	ASSESSMENT OF VIABILITY	82
3.1.2.1	ANNEXIN V AND PI	82
3.1.2.2	LDH ASSAY	85
3.1.2.3	HISTOLOGY	86
3.1.3	OPTIMISATION OF EXPERIMENTAL TECHNIQUE	87
3.1.3.1	OPERATIVE SAMPLING	87
3.1.3.2	NON-PERFUSED TIME	89
3.1.3.3	NUTRIENT MEDIA	90
3.1.4	OPTIMISATION THE CHIP	91
3.1.4.1	FLOW RATE	91
		92
3.1.5	STATIC TISSUE CULTURE	93
3.1.5.1	STATIC TISSUE VIABILITY	93
3.1.5.2	STATIC TISSUE LDH RELEASE	94
3.1.5.4	FURTHER HISTOLOGY STUDIES	97
3.1.6	DISCUSSION	99
3.1.6.1	RECRUITMENT AND SAMPLING	99
3.1.6.2	WARM ISCHAEMIC TIME AND THE EFFECT OF FLOW	101
3.1.6.3	NUTRIENT MEDIA	102
3.1.6.4	BLOCKAGES	106
4.1	<u>ANALYSIS OF GBM TUMOURS USING A MICROFLUIDIC DEVICE</u>	<u>108</u>
4.1.1	STUDY RESULTS	108
4.1.1.1	OVERVIEW	108
4.1.2	VIABILITY OF GBM ON CHIP	109
4.1.2.1	ANNEXIN V AND PROPIDIUM IODIDE	109
4.1.2.2	TRYPAN BLUE	111
4.1.2.3	LDH ABSORBANCE	113
4.1.2.4	H&E	116
4.1.2.4	IMMUNOHISTOCHEMISTRY	117
4.1.3	DRUG TREATMENT	120
4.1.4	CORRELATION WITH CLINICAL OUTCOMES	123
4.1.5	DISCUSSION	131

4.1.5.1	OVERVIEW	131
4.1.5.2	ANNEXIN V AND PROPIDIUM IODIDE AS BIOMARKERS	132
4.1.5.3	LDH AS A MARKER OF CELL DEATH/INJURY	134
4.1.5.4	IMMUNOHISTOCHEMISTRY	139
4.1.5.5	DRUGS	141
4.1.5.6	CLINICAL CORRELATION	143
5.1	CONCLUSION	146
5.1.1	DISCUSSION OF FINDINGS	146
5.1.2	LIMITATIONS	147
5.1.3	FURTHER RESEARCH	148
5.1.4	FINAL COMMENTS	151
	REFERENCES	152
	APPENDIX	177
	LIST OF ABBREVIATIONS	183
	NOMENCLATURE	185

List of Figures

Figure 1.1: GBM Histology specimen.	15
Figure 1.2: Three signalling pathways most affected in GBM tumorigenesis.	16
Figure 1.3: Metabolic drug targets of the RTK and PI(3)K pathways in GBM.	18
Figure 1.4: Different types of MF devices	24
Figure 1.5: Photolithography and the fabrication of MF devices.	27
Figure 1.6: ‘Christmas tree’ gradient generator integrated into the MF device.	29
Figure 1.7: Microphysiological systems.	33
Figure 1.8: Brain Slice and Microfluidic Designs.	37
Figure 1.9: Examples of submerged devices and different methods of improving oxygenation and tissue perfusion supply.	39
Figure 1.10: Microfluidic Perfusion Chamber	41
Figure 1.11: Microfluidics and Glioma 1	47
Figure 1.12: Microfluidics and Glioma 2	49
Figure 2.1: The basic units of the Microfluidic Device	63
Figure 2.2: Experimental Set-Up	67
Figure 2.3: Principles of IHC	71
Figure 2.4: The workings of a Flow Cytometer.	74
Figure 2.5: Emission spectra for FITC and Propidium Iodide	76
Figure 2.7: Summary of viability assays performed	80
Figure 3.1: Dot Plot (patient 16008) produced on CellQuest Pro software representing flow cytometric analysis of Annexin V and PI distribution.	83
Figure 3.2: Dot Plot (patient 16008) representing flow cytometric analysis of Annexin V and PI distribution sectioned into quadrants.	84
Figure 3.3: Flow Cytometric analysis represented as a Histogram	85
Figure 3.4: LDH absorbance in 72 h (AU – 490 nm).	86
Figure 3.5: Optimisation of histological techniques.	87
Figure 3.6: Variations in Histology from 4 different GBM patients	88
Figure 3.7: The effects of processing time on tissue viability	89
Figure 3.8: The effect of flow rate on tissue viability (matched pairs)	91
Figure 3.9: The effect of flow rate on tissue viability (whole cohort)	92
Figure 3.10: Tissue viability before and after the introduction of the mesh into the chip.	93
Figure 3.11: Differences in viability between chip tissue and static tissue	94

Figure 3.12: The differing patterns of LDH absorbance from effluent samples collected from chip and static tissue	95
Figure 3.13: Representative images of tissue sections from the 8 th patient – GBM IDH Wild Type (all at x400 Magnification)	96
Figure 3.14: Images of tissue sections from the 27 th patient (GBM = IDH Wild Type) stored for 1,2 and 3 days.	97
Figure 3.15: Summary of optimisation experiments detailing analysis undertaken and number of devices established.	98
Figure 4.1: Histogram of flow cytometric analysis of Matched Pairs (Fresh Tissue and Chip Tissue), used to quantify healthy cells (AV-/PI-).	110
Figure 4.2: Histogram of viability according to tumour grade.	111
Figure 4.3: Fresh and Chip Tissue viability according to Trypan Blue.	112
Figure 4.4: Correlation between two viability assays.	113
Figure 4.5: Average LDH absorbance over 72 h time period.	114
Figure 4.6: Effects of tissue lysis on LDH Absorbance	115
Figure 4.7: Representative images of H&E sections of GBM tissue	116
Figure 4.8: Representative IHC of GBM tissue (Ki67; n = 14)	117
Figure 4.9: Proliferation indices (Ki67 staining) of Fresh Tissue and Chip Tissue	118
Figure 4.10: Representative IHC of GBM tissue (Caspase 3; n = 13)	119
Figure 4.11: Apoptotic indices (Caspase 3 staining) of Fresh Tissue and Chip Tissue.	120
Figure 4.12: Effects of TMZ on GBM on Chip.	121
Figure 4.13: The effect of TMZ on GBM from Patient 16028.	122
Figure 4.14: Effects of ExoPr0 on GBM on Chip.	123
Figure 4.15: Patient Survival.	124
Figure 4.16: Histogram comparing viability of survivors with viability of deceased patients.	127
Figure 4.17: Correlation of patient survival with tissue viability.	128
Figure 4.18: Viability in patients with maximal (>90%) resection.	129
Figure 4.19: Viability of different GBM subtypes.	130
Figure 4.20: LDH Calibration Curve.	137
Figure 5.1: Redesigning the chip.	149

List of Tables

Table 1.1: Genomic expression/alterations and clinical features across Glioblastoma subtypes. _____	17
Table 1.2: Glioma and Microfluidics _____	52
Table 1.3: Cultured Human GBM Tissue _____	55
Table 3.1: Exosome-Depleted Media as a media substitute. _____	90
Table 3.2: aCSF as a media substitute. _____	90
Table 4.1: Histological types and demographics of patients included in the study. ____	109
Table 4.2: Extent of tumour resection, adjuvant therapy and performance status of GBM patients recruited into the study. _____	126

Preface

The planning, experimental design and execution of the studies and technical work involved in this thesis were all performed by the candidate, unless otherwise stated.

No part of this thesis has been submitted in support of an application for any degree or qualification in any other institute of learning.

Acknowledgements

I would like to thank my supervisors, Professor John Greenman and Mr. Shailendra Achawal. Professor Greenman for his continued support throughout every stage of the degree process; I remain indebted to him particularly for his patience and perseverance. Mr. Achawal for supporting my career break to venture into academia and his guidance and active role in ensuring the neurosurgical unit supported the study. I thank the neuro-oncology surgeons at the Hull and East Yorkshire Hospital - Mr. Gerry O'Reilly, Mr. Chittoor Rajaraman, Mr. Masood Hussein and Mr. Shailendra Achawal for providing me with access to patients under their care for recruitment into the study. I thank Dr. Robin Highley, Consultant Neuropathologist for his assistant and tutorials on all things histopathology related. I also owe Dr. Naomi Guppy and the staff at the UCL Advanced Diagnostics Laboratory my thanks, for their support with the histological preparations. A special thank you to the team from ReNeuron for their contributions, including providing me with access to the experimental drug, ExoPr0 for preliminary testing.

I am grateful to my colleagues, Craig Robson, Adam Razak, Daniel Brown, Veejay Bagga, Khalid Mohmoud, Nicholas McConnell, Syed Hussein, Efosa Ukponmwan, Omar Yaseen and Kostantinos Lilimpakis for helping me recruit patients. I would also like to thank those who I worked with in the laboratory, including Dr. Leigh Madden, Dr. Cordula Kemp, Linsey Malcolm and a particular thank you to Dr. Amy Dawson who supported me in those first few months as I made the transition from clinician to scientist. I am grateful to Dr. Victoria Green and Ruth Bower for their support and advice during the course of my experiments and Dr. Chao Huang of the Hull and York Medical School who assisted in my statistical analyses.

Lastly, I am eternally grateful to my wife, Linda Olubajo, whose support has carried me through the difficulties I have faced during my degree.

Declaration

I confirm that this work is original and that if any passage(s) or diagram(s) have been copied from academic papers, books, the internet or any other sources these are clearly identified by the use of quotation marks and the reference(s) is fully cited. I certify that, other than where indicated, this is my own work and does not breach the regulations of HYMS, the University of Hull or the University of York regarding plagiarism or academic conduct in examinations. I have read the HYMS code of Practice on Academic Misconduct, and state that this piece of work is my own and does not contain any unacknowledged work from any other source. I confirm that any patient information obtained to produce this piece of work has been appropriately anonymised.

1.1 GBM

1.1.1 Glioblastoma – What’s in a Name?

According to Cancer Research UK, in 2014, 10,981 new brain and central nervous system (CNS) tumours were registered in the UK.¹ This figure equates to 34 new intracranial tumour cases per 100,000 people with an equal split between male and females. Gliomas – central nervous system (CNS) tumours that originate from autochthonous glial cells, such as astrocytes, oligodendrocytes and ependymal cells, make up 81%² of brain tumours. Of the gliomas, Glioblastoma is the most prevalent^{3,4}, representing nearly half (47%)⁴ of all cases. Glioblastoma, previously known as Glioblastoma Multiforme (GBM) was originally categorised and named by Bailey and Cushing in 1925⁵ in the first major classification of brain tumours. The name Glioblastoma Multiforme was given to highlight the varied histological appearance within the tumour which is usually composed of a dense cellular structure with highly mitotic and pleomorphic nuclei, intermingled with necrotic tissue and proliferating vessels. Though not a true *blastoma* (*blastoma* refers to tumours originating from embryonic cell lines), it is likely that it was called one as the cells in GBM resemble *immature* glial cells⁶, predominantly astrocytes but occasionally oligodendroglia features can be present⁴. Commonly, within the same tumour, there can be markers of various cell lineages⁶, reinforcing the theme of heterogeneity that is prevalent within this tumour. Though the adjunct, *multiforme* is no longer in use, multiple forms of the disease, remain in existence today. The most recent World Health Organisation (WHO) classification of tumours of the central nervous system uses histological characteristics and genetic markers to identify 5 forms of GBM⁷, while The Cancer Genome Atlas (TCGA) group used genetic fingerprinting studies, patient demographics and survival to reveal 4 clinically relevant subtypes⁸. These classification methods are not mutually exclusive and are increasingly being combined to characterise an array of genetically and phenotypically different forms of GBM. Thus, the name remains the same, but the tumours are extremely diverse, with some, more common in different age groups and others, less resistant to current treatment modalities.

Yet, one thing unifies this assorted group of brain tumours. The diagnosis of a GBM is a devastating one, regardless of its denomination; 97.3% of those diagnosed die within 5 years.⁹ Such statistics have persisted despite all the advances in tumour biology, medical sciences, surgical techniques and oncological treatments. All treatments fail, and disease recurrence remains the rule. The prognosis of GBM is unchanged in over 90 years¹⁰ and regardless of what it is called, successful treatment of the group of tumours known as GBM remains one of the greatest unfulfilled ambitions of the 21st century.

1.1.2 GBM by Numbers

In England, the age-adjusted incidence of GBM is 2.05 per 100,000 persons.² In the UK, between 2007 and 2011, 6451 men and 4292 females were affected, giving an incidence rate 1.5 times higher in males compared to females.¹¹ Though the disease can affect patients of all ages, the median age at diagnosis is 62¹² with a reduced incidence in children and those over the age of 85.¹³ Age is, however, a negative prognostic indicator with older patients less likely to survive, having an almost linear decline in months of survival with increasing age.¹⁴ The disease affects Caucasians (80% of reported cases)¹⁵ more frequently than people of African (5.4%)¹⁵ or Asian (4%) origin⁴ and there appears to be an association with high socio-economic status.¹⁶ Though no definite environmental risk factors have been identified, 5% of gliomas^{17,18} result from the genetic mutations of certain hereditary syndromes,¹⁹ including Neurofibromatosis Type 1 & 2 and Turcot's syndrome.

GBM can present in any part of the neuro-axis but rarely involves the spinal cord²⁰ or brainstem. It has a predilection for the cerebral cortex with the frontal lobe affected 43% of the time, compared with 25% and 28% in the parietal and temporal lobes respectively; only 3% of tumours involve the occipital lobe²¹ and less than 1% of intracranial GBM is within the cerebellum.²² Regardless of site, the most common presenting symptom of brain tumours is a cognitive disorder²³ which is present in 74%-90% of patients,^{23,24,25} likely explained by the diffuse infiltrative nature of the disease. Seizures are also common, with an incidence of 30%-62% in different series²⁶ and there is a suggestion that seizures at presentation are associated with a

favourable prognosis;^{27,28} this is possibly related to seizures prompting an earlier presentation (and as such a smaller tumour upon presentation).²⁸ Headaches are usually present in about 50%²⁹ of gliomas but only occur as the sole symptom in 10% of brain tumours.³⁰ Depending on the location of the GBM, focal neurological deficit, including speech, motor and sensory disturbances can be forms of presentation.

Though brain tumours account for <2% of all malignancies³¹ the excessive mortality rates associated with a median survival of 12-15 months³² means malignant brain tumours are a great burden on the individual, with an average of over 20 years of life lost per patient.³³ This is the highest number of years lost per patient when compared with all other tumours in the UK.³³ Chang *et al.*³⁴ found that brain tumours ranked fourth in mean total direct medical costs per month at \$8,478 (amongst seven different cancer types). In the UK, prior to the introduction of Temozolomide (TMZ), it was estimated that management of malignant brain tumours cost £400,010 per quality adjusted life years (QALY).³⁵ Furthermore, a look at the employment status of people with brain tumours and the effect of the disease to the economy shows that 91% of patients were working prior to their diagnosis of a brain tumour with only a third ever getting back to work.³⁶ One study estimated all the indirect costs (sick leave, early retirement, and mortality) of brain tumours in one year to \$197.7 million for the Swedish population (\$22.5 million per million of population).³⁷

Currently, maximal surgical resection plus radiotherapy with concomitant TMZ is the standard treatment for GBM.¹⁸ Stupp *et al.*³² showed in their randomised controlled trial that the addition of TMZ to the regimen increased survival by 2.5 months compared to surgery and radiotherapy alone. But despite the modest increase in survival, the nature of the disease, which sees widespread permeation of tumour cells along tracts in the brain,³⁸ ensures that even novel therapies like TMZ fail. Median survival can range from 9-15 months^{39,40,41} however there are exceptions to this rule with approximately 2-5% of patients surviving beyond 3 years.^{42,43}

1.1.3 Understanding GBM

Though the minority, long-term survivors of GBM, present an opportunity to better understand the tumour. GBM used to be diagnosed based purely on histology. This was defined by the finding on histology of gemistocytic astrocytes, neovascularisation with endothelial proliferation and areas of necrosis with or without pseudopalisading⁴⁴ (*Figure 1.1*). Though these features are common within GBM tissue, basing diagnosis purely on histological features has its pitfalls as diagnostic concordance amongst pathologists assessing brain tumours ranges between 40-77%.⁴⁵⁻⁴⁷ Increasingly, histopathological diagnosis of tumours are requiring a new taxonomy that incorporates molecular and genetic alterations in tumour classification.⁴⁸ The new WHO classification of tumours of the CNS adopts this approach to GBM. According to WHO⁷, the diagnosis of GBM on histology now warrants clarification of the isocitrate dehydrogenase type 1 (IDH1) gene status; differentiating between a GBM with an IDH1 wildtype and one with a mutant IDH1. IDH1 catalyzes the decarboxylation of isocitrate to α -ketoglutarate and evidence points to the mutant enzyme converting α -ketoglutarate to the ‘oncometabolite’ 2-hydroxyglutarate.⁴⁹ Though only one of many genes affected in GBM, there is a plethora of evidence that supports the concept that GBMs with an IDH1 mutant have a better prognosis than those with the wildtype.^{7,35,36,42-45,53} The genetic and molecular variability within each tumour is likely to underlie the disparity in GBM patient survival. To understand the depth of this molecular heterogeneity, The Cancer Genome Atlas (TCGA) research network group looked at the genes involved in GBM, with the aim of establishing a comprehensive catalogue of genetic abnormalities driving tumorigenesis.³⁹

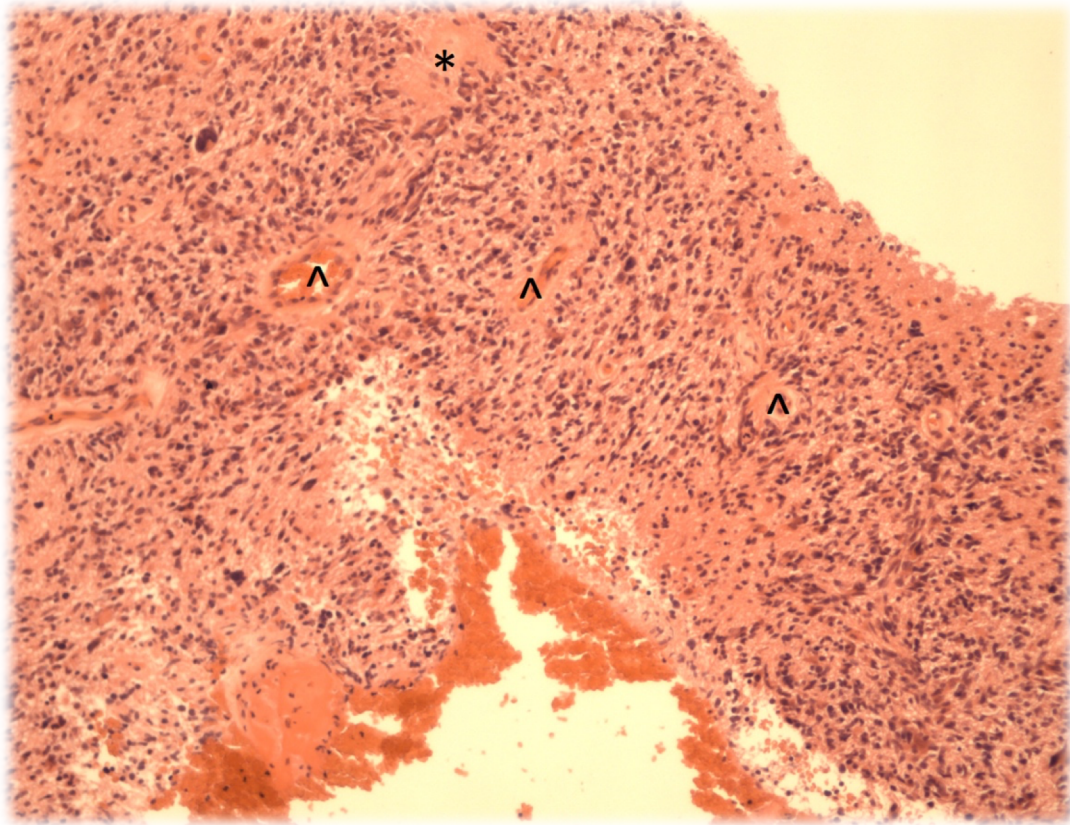


Figure 1.1: GBM Histology specimen.

This Glioblastoma has marked cellularity with hyperchromatism and pleomorphic nuclei. Note the prominent vascularity (^) as well as the area of necrosis ().*

TCGA analysed 91 matched GBM-normal pairs for detection of somatic mutations in 601 selected genes. The genes were selected based on previous molecular studies that had highlighted significant genetic events in the evolution of GBM. The group found recurrent mutations that led to dysregulation of three major signalling pathways: growth factor signalling via receptor tyrosine kinase (RTK) genes, p53 signalling and the retinoblastoma tumour suppressor (RB) pathway; with aberrations in 87%, 78% and 88% respectively (*Figure 1.2*).

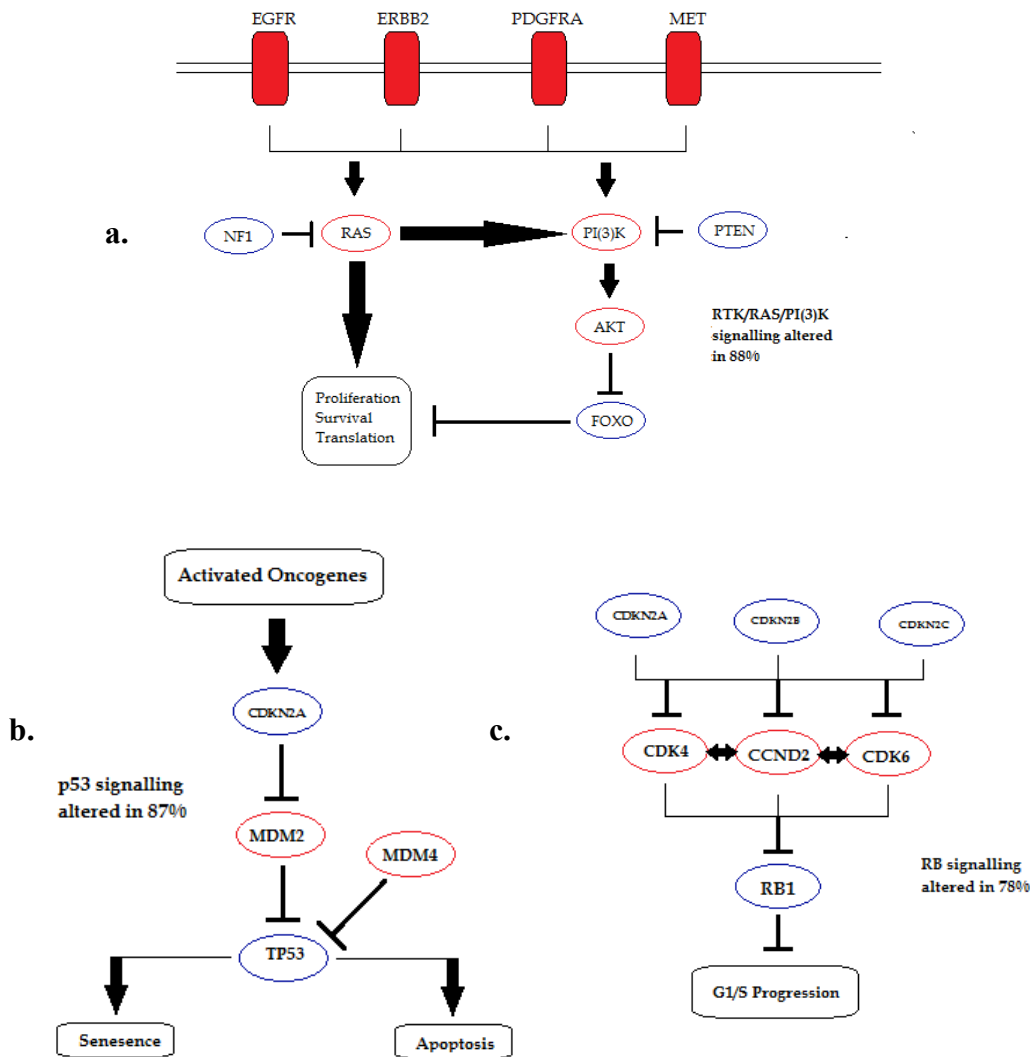


Figure 1.2: Three signalling pathways most affected in GBM tumorigenesis.

a. Receptor tyrosine kinase pathways **b.** Retinoblastoma Tumour Suppressor (RB) pathway **c.** p53 signalling pathways. Red indicates activating genetic alterations; conversely, blue indicates inactivating alterations. Adapted from McLendon *et al.*⁵⁴

These mutations appear to exist in varying degrees within different GBMs and particular genetic constellations confer certain cancer phenotypes. Verhaak *et al.* furthered the work of TCGA and integrated data from 200 GBM samples with consistent gene expressions. Using consensus clustering, the group identified four GBM subtypes based on their genetic profiles: Classical, Proneural, Neural and Mesenchymal (*Table 1.1*).⁵⁰

	Proneural	Neural	Classical	Mesenchymal
Chromosomes	4 (PDGFRA), 7, 10	7, 10	7 (EGFRvIII),10	17 (NF1)
Mutations	PDGFRA, IDH1, TP53	N/A	EGFR, TP53	NF1
Cell Markers	Oligodendroglial/Proneural	Neuronal	Neuronal and Stem Cell	Inflammatory
Age	Younger	Older	Older	Older
Secondary GBM	Represented	Not Represented	Not Represented	Not Represented
Prognosis	Longer (not statistically significant)	Shorter	Shorter	Shorter
Intensive Treatment	No Efficacy	Efficacy Suggested	Reduce Mortality	Reduce Mortality

Table 1.1: Genomic expression/alterations and clinical features across Glioblastoma subtypes.

Key: PDGFRA - platelet-derived growth factor receptor α ; EGFR - epidermal growth factor receptor; TP53 – tumour Protein p53; NF1 – Neurofibromatosis 1; IDH 1 – Isocitrate Dehydrogenase 1. Adapted from Verhaak et al.⁵⁰ & Masui et al.³⁹

The GBM subtypes were validated by an independent set of 260 GBM expression profiles with significant subtype reproducibility. Each subtype has a distinct set of mutations that represent its unique path to tumorigenesis, conferring a distinguishing phenotype. For example, the Classical subtype of GBM is linked with mutations of Epidermal Growth Factor Receptor (EGFR). This is usually a mutant variant known as EGFRvIII, where a truncated extracellular domain results in a constitutively active protein, promoting tumour growth⁴⁰ along the RTK pathway (as shown in *Figure 1.2a*). ‘Classical GBMs’, as well as being more likely to have a EGFRvIII mutation, are also significantly more likely to occur in elderly patients and all together, have a poorer prognosis.³⁹ Conversely, the Proneural subtype is more common amongst younger patients and is nearly always related to an IDH1 mutation. IDH mutation is thought to be an early event in glioma formation^{55,49} as well as a positive predictor of survival in GBM,⁵⁶ affording patient’s with Proneural GBMs, who are usually younger (another positive predictor of survival), a better prognosis.³⁹

This type of emerging evidence in tumour biology is promoting a modernised approach to tumour diagnosis and management, where clinicians and researchers can target specific abberations in cellular function to develop therapeutic agents.⁴⁰ Proof

of concept is exemplified in EGFR and Anaplastic Lymphoma Kinase inhibition in non-small cell cancer (NSCLC).^{57,58} In GBM, new targets include EGFR associated kinase activity with drugs like Erlotinib⁵⁹ or with therapies that target the downstream receptor tyrosine kinase signalling pathways (mammalian target of rapamycin - mTOR), such as Rapamycin⁶⁰ (Figure 1.3). It is vital to note however, that these new drugs will not be effective for every patient as the drug responses will depend on the particular genetic profile or subtype. For example in NSCLC, just 10% of patients have a rapid and dramatic response to Gefitinib (an EGFR inhibitor), because despite overexpression of EGFR in NSCLC, only a small proportion of these patients have the specific activating mutation within the tyrosine kinase domain of EGFR which Gefitinib inhibits.⁵⁷

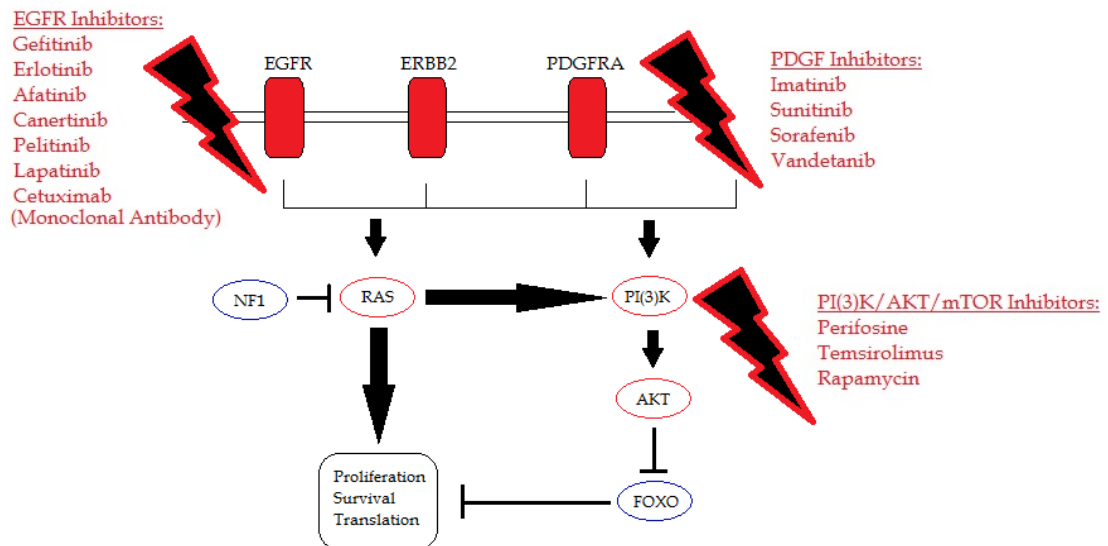


Figure 1.3: Metabolic drug targets of the RTK and PI(3)K pathways in GBM.

Figure displays drugs that inhibit EGFR, PDGF and PI(3)K pathways and hence have potential in treating GBM. Adapted from *The Cancer Genome Atlas Research Network*⁵⁴ and *Zorzan et al.*⁶¹

In GBM, despite prevalence within the research community, only a few genetic molecular markers are standard practice in clinical management. The most widespread molecular biomarker presently tested alongside histology is the epigenetic methylation of O⁶-Methylguanine-DNA methyltransferase (MGMT). MGMT protein, repairs DNA by removing alkyl adducts from the O⁶ position of

Guanine.⁴¹ MGMT methylation silences the gene and hence has a prognostic effect when TMZ, an alkylating agent is used to treat the tumour. The survival advantage of a patient with MGMT methylation treated with TMZ can be as high as 9 months.⁴¹ Such disparity in patient response, combined with the known variability in GBM subtypes, suggests that the ‘one-size fits all’ model for cancer treatment is incompatible with GBM development and heterogeneity. The evidence demands a shift to a personalised treatment paradigm that promotes defined treatments that correspond to specific subgroups which share similarities in tumorigenesis and molecular phenotype.

1.1.4 An Approach to the Gordian Knot

Finding a cure for GBM is more challenging than simply classifying tumour subtypes or heterogeneity. As far back as the 1920s, Walter Dandy resected entire cerebral hemispheres in an attempt to cure his patients of GBM.^{17,62} Removing a whole hemisphere was to ensure complete excision far beyond the tumour margins and reduce any chance of recurrence. Unfortunately, these patients still died from the disease, an indication of how pervasive GBMs are. Autopsies in the 1990s revealed that up to 39% of GBM patients were dying without any evidence of raised intracranial pressure.⁶³ Again the assumption was that invasive cancerous cells within the brain were part of the disease alongside the intracranial mass. This has led to the hypothesis that underlying every GBM is a sub-population of self-renewing tumour initiating ‘stem-cells’⁶⁴ that propagate the growth of a tumour. Though various theories are in competition as to the exact genesis of these cells¹⁷, all theories are in concordance that this population of cells is distinct from the tumour mass and diffusely invade the brain along white matter tracts. Along with the issue of glioma stem cells, treatment for GBM also has to overcome intra-tumoral heterogeneity; where the same tumour expresses regional differences in molecular markers and tumour behaviour.^{65,66} For example, Baysan *et al.* found an array of glioma stem cells within resected GBM and brain specimens taken from the same patient from seven distinct locations and at two different time points, a year apart.⁶⁷ The glioma stem cells showed polyclonal development, with distinct populations based on the part of the brain/tumour sampled as well as the timing in relation to the patient’s

treatment. Most importantly, the group were able to show that after treatment, recurrent tumours represented a tissue-wide expansion of a new set of tumor clones, progenies of the dominant clone within the initial resected tumor. This spatiotemporal heterogeneity within GBM explains how the disease is able to modify its phenotype in response to treatment. The net effect of self renewal, tumour growth, treatment resistance and thus prognosis is difficult to predict based on just molecular markers when different regions within the same tumour have different cellular niches and properties. Not surprisingly, the evidence points to increased intratumour heterogeneity being linked to higher mortality rates,⁶⁶ suggestive of the fact that intratumoral heterogeneity affords GBMs a greater degree of adaptability and tumour survival regardless of treatment. Glioblastoma is equipped to adapt but yet, current approaches to treatment are unable to adapt to individual tumours.

In the last 5 years, there were 194 trials registered that were considering therapeutic strategies to treat GBM¹⁰. As of April 2017, there were 294 ongoing trials (<https://clinicaltrials.gov>) looking at GBM and its therapeutic options. Most of the emerging therapies for GBM are based on sound scientific principles on cancer genetics and the molecular nuances in GBM development. However, history suggests that a lot of these trials will fail to show a significant benefit to patient survival. In fact, a lot of the studies looking at EGFR tyrosine kinase receptors have already failed to show any benefit, with only a few studies progressing beyond phase 2 trials.⁶⁸ Patients will continue to die despite all that is known about the disease. Two of the reasons why many trials investigating GBM will/have failed are proposed here:

1. Firstly, the process of drug selection/screening is flawed as *in vitro* models and pre-clinical trials do not have an optimised model for GBM. Cell cultures, currently the mainstay of pre-clinical assays, do not recapitulate the infiltrative nature of the tumour and possess significant molecular and pathological differences from human gliomas.^{69,70} Currently, only 2% of all drug development failures are screened in the preclinical stage.⁷¹ Mouse models⁷² and patient derived xenografts (PDX)^{70,73} provide a solution to this particular issue but are costly and time consuming.

2. The second issue with the failures in the drug trials is to do with heterogeneity – trial samples include a heterogeneous group of GBM subtypes and while some may benefit from the treatment, most do not, giving an overall response that is not significant. Like people, GBMs are highly varied and it is unlikely that one drug/treatment modality will be effective against all. Patient selection should be based on individual tumour behaviour and not just diagnosis.

Both these issues potentially have a similar solution. The ideal scenario is to be able to study real patient tumours in the laboratory; freshly biopsied at the time of surgical debulking, kept in a viable state long enough to analyse response to various treatment modalities, and offer treatment to the patient based on those results. Just as microbiologists rationalise their treatments of infections based on culture and sensitivity, an approach that allows prior drug testing and analysis of human GBM tissue (*hGBM*) *ex vivo* could help improve patient outcomes. As a pre-clinical model, such a system would effectively mimic the native tumour micro-environment, while avoiding prolonged incubation periods required with PDX. As a clinical model, it would allow testing of individual tumour samples within a short time frame; potentially, allowing key analyses of the tumour to assess for subtype, response to specific treatment as well as allow stratification of the patients to particular drug sensitivities. The issue of intra-tumour heterogeneity can be overcome by real-time measurements of the net response of the tumour to a single agent or combination therapy. Such a system introduces the desired degree of flexibility to deal with an adaptive tumour like GBM and would significantly enhance clinical research, aiding scientists and clinicians in pre-clinical drug development, patient stratification for drug trials and predicting responses to treatment in the clinic. Currently, no such model exists. The development of such a model may very well be instrumental in reducing the mortality associated with the disease and bring the elusive cure closer to our reach.

1.2 Microfluidics

1.2.1 Overview

Currently, the scientific community relies on a combination of *in vivo* animal studies and *in vitro* methods like cell and tissue culture in pre-clinical scientific research. Importantly, these methods are the mainstay of drug development, efficacy and toxicology. *In vitro* methods are widely used as they are quick, reliable, cheap⁷⁴ and high-throughput⁷⁵ methods, vital in understanding novel drug pharmacodynamics and pharmacokinetics. However, *in vitro* studies have less regard for the normal physiological environment of the cell and do not incorporate the complexity of tissue architecture⁷⁶ or cellular signalling in the analysis – failing to recapitulate the right disease micro-environment and hence providing a simplified understanding of drug interactions. Animal research is a method that works in parallel to *in vitro* testing. Testing of animals can help predict how human cells and tissues will respond to the same parameters and the scientific community infer much from these experiments, particularly to provide an insight into toxicology and the safety profile prior to human testing,^{77,78} while allowing an understanding of drug effects on the *whole* organism. However, these studies are also limited particularly with high costs, labour intensive procedures including breeding of the animals, which is time consuming,⁷⁹ as well as the moral ambiguity of animal testing. This last point is exemplified by a survey of 987 people across Great Britain that found 26% believe a ban on all animal research was necessary, and 74% felt more work needed to be done in identifying alternatives to animal research.⁸⁰ The biggest disadvantage of pre-clinical models though, is poor efficacy, with a clinical approval rate for new drugs estimated at 11.8%⁸¹. The highest failure rates for drugs in development are not during *in vitro* or animal studies but during human testing, with peaks in Phase 2 clinical trials where 51% of failures are due to poor drug efficacy and 19% due to drug safety concerns.⁸² According to the Pharmaceutical Benchmarking Forum, only 29% of drugs successfully progressed beyond phase 2 trials (between 2005 and 2010), despite 63% being deemed viable options from pre-clinical studies.⁸³ In the quest to cure GBM and other diseases alike, a pre-clinical model, which better predicts human responses is required to efficiently screen for potential failures, earlier in the product pipeline, avoiding costly investments in drugs or techniques that are doomed to fail.

Herein lies the drive towards effective *in vitro* models that accurately predict *in vivo* outcomes. Models that exist outside the organism but accurately mimic *in vivo* physiology. Microfluidics (MF) is a fast-growing area of research that allows experimentation with mimicry of natural conditions; so-called *ex vivo* experiments. Fluid flow through micro-devices takes place at a sub-millilitre scale, with Reynolds number much less than 100,⁸⁴ where viscous as opposed to inertial forces dictate flow. This results in laminar flow, with diffusion becoming the predominant form of molecular interactions; as it is in cells and tissues. The dynamics of fluid at the micro-scale has been exploited with a variety of biological applications, such as protein crystallization, polymerase chain reactions (PCR), single cell analysis, chemotaxis, and evolutionary biology.⁸⁵ Manipulation of fluid at such small scales offer a number of distinct advantages including low costs, low consumption of reagents, shorter processing times,⁸⁶ and greater sensitivities for target molecules.

In comparison to two-dimensional cell cultures, microfluidic systems are a better physiological mimic of the micro-environment, with regards to fluid forces and shear stress on the cells. With respect to animal experiments, it has the potential to obviate the need to breed animals for science, while also avoiding the pitfalls that will inevitably arise from the physiological differences between animals and humans. Its application to biological systems has taken off at an exponential rate and created a completely new field of research, which in 2013 was valued at \$1.59 billion.⁸⁷ This exciting field is creating a window into the nature of complex biological processes.

Types

MF devices can be categorised into two, depending on the type of flow through the device – *droplet-based microfluidics* and *continuous flow microfluidics*. Droplet based devices are an important branch of microfluidics that utilise the immiscible properties of water and oil (or gas) to allow encapsulation of single molecules or cells within aqueous microspheres of a controlled size. Cells or molecules can be maintained at ambient conditions for months, with cells cultured within the droplets viable for up to 7 days.⁸⁸ Each droplet contains on average, one molecule or cell and depending on the device specification, can be coupled to a number of reactions, including protein and genomic analysis such as PCR; in this case referred to as droplet digital PCR. The key here, is in the ability to measure very low levels of

proteins, cell surface markers and DNA/RNA with higher sensitivities than was possible with traditional PCR or ELISA techniques (see *Figure 1.4a*).

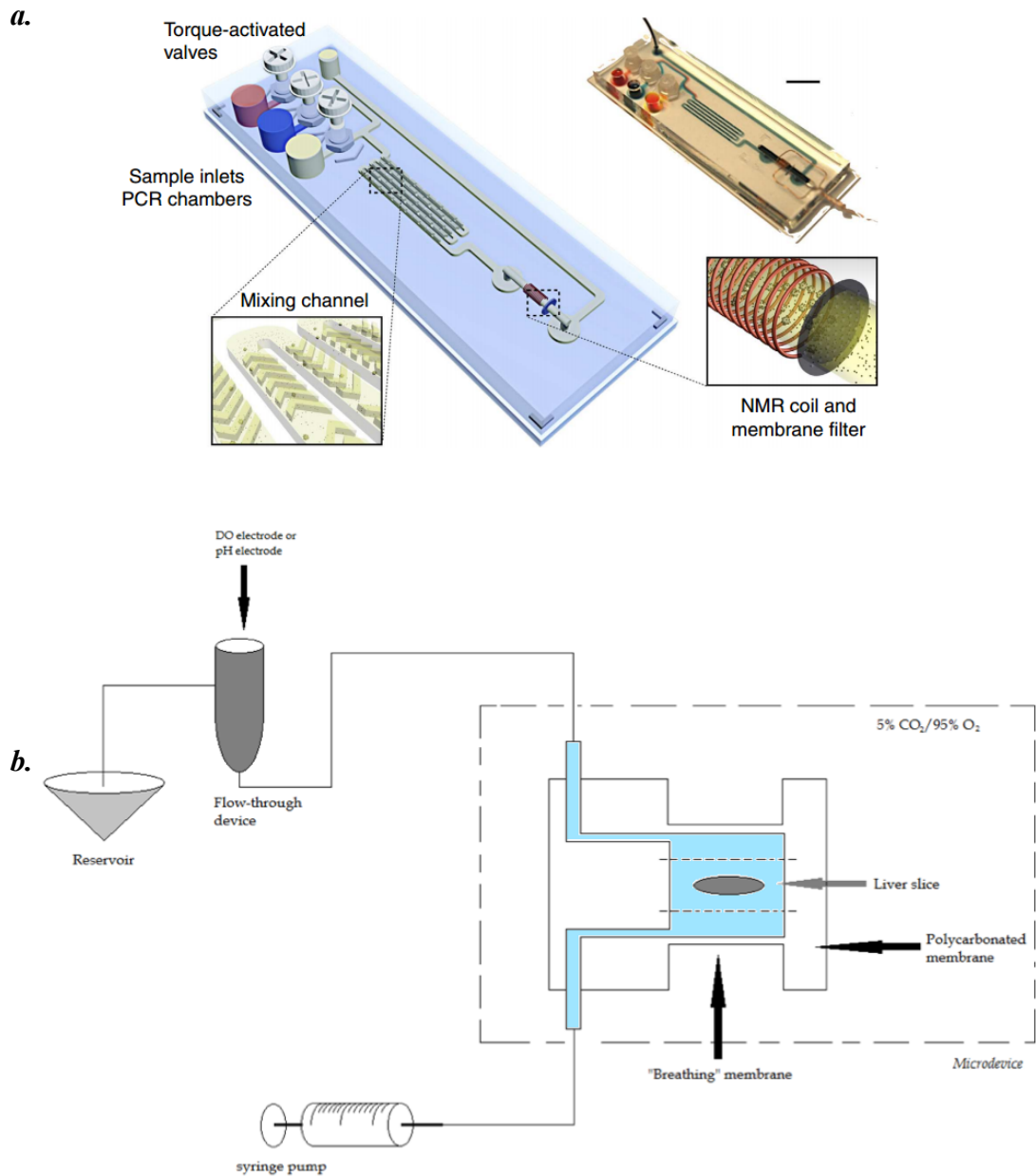


Figure 1.4: Different types of MF devices

a. On a 2.5 x 7.5 cm cartridge, DNA extracted from sputum samples is amplified in the chambers on the left. TB-specific sequences are magnetically labelled in the microfluidic mixing channels in the centre and detected by passage through the micro-NMR coil on the right. Copied from Liong et al.⁸⁹ **b.** Continuous flow microfluidic device housed in an air permeable PDMS membrane can maintain precision cut liver slices. Adapted from Van Midwoud et al.⁹⁰

While droplet-based microfluidics is becoming an important tool in analysing proteins and genetic material, continuous flow-based microfluidic devices are providing a new way to understand cell and tissue function. These devices involve continuous flow of nutrients or reactants to a cell or tissue and have been manufactured to assess all manners of cellular function, ranging from cell migration,⁹¹ embryonic development,⁹² physiological processes like axonal growth⁹³ and angiogenesis,⁹⁴ and disease modelling including, axonal injury,⁹⁵ renal stone formation,⁸⁶ and infection.⁹⁶ Though there are a variety of continuous flow based devices, with an array of complex channels and networks, the principles remain simple - a continuous inflow of media or reactants connected via microchannel(s) to a cell or tissue within a reservoir, which leads to an outlet for effluent collection (see *Figure 1.4b*). The use of glass or PDMS in these devices, means they are easily incorporated into standard microscopes and allow real-time visualisation of processes.⁹⁷⁻⁹⁹ Unlike static cultures, microfluidics allows continuous nutrient supply and waste removal, at a rate similar to human capillary flow,¹⁰⁰ thus maintaining a stable culture environment in keeping with the natural *in vivo* state. Culture of seeded cells within bioengineered MF devices are able to simulate functional units of human organs such as the lung⁹⁶ and liver,⁹⁰ or a physiological barrier like the blood brain barrier.¹⁰¹

With increasingly sophisticated microfabrication techniques, integration of a multitude of functions within one device, can streamline lab processes with a one stop 'lab on a chip'¹⁰⁰ with pumps, valves, temperature control and detection systems all within one point of care device.^{102,103}

Fabrication

The term *chip* stems from the original fabrication method of MF devices; a form of photolithographic etching used to manufacture computer chips.⁸⁴ This fabrication technique allows precise design of surface features, shapes and sizes on a micro-scale equivalent to living tissue/cells. Photolithography is the process of using light to transfer geometric patterns from a photomask (plate with holes or transparencies that permit light in a pre-defined pattern) to a light-sensitive *photoresist*. The exact sequence of events may vary depending on the substrate but typically involves spin-coating a thin film of photoresist onto a silicon or glass *master*. The master material

is then overlaid with the photomask which shields regions of the photoresist during exposure to high-intensity ultraviolet (UV) light. In the case of a polydimethylsiloxane (PDMS) chip, the silicon master acts as a mould onto which liquid pre-polymer PDMS is poured onto the photoresist pattern, cured and peeled off. This can then be trimmed, punched and sealed. With glass, the photoresist pattern is treated with a developer solution and the pattern is etched into the glass (*see Figure 1.5*). Ultimately, the fabrication technique allows the creation of micro-channels of sub-millilitre size within one layer of the device, while, corresponding holes can be drilled for inlet/outlet channels, prior to the bonding together of the layers. Fabrication of devices is usually inexpensive and amenable to mass production and because of the wide array of microfluidic applications, there are a multitude of different chip designs. This is not always an advantage, though, as the assorted mix of devices means there isn't always a cohesive approach to a specific microfluidic question. For example, a PubMed database search in November 2017, using the search terms "blood brain barrier model" AND "microfluidics" identified 12 different blood-brain barrier (BBB) microfluidic models, each unique in its own way.^{101,104,113,114,105-112} The overwhelming array of different devices and the boundless applications in existence means the field is not moving in a defined direction. This could explain why the field is yet to breakthrough into the mainstream.

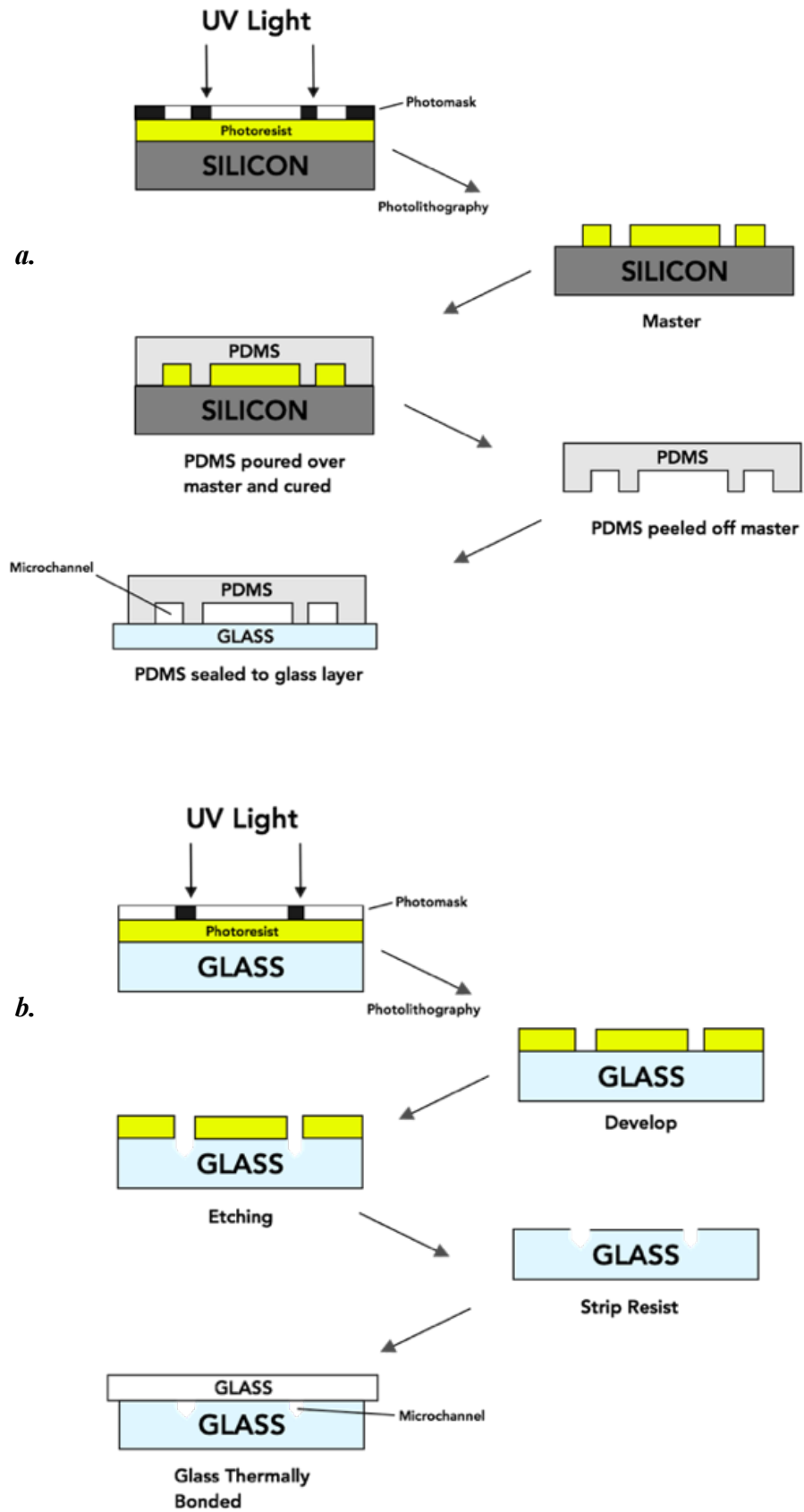


Figure 1.5: Photolithography and the fabrication of MF devices.

a. Chip fabrication using PDMS and glass substrates. **b.** Chip fabrication with microchannels etched into the bottom glass layer.

1.2.2 Application

Though MF devices are capable of a multitude of applications, the use of these devices as an alternative to *in vitro* and *in vivo* experiments, particularly for drug testing and disease modelling, aligns best with addressing a problem as complex as GBM. Microfluidic studies have involved all stages of ontological development; from embryos, to tissue and organ models that provide insightful and previously inaccessible information. It is beyond the scope of this thesis to provide a complete overview of all ranges of microfluidic applications so the papers highlighted here are done to emphasise the level of quantitative detail that can be achieved with MF applications, as well as to underscore a number of interesting devices that are astutely fit to purpose.

1.2.2.1 Embryos and Cells

Due to the sub-millimetre scales involved, microfluidics allows the creation of culture systems on a measure that suits the characteristic diameter of single cells and embryos. Within the field of assisted reproduction micro-channels have been used for sperm selection, removal of the zona pellucida, fertilization, maturation and culture¹¹⁵. Traditionally, gametes and embryos have been cultured in inert plastic vessels ranging from test tubes to various configurations of petri dishes⁹² but there is a trend towards platforms that utilize smaller volumes of media with a confined surface area; offering an efficiency in concentrating chemicals involved in autocrine/paracrine signalling. Faster rates of cell cleavage and production of more blastocysts have been noted with microfluidic structures when compared to ‘control embryos’ cultured in traditional culture dishes.¹¹⁶ Devices have been created to monitor detailed energy consumption, including the oxygen and glucose consumption of embryos.¹¹⁵ With respect to drug testing, Yang *et al.*¹¹⁷ created a chip that allowed evaluation of the toxicity and teratogenicity of drugs on zebra fish embryos using an integrated microfluidic device. The chip had a top glass layer, etched with a “Christmas tree” gradient generator (*Figure 1.6*) and seven embryonic inlet arrays; this was bonded to a middle plate containing an array of independent embryonic culturing chambers to correspond with the embryonic inlets of the top layer. The completed device exposed confined embryos to well-defined drug

concentrations, allowing simultaneous testing of different drug doses in parallel to culture and real-time monitoring of the cytotoxic effects of the drugs on the embryos.

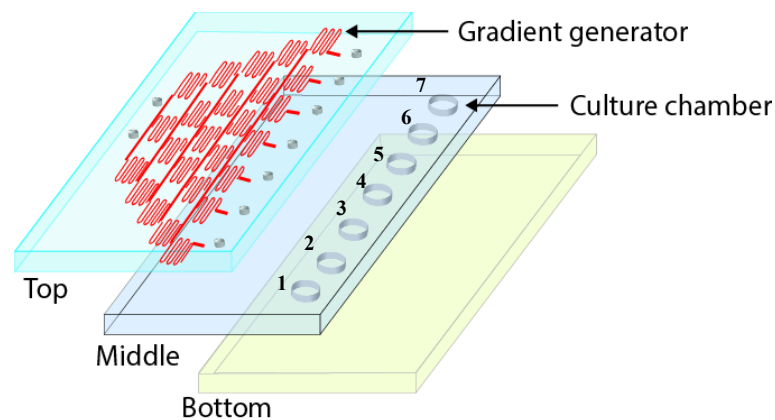


Figure 1.6: ‘Christmas tree’ gradient generator integrated into the MF device.

A three-layer microfluidic chip with a top plate with a concentration gradient generator and embryonic inlet array, a middle plate with a set of independent array chambers (1–7) for embryo culturing, and a bottom layer. When assembled contains two inlets for different solutions (medium and medium + drug) allowing different drug gradients to be exposed to embryos within the culture chambers. Adapted from Yang et al.¹¹⁷

Developments in research studying cellular mechanics is a good example of how technical limitations of traditional culture techniques can be overcome with microfluidic principles. In neurone and axonal development, for example, traditional techniques usually expose neuronal cell bodies and complex system of axons to a single culture medium bath. As such, chemical treatments are effective on both the soma and axons simultaneously, making it impossible to distinguish the impact on each cell component.¹¹⁸ Also without restricting the axons to a confined compartment, neuronal processes extend in random directions and form extensive tangles between axons and dendrites, making quantitative analyses of growth very difficult. Park *et al.* created a microchip made of three PDMS components that when assembled allowed confinement of axons to a central soma compartment while allowing axons to grow into a radial arrangement of six surrounding axon microchannels.⁹³ The chip was used to study how neurons from embryonic rats responded to different extracellular matrix (ECM), with a particular focus on axonal growth. Visualising axons with the aid of Calcein-Am (a fluorescent dye), the effects

on axonal growth under microscopy of four different ECM was studied. The benefit of this device was the specificity it allowed in identifying the effects the ECMs had on distinct parts of the cell with differential growth depending on whether the ECM was exposed to the cell body or the axon compartment. When the ECMs were exposed to the axonal compartment, all four factors promoted axonal growth by allowing 35-50% greater length, with a particular ECM, Matrigel, as most effective and Collagen, the least effective. Local exposure of ECMs to the cell bodies, on the other hand, revealed different results with Matrigel, Laminin and Collagen treatments promoting the most axonal growth. Kim *et al.* used similar principles for high throughput drug screening of axons with a device containing 24 axon compartments.¹¹⁸ Other devices have been used to study axonal regeneration after injury¹¹⁹ and even the process of myelination within axons (with co-culture of neurones and oligodendrocytes).¹²⁰

MF devices have also been able to mimic and manipulate the cellular microenvironment to enhance our comprehension of the workings behind cell movement and migration. With a similar device to the 'Christmas tree' gradient generator used by Yang, Jeon *et al* created a chip to study neutrophil migration.¹²¹ Their gradient generator incorporated a branched network of microchannels (50 μm wide) downstream of chemoattractant inlets. With laminar flow, the multiple streams of solution created stable gradients of interleukin-8 (IL-8) and their effects on neutrophil chemotaxis was studied. Smooth linear gradients, as well as complex gradients with sharp 'cliff edge' drops in concentration, were developed and the group proved the existence of a previously unidentified sensing mechanism that allows neutrophils to detect a precipitous drop in a chemoattractant despite an inability to react quickly to a gradual decline. Such detailed insight into cellular responses is made possible by the *stable* concentration gradients that can be created with the scaling down of flow rates. Migratory behaviour is also critical in our understanding of how cancer cells invade adjacent tissues and metastasise through the blood, and increasingly more accurate models are being developed with the aid of microfluidics. Behaviour in breast cancer cells co-cultured in a microfluidic device was tested with the use of a chip composed of two culture chambers, interconnected via microchannel arrays.¹²² The device allowed different models of mild, moderate and severe cancer to be investigated and the effects on cancer migration, as well the

inhibitory effects of chemotherapy agents were able to be tested. Similar work has been carried out in lung,¹²³ colon¹²⁴ and brain cancer (*see Section 1.2.5*). The role of proteins secreted from endothelial cells as well as the importance of the endothelium in promoting cancerous migration can also be studied in real time using microfluidics.¹²⁵ It is fair to say that as the technology to accurately mimic components of the cellular microenvironment improve, along with the ease of incorporating the microscope to microfluidic devices, we will gain greater insights into how cell polarity,¹²⁶ migration, and the metastatic behaviour of cells affect us in health and disease.

1.2.2.2 Tissue Chips

Beyond understanding detailed cellular machinations, microfluidic devices are also able to create complex physiological systems. These systems position cells into three-dimensional structures to imitate functional organs. These ‘tissue chips’ are able to react in a physiological manner, as well as respond to drugs, cell signalling molecules and biomechanical stressors.¹²⁷ The ease and precision of device manufacturing and the complementary developments in bioengineering mean that the boundaries of possibility are constantly being tested. One of the most frequently cited publications within the microfluidic literature is that by Huh *et al.* where a ‘lung’ was reconstituted on a chip.⁹⁶ Huh and colleagues cultured human alveolar epithelial cells and microvascular endothelial cells on opposite sides of a thin (10 µm), ECM coated PDMS membrane. Once the cells were confluent, air was introduced into the epithelial compartment to create an air-liquid interface and more precisely mimic the lining of the alveolar air space. Stretching of the PDMS membrane was pressure-driven, accomplished by the incorporation of lateral chambers, in which a vacuum was applied, producing elastic deformation of the wall separating the cell-cultured micro-channels from the side chambers (*see Figure 1.7*). When the vacuum was released, elastic recoil of PDMS caused the membrane and adherent cells to relax to their original size. The cyclical respiratory pattern of physiological breathing was maintained by integrating the device with a computer-controlled vacuum to produce rhythmic stretching of the tissue-tissue interface. With an accurate model of the alveolar-capillary interface, the group used the device to explore the rate of absorption of nebulised nanoparticles into the lung ‘vasculature’

as well as the effects of living *Escherichia coli* bacteria on activating the endothelium to promote migration of human neutrophils through the vascular microchannel. The biomimetic system was able to reconstitute multiple physiological functions and is in part responsible for the exponential growth in microfluidic systems aimed at organ mimicry. Grosberg *et al.* were able to assess the effects of epinephrine on measured contractility of cultured rat myocytes, within a ‘heart on chip’ device.¹²⁸ Wei *et al.*⁸⁶ created a MF model of renal tubules and recapitulated the physiological process of calcium phosphate crystal genesis to gain a better understanding of how pathological kidney stones are created *in vivo*. Other organs including the liver,¹²⁹ spleen¹³⁰ and bioengineered arteries^{131,132} have been modelled with microfluidic devices. The possibilities available with such devices rises exponentially when different groups collaborate with the concept of a Body-on-a-chip (BOC),¹³³ allowing complex interactions between different ‘organ’ modules. Though still in its infancy, there are currently models already described that combine 3-4 different organic functions.^{134,135} Such models have the hypothetical potential to allow intricate and accurate *in vitro* studies, which can completely eliminate the need for animal testing or patient derived xenografts and provide a time and cost effective approach to drug testing.

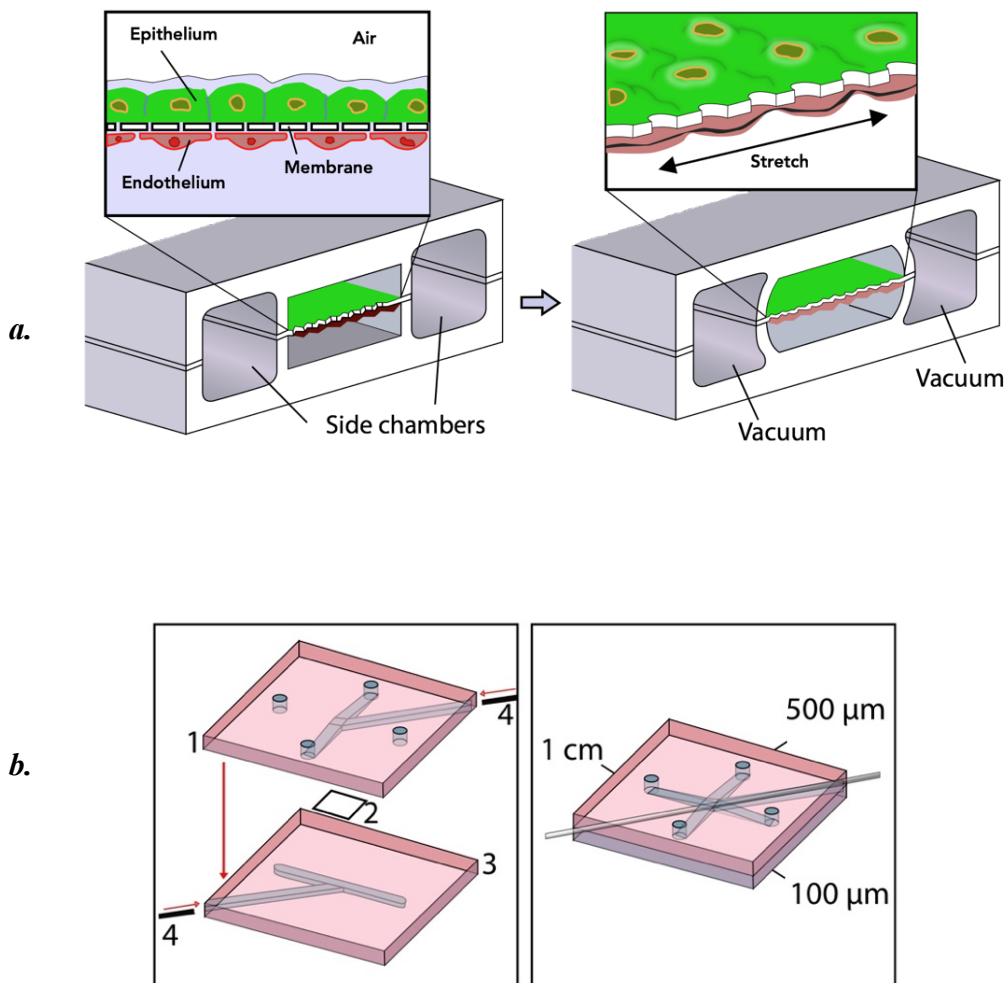


Figure 1.7: Microphysiological systems.

a. Schematic of part of the PDMS chip devised by Huh et al. in which epithelium and endothelium were co-cultured on either side of an ECM coated membrane. Physiological breathing was recreated by applying vacuum to the side chambers causing stretching of the membrane. Adapted from Huh et al.⁹⁶ **b.** Representation of the BBB chip from Griep et al. Left sided image shows the chip components including (1) Top layer, (2) Transwell membrane, (3) bottom layer, (4) Platinum electrodes. Right sided image shows the assembled chip. Adapted from Griep et al.¹⁰¹

One of the major hurdles in treating CNS diseases, including GBM, is the BBB, an ultra-selective membrane composed of tight junctions between CNS endothelial cells that blocks access of nearly all polar or large compounds to the nervous system. Regardless of drug efficacy, countless chemotherapeutic agents and antibiotics are deemed ineffective in treating CNS conditions as they are excluded by this barrier.

An accurate BBB model is a welcomed development in the field of neuroscience as it allows the testing of drugs for CNS penetration and suitability. Griep *et al.*¹⁰¹ cultured immortalised human brain endothelial cells (hCMEC/D3) for up to seven days in a BBB chip composed of two PDMS membrane separated by a 10 µm thin transwell polycarbonate membrane (pore size of 0.4 µm). Each membrane layer had a microchannel which was 1 cm in length, 500 µm in width, and a depth of 100 µm. The channel of the top layer was rotated 90° to the bottom layer so that both channels crossed each other, and the channels permitted flow through the device (*See Figure 1.7*). Crucial to proper endothelial cell function is shear stress and applied MF principles meant that the experimenters could manipulate flow rates of media through the microchannels that created physiologically relevant shear stress values and optimise the integrity of the model. Tightness of the membrane was measured by assessing the trans-endothelial electrical resistance via platinum electrodes incorporated into the device. The clear PDMS chip was visualised via confocal microscopy and the validity of the BBB monolayer was confirmed by the presence of stained Zona Occludens-1, a key transmembrane protein, within cell tight junctions. Yeon *et al.* used a combination of astrocytes and endothelial cells trapped in micro-holes connecting two fluid chambers for their BBB model. Another PDMS device, their BBB model was verified by microscopic confirmation of a consistent cell membrane layer with expression of Zona Occludens-1, as well as permeability assays of a number of drugs, with a good correlation with *in vivo* data.¹¹² Other models exist,^{113,114,136} most revealing similar insights and allowing detailed conclusions that can be applied and incorporated into CNS drug development. The gains are beyond just within neuroscience and some chips are now able to couple multiple physiological systems, including liver, kidney and blood-brain barrier models to better understand inter-organ interactions on drug metabolism.^{127,137} As such, these ‘tissue chips’ are gaining increasing popularity as the microfluidic community comes to terms with what is possible. The technology is behind the company Emulate Inc., a privately held company that has employed microfluidic and engineering principles in the “development of a wide range of chips and disease models through collaborations with industry partners and internal R&D programs.”¹³⁸

These impressive developments in tissue engineering are invaluable tools in emulating organs and systems and may be key in ushering a new era of personal

health medicine. But their necessity only results from the absence of a better model. Such innovations will not be required if we could preserve tissues outside the body. If the aim is to mimic an organ, no model can be as accurate as the organ itself, preserved *ex vivo*. What better model of the liver could there be, than an actual liver maintained and studied outside the body? If not the whole organ, perhaps even functional tissue sections of a liver. Attempts at preserving human organs or tissues in a working physiological state date back as early as 1903, when the then director of research of the Royal College of Surgeons devised a reliable pump to perfuse aeriated blood to excised animal organs.¹³⁹ Fell in 1940 performed successful *in vitro* cultures of embryonic organs and immature neonatal tissues¹⁴⁰ and later in 1959, Trowell published his extensive research on ‘the culture of mature organs in a synthetic medium’ where he devised a static culture system housed in an aluminium gas chamber. Within this device, he was able to culture up to twenty, 2 mm tissue or organ sections, using histological stains to confirm viability of up to 6 days. The experiments were repeated on a variety of animal organs, including renal, glandular, lung and central nervous system tissue.¹⁴¹ In 1966 Röller *et al.* published their experience of culturing 91 human tumour specimens, using a modification of Trowell’s technique, which were maintained for 4, 7 and 11 days. Scoring the tissue sections on the morphological appearance of H&E sections, viability of the tissue was estimated at 43%, based on the tissue retaining histological characteristics of normal living tissues.¹⁴² Leading on from Trowell’s techniques, several groups cultured tissues and human tumours with varied success rates,^{141–149} but there is still a paucity of examples within the literature, suggesting that the practise is yet to be adopted by the mainstream. This may be due to the short culture times and poor viability of current methods when compared to cell and 3D-cultures. The introduction of microfluidic principles to tissue culture, however, is instigating a new wave of exciting developments that is raising the profile of the method as a scientific model for understanding human biology and disease mimicry. Interestingly and rather relevant to GBM, the story of tissue culture, or more specifically in these cases, *tissue maintenance*, has a significant facet involving the central nervous system and brain tissue slice.

1.2.3 Brain Slice on a Chip

The human brain represents 2% of total body weight, yet receives 15% of the cardiac output and 20% of total body oxygen.¹⁵⁰ The high blood and oxygen requirement means that brain tissue cannot maintain proper function without adequate oxygenation for even a few minutes.¹⁵¹ The well evolved nature of the cerebrovascular system, means that it is perfectly adapted at providing nutrients and oxygen to every part of the brain in a highly regulated manner to match the high metabolic demand of CNS neurones. Sequestering and maintaining tissue outside this complex environment, requires an accurate reproduction of the *in vivo* system for nutrient and oxygen delivery. This remains one of the main obstacles to overcome when maintaining acute brain tissue *ex vivo*.

A more defined approach to the problem of brain tissue maintenance was provided by Huang *et al.*, who suggest that there are 3 key issues that a successful brain slice culture paradigm must overcome: (1) efficient delivery of oxygen and nutrients with the successful removal of waste; (2) finite control over (neuro)chemical environments; (3) access to modern microscopic and electrophysiological techniques.¹⁵¹ Applying microfluidic technology to tissue slices allows for inventive ways to address these essential concerns, in particular, that of slice oxygenation and viability.

1.2.3.1 Interface Chamber

The earliest experiments focused on maintaining active tissue sections were on rat/mice brains, motivated by a desire to minimise disruption of intact neural networks while studying the tissues of the brain. These experiments attempted to achieve adequate viability and function by exposing a tissue slice to both media (for nutrient supply) and air (for oxygenation); a so-called interface chamber (*Figure 1.8*). The Haas interface chamber, leads on from the works of Fell and Trowell and was first described in 1979 to provide a stable platform for intracellular recordings and rapid exchange of perfusion fluids.¹⁵² It consisted of tissue sections mounted onto a nylon mesh atop a rectangular water bath, which was filled with 'fluid' via polyethylene tubing connected to a three way tap. The perfusion of the tissue was

passive, via capillary action along the nylon mesh and the group could maintain brain tissues for up to 12 h. Reynaud *et al.* developed an interface chamber with similar principles but with more complex machinery incorporating peristaltic pumps, bubble traps and thermistor probes to maintain 400 μm thick rat brain slices.¹⁵³ Decades later, the interface technique was refined using a flat microfluidic chamber with an open channel flow of the perfusate.¹⁵⁴ Rather than a nylon mesh, Passeraub and his colleagues used an array of micro-pillars that upheld the brain slice and maximised surface contact between the tissue and the artificial CSF (aCSF) perfusate. As with all interface models, only the inferior surface of the brain slice was in contact with the aCSF, with the superior aspect aeriated with Carbogen (95% Oxygen/5% Carbon Dioxide). Using this set up, the researchers confirmed viability of brain slices over 5 h as the tissue slices produced spontaneous epileptiform activity.

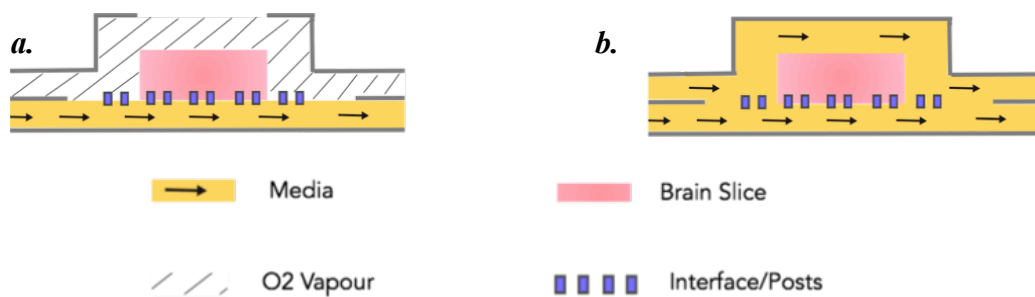


Figure 1.8: Brain Slice and Microfluidic Designs.

a. Interface flow chamber with tissue slice laid on posts and in contact with media (bottom) and air (top). **b.** Submerged MF type set-up with a closed system without any direct exposure to air oxygenation and whole tissue submerged in media.

1.2.3.2 Submerged Chamber

In 1980, only 18 months after Haas first introduced the interface chamber, Nicoll and Alger developed a competing approach to maintaining tissue slices.¹⁵⁵ Their device consisted of two interconnected wells, with the tissue slice completely submerged within the perfusate, firmly placed within a receiving well and enclosed within two nylon membranes. The so-called ‘submerged chamber’ developed almost in parallel to interface techniques and would address some of the short comings of Haas’ chamber; particularly, as these devices were able to promote active *interstitial* flow - where fluid flow is forced through the tissue, as opposed to the arrangement in

interface models where a tissue slice wicks medium from the channel below, solely by capillarity.¹⁵⁶ As a result, these new chambers could address the problem of central necrosis, where nutrients failed to diffuse into the depth of thick tissue slices. However, as the brain slice is completely immersed within the media, alternative approaches to improve tissue oxygenation were also required. Hajos and Mody found that improved oxygenation of submerged brain slices could be achieved by reducing the total volume of the perfusion chamber, while increasing the flow rate of the media solution to improve tissue perfusion.¹⁵⁷ As high flow rates can cause increased shear stress and hence damage the tissue, other methods including using hyper-oxygenated solutions or reducing the oxygen demand of the tissue by lowering the temperature of the preparation were also necessary.¹⁵¹ Another approach to improve tissue oxygenation is to minimise the thickness of the slice, thereby reducing the depth of nutrient diffusion, hence most acute brain slices are less than 500µm thick.¹⁵¹ Despite these modifications, oxygenation can be suboptimal with submerged devices and a lot of researchers incorporate PDMS or other gas permeable materials in their device.^{151,158–162}

Examples of submerged devices, heavily focused on optimising interstitial flow include a device which used inlet channels *within* micro-needles to penetrate the brain slice.¹⁵⁸ The microneedles perfused tissue slices at a flow rate of 40 µl per hour and were able to ensure nutrients were infused directly into the tissue; much the same as how capillaries, delivering oxygenated blood, are embedded within the tissue (*see Figure 1.9a*). Unfortunately, viability in this model was not impressive, lasting only 4 h. Another submerged chamber utilised a three-layer PDMS device constructed with perfusion layers above and below a tissue chamber. The brain slice was held in place by microposts, arranged in a diagonally-alternating pattern to optimise the flow of nutrients and oxygenation on either side of the tissue. There were 3 inlet channels leading to the tissue chamber and the flow within the channels could be varied independently to maintain a focused laminar flow down the centreline area of the brain slice, in either the bottom or the top of the slice (*See Figure 1.9b*).¹⁶³ The experimenters displayed the strength of the device by focusing a stream of Na⁺-free solution onto one half of a medullary slice to abolish spontaneous neural activity in that half of the brain slice, while the other half remained active. Overall viability was not tested beyond 3 h, but the group could confirm spontaneously produced motor

output during that time period.

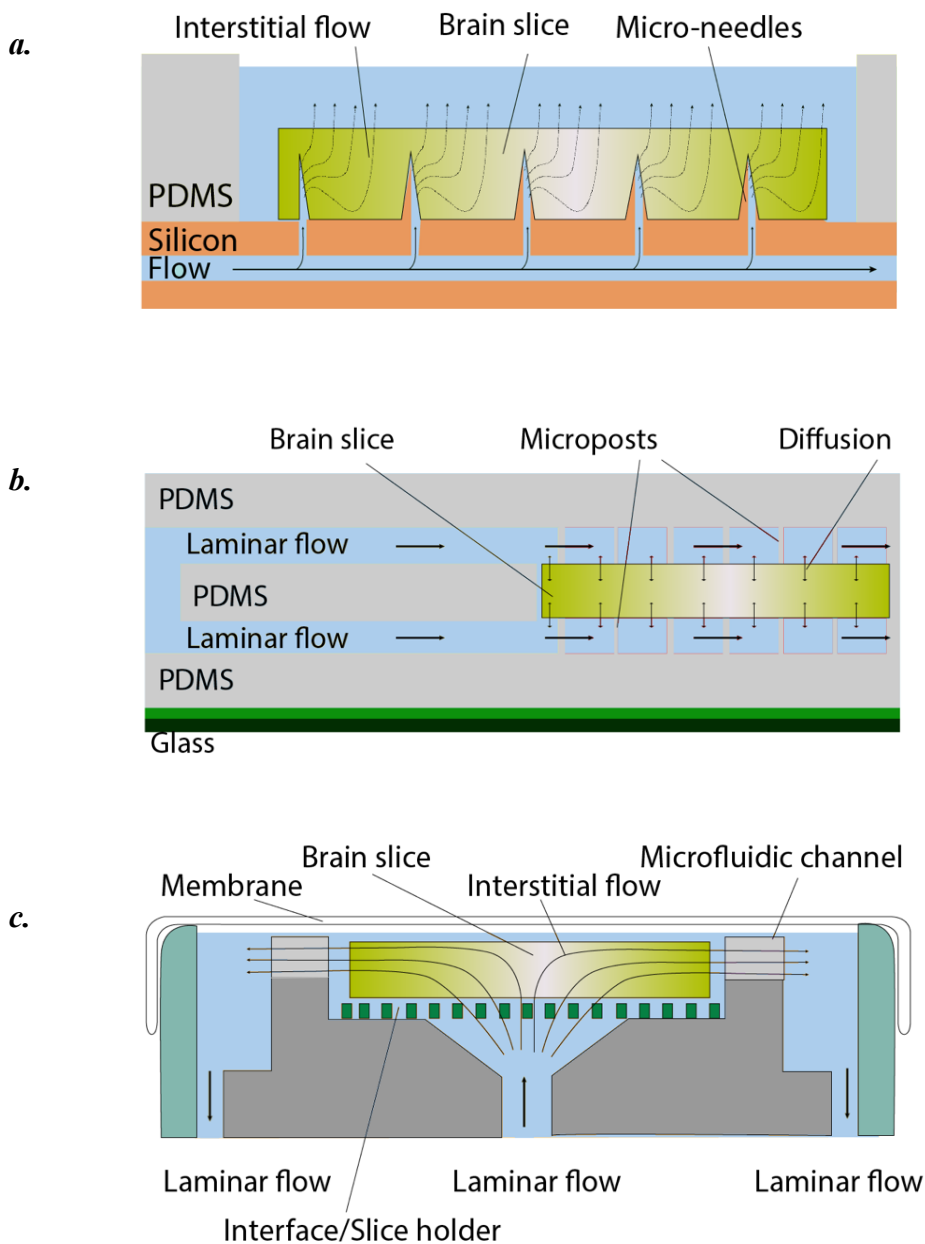


Figure 1.9: Examples of submerged devices and different methods of improving oxygenation and tissue perfusion supply.

a. Schematic of flow through MF device as set up in Choi et al.¹⁵⁸ with microneedles piercing and perfusing media through the tissue (green) **b.** Schematic of flow through MF device as set up in Blake et al.¹⁶³ where the tissue is supported above and below by microposts and media flow is pushed through channels above and below the tissue. **c.** Schematic of flow through MF device as set up in Rambani et al.¹⁵⁹ This system promoted flow through the tissue by forcing flow from below the tissue and placing microchannels around the infusion chamber that facilitated the lateral outflow of culture media into the withdrawal chamber and thus promoted interstitial flow.

Able to resolve the challenges of tissue oxygenation within a submerged device, Rambani *et al*, created a device that was sealed with a gas permeable membrane.¹⁵⁹ Their microfluidic device had a unique micro-perfusion chamber that promoted flow through the entire brain slice. The micro-perfusion chamber consisted of an inner infusion (culture) chamber, an outer withdrawal chamber; and respective inlet and outlet ports. A gold electron microscopy grid was used as the substrate to seat the tissue, which was sealed to the chamber via an adhesive layer of laminin. The nutrient medium was delivered into the infusion chamber via the inlet port that projected upwards into the gold plate housing the tissue. The infusion chamber was in direct fluidic communication with the withdrawal chamber by way of 150 μm wide microchannels that facilitated the lateral outflow of culture media into the withdrawal chamber. A gas permeable and water impermeable membrane composed of fluorinated ethylene-propylene (FEP) was stretched and securely fitted over the perfusion chamber to ensure gas exchange. Using this method, a convection-enhanced delivery (see *Figure 1.9c*) of nutrient and oxygen with forced interstitial perfusion was established with flow characterised by the radial spreading of the media solution. Slice viability was 84.6% at 5 days using Propidium Iodide (PI) for staining dead cells. More recently, a similar device has incorporated perforated microelectrode arrays for easier electrophysiological monitoring while maintaining the brain tissue.¹⁵⁶

By improving the viability of brain tissue slices, the ultimate goal of studying long term processes can be achieved with these cultures. The complex processes involved in tissue hypoxia were studied in real time with a recreated microfluidic model that allowed finite control of the tissue microenvironment. With several independent microchannels located at different regions of the tissue slice, spatial and temporal variability in oxygen concentrations were manipulated to simulate a stroke.¹⁶⁴ As well as manipulating the oxygen concentration, devices have been created that allow finite control of the chemical environment with localised chemical stimulation of a tissue slice available within a device, where perfusion inlet and outlet sites replace microposts on which the brain slice sits atop.¹⁶¹ Innovations such as in the case of Tang *et al*. incorporate fluid ports amongst the micro-posts that could introduce or siphon off media contents, to ensure tight control of the tissue slice microenvironment (see *Figure 1.10*). Brain sections inserted into the device and

perfused with an artificial cerebrospinal fluid medium could be exposed to localised injections of potassium chloride through the ports to induce a spreading depolarisation within a specific focus of cells. Similar chemical delivery methods have been used to measure the effects of focal concentrations of cocaine on Dopamine release within the tissue slices.¹⁶⁵

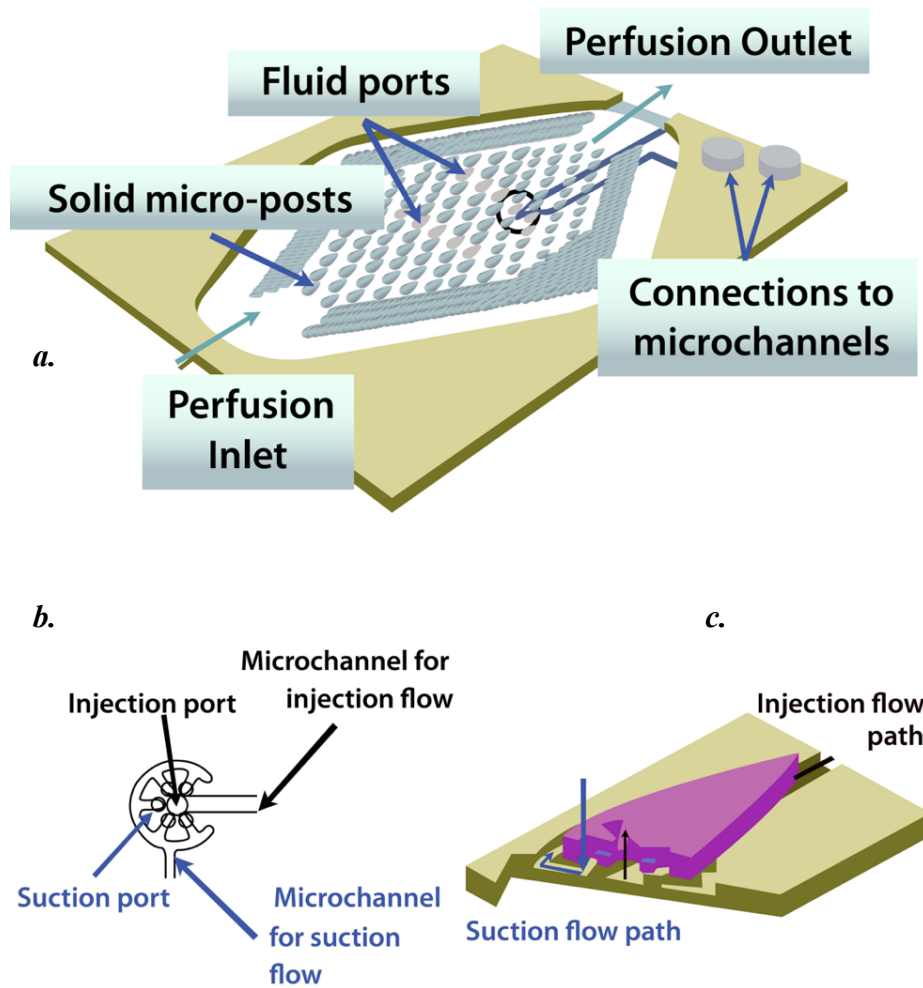


Figure 1.10: Microfluidic Perfusion Chamber

a. Schematics of the perfusion chamber devised by Tang et al., incorporating an integrated fluid injection/suction ports for the localised chemical stimulation of the brain tissue slice. Tissue is placed on top of the perfusion chamber, so that most of the stimulation occurs on inferior portion of tissue *b.* Top view and *c.* cut view of the fluid port which contains one injection port surrounded by suction ports. The tissue is represented by the pink disc. Adapted from Tang et al.¹⁶¹

1.2.3.3 Organotypic Slices

The term organotypic slice is used interchangeably with acute tissue slice, likely because of the subtle differences between the two. To a purist, organotypic slice refers to the culture of a layer of perinatal tissue attached to a semipermeable membrane,¹⁴¹ glass coverslip (within roller-tube cultures)¹⁶⁶ or in the case of the earliest work, within the anterior chamber of a rodent's eye.¹⁶⁷ The tissue is usually from an animal that is postnatal day 0-12, and though there is evidence of culture slices from adult animals, the older the animal, the less the tissue survives.¹⁶⁸ During culture, the slice morphology and cytoarchitecture alters as the tissue mantle spreads out into a thin layer of 1 to 4 cells.^{151,168} The thinning and re-organisation of the tissue layer allows culture of the tissue for weeks or even months and is the reason behind the term 'organotypic', since the cultures are altered from the tissue of origin and as such different to the acute culture techniques mentioned earlier. Organotypic cultures date back to the 1950s with varied procedures involved in the long-term study of tissue cultures and electrophysiological parameters. Recently scientists are adapting organotypic culture chambers with microfluidic add-ons with interesting effects.

Concomitant culture of organotypic tissues provide great insights into the development of axons. Berdichevsky *et al.* performed the co-culture of organotypic (hippocampal) tissue slices interconnected by microchannels.¹⁶⁹ Each compartment had a separate fluid inlet and outlet site and the compartments were completely isolated from the other except for series of interconnected microchannels. Slices of rat hippocampus cortex were maintained in the compartmentalised devices for up to 4 weeks and the axonal outgrowths developed within 3 days of co-culture as viewed under microscopy. The process of synapse formation was evidenced by the synchronization of electrical activity within both cultures. Synchronisation only occurred after 16 days *in vitro*, proof that it occurred as a result of new connections as well as highlighting the importance of long-term culture techniques to study long term processes. Dolle *et al* were also able to culture interconnected organotypic slices on a MF device while focusing on the effects of axonal injury by mechanically inducing strain to the axons. Using a pneumatic cavity within a PDMS MF device, they were able to increase the pressure within the cavity, stretching and injuring the

interconnected axons overlying the pressure chamber, creating a platform for studying the chronic effects on nervous tissue.¹⁷⁰ Similar to submerged chambers described above, devices have also been manufactured to allow finite control of the microenvironment of organotypic slices with multiple inlet channels under the semipermeable membrane for long term culture,¹⁷¹ and recently a microfluidic set up incorporated a perfused drop organotypic slice with a PDMS microfluidic channel for the development of high throughput drug screening of tissue cultures.¹⁷²

Though mainly focused on animal brain tissues, the literature on the use of microfluidic technology shows how a tissue culture paradigm has developed that allows culture of thick tissue slices for hours to days, with good viability. The ingenuity encouraged by microfluidic methods has allowed inventive ways to overcome the challenges of tissue oxygenation *in vitro* and the finite control of the microenvironment. Devices have been able to utilise whole tissue cultures to provide insights into the complex nature of neurobiology,^{152,162,173,165,166} stroke,^{164,176} trauma,⁹⁵ neurodegeneration¹⁷⁷ and the realisation of high throughput drug screening models to replace conventional methods is near.¹⁷²

1.2.4 Non-CNS Tissues on Chip

Translating the principles of tissue maintenance using microfluidic devices to non-CNS tissue, has allowed various research groups to mimic normal tissue function in a variety of organs. Van Midwoud *et al.* were the first to maintain non-CNS tissues *en bloc* within a microfluidic device consisting of two separate inlet and outlet stacks of integrated PDMS membranes bond together with a polycarbonate clamp.⁹⁰ In this system, rat Precision Cut Liver Slices (PCLS) remained viable for up to 24 h, as evidenced by Lactate Dehydrogenase (LDH) assay and the stable activity of the metabolite 7-ethoxycoumarin (a cytochrome p450 mediated metabolite). *In vivo*, liver function is rarely in isolation of other tissues and the true power of MF devices is in allowing a better understanding of the interplay between two different organs, which the group were able to explore through sequential perfusion of micro-chambers containing different organ specific tissue slices. In particular, the influence of the intestine on the production of bile acids in the liver was studied when the outlet of a micro-chamber containing rat intestinal slice was coupled to the inlet of a

micro-chamber containing a rat liver slice.¹⁷⁸ When exposed to medium containing the bile acid, chenodeoxycholic acid (CDCA), the intestine produces fibroblast growth factor 15 (FGF15), a protein that deregulates the enzyme, cytochrome P450 7A1 (CYP7A1), responsible for bile acid synthesis in the liver. This downregulation was reproduced *in vitro* using an integrated microfluidic platform; with the expression of CYP7A1 unchanged when rat intestinal slice was perfused in front of a liver slice in the absence of CDCA (control) but decreased by 60 % with the introducing of 50 mM CDCA into a system with an intestinal slice. This was explained by the excretion of the FGF15 protein by the intestine, which was also measured to have as increased.

Webster *et al.* publish their experience of whole tissue culture of non-CNS tissue biopsies in a microfluidic device the same year as Van Midwoud's liver experiments. They developed a device made from two layers of glass that enclosed 50 µm deep micro-channels and a central 3 mm tissue cavity, when bonded together. The device had 1.25 mm diameter holes to accommodate 3 inflows and 1 outlet tubing. Once connected to a peristaltic pump delivering gas saturated media, the group were able to maintain colorectal and neoplastic tissue of 2 mm³ for 3 days and assess the response of the tissues to degrees of hypoxia; measured by the release of vascular endothelial growth factor into the media. Hattersley *et al.*¹⁷⁹ adapted the same device to maintain head and neck squamous cell carcinomas (HNSCC) and progressed the method further by assessing the response of the tissue to chemotherapeutic agents over a 7-day period. As well as measuring the LDH release from the effluent, they analysed Water Soluble Tetrazolium (WST-1) as a marker of metabolic activity. Evidence of viability was confirmed by low LDH levels and high WST-1 concentrations. Using two chemotherapy drugs – Cisplatin (CDDP), 5-Fluorouracil (5-FU) and a combination of the two, the researchers could compare the effects of these drugs on viability assays. Significantly raised LDH release was noted in the chemotherapy cohorts (highest with the combination of 5-FU and CDDP) compared to control samples. Cell viability assays with Trypan Blue staining of disassociated cells confirmed the results with the highest percentage of viable cells seen in the untreated samples, and the lowest in the samples treated with dual chemotherapy agents. Building on from this, Carr *et al.*¹⁸⁰ used the same device to examine the effects of radiotherapy regimens on the tissue within the microfluidic devices.

Irradiation was performed using a 6 MV photon beam from a Varian Linear Accelerator, with the microfluidic device housed inside a Perspex phantom and there was a significant release of LDH from tissue that was exposed to 20 Gy of radiotherapy at 24 h (compared to the control). Immunohistochemical staining of the caspase-cleaved cytokeratin with M30 revealed a significant increase in the apoptotic index in samples that had been exposed to 2 Gy and 10 Gy of radiotherapy compared to radiation naïve samples. There was also an increment in the apoptotic index between the two radiation groups with a higher apoptotic index in the group exposed to a higher dose of radiotherapy.

These proof of concept studies paved the way for a number of follow-up experiments that confirm that human and animal tissues can be maintained *en bloc* within microfluidic devices as viable models for disease and drug testing. Since the earlier works mentioned above, Astolfi *et al.*¹⁸¹ has used a very different microfluidic device, that catered for smaller tissue sections, with the rationale that sub millilitre tissue dimensions help to maintain viability by reducing hypoxia in the centre of the specimen. Tissues of 300 µm thickness, including human ovarian and prostate cancers, were maintained within microfluidic wells for a period of 8 days, with high cellular viability, between 50 and 85 %. Exposure of the micro-dissected tissues to Carboplatin at concentrations of 350 µM for 3 days significantly reduced cell viability compared to untreated controls. Cheah *et al.* maintained viable heart tissue samples from rats and humans for 5 and 3.5 h respectively,¹⁸² Dawson *et al.* were able to maintain full thickness bowel tissues of 5 mm diameter within a dual flow device, with tissue viability maintained for up to 72 h¹⁸³ and Zambon *et al.* who were able to maintain adipose tissues for the high throughput screening of insulin sensitivity.¹⁸⁴

1.2.5 Glioma on Chip

Though there have been a number of experiments in which glioma cells and material have been the substrate of microfluidic experimentation, there is yet to be a study that focused on the use of a microfluidic device to maintain primary GBM tissue. The closest description is with the maintenance of patient derived (GBM8 cell lines)

xenograft tissue slices within a microfluidic device.¹⁸⁵ A bottomless 96-well plate was modified so that the central 4 x 4 well area was sacrificed to fit a square microfluidic chip in the centre, ensuring the device only accepted 80 inputs. This top layer of the bottomless '80 well plate' was affixed to a PDMS layer with 'through holes' that corresponded to the bottomless wells, a microchannel network layer that connected the through hole to the central layer which contained a microfluidic chip with 80 parallel open channels. Xenografts were prepared by injecting GBM8 cells (200,000 viable cells) into immunodeficient mice and then biopsied, which were interrogated on chip. The device allowed for selective fluid delivery to the tissue slice at several predefined locations of TMZ; and confirmed the disappearance of green fluorescent protein (GFP) labelled glioma cells at the sites of TMZ delivery after 48hours.

Though this is the only example of glioma 'tissue' being maintained in a microfluidic device, there are a number of experiments in which microfluidic principles have been applied to the understanding of GBM. A number of microfluidic devices have been used to sort different glioma cells, such as a spiral device that used inertial forces created within a spiral chip for size dependent sorting of glioma cells.¹⁸⁶ Microfluidic diffusive mixers have also been used to manipulate the gradients of U87 glial cells to study the effects of spatial and temporal heterogeneity on tumour development on chip¹⁸⁷ and mimic hallmark histopathological pseudopalisades.¹⁸⁸ The migratory behaviour of glioma cells have been studied by a number of groups using microfluidic devices^{97,189-191}; Huang *et al.*⁹⁷ looked at migration of brain tumour stem cells seeded into PDMS micro-channels coated with ECM (*Figure 1.11a*) to study the migratory behaviour of brain tumour stem cells (BTSC). They showed that the BTSC had the ability to migrate from a seeding chamber to a parallel receiving chamber through micro-channels and that migration was aided by the formation of cell polarisation and protrusions. Subsequently, the cells were enzymatically detached from the microfluidic device and then isolated into two populations of BTSC; migratory and non-migratory subsets. The rationale being able to analyse the genetic phenotypes that promoted a migratory signature, with potential for gene targeting. Able *et al.* also connected inlet and outlet reservoirs with microchannels to study the effects of different growth factors on mouse glial progenitor cells¹⁹⁰ while Wan *et al* experimented on the

effects EGFR blockage has on glioma cell migration using real time microscopy.¹⁹¹

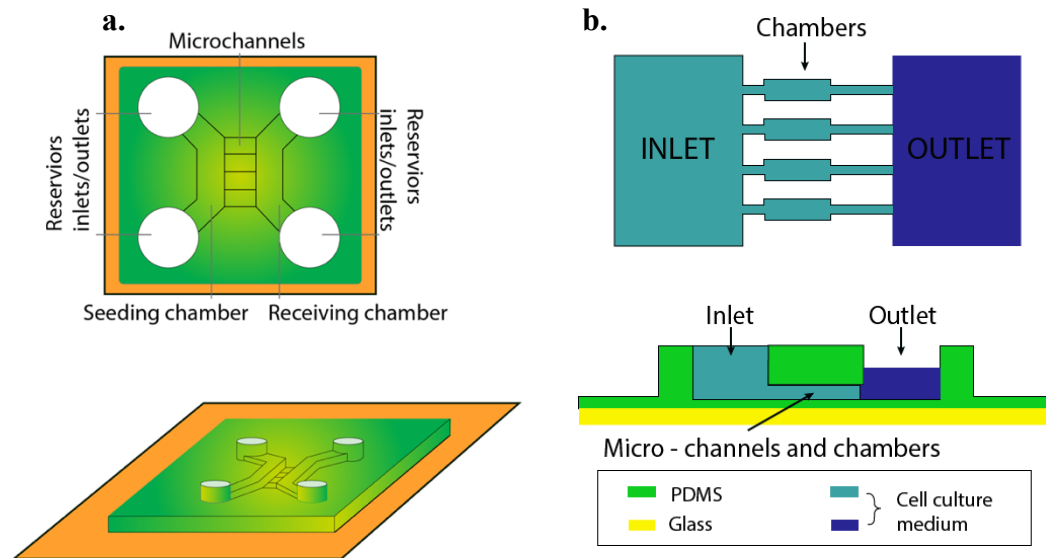


Figure 1.11: Microfluidics and Glioma 1

a. PDMS device with microchannels connecting receiving and seeding chamber to allow monitoring of glioma cell migration. Cells are placed into the reservoirs and migration across the reservoirs is observed (adapted from Huang *et al.*⁹⁷) **b.** Configuration of MF device with four parallel culture chambers used for drug screening (adapted from Liu *et al.*¹⁹²)

A number of microfluidic devices have been created to test the effects of drugs on glial cells. Liu *et al.*¹⁹² used a microfluidic device that contained four parallel cell culture chambers as well as separate inlet and outlet channels (Figure 1.11b) that allowed unrestricted flow within the channels, while in turn maintaining rat glioma cells and exposing them to varied concentrations of Colchicine. Results, with phase contrast and fluorescent images, showed Colchicine concentration correlated with cell death. The same group have utilised 3D spheroids to mimic the tri-dimensionality and cellular density of GBM tissues.¹⁹³ Creating an innovative MF device for cell trapping; by using a gas activated pneumatic microstructure, they were able to turn 2D posts into 3 dimensional posts and as such, could seed U251 human glioma cells into their MF device, trap the cells long enough to confirm ‘tumour’ formation and then release the cells for collection/analysis. Tumour viability was confirmed with fluorescent staining of actin filaments, as well as a steady increase in the diameter of the spheroids. The effects of treatment with

Vincristine and Bleomycin was revealed as a dose dependent increment in the number of dead cells as portrayed by PI staining.

Pang *et al* created an integrated device composed of fluidic channels with pores within filter units for the capture of single cells (see *Figure 1.12a*). The filter units decreased in width by 2 μm to capture different sized cells, and the device allowed single cell capture and subsequent infusion with drugs (Vincristine); and as such was utilised to assess the correlation between size of tumour cells and resistance to Vincristine – induced (larger) cells showed greater resistance.¹⁹⁴ Other high throughput microfluidic screening models have been used to study the effects of experimental drugs, including the EGFR inhibitor Erlotinib,^{195,196} Irinotecan¹⁹⁷ and even the interaction of GBM cells with nanoparticles.¹⁹⁸

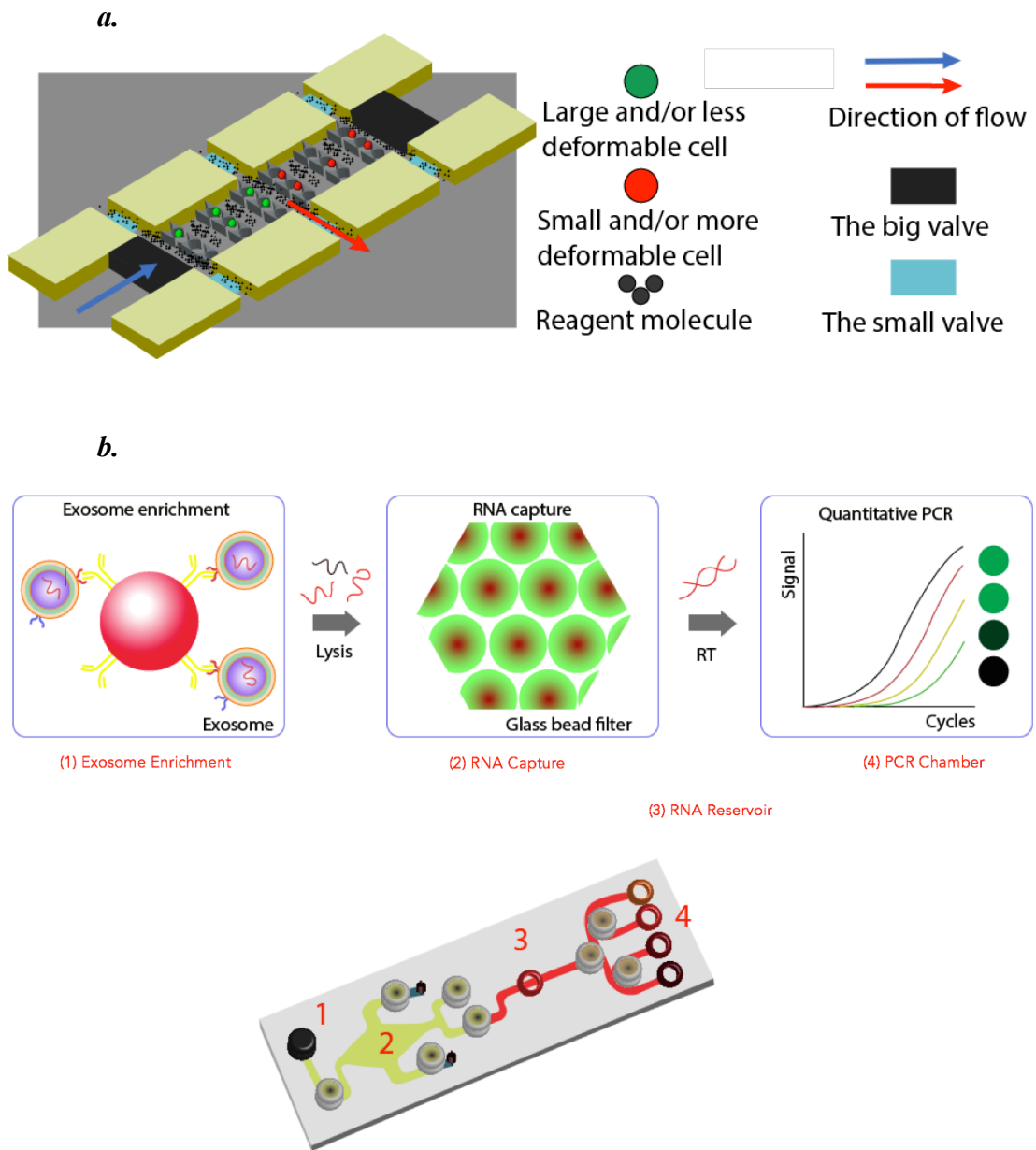


Figure 1.12: Microfluidics and Glioma 2

a. Magnified schematic to represent single cell sorting – cell sorting is achieved by a cell infusion in the direction highlighted by the blue arrow; large and less deformable cells are trapped by the larger filter units; smaller cells are captured in the slightly smaller filters which are 2 mm narrower. Once cell capture is achieved, big valves are closed and reagents including drugs are introduced in perpendicular direction (red arrow). (adapted from Pang et al.). **b.** Integrated device that incorporates exosome enrichment, RNA capture and PCR for tumour prognostication (adapted from Shao et al.¹⁹⁹)

Integrated microfluidic devices have also been shown to be useful in the study of GBM cells. Wei *et al.* were able to capture glioma cells and use their device which contained a bar code array for cell profiling and assess the effects of different partial pressures of oxygen on glioma cell regulation.²⁰⁰ Shao *et al.* were able to integrate all the features for quick PCR analysis of patient's MGMT status using tumour exosomes from the patient's blood on a 'lab on a chip' (see *Figure 1.12b*),¹⁹⁹ and a similar device was used to effectively screen patient tumour samples for their IDH1 status.²⁰¹

Table 1.2 summarises the studies in which microfluidic devices were used to study Glioblastoma. The literature is extensive and includes well thought out GBM models on chip, some of which have been validated as promising replicas of GBM *in vivo*, allowing the observation of pathophysiological processes and quite a few devices focused on drug screening models. Yet, these models still pose a risk of being imprecise because they are based on immortal cell lines and spheroids that lack the normal matrix protein content, mechanical and microstructural properties, and growth factors that exist within the tumour *in vivo*.¹⁸⁷ Drug screening using these models will also provide conclusive errors as the cell lines used behave very differently from the primary tumour; for example, just under 100% of rapidly replicating glioma cell lines are within active phases of the cell cycle at any given time, yet the proliferation index of most GBMs *in situ* is usually less than 20%.²⁰² Most chemotherapeutic drugs preferentially target highly mitotic cancer cells as opposed to normal tissue with lower proliferation indices. Basing treatment response *in vivo* on immortal cell lines can overestimate response to treatment and lead to inefficiencies in the development of drugs. The high mortality and morbidity associated with GBM demand that other viable options are explored.

Reference	Summary
Kuntaegowdanahalli <i>et al.</i> (2009) ¹⁸⁶	Created a device under the principle that under inertial forces, neutrally buoyant particles flowing in a microchannel migrate to a single equilibrium position near the inner (central) microchannel wall. The spiral lab-on-a-chip was used for size-dependent sorting of particles at distinct equilibrium positions. The device exhibited 80% separation efficiency of glioma cells. The technique was comparable to the rates obtained with commercial macroscale flow cytometry techniques.
Liu <i>et al.</i> (2010) ¹⁹²	A microfluidic device that contained four parallel cell culture chambers as well as separate inlet and outlet channels (see <i>figure 7 a & b</i>) that permitted unrestricted flow within the channels, while in turn maintaining rat glioma cells in suspension. Cell growth rates persistently increased over 7 days and the effects of different doses of colchicine (chemotherapeutic agent) was measured with fluorescence of PI.
Huang <i>et al.</i> (2011) ⁹⁷	A PDMS chip composed of a seeding chamber in continuation with inlet/outlet reservoirs connected via microchannels to a receiving chamber that mirrors the seeding chamber (see <i>figure 6a</i>). Able to characterise the initiation, expansion and retraction involved in BTSC and study the genetic phenotypes that promoted a migratory signature, with potential for gene targeting.
Gallego-Perez <i>et al.</i> (2012) ¹²⁴	Fabricated a tissue culture polystyrene platform with 5 μm wide microchannels to study the migratory behaviour of glioma cells as well as brain metastases from primary lung and colon cancer patients using time lapse microscopy at the single cell level. Glioma cells were observed to have the most unidirectional migratory behaviour as well as the lowest velocities.
Able <i>et al.</i> (2012) ²⁰³	A microfluidic device consisting of 'sink' and 'source' reservoirs connected by a microchannel was used to examine the effects of three growth factors: Hepatocyte Growth Factor, Platelet-Derived Growth Factor-BB and Transforming Growth Factor- α on the migratory behaviour of genetically modified mouse glial progenitor cells. Significantly, the group identified that counter to intuition, migration was enhanced by ultra-dilute concentrations of growth factors.
Wan <i>et al.</i> (2013) ¹⁹¹	Culture of glioma cells in a microfluidic device with inlets 20 μm that gradually tapered down along the channel to 5 μm at the distal end was used to study the effects of an EGFR blockage on glioma cell growth and migration using real time microscopy.
Wang <i>et al.</i> (2013) ¹⁹⁵	PDMS chip containing 5 microchannels for 5 distinct assay conditions, each with a corresponding inlet and outlet channel (see <i>figure 7a</i>). U87 cells were cultured in cell capture chambers and the effect of drug treatment, in this case Erlotinib (an EGFR inhibitor) on ¹⁸ F-FDG uptake was studied. Direct radio-assays of multiple cells within 30 mins of treatment with Erlotinib, showed significant decrease of ¹⁸ F-FDG uptake in the U87 cells using a B-particle imaging camera on the chip.
Wei <i>et al.</i> (2013) ²⁰⁰	Used an integrated microfluidic device that contained a single cell DNA bar code array, for highly efficient glioma cell capture and subsequent profiling of single cell proteomic assays (secreted and intracellular proteins). Were able to culture glioma cells in different pO ₂ and assess the effects on protein expression. Identified dysregulation and uninhibitable mammalian target of rapamycin (mTOR) levels near pO ₂ of 1.5%
Changa <i>et al.</i> (2014) ¹⁸⁵	Microfluidic platform incorporating modified 96 well plate that allowed maintenance of GBM xenograft from mice brain for 7 days. The device allowed for selective fluid delivery to the tissue slice at several predefined locations through a removable porous membrane resting on top of the micro-channels. Temozolomide (TMZ) was tested in the device on the GBM xenografts and through seven parallel fluid streams (containing 1mM of TMZ).
Pohlmann <i>et al.</i> (2015) ¹⁹⁸	Microchip used to study glioma cell interaction with nanoparticles. Instilled a cell suspension containing glioma stem cells into a silicon nitride microwell-integrated microchip that contained 10 μm diameter wells for capture of stem cells. Chip was coated with monoclonal antibodies against NOTCH 1 protein to capture glioma stem cells that express NOTCH1 protein and once trapped on the microchip, the interaction of the cells with gold nanoparticles was studied with electron microscopy.
Shin <i>et al.</i> (2015) ¹⁹⁶	Follow up study (of Wang <i>et al.</i> 2013) with modified design that permits single cell study of ¹⁸ F-FDG metabolism with a positron-sensitive photodiode detector. New chip design allows the trapping of individual cells and thus analysis of single cells over a 1 h time period.
Liu <i>et al.</i> (2015) ¹⁹³	Created a MF device for cell trapping; by using a gas activated pneumatic microstructure that turned flat posts into 3 dimensional posts that could seed U251 human glioma cells into their MF device, trap the cells long enough to spheroid formation and then release the cells for collection/analysis. The effects of treatment with Vincristine and Bleomycin was revealed as a dose dependent increment in the number of dead cells with PI staining.
Shao <i>et al.</i> (2015) ¹⁹⁹	Integrated immunomagnetic exosomal RNA platform composed of three units in one (see <i>figure 7c</i>): (1) chamber with magnetic microbeads with affinity ligands (to EGFRvIII) that enrich exosomes; (2)

	chamber containing glass bead filters that adsorb RNA from exosomes with collected RNA eluted and reverse transcribed in PCR chamber; (3) PCR analysis of tumour exosomes from blood were enriched. Quick (~ 2 h) blood screen for RNA of molecular markers of drug resistance such as MGMT.
Pedron et al. (2015) ¹⁸⁷	Utilised a microfluidic diffusive mixer with staggered herringbone features to manipulate the gradients of U87 glioma cells, gelatin and hyaluronic acid so as to produce hydrogels with a steady gradient of the 3 components of the tumour microenvironment. Once the gradients were formed and established, the group were able to study the effects of spatial and temporal heterogeneity in matrix, cell and biomolecular content on tumour development.
Aibaidula et al. (2015) ²⁰¹	Integrated device that contained a lysis chamber where tumour particles were lysed to release proteins of interest (IDH1) into solution, and an immune chamber, containing microspheres immobilised with anti-IDH1 antibody. 5 mg of tumour samples were inserted into the device for IDH immune analysis. On chip staining of IDH1 mutation with Anti-IDH Antibody and FITC of GBM samples within 30 minutes of tumour sampling.
Pang et al. (2016) ¹⁹⁴	Integrated device composed of fluidic channels with pores within filter units ('H' shaped microstructures) for the capture of single cells (see <i>figure 7e</i>). The filter units decreased in width by 2 µm, to capture different sized cells. Device allowed single cell (U251 GBM cells) capture and then reagent infusion, including media mixed with concentrations of Vincristine; used to distinguish between normal (smaller) and induced cells (larger). As such, device could differentiate cells according to size and deformability translated to difference in resistance to Vincristine – induced (larger) cells showing greater resistance.
Mongersun et al. (2016) ²⁰⁴	Developed a droplet based microfluidic device for the encapsulation of single U87 glioma cells and subsequent quantification of lactate released from individual cells by measuring the fluorescence of the end-product of a lactate enzyme reaction.
Fan et al. (2016) ¹⁹⁷	A chip consisting of four reservoirs (3 inlet and one outlet) with a Christmas tree shaped channel that decreased gradually from 300 µm to 100 µm sprouting a culture array that had 24 culture chambers (micro-wells) that drained to the outlet chamber. Capture and culture of 3D spheroids of GBM cells (U87) in the micro-wells with development observed on microscopy and fluorescence. Able to screen the effect of two drugs Ironetecan and Pitavastatin on GBM cells. Created simple, cost effective MF device for high through-put drug screening of U87 cells.
Logun et al. (2016) ⁹⁸	A device made of three microfluidic channels with trapezoidal barriers between channels. Each channel was 10 mm in length and 1000 µm in width. 300 µm trapezoidal barriers lined the junctions where two channels met with 100 µm spaces between barriers. Able to study the effects of different extracellular matrix models on glioma cell (U87) migration by infusing cells into a central channel, either side of different ECM-like hydrogel channels. Found U87 cells had a preferential affinity to sulfate rich environments when compared to hydrogel matrices.
Han et al. (2016) ²⁰⁵	The group designed a chip containing an array of 488 hexagonal microchambers with microslits in the peripheral chambers that allowed drug and nutrient flow. Cultured U87 cells loaded into the device were treated with a range of Doxorubicin concentrations, resulting in an initial decrease in the number of cells at day 3-5, only to repopulate at day 7. The group maintained that this was evidence of drug resistance of the cells and confirmed this by showing up-regulation of genes involved in relevant to the established mechanism of Doxorubicin action.
Gu et al. (2017) ²⁰⁶	Studied the migration of glioma cells and microglia cultured at opposite culture chambers connected by migration channels to better understand the relationship between both cell types in glioma development and invasion. Discovered that migration was greater when both cells were cultured together as opposed to when only one cell type was cultured, suggestive that there was some chemoattraction between the cells. By changing concentrations of the different cells, could mimic, the early stages of glioma development (high glioma; low microglia concentration) where it was noted that microglia contributed to glioma invasion.
Ayuso et al. (2017) ¹⁸⁸	A micro-device with a central micro-chamber for GBM cells (U-251) embedded within a hydrogel and allowing three-dimensional migration. On both sides of the micro-chamber, lateral microchannels filled with culture media allowed diffusion into the micro-chamber. Flow through one of the lateral microchannels was obstructed by media with 1% spheres suspension, creating a nutrient gradient away from the obstructed channel (see <i>figure 7d</i>). By controlling media flow through the lateral microchannels, could mimic GBM-associated thrombotic pathophysiological conditions. Able to use fluorescent labelled Ki67 to prove hypothesis that once pseudopalisading is formed GBM cells change from migratory state to proliferative state.

Table 1.2: Glioma and Microfluidics

A summary of studies in which microfluidic devices were significant in the methodology utilised to study glioma cells/tumours (over the last 10 years). A Pub Med database search using the criteria “glioma” OR “glioblastoma” AND “microfluidics” was screened for relevant studies. Papers (from 2001-2017) which fulfilled the search criteria were included.

1.2.6 Human GBM Tissue Culture

Though there are no examples of GBM tissue cultivated within a microfluidic device, a few researchers have attempted to maintain human GBM (*hGBM*) tissue within static cultures for various periods of time; In 1971, Holmström and Saksela maintained 35 brain tumours, including GBMs by dissecting small pieces of tumours from operated patients and cultivating them on a matrix of human fibrin foam in a culture media.²⁰⁷ They found that using histological appearances as a marker of viability, the viability decreased from 85 % at 3 days to 70 % at 14 days. Rubenstein *et al.* maintained cultures of *hGBM* tissue from five patients, with tumours ‘grown’ in small plastic Falcon culture dishes on top of a small piece of gelatin sponge foam rested on a steel grid within the central well of a culture dish.²⁰⁸ The tissue was maintained within an open system, with the tissue exposed on its surface to an atmosphere of 3 - 4 % CO₂, 96 % Oxygen and exposed to nutrient media diffused in from the gel foam, changed twice weekly. Using this method, the GBM explants were successfully maintained for 21-75 days as observed with histological examination. Although the tissue remained viable, there was a change in the pattern of the tissue architecture with flattening of the tissue as seen with organotypic cultures and though mitotic figures and occasional giant cells were present, the explants did not exhibit focal necrosis, pseudopalisading or vascular endothelial proliferation that are characteristic of GBM *in vivo*. The group found the tumour explants invaded the spaces within the gel foam but most of this invasion was in the form of tissue outgrowths of the explants where fibroblasts mixed with anaplastic tumour cells developed beyond the original tissue margins. Another publication from the same group looked at the electron microscopy appearance of the cells cultured and found that the cells cultured differentiated to highly fibrillary astrocytes.²⁰⁹ A few years later the same group, published their findings on tissue growth using autoradiography to determine the growth fraction of the tissues and found using pulse-labelling that as well as tissue maintenance, of the viable tumour, there was also continued DNA synthesis.²⁰⁹

With tissue culture techniques established, Saez *et al.* used the same culture techniques adopted by Rubenstein to culture GBMs, using their tumours as an analogue of the *in vitro* tumour for chemotherapeutic trials in culture.²¹⁰ Cultured

GBMs exposed to 4 days of drug treatment were monitored for microscopic changes, while measuring the extent of cell damage by measuring the levels of reduced NADH. Results showed 7 out of 10 GBMs remained viable for at least 11 days and cytotoxic assays showed a significant increase in reduced NADH in samples treated with a number of drugs including cyanide and luciferase, compared to samples untreated. Yuki *et al.* followed up this work by maintaining *h*GBM tissue and mouse xenografts of 2 x 2 x 1 mm on specialised collagen gel matrices derived from pig skins and tested the response of the tissues to a variety of chemotherapeutic agents.²¹¹ They found drug concentration correlated with inhibition of growth as measured by incorporation of tritiated thymidine.

Despite these pioneering works in the 1970s and 80s, through the next two decades, there was little progress in the field until 2007, when Ono *et al.* repeated the works of Yuki *et al* by culturing 26 GBM patient tumours on collagen matrices and performed further chemotherapy sensitivity assays, measuring drug inhibitory rates with 3-[4,5-dimethylthiazol-2-yl]-2,5-diphenyl-tetrazolium bromide (MTT) assay.²¹² They matched the response of the tumours to the drugs *ex vivo* to the survival of patients who were given the same drugs only to find that there was not a significant correlation in tumour inhibitory rate of the drug *ex vivo* and patient survival, despite being given the same drugs. In 2013, a group cultured slices of GBM explants in 6-well plates and observed the long term culture of 350 μm thick GBM tissues for up to 4 weeks and showed that the tissues maintained normal tissue architecture as compared to control samples obtained fresh from the patient and they were also able to test the tissue response to 50 μM – 200 μM of TMZ, showing a significant increase in PI positive cells in samples treated with TMZ compared to control.²¹³ There was also a significant increase in apoptosis, based on caspase 3 immunohistochemistry (IHC), in tissues that were treated with both TMZ and X-Ray irradiation.

Recently, *h*GBM tissue has been maintained *ex vivo* to study the effects of Tumour Growth Factor β inhibitors on sensitising tumours to radiation.²¹⁴ This and all the other studies in which *h*GBM tissue has been maintained in a viable state has been summarised in *Table 1.3* and they provide insight into what can be achieved with tissue explants of *h*GBM and their suitability for pre-clinical drug screening.

Study	Culture	Method	Viability/Results
<i>Growth of Human Brain Tumour Explants in Matrix Cultures in Different Human Sera (1971)</i>	Cultured benign and malignant tumours including 10 Gliomas.	Cultured on matrix of human fibrin foam on a petri dish. Compared autologous human serum to 'pooled' random human serum as media.	Maintained for 3, 7, 11 and 14 Days. Histological analysis showed better tissue maintenance with autologous sera
<i>In Vitro Characteristics of Human Glioblastomas Maintained in Organ Culture Systems (1973)</i>	Obtained small fragments from 5 GBM patients for organotypic culture	Compared cultures maintained on gelatin foam within a culture dish with cultures maintained on a small Millipore filter.	Maintained for up to 75 days. Initial morphology similar to primary tumour followed by fibrillary differentiation
<i>Chemotherapeutic Trials on Human Malignant Astrocytomas in Organ Culture (1977)</i>	Obtained samples from 8 GBM samples	GBM samples on a pledget of gelatin sponge rested on a platform at the surface of the media.	7 out of 3 GBM cultures were viable over 11- 42 days. Cytotoxic drug effects noted with Cyanide and Luciferase.
<i>The Kinetics of Human Glioblastoma Maintained in an Organ Culture System (1983)</i>	Obtained small fragments from 7 GBM patients for organotypic culture	Tumour specimens placed on a cube of gelatin foam that had been previously moistened with media. Media changed every 2 days.	Cultures for 29 days. Pulse labelling experiments confirmed growth fractions similar to <i>in vivo</i> tumours
<i>In Vitro Chemosensitivity Test of Human Brain Tumours using a Three-Dimensional Organ Culture with a Collagen Gel Matrix (1994)</i>	16 tumour specimens from 14 patients. 5 of the patients were GBM	GBM tumour specimens placed on a specialised collagen gel matrix from pig skin. Media changed after 7 days of culture	Tumours cultured for 14 days and showed tumour cell invasion of the gel matrix
<i>Collagen Gel Matrix Assay as an In Vitro Chemosensitivity Test for Malignant Astrocytic Tumours (2007)</i>	26 Glioblastoma patients (24 Astrocytomas)	Tumour samples cut were placed on a collagen gel matrix in six-well tissue culture plates.	Growth inhibition between 23 - 42 % with varied drugs including cisplatin, carboplatin and Etoposide using MTT assay and compared effectiveness of drugs <i>in vitro</i> with patient survival.
<i>Organotypic Explant Culture of Glioblastoma Multiforme and Subsequent Single-Cell Suspension (2011)</i>	Describes Protocol for GBM tissue culture	Places GBM explants (2 mm ²) into millicell inserts wet with 50 µl of fibronectin. Media replenished every 2 days.	Cultures kept for up to 3 weeks with Ki67 index comparable with original tumours (18.5 % and 16.7 %)
<i>Organotypic slice cultures of human glioblastoma reveal different susceptibilities to treatments (2013)</i>	12 GBM patient samples maintained in culture	350 µm thick GBM samples were cut with a vibratome and then maintained on a Millipore placed within 6-well plates. Able to test effects of TMZ and X-Ray radiation.	Maintained morphology on H&E stains for two weeks. Reduction in proliferation index on samples treated with TMZ and Radiation over 24 h.
<i>Patient-Specific Screening Using High-Grade Glioma Explants to Determine Potential Radiosensitization by a TGF-β Small Molecule Inhibitor (2016)</i>	7 GBM samples (6 newly diagnosed and 1 recurrent).	Samples cultured on laminin-coated filters in the upper chambers of Transwell inserts. Cultures flattened after 4 days.	Used a Tumour Growth Factor β inhibitor as a radiosensitiser to improve radiation induced death in 5 of the 7 GBM samples.

Table 1.3: Cultured Human GBM Tissue

Table summarising studies in which hGBM tissue have been maintained or cultured *ex vivo*. A Pub Med database search using the criteria “glioma” OR “glioblastoma” AND “tissue culture” OR “*ex vivo* tissue”, was screened for relevant studies. All relevant papers from 1970 to the present were included.

1.3 Study Aims

Microfluidic devices have been used to explore a wide range of biological processes, from embryological machinations to intricate cellular mechanisms. Devices have been created that mimic complex organs or facilitate molecular tests. There is however a paucity of research evidence incorporating *h*GBM tissue into a microfluidic device for viability testing. The aim of the current research project is to establish a microfluidic tissue culture paradigm for the maintenance of human glioblastoma tissue biopsies. Glioblastoma continues to elude current therapies, and this is in part to do with genetic and epigenetic markers specific to the individual that results in molecular heterogeneity. Treatment of these tumours require a personalised approach that addresses the specific molecules of tumorigenesis in each individual. Currently, although some models exist²¹⁵, there is not a realistic or cost-effective way to examine tumour heterogeneity on a case by case basis. The aim is to translate the principles established by the research group in the University of Hull in microfluidic tissue maintenance in liver, colorectal cancer and head and neck tumours into effective GBM management.

Main Objectives:

- The study aims to compare the viability of fresh GBM tissue biopsied with that of tissue maintained within the microfluidic device for 3 days and analyse what factors promote or hinder tissue maintenance on chip, including:
 - Length of tissue maintenance
 - Optimal nutrient media used to perfuse the tissue
 - Rate of nutrient flow
 - The effect tissue flow has on tissue maintenance by comparing tissue maintained in systems with and without nutrient flow.
 - Non-perfusion time i.e. the time it takes from biopsy in theatre, to perfusing on the MF device.
 - The chip design, including adaptations to the device.

- Understand what drugs can be studied within the microfluidic device, exploring options such as chemotherapy and radiotherapy as well as experimental drugs.
- Correlate the results of the *ex vivo* GBM experiments with patient outcome data, in particular survival and assess how comparable GBM behaviour on chip is to *in vivo* GBM.
- Assess the effect of patient factors, as well as known tumour characteristics, such as histological diagnosis, IDH 1 status and MGMT methylation have on tumour behaviour on chip.

The study design and framework are intended to explore the aspiration of a personalised treatment standard that incorporates patient tumour biology into the treatment decision algorithm. Current GBM treatment starts with maximal safe resection and there is on average, 6 weeks between surgical resection and adjuvant therapy.²¹⁶ There is a potential to use this “lag” time to study the individual characteristics of a tumour biopsy in MF device and to tailor the adjuvant therapy based on biological testing. More enticing is the possibility of a new pre-clinical drug model for the investigation of novel therapies to treat GBM. This pilot study aims to explore the feasibility of the ‘lab on chip’ model being utilised in GBM research and treatment.

2.1 Materials

2.1.1 Materials, Reagents and Equipment

Material	Supplier
2.1.1.1 Microfluidic Device	
Araldite 2-Part Epoxy Adhesive	B&Q, UK
Schott B270 Glass (x 2)	H.V. Skan, UK
BD Plastipak 3-Part Luer Slip Syringes (20ml)	Becton Dickinson (BD) Biosciences, USA
Cell Strainer (40 µm and 100 µm Pore Size)	VWR, UK
Ethylene Tetrafluoroethylene (ETFE) tubing	IDEX, Germany
Ferrules Graphitised Vespel Ferrule for 1/16" Fitting	Kinesis, UK
HiQA Coverslips No 1.5 22x50mm	CellPath, UK
Polyether Ether Ketone (PEEK) Microport and Microport Adaptor	Anachem, UK
Polydimethylsiloxane (PDMS)	Dow Corning, UK
Polytetrafluoroethylene (PTFE)	B&Q, UK
2.1.1.2 Reagents	
Annexin V-FITC Apoptosis Detection Kit	Sigma-Aldrich, UK
Bovine Serum Albumin	Thermo Fisher Scientific, UK
Carbogen (95% Oxygen, 5% Carbon Dioxide)	Brin's Oxygen Company (BOC), UK
Collagenase (type IV; 356µl stock solution)	Sigma-Aldrich
Cytotoxicity LDH Kit ^{PLUS}	Sigma-Aldrich
DNase (type 1; 300µl stock solution)	Sigma-Aldrich
Foetal Bovine Serum (FBS)	Labtech Int., UK

Lonza Dulbecco's Modified Eagle Serum (4.5 Glucose with L-Glutamine 500ml)	Lonza, Switzerland
Lonza HEPES Buffered Saline Solution	Lonza
Lonza Penicillin-Streptomycin (10:10UI/ml)	Lonza
Lonza Sodium Pyruvate	Lonza
L-Lactate Dehydrogenase (L-LDH)	Sigma-Aldrich
Trypan Blue (0.4% w/v)	Sigma-Aldrich

2.1.1.3 Histology/Immunohistochemistry

4% (w/v) Paraformaldehyde	Sigma-Aldrich
100% Ethanol	VWR
Eosin Y	Thermo Fisher Scientific
Mayer's Haematoxylin	Surgipath Medical Industries, USA
Leica Bond Polymer Refine DAB Detection Kit	Leica, Germany
Leica Epitope Retrieval 1 Solution	Leica
Leica Epitope Retrieval 2 Solution	Leica
2-Methylbutane	Sigma-Aldrich
Polysine Microscope Slides	Thermo Fisher Scientific
Xylene	Thermo Fisher Scientific

Antibodies

Mouse clone MIB1 (M7240)	Dako, USA
Rabbit polyclonal D175 (#9961)	Cell Signaling Technology, USA

2.1.1.4 Drugs

Doxorubicin (DOX)	Sigma-Aldrich
ExoPr0	ReNeuron, UK
Irinotecan Hydrochloride (IRT)	Sigma-Aldrich
Temozolomide (TMZ)	Sigma-Aldrich

2.1.1.5 Equipment

BD FACSCalibur	BD
ClearVue Coverslipper	Thermo Fisher Scientific
Eclipse 80i Digital Microscope	Nikon, Japan
EG 1160 Paraffin Wax Embedder	Leica, Germany
Harvard PhD 2000 Syringe Pump	Harvard, UK
Infinity 3 Lumenera Microscope Camera	Roper Technologies, USA
Leica Autostainer XL (Automated Slide Stainer)	Leica
Leica Bond III Automated Immunostaining Platform	Leica
LSM710 Fluorescent Microscope	Zeiss, Germany
Multichannel Oxygen Sensor Probe	PreSens, Germany
Shandon Finesse 325 Microtome	Thermo Fisher Scientific
Synergy HT Plate Reader	BioTek, USA

2.1.1.6 Solutions

Preparations of Solutions

Annexin V/Propidium Iodide Buffer Solution	1 ml of Buffer Solution (containing HEPES buffer) mixed with 9 ml of Distilled Water
Disaggregation Solution	15 mL of DMEM media + 0.02% (w/v) collagenase (type IV; 356µl stock solution) and 0.02% (w/v) DNase (type1; 300µl stock solution).

Histological Reagents

0.5 % (v/v) Acid Alcohol	0.5 ml of hydrochloric acid is added to 99 ml of 70% alcohol
1% (w/v) Eosin	1 g of Eosin per 100 ml of alcohol
5 % Sodium Bicarbonate	5 g of Sodium Bicarbonate dissolved in 100 ml of ddH ₂ O

LDH Reagents

1% (w/v) Bovine Serum Albumin (BSA)	0.1 g of Bovine Serum Albumin (BSA) in 10 ml PBS
LDH Control (1 U/ml)	Mix 2 µl of L-Lactate Dehydrogenase with 5.5 ml of 1% BSA
Phosphate Buffered Saline (PBS)	2 tablets of PBS added to 1 L of distilled water
Reaction Mixture (LDH Analysis)	Mix 125 µl of Catalyst with 5.625 ml of Reaction dye

2.2 Methods

2.2.1 Fabrication and Assembling the Chip

The microfluidic device used in this study has previously been described by the group in Hull.^{179,217} It was fabricated using standard photolithography and wet etching techniques. In brief, a photomask containing the layout of the microchannel network is developed by photo-reduction of a laser printed drawing, with a computer-assisted design package - AutoCAD[®] LT software (*Autodesk Ltd., UK*). The photomask is aligned onto a 30 mm x 30 mm crown white glass, pre-coated with photoresist. The pre-coated glass, left in contact with the photomask is exposed to UV radiation for just over a minute, creating the desired photoresist pattern and allowing further development and etching in 1% (v/v) hydrofluoric acid at 65° C in a heated ultrasonic bath. The etched glass chip is then cleaned and thermally bonded with a corresponding top or bottom layer at 600° C for 3 hours. The completed device consisting of the two glass plates bonded together is represented in the diagrams in *Figure 2.1*. The whole device is 30 x 30 x 4 mm and consists of a thick top layer (3 mm) in which access holes and a central chamber (diameter 3 mm), analogous to the bottom layer are drilled. The thinner bottom (1 mm) layer has a channel network with microchannels 190 µm in width and 70 µm in depth, which diverge into three exit micro-channels.

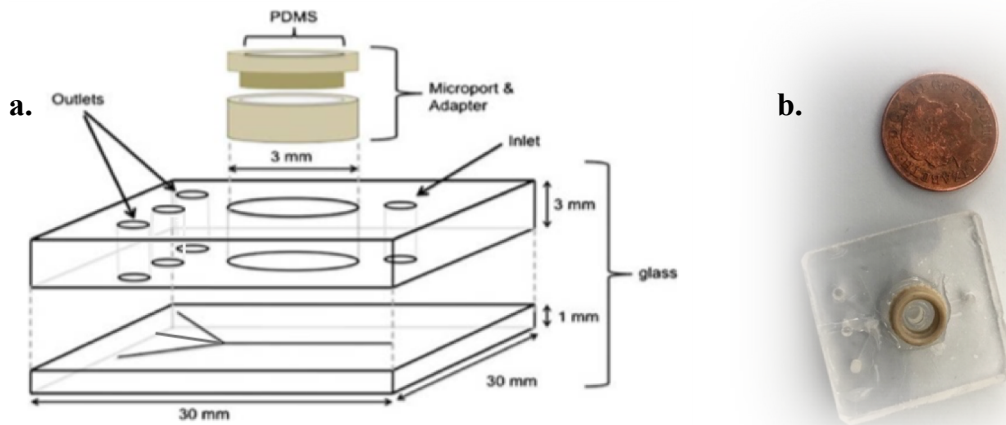


Figure 2.1: The basic units of the Microfluidic Device

a. Inlet and outlet (access) channels as well as a central channel were drilled into the top glass layer. Channel networks were etched into the bottom layer, producing channels 190 μm in width and 70 μm in depth. The tissue chamber was sealed with a microport and PDMS filled adaptor. The tissue chamber has a volume of approximately 20 μL . Adapted from Hattersley et al.²¹⁸ **b.** Pictures of the chip. Note: Two outlet holes glued with glass coverslip.

This basic unit required further modifications, prior to tissue analysis. First, a circular mesh cut out of a 100 μm pore size cell strainer (*VWR*) with a diameter to match the tissue cavity (3 mm diameter) is secured into the bottom of the tissue cavity chamber, forming a semipermeable barrier between the microchannels and the tissue cavity. A PEEK microport (*Anachem*) is sealed with epoxy to the surface of the top glass layer such that the circular tissue cavity could be enclosed using an English-threaded adapter (*Anachem*). The adapter contains a hollow central portion which is filled with PDMS (*Dow Corning*) to allow gaseous exchange into the tissue compartment. The fabricated device microchip is finalised by connecting 0.8 mm (internal diameter) by 1.58 mm (external diameter) Ethylene Tetrafluoroethylene (ETFE) Teflon[®] tubing (*Anachem*) to the inlet and outlet channels with epoxy adhesive and a graphite ferrule. To ensure a watertight seal, the PDMS filled adapter was enveloped with a length of polytetrafluoroethylene (PTFE) (*B&Q*) tape to ensure an adequate watertight seal within the microport hub. For these experiments, only one inlet and one outlet channel was required to allow direct flow in and out of the chip (the other two outlet channels were sealed using a microscope glass coverslip

and epoxy glue). The completed device was sterilised within a sterilised with 70% (v/v) ethanol/distilled water flushed through the tubing and channels for 15 minutes at $10 \mu\text{l min}^{-1}$. At this instance, any leaks were identified and sealed. Once sterilised with alcohol, the device was irrigated for 30 minutes at a rate of $5 \mu\text{l min}^{-1}$ with the standard supplemented media and thus ready for tissue maintenance.²¹⁹

2.2.2 Tumour Samples

Case notes, clinical imaging and MDT outcome of potential participants admitted to the Hull Royal Infirmary (Hull and East Yorkshire NHS Trust) were reviewed to identify cases where a GBM tumour was suspected. In particular, patients with a ring-enhancing intracranial mass on magnetic resonance imaging (MRI), without evidence of systemic disease on a Computed Tomography (CT) scan were approached to be included in the study. Prior to surgery, informed consent was obtained, once participants had read the patient information sheet and any questions raised had been answered. All patients included in the study gave written permission to allow a sample of tissue from their resected tumour or a sample from surplus tissue during diagnostic biopsy, to be utilised in microfluidic studies. This was under the remit of Local Research Ethics Committee and NHS Trust R&D approval (IRAS Project ID: 196595). Consent was obtained either on the day of surgery or the day before and usually, the patient was reviewed prior to their operation to ensure they were happy to proceed. Copies of the patient information sheets and consent forms are available in the Appendix.

Inclusion criteria

Patients > 18 undergoing a diagnostic procedure or planned tumour resection where a sample of brain tumour tissue is expected to be taken by the surgeon; the principal diagnosis is suspected to be one of GBM.

Exclusion criteria

Participants lacking capacity to give informed consent.

2.2.3 Experimental Set Up

2.2.3.1 Culture Medium

The completed standard media was composed of Dulbecco's Modified Eagle Medium (DMEM), fortified with 4.5 g/L of glucose supplemented with 10 % (v/v) heat inactivated Foetal Bovine Serum (FBS), as well as a penicillin (0.1 U/ml)/streptomycin (0.1g/ml) mixture. In addition, the media contained a final concentration of 5 mM Sodium Pyruvate and 25 mM HEPES were added.

The efficacy of the standard media at maintaining the GBM tissue was compared to two alternative culture media. The first, exosome depleted media, was supplemented with *exosome-depleted* FBS (10 % (v/v)) as opposed to standard FBS; with all other supplementations identical to the standard media.

The second alternative media was an artificial cerebrospinal fluid (aCSF) solution which was composed of final concentrations of 119 mM NaCl, 26.2 mM NaHCO₃, 2.5 mM KCl, 1 mM NaH₂PO₄ and 1.3 mM MgCl₂ diluted in 1L of ddH₂O, supplemented with 10 mM of glucose and insufflated with 5% CO₂/95% O₂ for 10–15 min. The solution was completed with the addition of 2.5 mM of CaCl₂.²²⁰

2.2.3.2 Tissue Maintenance

Microfluidic devices were assembled and tested for leaks 1-5 days in advance, so as to ensure their availability on the day of surgery. At operation, during tumour resection and once appropriate specimens had been collected for histological assessment, the most cellular portion (i.e. avoiding necrotic tissue) was acquired (either under direct vision with a microscope or with the aid of neuro-navigation and a biopsy needle) and immediately placed in a 50ml polypropylene tube containing the maintenance media. The sample was transferred in a safety box directly to the laboratory (approximately 20 minutes away from the hospital). Within a sterilised Class II Biological safety cabinet, samples were sectioned into 10-15 mg slices. Sections were placed into the central chamber of the microfluidic device and sealed

with the microport adaptor. The tumour containing chip was connected to a 20 ml 3-Part Luer Slip Syringe (*BD*) containing the appropriate media.

The assembled device was attached to a calibrated PhD 2000 Syringe Pump (*Harvard*) within a Perspex box with a thermostat regulated temperature of 37° C. Media was infused into the chip and tissue at a rate of 4 $\mu\text{L min}^{-1}$ (a picture of the set-up is detailed in *Figure 2.2*). In conjunction with tissue maintained within the microfluidic device, a piece of fresh GBM tissue was prepared for histology and immunochemistry, enzyme assays, and tissue disaggregation, in preparation for flow cytometry studies.

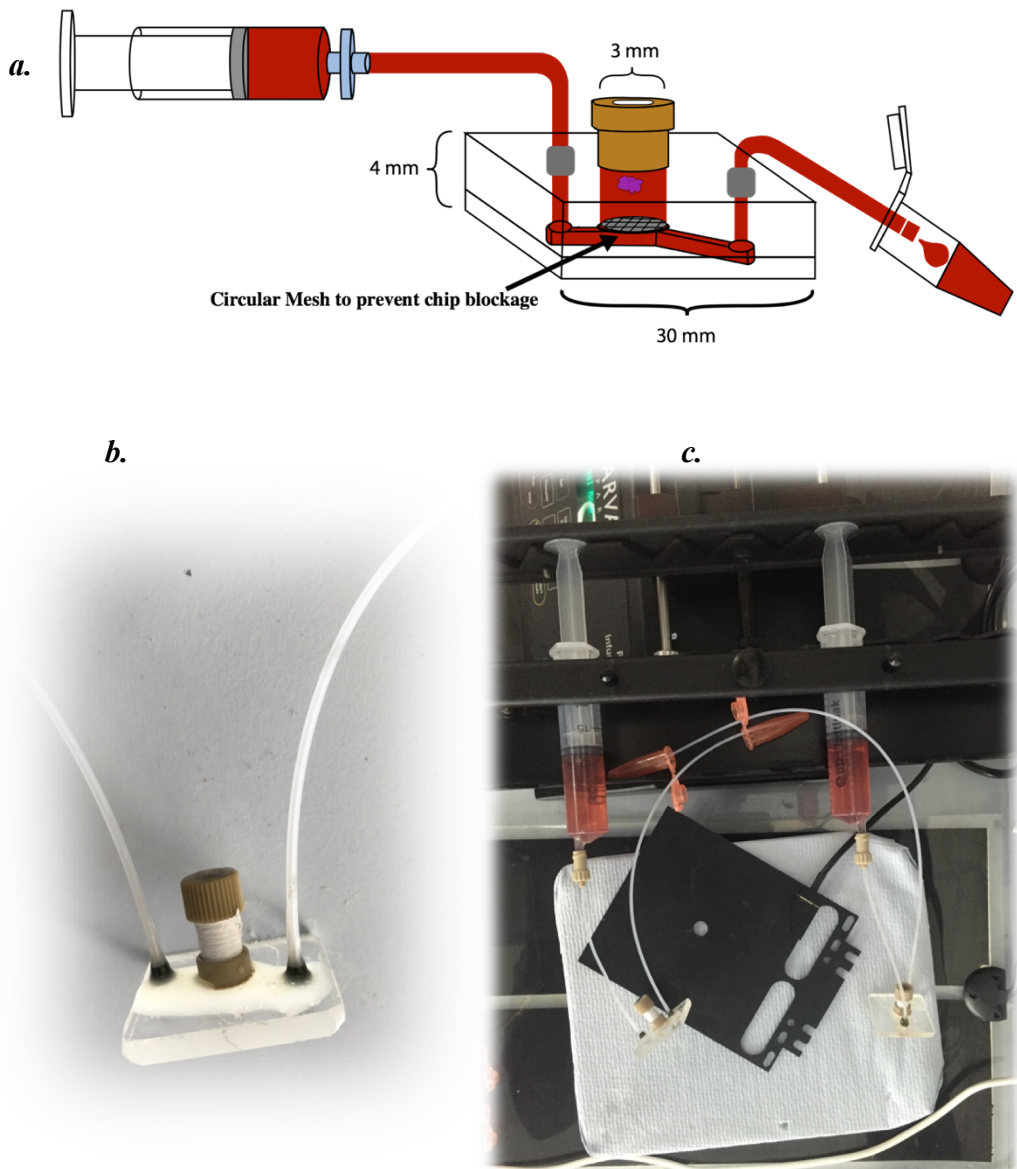


Figure 2.2: Experimental Set-Up

a. Schematic of microfluidic set up (Adapted from Dawson et al.⁷⁶). *b.* A picture of the assembled microfluidic chip and *c.* The device with GBM tissue, connected to syringes and syringe pump.

2.2.3.3 Protocol

The standard protocol involved infusing the tissue continuously for 72 h. Effluent samples were collected every 2 h (into a 1.5ml polypropylene tube) during the day and the overnight samples were collected over a range of 12-18 h; collected effluent samples were stored at 4° C for subsequent analysis. Interruption of infusions was

occasionally necessary to change media, add drugs or lysis solution. Infusions were stopped after 72 h and tissue samples were removed from the device for post-chip analyses. Used chips were disassembled, sterilised in 70 % (v/v) alcohol/distilled water overnight, autoclaved at 126° C and 1.4 Bar for 22 mins (and stripped of any excess glue). The glass components were placed in a furnace at 500° C for 2 hours prior to repeat use.

2.2.3.4 Static Tissue

A number of tissue samples were also studied in parallel to the tissue on chip; with tissue maintained for the same time period in an Eppendorf containing media. In these experiments, the weighted tissue was prepared in the same manner as the 'chip tissue' within a sterilised Class II Biological safety cabinet; sectioned into 10-15 mg slices and then sections were placed into a 1.5 ml or 15 ml Eppendorf with a specific volume of media and then housed in the same Perspex Box as the microfluidic tissue. The amount of media used to maintain the tissue was based on the microfluidic experiments and to ensure tissues were exposed to the same amount of media, the tissue was allowed to sit in 480 µl of media. The media was changed every 2 h; collected and stored at the same time, the microfluidic effluent was collected. Overnight, samples were maintained within media for longer periods of time and with this, were sat overnight within larger volumes of media, more specifically, 3.36 ml of media (to match the same amount of media that was flowed through the microfluidic tissue over 8 h – 4 µl per hour for 14 h). At the end of the 72 h period, the tissue was removed from the media solution and analysed in the same manner as the microfluidic tissue were. Similarly, the collected media samples were analysed for LDH levels as described in 2.2.4.3.

2.2.4 Post Chip Analysis

Samples removed from the microfluidic device underwent a number of different analyses: 1) they were placed in 1.5 ml of 4% paraformaldehyde for histological preparation; 2) were maintained in a lysis solution for 24 h to assess the amount of LDH retained within the tissue and 3) were disaggregated with a tissue disaggregation solution to allow single cell analysis with flow cytometry. The

effluent samples collected during the experiment were analysed using an LDH assay to estimate cell death.

2.2.4.1 Histological Preparations

A standard operating protocol for histological preparations was utilised with modifications as directed by the histological department at Hull Royal Infirmary.²²⁰ Samples for histological analysis were treated with 4% (w/v) paraformaldehyde for at least 18 h to allow penetration through the entire tissue. After this, samples were dehydrated in increasing concentrations of alcohol: 1 h in 70% (v/v ethanol/distilled water) alcohol, followed by an hour each in 80%, 90%, 100% alcohol and then 50% (v/v) pure alcohol/Histoclear solution. The sample was then left in 100% Histoclear for 24 h and subsequently immersed in liquid wax for 2 h (the wax is changed once after an hour) and then allowed to set within wax in a histology tissue cassette in an EG 1160 Paraffin wax embedder (*Leica, Germany*). Cassettes were placed on the Shandon Finesse 325 Microtome (*Thermo, USA*) and 5 µm thick sections were cut and allowed to dry on polylysine microscope slides.

Haematoxylin and Eosin

Haematoxylin & Eosin (H&E) is one of the most essential staining techniques used in the histological analysis of tissue sections.^{221,222} As the name suggests, it works on the basis of two primary dyes – Haematoxylin and Eosin. Haematoxylin is a basophilic dye; a product of a complex formed between aluminium ions and haematin. The aluminium in this case, holds the acidic properties and acts as a mordant, affixing the haematin as it binds to negatively charged substances within the cell, such as DNA and RNA. As a result, the haematin/aluminium complexes bind and stain nucleic acids. This is usually a dark blue/purple stain and usually represents the nuclei of a cell. Eosin is an acidophilic dye and it binds to positively charged amino acids, present on most proteins within the cytoplasm of cells.²²³ As such, the pink stain of eosin, usually represents the cytoplasmic contents of a cell. The combination of both dyes in a tissue specimen allows characterisation and interpretations of cellular and tissue architecture.

H&E staining was performed by University College London's Advanced Diagnostics Laboratory using the Leica Autostainer XL (*Leica, Germany*) automated staining platform. Briefly, slides were dewaxed in the oven at 60° C for 5 min. They then had 2 washes in Xylene (each for 2 min), followed by rehydration with immersion in a series of graded alcohols (100% - 70%). After a 2 min tap water wash, nuclei were stained in Mayer's Haematoxylin (*Surgipath Medical Industries, US*) for 6 min, differentiated in 1% acid alcohol for 2 sec and *blued* in tap water for 3 min and 30 sec. Cytoplasm counterstaining was performed with 1% aqueous Eosin (*Thermo Fisher, UK*) for 1 min and the slides were washed for 10 sec prior to dehydration in graded alcohols (95% - 100%). Dehydrated slides were finally rinsed in 2 changes of Xylene and mounted with a coverslip using ClearVue Mountant (*Thermo Fisher, UK*) with the ClearVue Automated Coverslipper (*Thermo Fisher, UK*).

Immunohistochemistry

IHC refers to the microscopic identification of specific antigens within tissues by staining with antibodies labelled with pigmented markers.²²⁴ The process involves exposure of tissue sections to a primary antibody specific for a protein epitope. The tissue is then treated with a secondary antibody which has a high specificity for the first antibody (the two antibodies are usually from different animal species). The secondary antibody is biotinylated, which means it is coupled with biotin (vitamin H). After washing away any unbound antibodies, the tissue is incubated with an avidin/horseradish peroxidase (HRP) complex. As biotin binds strongly to the four binding sites on each avidin molecule, this concentrates the HRP complexes to the site of the secondary antibody.^{225,226} Subsequently the presence of the antibodies, and thus the antigen, can be visualised by the action of HRP on the chromogen, 3,3' Diaminobenzidine (DAB), transforming the substrate into a brownish precipitate that is deposited in the tissue at the site of the reaction (*Figure 2.3*).

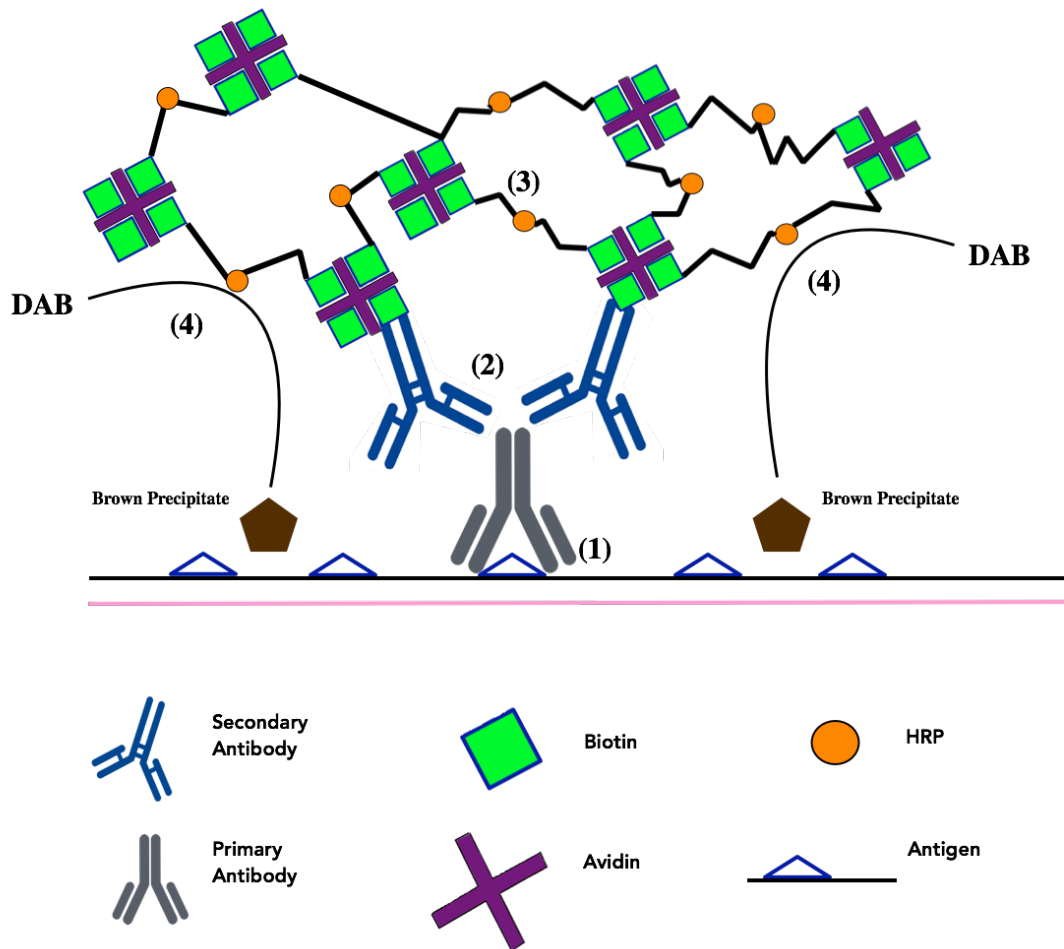


Figure 2.3: Principles of IHC

(1) Detection of an epitope by a primary antibody. (2) After the epitope-antibody binding event, a biotinylated secondary antibody binds the primary antibody with high specificity. (3) Avidin/Biotin/HRP Complex bound to secondary antibody. (4) A chemical substrate (DAB) is added which is reacted on by HRP to produce a coloured precipitate at the site of the whole epitope-antibody complex.

Within this study, the IHC was performed by University College London's Advanced Diagnostics Laboratory. Staining was performed, using the Leica Bond III automated immunostaining platform (*Leica, Germany*) in conjunction with the Leica Bond Polymer Refine DAB detection kit (*Leica, Germany*), as per the manufacturer's guidelines. This kit contains a peroxide block and protein blocking agents. Dewaxing, epitope retrieval and peroxide blocking steps are all performed in an automated manner.

The following primary antibodies were used:

MIB1: a monoclonal antibody directed against Ki67; a nuclear protein associated with cellular proliferation. Ki67 IHC involved on-board epitope retrieval for 20 minutes at 99° C using Leica Bond Epitope Retrieval 2 solution (*Leica, Germany*). Endogenous peroxidases were blocked with hydrogen peroxide (as per the kit) for 5 minutes at room temperature. The primary antibody **MIB1** M7240 (*Dako, USA*) was diluted 1/120 in Leica Bond Primary Antibody Diluent (*Leica, Germany*) and applied for 15 minutes at room temperature. Leica Bond rabbit anti-mouse post primary reagent was applied for 15 minutes at room temperature followed by Leica Bond anti-rabbit Polymer for 20 minutes. Leica Bond DAB was applied as for 10 minutes and 0.5% copper sulphate DAB enhancing solution was subsequently applied for 5 minutes. The final step involved applying a Haematoxylin counterstain for 30 seconds at room temperature.

ASP175: polyclonal antibodies against Cleaved Caspase 3; commonly considered a critical “executioner” of apoptosis. Caspase 3 IHC started with on-board dewax at 97 ° C and on-board epitope retrieval for 30 minutes at 99° C using Leica Bond Epitope Retrieval 1 solution (*Leica, Germany*). Endogenous peroxidases were blocked with hydrogen peroxide for 5 minutes and the primary antibody **ASP175** D175, #9961 (*Cell Signaling Technologies, USA*) was diluted 1/300 in Leica Bond Primary Antibody Diluent (*Leica, Germany*) and applied for 40 minutes at room temperature. Leica Bond anti-rabbit polymer was applied for 20 minutes, followed by Leica Bond DAB for 10 minutes. 0.5% copper sulphate DAB enhancing solution was applied for 5 minutes at room temperature and a Haematoxylin counterstain 30 seconds at room temperature finalised the process.

The IHC process was monitored with the use of positive and negative control samples. Positive controls included examine a tissue type that is known to expresses the protein of interest. In this instance, human tonsillar tissue was used as per manufacturer’s guidelines. The negative tissue control was based on a tissue that was processed as normal except for the exclusion of the primary antibody and is vital in identifying non-specific staining.

Once finalised, all H&E and IHC slides were viewed by the principal investigator using an Eclipse 80i microscope (*Nikon, Japan*) and digital images were acquired with an Infinity 3 Microscope Camera (*Roper Technologies, USA*) using Image Pro Premier Software (*Media Cybernetics, USA*). Digital images of the IHC slides were analysed using ImmunoRatio, a free web based application for automated image analysis of immunostained tissue sections.^{227–229} Proliferation and apoptotic indices were calculated as the number of positively stained cells divided by the total number of cells, multiplied by 100. For each slide, this was performed on a randomly chosen high-power field (400- fold magnification) image that contained positively stained cells.

Review of all histological and immunohistochemistry images was performed under the supervision of Dr. Robin Highley (Consultant Histopathologist, Hull & East Yorkshire NHS Trust).

2.2.4.2 Flow Cytometry

Flow Cytometry allows information on cell populations to be obtained by converting the light scattering and fluorescent properties of cells into electronic impulses that can be processed by a computer. This is achieved by a fluidic system that presents cells sequentially to an argon laser beam (488 nm) for interrogation; the laser causes temporary excitation of the cells and subsequent emission of a characteristic wavelength of light.²³⁰ Each cell's distinct signature is registered within the cytometer as the light 'scattered' is dependent on the cell size (Forward-scattered light – FSC), granularity or internal complexity (side-scattered light – SSC) and the fluorescent nature of the cell. Mirrors and optical splitters route specific emissions from the cells to photomultiplier tubes (PMT) that detect specific ranges of light. For example, the PMT that detects Fluorescein Isothiocyanate (FITC) only detects light within the range of 515 nm to 545 nm. All of this feed to an electronic system that converts the light impulses into data, processed by a computer (*see Figure 2.4*).

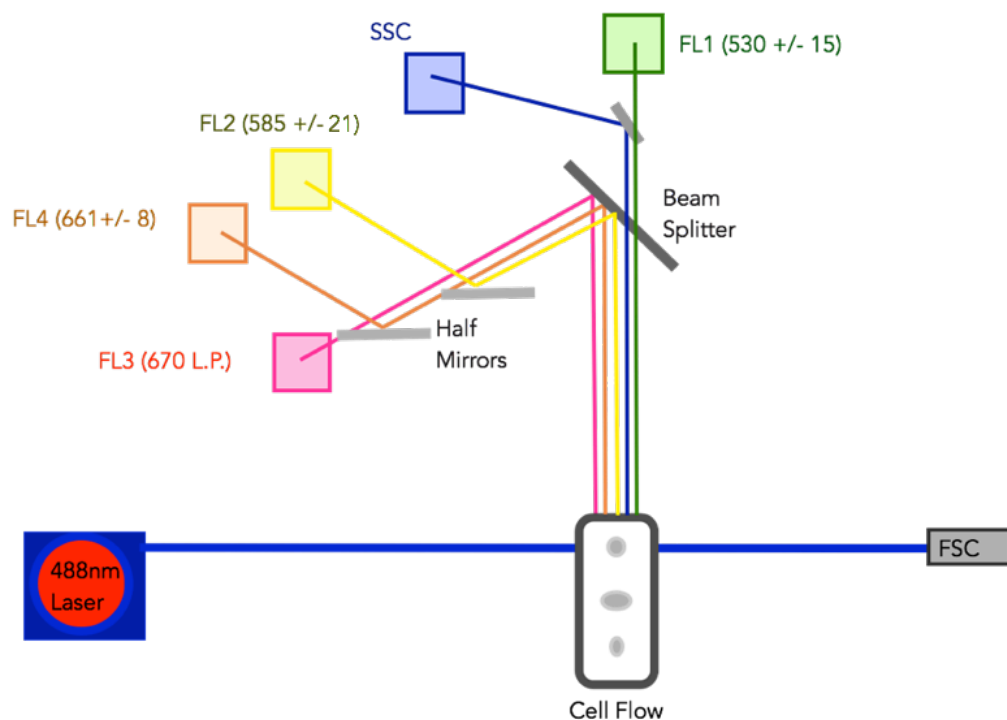


Figure 2.4: The workings of a Flow Cytometer.

Cells with varied cell size, granularity and fluorescent properties are illuminated with a laser and the light emitted by each cell is recorded by PMTs (coloured boxes) which convert the light signal into a specific electrical impulse that allows cell stratification of the cell population.

Annexin V and Propidium Iodide

The Annexin V-Fluorescein Isothiocyanate (FITC) Apoptosis Detection Kit (*Sigma Aldrich, UK*) is based on the translocation of phosphatidylserine (PS) from the inner to outer plasma membrane of cells, that occurs during apoptosis.²³¹ Annexin V is a Ca^{2+} dependent phospholipid-binding protein with a high affinity for translocated PS. Translocation of PS also occurs during cell necrosis and as such, the measurement of bound FITC-labelled Annexin V (green fluorescence) is coupled with a dye exclusion test. Propidium Iodide, a (red) fluorescent molecule that intercalates with DNA, is unable to cross through intact cell membranes, making it a valuable stain for identifying necrotic cells, as well as those at the end stages of apoptosis. While Annexin V staining only occurs in apoptotic cells, PI staining will be seen in any cell with a disrupted cell membrane. With flow cytometry, the cells can be stratified into

three distinct populations – intact cells (FITC-/PI-), apoptotic cells (FITC+/PI-) and necrotic cells (FITC+/PI+).²³²

The analysis in the setting of GBM, required the tissue to be cut and dissociated into single cells following the removal of fat, blood and necrotic areas with a scalpel. The tissue was further cut whilst covered in media using criss-cross actions and periodically rotating the petri dish. The dissected tissue was added to a 1.5 ml polypropylene tube containing 1 ml of a tissue disaggregation solution (300 µl of 0.02% DNase type I and 356 µl 0.02% collagenase type IV in 15 ml of DMEM media). The tissue was kept in an incubator at 37° C for 2 hours on a tube rotator. The disaggregated solution was then filtered through a 40 µm cell strainer (*VWR, UK*) and the collected solution centrifuged at 400 x g for 5 min. The supernatant was discarded, and the pellet mixed with 1 ml of the HEPES buffer solution provided with the Annexin V-FITC Apoptosis Detection Kit (*Sigma Aldrich, UK*). Both Annexin V (5 µl) and PI (10 µl) were then added to a 500 µl of the cell suspension, allowed to mix for 15 min in the dark and the solution analysed within a BD FACSCalibur flow cytometer (*BD, UK*). Data acquisition was performed with the BD CellQuest Pro software and allowed the production of a dot plot chart that plotted the cell signals with relation to their emission spectrum. Gating based on side-scatter detection was applied to eliminate cell debris and doublet formation. For these experiments, Annexin V was labelled with FITC, which has a maximum emission at 530 nm, and this was measured on the flow cytometer with the FITC channel *FL1*, which detects wavelengths between 515-545. PI has a maximum emission at 620 nm and the red channel *FL3*, which detects light with wavelengths of 670 nm, was used to detect PI. Though the *FL2* channel (detects light within 564-606 nm) can also detect PI, its range of detection overlaps with the emission of FITC and hence, *FL3* was selected because of the improved separation of fluorescence (*see Figure 2.5*). Using the clustering of cell events, the graphs could be sectioned into four distinct populations – cells with minimal or negative Annexin V and PI (low *FL1* and *FL3* - healthy); cells which are positive for Annexin V but with the cell membrane still intact and hence, excluding PI (high *FL1* but low *FL3* – early apoptosis); cells that have undergone irreversible apoptotic changes that mean the cell membrane has lost its integrity and is permeable to PI (high *FL1* and *FL3* - late

apoptosis); and lastly cells that have not gone through the apoptotic pathway and died via necrosis (low FL1 but high FL3 - necrotic).

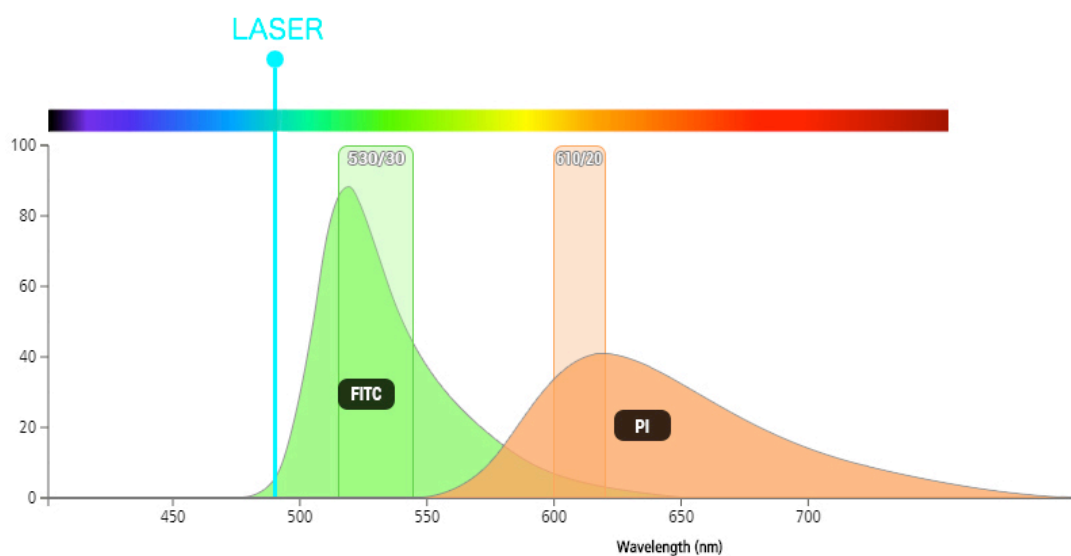


Figure 2.5: Emission spectra for FITC and Propidium Iodide

There is a region of overlap between 550 and 650 nm between the emission spectra of FITC and PI; hence FL3 which detects emissions at 670 nm was used instead of FL2 (which detects 564-606 nm wavelength) to specify PI.

2.2.4.3 LDH Analysis

Cell viability was also assessed using a colorimetric cytotoxic assay - Lactate dehydrogenase (LDH) Cytotoxic Kit (*Sigma Aldrich, UK*). LDH is an intracellular enzyme that is released from cells into the culture medium once cell damage occurs. As it is a stable enzyme, its presence in the assay can be used to evaluate cell or tissue death.^{233,234} The kit was used per the manufacturer's protocol on the effluent that was collected from the microfluidic device. It works on the principle that LDH in the collected medium catalyses the reduction of NAD⁺ to NADH/H⁺, while converting lactate to pyruvate. The catalyst, diaphorase concomitantly transfers H⁺ from NADH/H⁺ to the tetrazolium salt iodotetrazolium chloride, which is reduced to a formazan dye (see *Figure 2.6a*). As cellular damage increases, there is an increase in the release of LDH and thus LDH activity in the effluent was directly correlated to the amount of formazan produced. Red formazan has a maximum absorbance at around 490 nm and the degree of absorbance by the effluent at this wavelength is an indirect measure of cell damage/injury. The LDH Kit contains all the substrates and

enzymes in this reaction, including a *reaction dye* (containing Iodotetrazolium chloride and sodium lactate) and a *catalyst* solution (containing a mixture of Diaphorase and NAD⁺).²³⁵

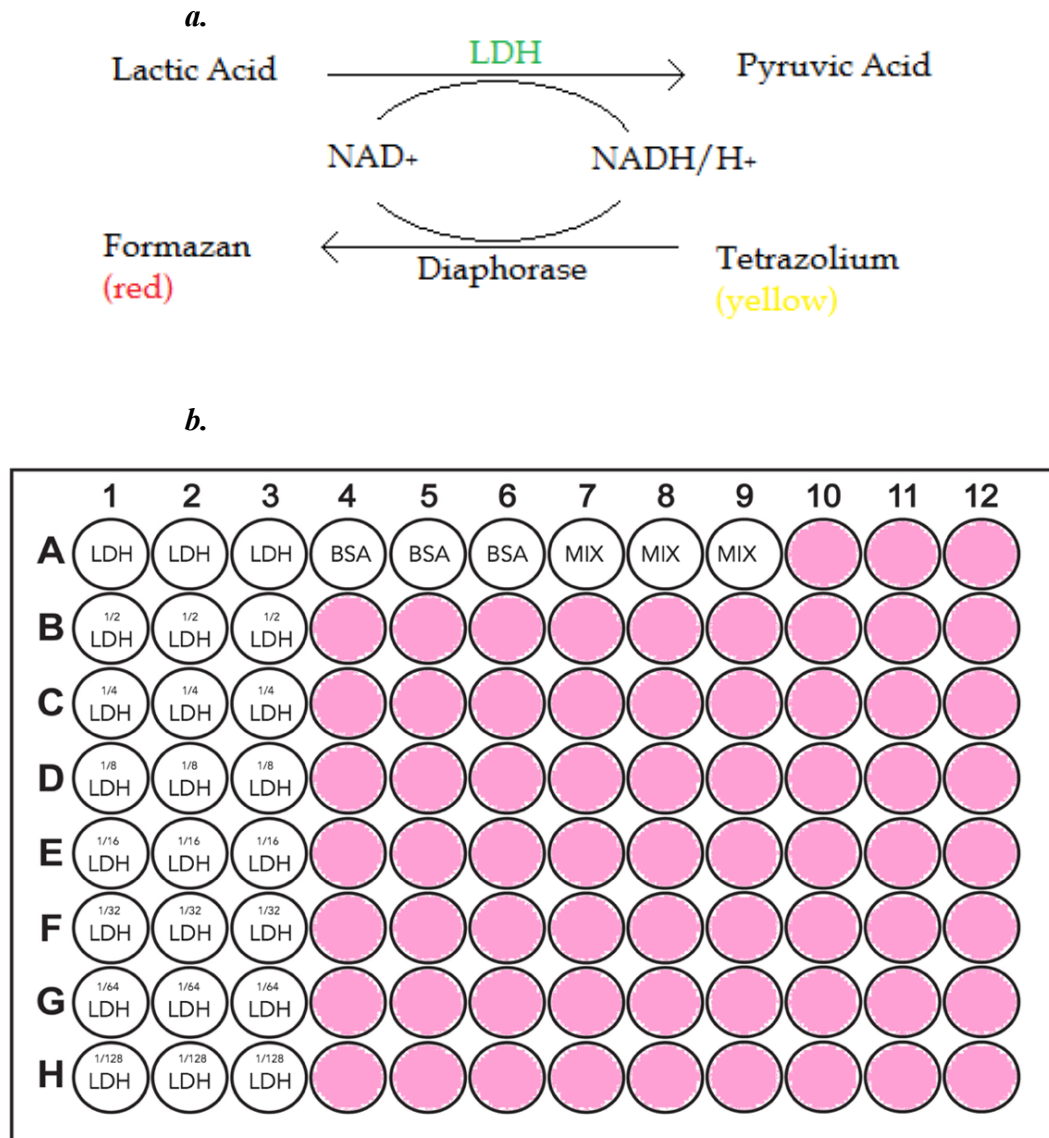


Figure 2.6: Understanding LDH Analysis

a. Reactions catalysed by LDH and Diaphorase utilised in LDH quantification. **b.** Typical set up of 96 well plate for LDH analysis. Key: LDH = LDH Control (1 u/ml); BSA = 10% (w/v) Bovine Serum Albumin; Mix = Reaction Mixture; Coloured Wells = Collected Samples in triplicates.

Effluent flowed through the microfluidic device was collected at set time points (usually, every 2 hours) and stored at 4° C until the experiment completed. Once all

effluent samples had been collected, a 96 well plate was prepared (see Figure 2.6b): adding 50 μ l of 1% (w/v) BSA in PBS into every well except for the top 3 LDH control wells (A1-A3) and those used as a reaction mixture control (A7-9). LDH control (100 μ l; made by mixing 2 μ l of L-Lactate Dehydrogenase with 5.5 ml of 1% BSA) was added into the three LDH control wells. To prepare a 50% LDH control, 50 μ l was taken out of each of these wells and added into the previously described BSA solution into wells B1, B2, B3. This was repeated until a range of concentrations from 1 to 1/128 were obtained (see figure 2.6b). Collected effluent samples (50 μ l) were also added into corresponding wells, in triplicates, followed by 50 μ l of the reaction mixture (Reaction Mixture: 125 μ l of *catalyst* with 5.625 ml of *reaction dye*). The plates were kept in the dark for 30 min and then the stop solution (Hydrochloric Acid) was added. Plates were subsequently placed on a plate shaker for 30 secs at 250 rpm and once clear of any bubbles, the plate was read on a Synergy HT Plate Reader (*BioTek, USA*) at 490 nm, using the Bio-Tek KC4 application (*BioTek, USA*). The results of the assay were analysed using Microsoft Excel 2017 (*Microsoft, USA*).

For the determination of viability after perfusion a number of GBM control samples in devices, were perfused with 10% (v/v) of the Lysis Solution from the Cytotoxicity Detection Kit (in DMEM media). The Lysis Solution was introduced 1 hour before the termination of the experiments (for example, if the device was run for 72 h, the lysis solution was introduced at 71 h, allowing an extra hour to obtain the released LDH from the effluent).

2.2.4.4 Trypan Blue Staining and Cell Counts

Trypan Blue is a molecule that is impermeable to the cell membrane and as such, can only enter a cell if the membrane is compromised. Upon entering the cell, it binds to intracellular proteins, thereby staining the cell its characteristic bluish colour. Because of its specific properties, cell viability can be measured by a trypan blue exclusion test.²³⁶

The disaggregated tissue cell suspension (10 μ l) was mixed with 10 μ l of 0.4% Trypan Blue Solution. The mixture was pipetted onto a haemocytometer and the

viable percentage was calculated by dividing the number of viable cells (cells that excluded the dye/unstained) by the total number of cells (stained and unstained) multiplied by 100.²³⁷

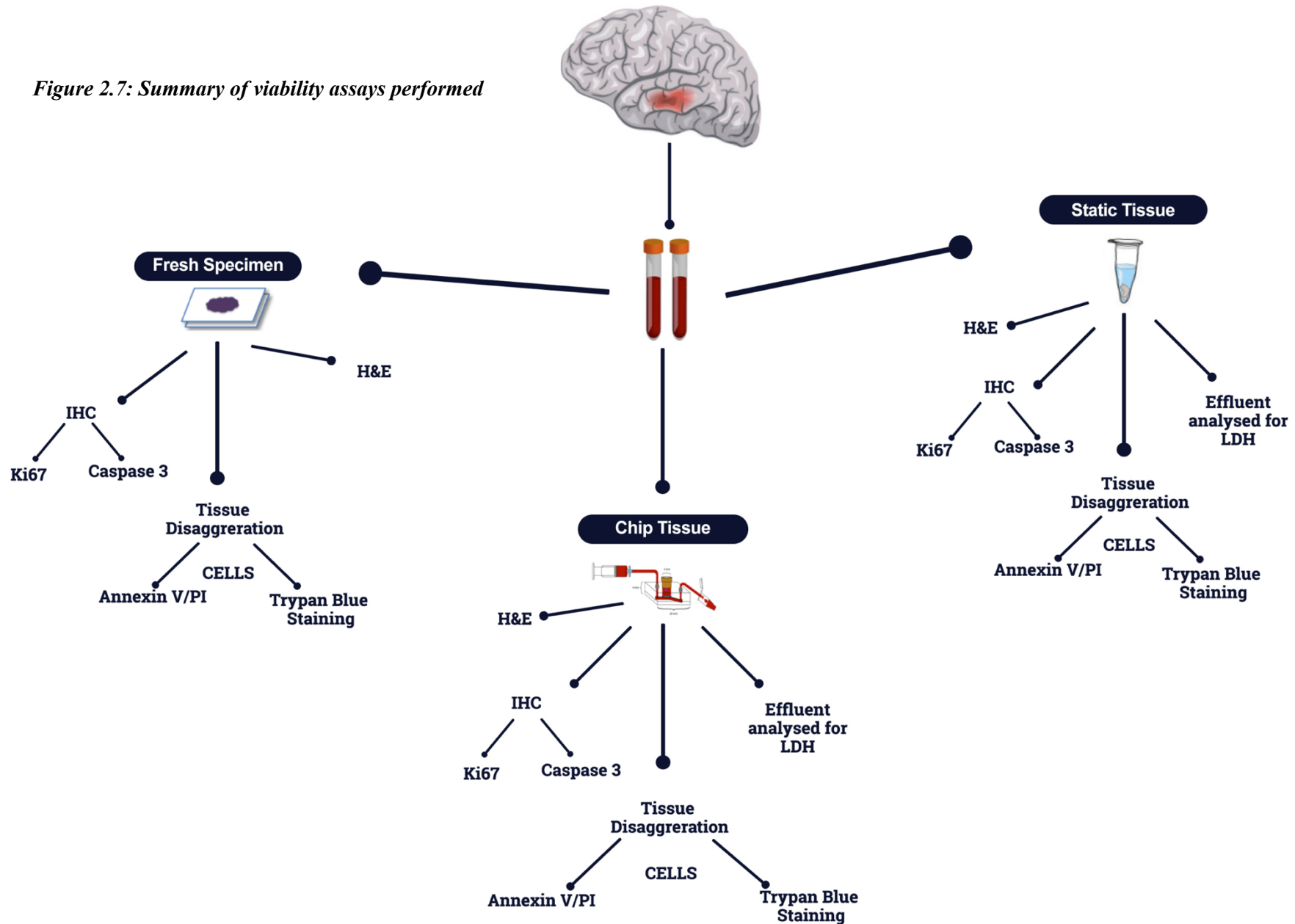
2.2.4.5 Drug Treatments

Effect of cytotoxic drugs on the GBM tissue was tested with two drugs: Temozolomide (TMZ) and ExoPr0.

Temozolomide is a prodrug that is converted into the active drug MTIC (5-(3-methyl-(triazene-1-yl)imidazole-4-carboxamide in physiological pH, without hepatic activation.^{238,239} Previous studies have shown that the plasma and CSF concentrations of TMZ are approximately 100 μM and 10 μM , respectively.^{240,241} As such within this study, a final concentration of 100 μM of TMZ initially dissolved in DMSO (10 mg of TMZ dissolves in 1 ml of DMSO) was used to treat GBM tissues maintained on chip after optimising the tissue on chip for 24h. At 24 h, the 100 μM TMZ/media solution was perfused at a rate of 4 $\mu\text{l}/\text{min}$ for 24 h. As the half-life of MITC is 2 h,²⁴² the TMZ solution was replenished after 24 h and the tissue perfused for another day, ensuring that the GBM was exposed to 48 h of TMZ perfusion. A GBM control sample was also exposed to the corresponding volume of DMSO (0.2% v/v) to ensure that any presumed drug effects were not as a result of DMSO.

ExoPr0 is an exosome product derived from CTX, a conditionally immortalised human neural stem cell line currently being developed by the company ReNeuron. Preliminary studies within the ReNeuron group has shown efficacy of the drug in treatment of GBM cell lines. To test the efficacy of ExoPr0 in treating GBM tissue, various concentrations of the drug were added to exosome-depleted media. As the use of exosomes to treat GBM is still in the pre-clinical stages, the doses were per manufacture guidance and ranged from 1×10^9 – 2×10^{11} particles within 20 ml of media.

Figure 2.7: Summary of viability assays performed



2.2.5 Statistical Analysis

Statistical analysis was carried out using Graph Pad Prism (*Graph Pad Software, USA*). A combination of paired and unpaired t-tests was used to determine statistical significance between fresh tissue assays and assays within the microfluidic device as appropriate. A p value of ≤ 0.05 was considered to be significant and thus reject the null hypothesis that the differences in the results were due to chance. All graph error bars display the standard error of the mean, except where indicated. Statistical analysis support was provided by Dr. Chao Huang of the Hull and York Medical School.

3.1 Optimisation and Results

3.1.1 Overview

A total of 148 GBM tumour specimens (obtained from 33 patients) were maintained within a microfluidic device. The average wet weight of the tumour samples was 12.1 mg (\pm 2.2 mg). Tissue maintenance was for an average of 70.2 h (\pm 6), with 2 experiments that ran for the shorter length of 48 h, and 2 devices maintained for longer than 72 h; one for 5 days and another for 7 days. Effluent collection occurred every 2 hours during the working day and was left overnight for an average of 12-18 h. A further 22 tissue samples were maintained as static cultures within a 1.5 ml polypropylene tube, with media replenished every 2 hours during the day and left overnight without any change of the media for 12-18 h. The *static culture experiments* were used as a control, to compare the effects of tissue culture, without microfluidic flow and as such, the volume of the media used, and the timings of media exchange corresponded with effluent collection from the microfluidic devices that were running in parallel. The static culture tissues were on average, heavier than the microfluidic tissue at 14.5 mg (\pm 6.3 mg).

3.1.2 Assessment of Viability

3.1.2.1 Annexin V and PI

For each patient recruited into the study, both fresh tissue and chip tissue were disaggregated into single cell suspensions as described in section 2.2.4.2. The Annexin V and Propidium Iodide assay was performed and analysis with flow cytometry produced a dot plot of 10,000 cellular events with each cellular event represented by a point on the chart, the location of which was determined by the presence or absence of Annexin V and Propidium Iodide. *Figures 3.1-3.3* show an example of chip tissue that was processed using the method.

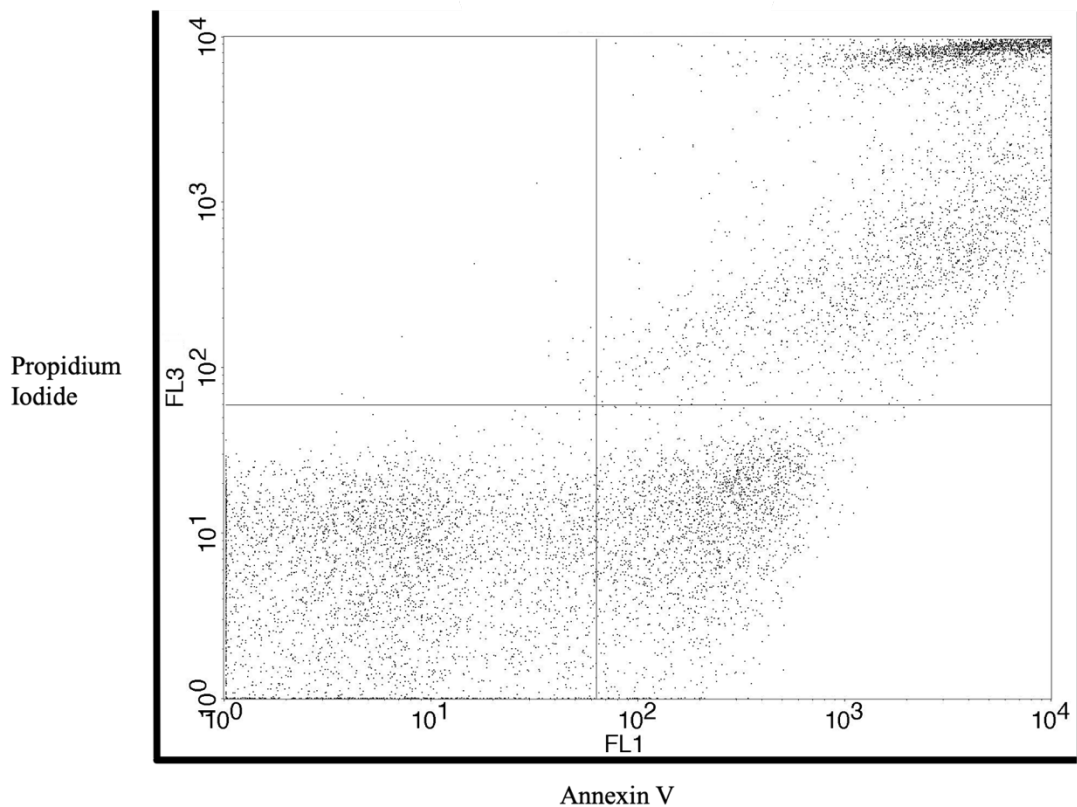


Figure 3.1: Dot Plot (patient 16008) produced on CellQuest Pro software representing flow cytometric analysis of Annexin V and PI distribution.

The chart shows the proportion of cells (from a total of 10,000 cells) that are labelled with Annexin V and/or PI. The x axis denotes FL1 and represents cells emitting light around 530 nm, corresponding to FITC-labelled Annexin V. FL3 (y axis) corresponds to cells emitting light at 670 nm, which in this case would be cells with intracellular PI. NB: The scales are logarithmic.

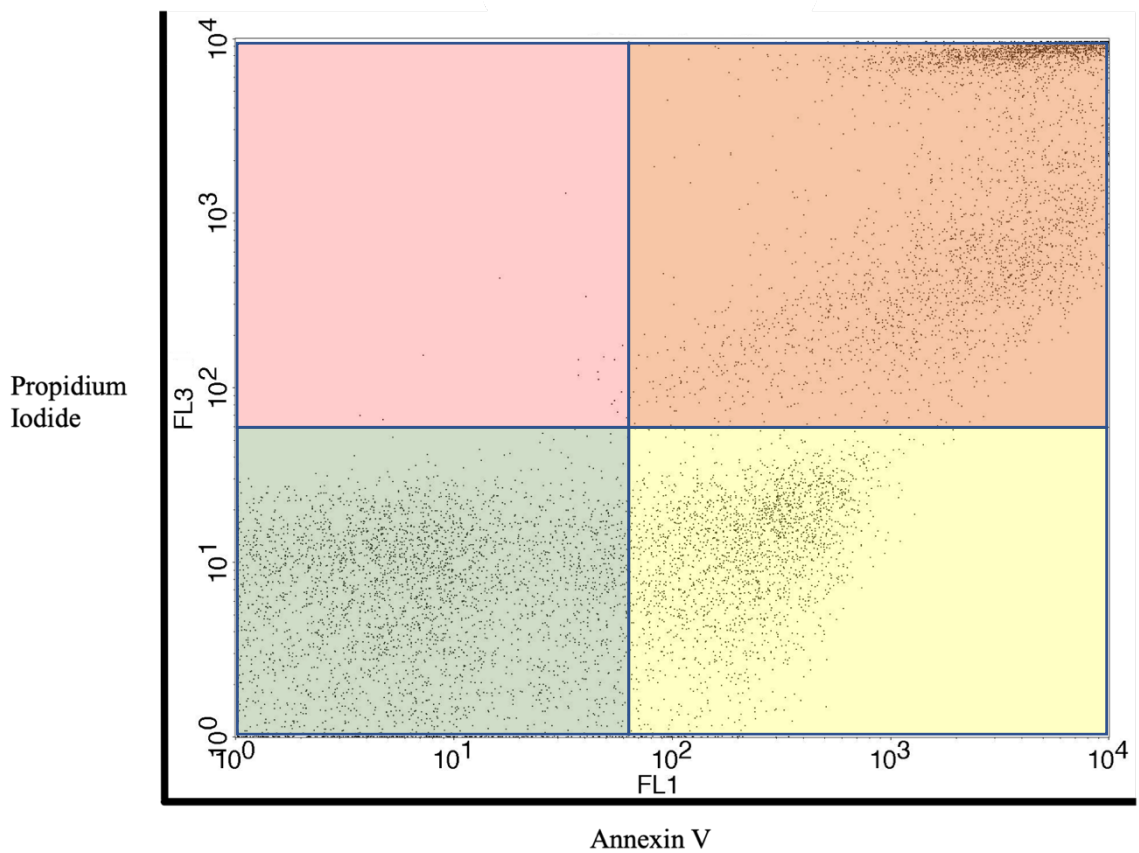


Figure 3.2: Dot Plot (patient 16008) representing flow cytometric analysis of Annexin V and PI distribution sectioned into quadrants.

Using the clustering of the cell events the dot plot produced can be sectioned into four distinct populations – healthy/live (AV-/PI- in Green); early apoptosis (AV+/PI- in Yellow); late apoptosis (AV+/PI+ in Orange); necrosis (AV-/PI+ in Red).

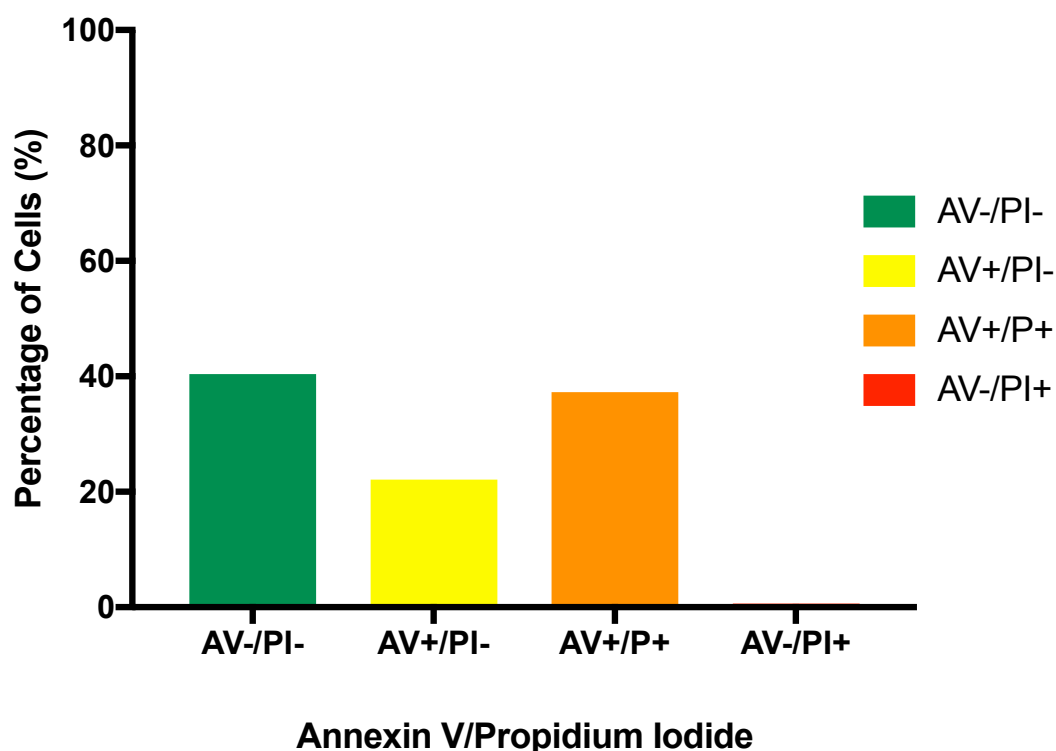


Figure 3.3: Flow Cytometric analysis represented as a Histogram

The percentage of the total cells in each quadrant is calculated and plotted onto a histogram to better visualise the different cell populations. This can be used to determine the population of cells that are healthy (AV-/PI-) in Green and thus measure viability.

3.1.1.2.2 LDH Assay

All patient samples within the microfluidic device and those maintained with static culture techniques were analysed for LDH release. The LDH assay was performed as described in section 2.2.4.3. The results of the assay were used to calculate the average absorbance for a certain period of time. As the effluent samples were analysed in triplicate the average of the 3 samples was obtained. This average was then subtracted from the average absorbance from the reagents used, e.g. the absorbance from the BSA control and the reaction mixture control. This final figure was plotted as an absorbance value against the hour it was collected from the start of the experiment. A worked example for patient 16024, Sample 1 is below -

The absorbance figures for the effluent sample collected at 2 h were:

Triplicate samples - 0.478, 0.477 and 0.497. The average was 0.484.

From this figure, the background absorbance (average absorbance of reagents – BSA and reaction dye) is subtracted:

$$0.484 - 0.047 = 0.436$$

This figure is plotted as the absorbance value against the time it was collected. The same process is repeated for each effluent sample collected over the length of the experiment. Note that overnight samples were not changed as frequently as every 2 h and instead changed on average every 14 h. The initially high LDH absorbance is thought to be related to tissue damage resulting from tissue dissection and handling, which settles once the tissue has acclimatised to the chip environment.¹⁸⁰

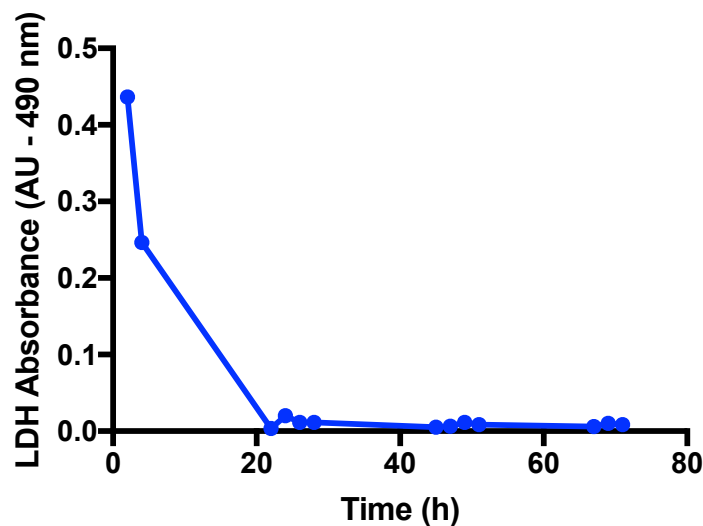


Figure 3.4: LDH absorbance in 72 h (AU – 490 nm).

LDH absorbance compiled from effluent samples collected every 2 hours and 12-18 (overnight). The graph shows an initial high absorbance value that plateaus to a low absorbance value for the rest of the experimentation period.

3.1.2.3 Histology

Histological analysis of specimens was obtained for all patients recruited (fresh tissue and chip tissue). All wax embedding of tissues was performed by the principal investigator. The initial protocol for tissue sections and staining was a manual process that was optimised after the 12th patient to include a ‘blueing’ process, as the quality of the slides were inadequate (see *Figure 3.5*). After the 18th patient and

despite amendments to the protocol, there was not a significant improvement in quality of histological slides and as such, the services of UCL Advanced Diagnostics Laboratory (UK) were sought for all histological and immunohistochemical preparations. The finalised protocol is summarised in *section 2.2.4*. H&E sections were developed for 30 patients. Immunohistochemical analysis was processed for the last 16 patients (both Ki67 and Caspase 3)

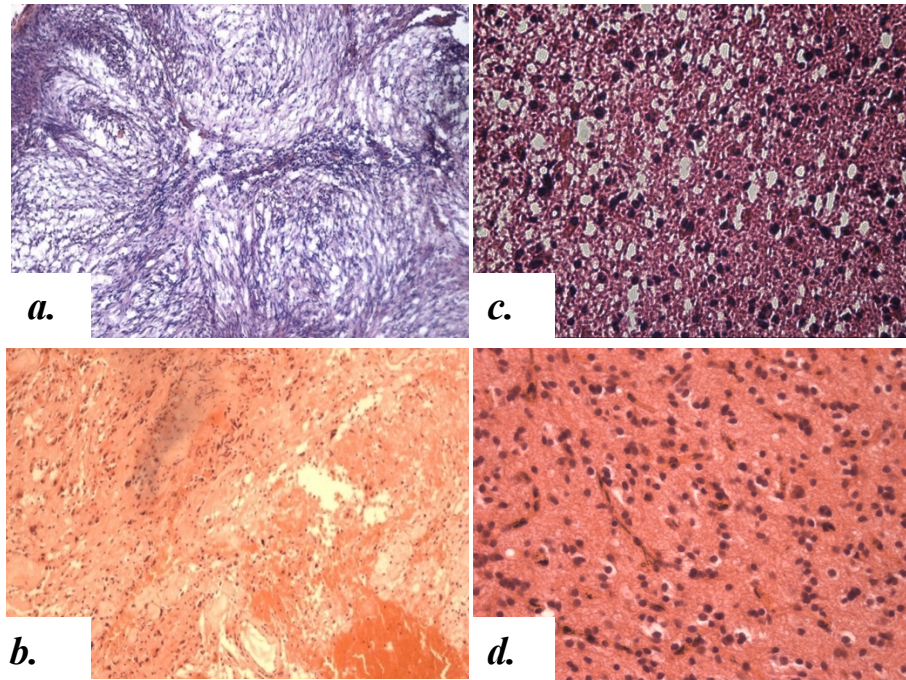


Figure 3.5: Optimisation of histological techniques.

*Comparison of initial H&E protocols **a&c** with final protocols **b&d**. Note the greater contrast in colour between nuclei (Haematoxylin) and cytoplasm (Eosin) in finalised protocol, providing greater differentiation (**a&b** x100 Magnification; **c&d** x 400 Magnification).*

3.1.3 Optimisation of Experimental Technique

3.1.3.1 Operative Sampling

Tumour samples were deemed appropriate for specimen acquisition during surgery based on macroscopic appearances and knowledge of the relationship of the tumour to normal brain. Sampling errors were defined as tissue without evidence of GBM on

histological examination. This occurred once, amongst the 33 patients, with histological examination not showing any evidence of GBM tissue; the analysis was consistent with normal brain (*see Figure 3.6*). There were 3 instances where the bulk of the tissue obtained contained perilesional tissue and there were 2 occasions where the tissue contained minimal or no nuclei, likely representing tumour necrosis. These findings were consistent in histological analysis of both fresh tissue and chip tissue.

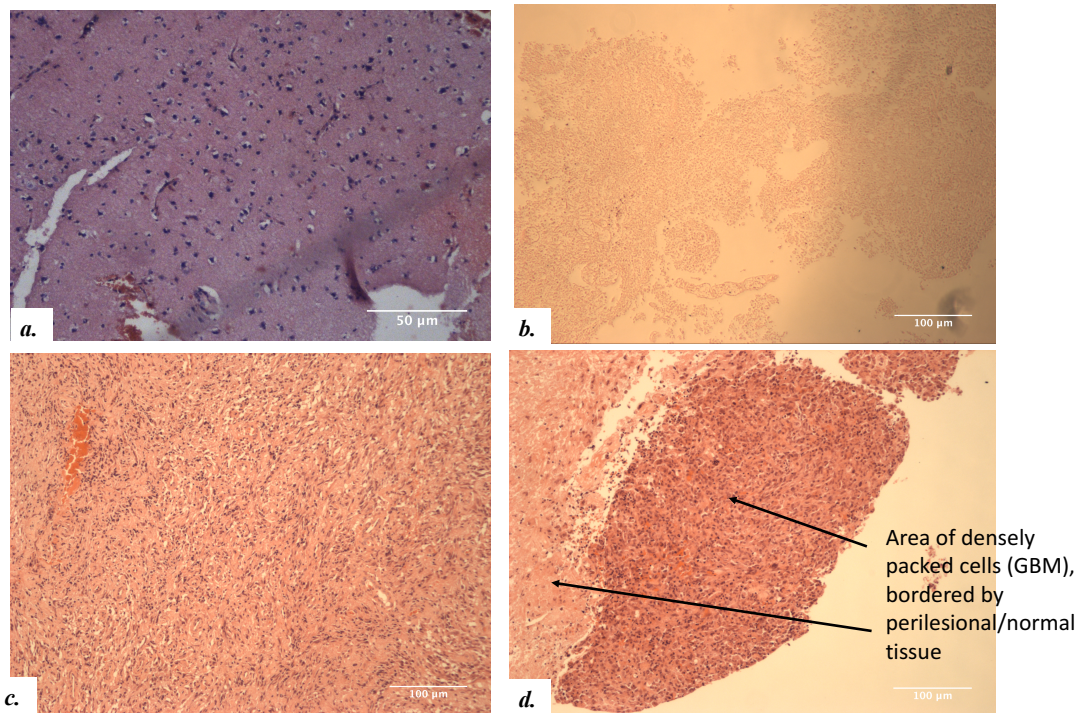


Figure 3.6: Variations in Histology from 4 different GBM patients

a. Specimen without obvious cancerous tissue, most consistent with normal brain (*x200 Magnification*); **b.** Anuclear specimen, likely representative of a dense area of tumour necrosis (*x100 Magnification*); **c.** Grossly uniform tissue specimen with high cellularity, vascular proliferation, consistent with GBM (*x100 Magnification*); **d.** Tissue with localised area of densely packed cells with high cellular pleomorphism and mitotic activity, adjacent to areas of perilesional tissue (*x100 Magnification*)

Despite strict adherence to the inclusion and exclusion criteria, 5 of the 33 patients did not have a diagnosis of a GBM, including one patient who had a non-glial tumour (a Grade 1 Schwannoma, which mimicked a GBM on imaging).

3.1.3.2 Non-Perfused Time

On average the time between obtaining the sample and perfusing the tissue within the microfluidic device was 69 mins (with a range of 40 - 120 mins). The timing shortened with experience with the last 10 sample acquisitions being perfused within 60 mins of surgical resection (with a mean of 56.2 mins +/- 15.8). Optimisation experiments were carried out to see if the length of time prior to processing the tissue affected viability; fresh tissue was disaggregated immediately, and an Annexin V/PI assay was performed. These results were compared with assays on tissue that was left in nutrient media for an hour prior to starting the same process. The viability of tissue processed immediately was 81.4 % (+/- 11.7) compared to tissue that was processed an hour later 62.9 % (+/- 5.7). A paired t-test showed that the difference between the matched pairs (n=3) was statistically significant; $P = 0.043$. However, there was no correlation between the non-perfused time and viability when samples were analysed (n = 28) using Pearson's correlation coefficient with an r^2 value of 0.027 and P value of 0.41, indicative that the variance between timing of chip processing and viability is not shared. *Figure 3.7* summarises the data on the length of time the tissue was without perfusion.

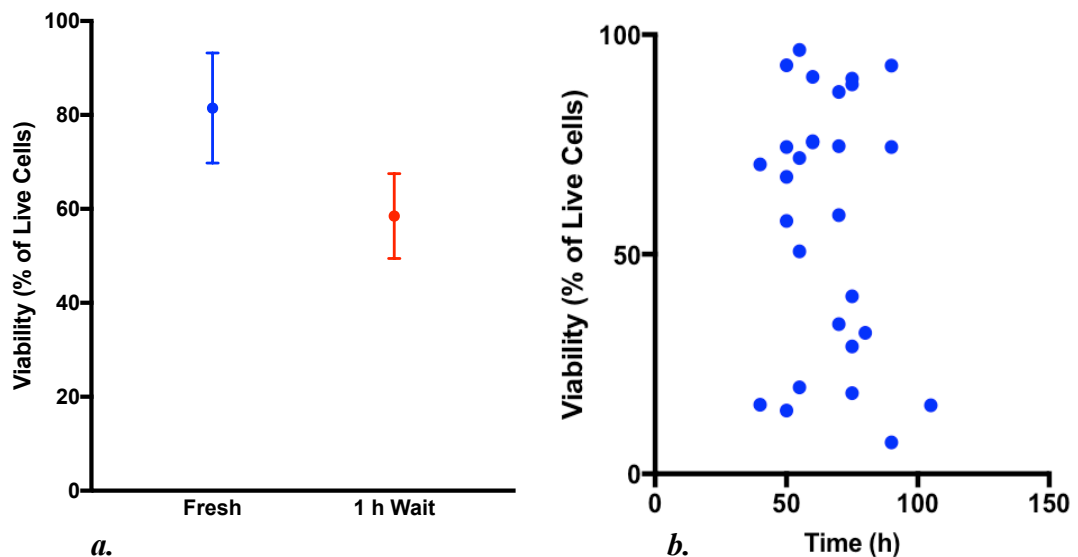


Figure 3.7: The effects of processing time on tissue viability

a. Viability of tissue processed immediately (Fresh) and that processed an hour later (1 h Wait); p value = 0.043 (n=3). **b.** Scatter graph showing correlation between length of time taken to process tissue and viability. Pearson's correlation – $r^2 = 0.027$; $P = 0.41$.

3.1.3.3 Nutrient Media

To assess the efficacy of different nutrient media solutions in maintaining GBM tissues *ex vivo*, the standard media, utilised as the media solution in 98 microfluidic devices, was compared with exosome-depleted media (n = 22) media and an artificial CSF solution (n = 8). There was no statistical difference in cell viability when tissue and effluent maintained with standard media was compared with tissues maintained with exosome-depleted media, nor when the standard media was compared to aCSF. The results of the differing media types are summarised in *Table 3.1 and 3.2*.

	Standard Media FBS	Exosome-Depleted Media <i>Exosome-Depleted FBS</i>	T-test (Wilcoxon) <i>n = 7</i>
Viability (%)	49 (+/- 30.7)	31.6 (+/- 19.5)	<i>P = 0.19</i>

Table 3.1: Exosome-Depleted Media as a media substitute.

Table comparing the viability in tissues maintained in standard media and those maintained in exosome-depleted media.

	Standard Media FBS	aCSF	T-test (Wilcoxon) <i>n = 8</i>
Viability (%)	73.3 (+/- 28.8)	65.6 (+/- 27.1)	<i>P = 0.05</i>

Table 3.2: aCSF as a media substitute.

Table comparing the viability in tissues maintained in standard media and those maintained in aCSF.

3.1.4 Optimisation the Chip

3.1.4.1 Flow Rate

Previous studies that utilised microfluidic devices to maintain human tissue had used flow rates of 1 $\mu\text{l}/\text{min}$ ²⁴³, 2 $\mu\text{l}/\text{min}$ ^{179,218,244,245} and 4 μl .²⁴⁶ As this was the first time biopsies of brain tissue had been maintained within the device, there was uncertainty about the optimal flow rate for tissue maintenance and as such flow rates through the chip were altered between 2 $\mu\text{l}/\text{min}$ (n = 49) and 4 $\mu\text{l}/\text{min}$ (n = 79). There was a statistically significant difference between the viability of the tissue maintained within the devices, as measured with Annexin V and PI; with tissue perfused at a rate of 4 $\mu\text{l}/\text{min}$ having significantly higher viability (66.2 % +/- 26) than tissue maintained with flow rates of 2 $\mu\text{l}/\text{min}$ (44.6 % +/-28.1); $P = 0.0314$. The effect of flow on viability is summarised in *Figures 3.8* and *3.9*.

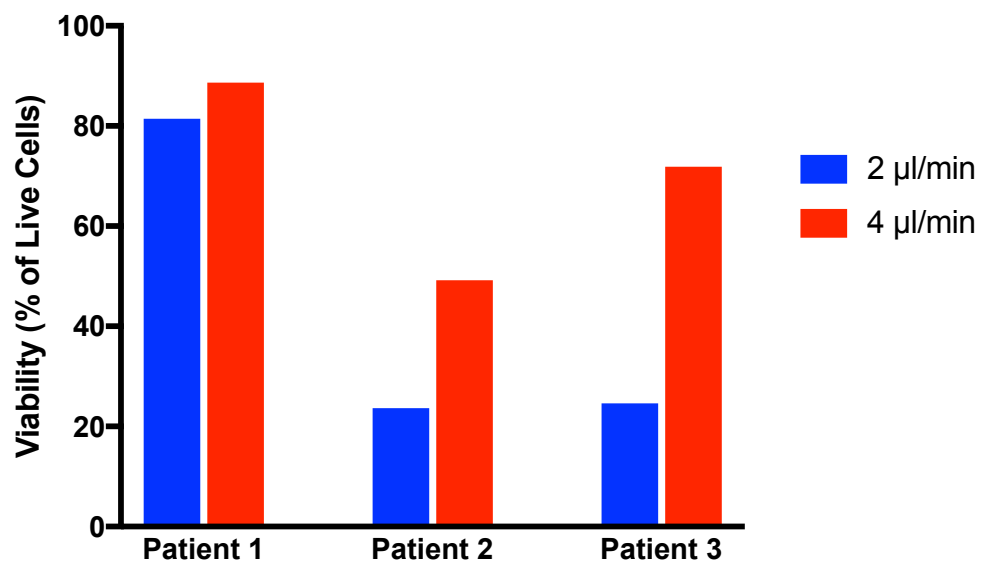


Figure 3.8: The effect of flow rate on tissue viability (matched pairs)

Matched pair samples (n=3) from the same patients assessing the effects differing flow rates (2 μl and 4 μl) had on tissue viability (assessed with Annexin V and PI).

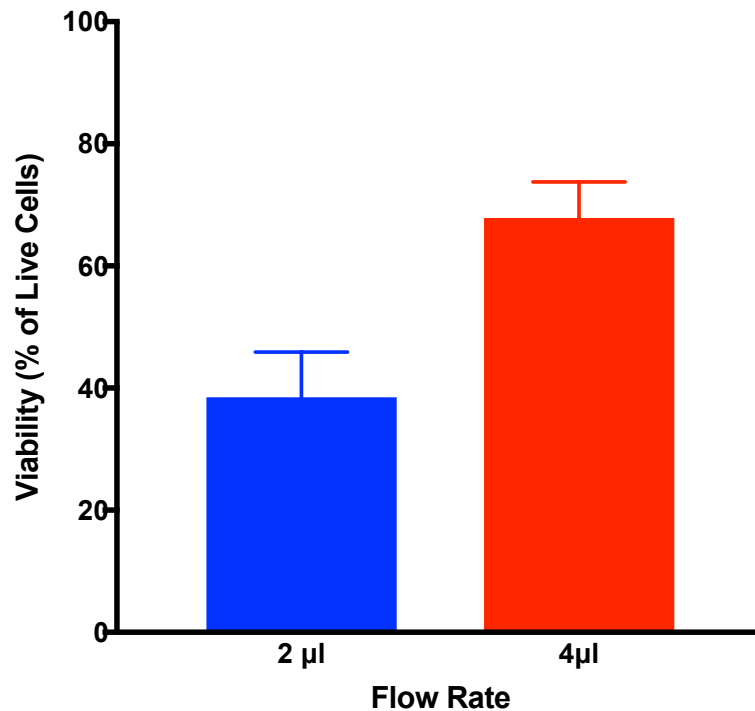


Figure 3.9: The effect of flow rate on tissue viability (whole cohort)

Viability of tissues perfused with 2 µl/min (n= 49) and 4 µl/min (n =79) as measured by Annexin V and PI assay. There was a statistically significant difference in the viability of the cells with a P value of 0.03 (unpaired t-test).

3.1.4.2 Blockages and Leaks

In total, 20 out of 148 devices, either blocked or leaked to the extent that the experiments were abandoned. Blockages meant experiments were not able to run their course and results could not be interpreted accurately. To limit this problem, the microfluidic device required an adaptation. Optimisation of the microfluidic device required the introduction of a nylon mesh to separate the tissue culture chamber from the microfluidic channels. This idea incorporated aspects of the perfusion chamber devised by Rambani *et al.*, where the tissue was placed on a gold electron microscopy grid.¹⁵⁹ The current experiment, introduced the nylon mesh after the first 11 patients had been recruited (38 tumour samples). This increased the efficiency of the devices; with chip disruptions of 44.7 % (17/38) prior to the introduction of the mesh reducing to 3.3% (3/90) after the mesh was introduced. On 3 occasions, prior to the introduction of the mesh, there was no tissue in the device at the end of the experiment, with the likelihood that that the tissue had been flushed through the

device. Though this was rare, it highlighted the importance of a physical barrier between the microchannel and the tissue chamber. As well as reducing the incidence of device disruption, tissue viability was significantly improved (unpaired t-test – $P = 0.019$) after the introduction of the mesh. *Figure 3.10* compares tissue viability with and without the mesh within the device.

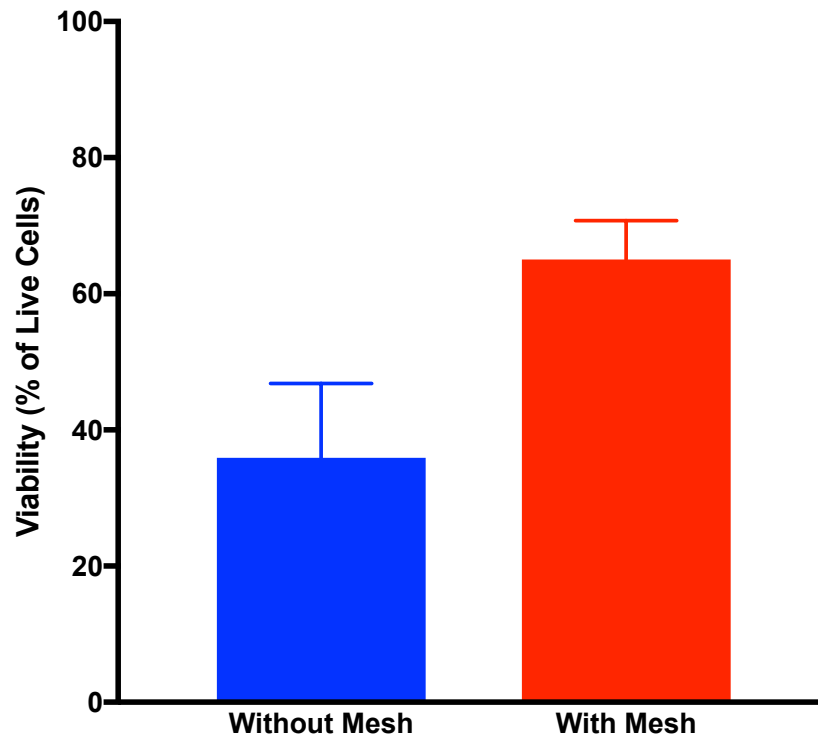


Figure 3.10: Tissue viability before and after the introduction of the mesh into the chip.
There was a significant increase in the viability of the tissue with the introduction of the mesh – With Mesh; $n = 90$ and Without Mesh; $n = 38$ (Unpaired t-test; $P = 0.019$).

3.1.5 Static Tissue Culture

3.1.5.1 Static Tissue Viability

Static tissue cultures were used as control conditions to compare the effect of microfluidic flow on tissue maintenance. 22 tissues were maintained in static culture conditions with media replaced every 2 hours during the day. To ensure conditions were comparable to the chip tissue, the same volume of media was used as that used to perfuse the chip tissue, e.g. experiments with chip tissue maintained with $2 \mu\text{l}/\text{min}$

would have 240 μ l of nutrient media every 2 h. This was doubled when the flow rates within the chip tissue was doubled to 4 μ l/min and an equivalent volume used to maintain tissue that was kept overnight. The media in which the static cultures were maintained were collected and stored for LDH analyses at the end of the experiment run as described in section 2.2.3.4. When matched pairs were compared ($n = 9$), there was a statistically significant difference (paired t-test - Wilcoxon) in the viability of chip tissue compared with static tissue maintained over 72 h, with a mean viability of 73.6% (+/- 26.5) in chip tissue compared to static tissue, which had a mean viability of 52.1 % (+/- 30.8). $P = 0.036$). *Figure 3.11* displays this graphically.

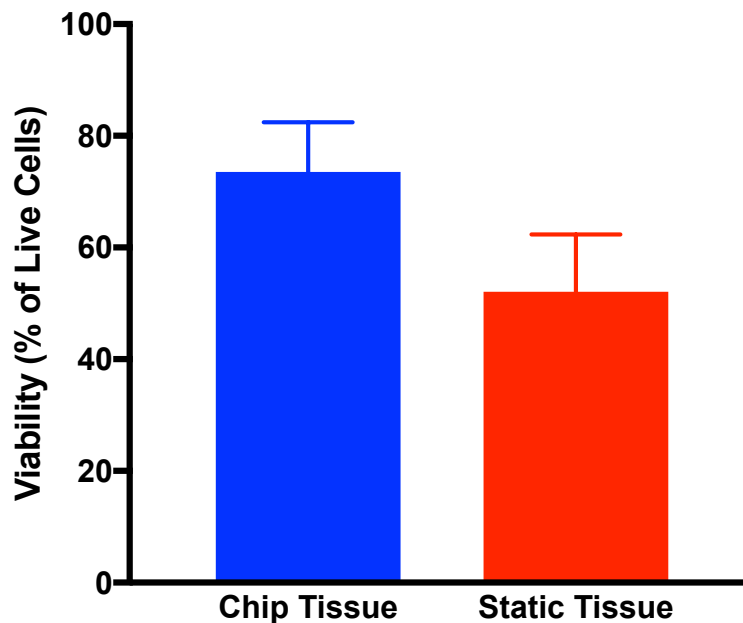


Figure 3.11: Differences in viability between chip tissue and static tissue

Matched pairs (n=9) comparing viability of chip tissue with static tissue using Annexin V and PI assay. Mean viability for chip tissue was 21.5 % greater than static tissue.

3.1.5.2 Static Tissue LDH Release

There was a distinct difference in the LDH absorbance in the effluent collected from static cultures when compared to chip tissue. *Figure 3.12* demonstrates LDH absorbance curves of matched pairs (the 12th and 21st patient) of chip tissue and static

tissue demonstrating representative LDH absorbance with reduced absorbance levels after an initially high absorbance with chip tissue compared with erratic and high absorbance in tissue without microfluidic flow.

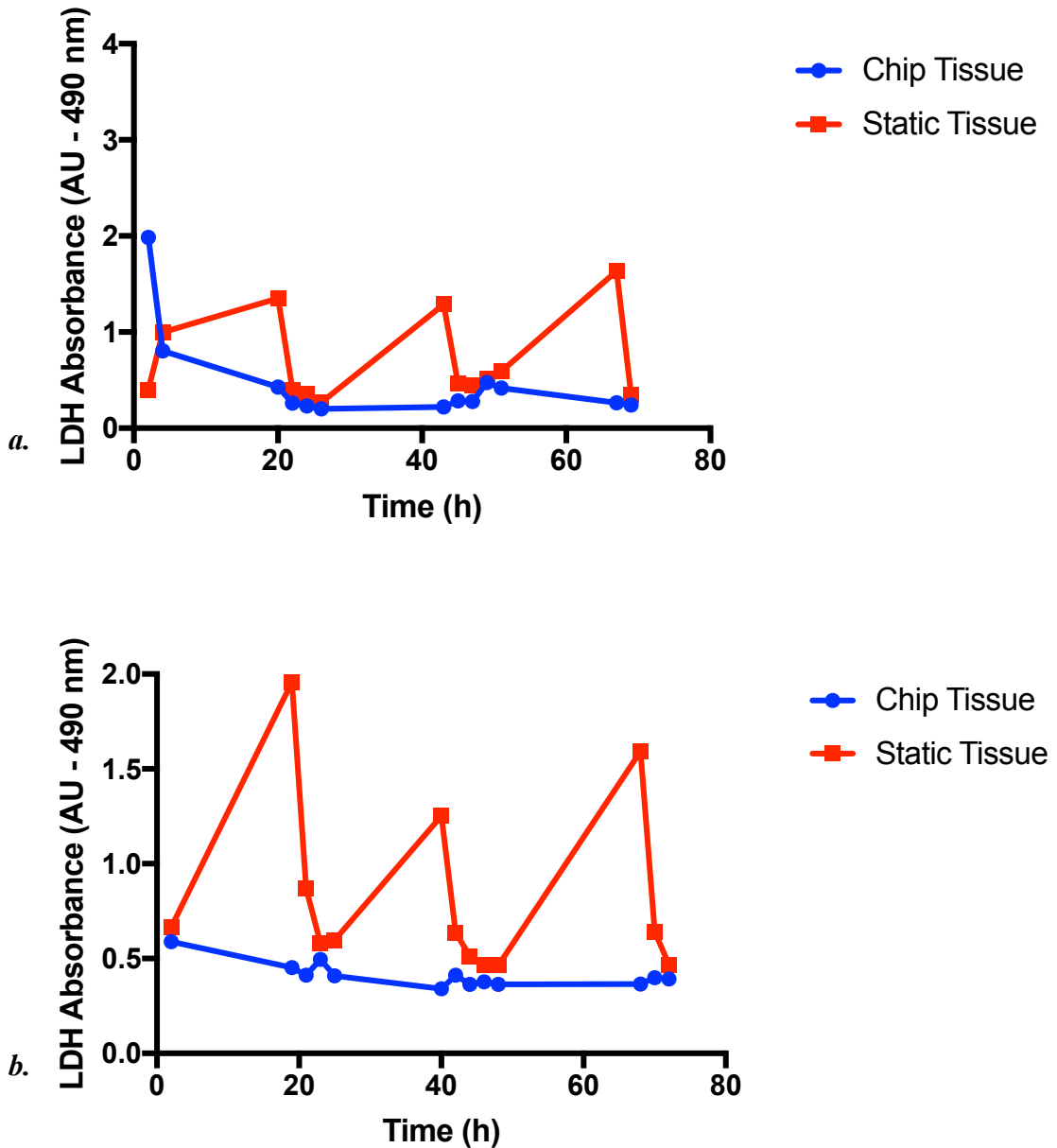


Figure 3.12: The differing patterns of LDH absorbance from effluent samples collected from chip and static tissue

a. LDH absorbance over 72 h period with tissue maintained within the microfluidic device compared to LDH absorbance over 72 h period with static tissue culture (Patient 16012) b. Same comparison for Patient 16021.

3.1.5.3 Histology of Static Tissue

There was a difference in the histological appearance of tissue maintained without microfluidic flow. H&E sections of 3 patients in which all three tissue types (fresh, chip and static) were compared for histological differences showed that static tissue lost part of the structural integrity of the extracellular matrix and took on a “woolly” appearance with large holes in the tissue. There was also a consistent reduction in the intensity of eosin staining, which could indicate a reduction in cytoplasmic proteins. Ki67 staining of the static tissue compared with fresh and chip tissue showed reduced staining in static tissue, suggestive of reduced cellular proliferation of this tissue. *Figure 3.13* demonstrates comparable images from a patient with GBM with histological slides for fresh, chip and static tissue and highlights the different proliferation index in the different tissues.

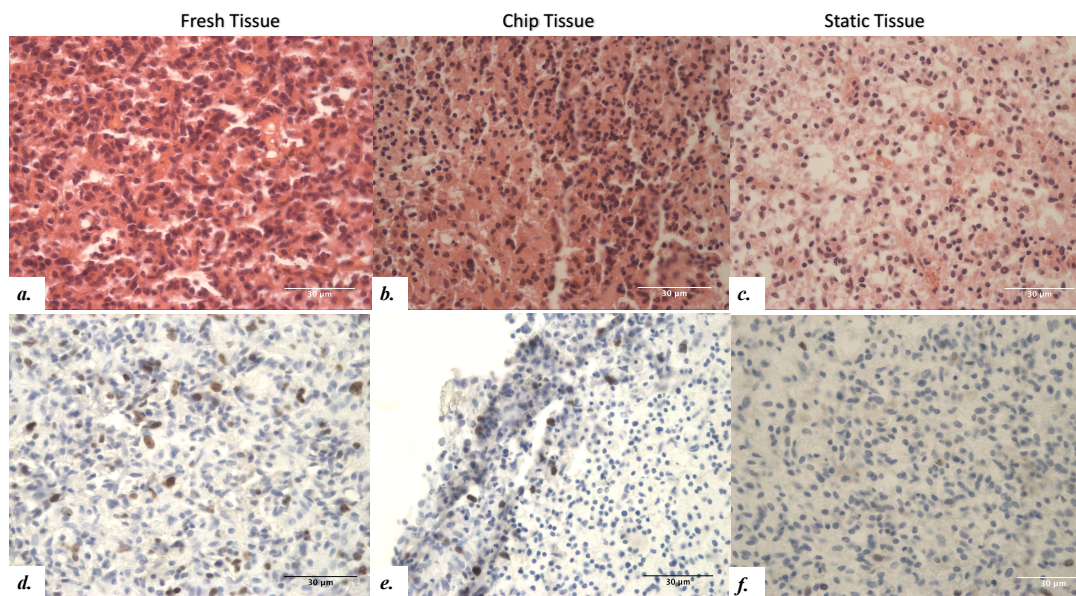


Figure 3.13: Representative images of tissue sections from the 8th patient – GBM IDH Wild Type (all at x400 Magnification)

- GBM sections from fresh tissue (a. H&E d. Ki67 IHC proliferation index of 11.3)
- GBM sections from chip tissue (b. H&E e. Ki67 IHC proliferation index of 5.1)
- GBM sections from static tissue (c. H&E f. Ki67 IHC proliferation index of 2.2).

Note the reduced intensity of eosin (red/pink) staining in the tissues on the top row (fresh tissue > chip tissue > static tissue) that may be related to reduced extracellular matrix/cytoplasmic content.

3.1.5.4 Further Histology Studies

To assess the pattern of tissue degradation once removed from the body, tissue was stored in media for 1, 2 and 3 days without changing the media and then processed for histological analysis. Tissue maintained its cellular and structural architecture for the 3 days without any media change or flow. Immunohistochemical analysis of proliferation with Ki67 staining did not show any nuclei staining for any of the days, indicative of a lack of cellular proliferation after 1 day (*Figure 3.14*).

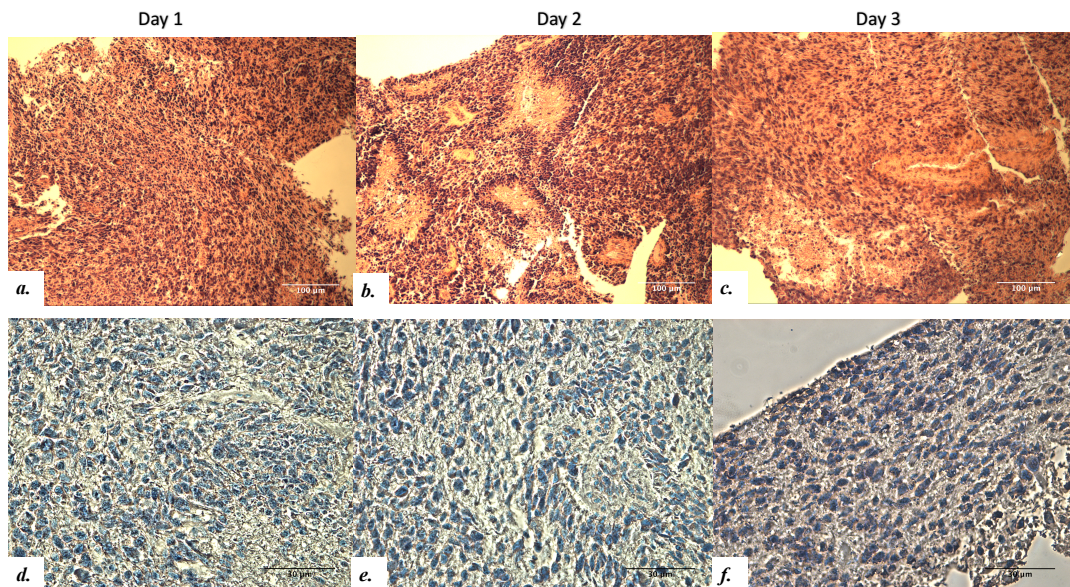


Figure 3.14: Images of tissue sections from the 27th patient (GBM = IDH Wild Type) stored for 1,2 and 3 days.

- GBM sections from tissue stored in media for 1 day - **a.** H&E (x100 Magnification)
d. Ki67 Immunohistochemistry without any nuclei staining positive for Ki67 (x400 Magnification)
- GBM sections from tissue stored in media for 2 days - **b.** H&E with typical areas of necrosis and pseudopalisading (x100 Magnification) **e.** Ki67 Immunohistochemistry without any positive nuclei staining (x400 Magnification)
- GBM sections from tissue stored in media for 3 days - **c.** H&E (x100 Magnification)
f. Ki67 Immunohistochemistry (x400 Magnification)

3.1.6 Summary of Optimisation Techniques

Summary of optimisation techniques are displayed in *Figure 3.15*.

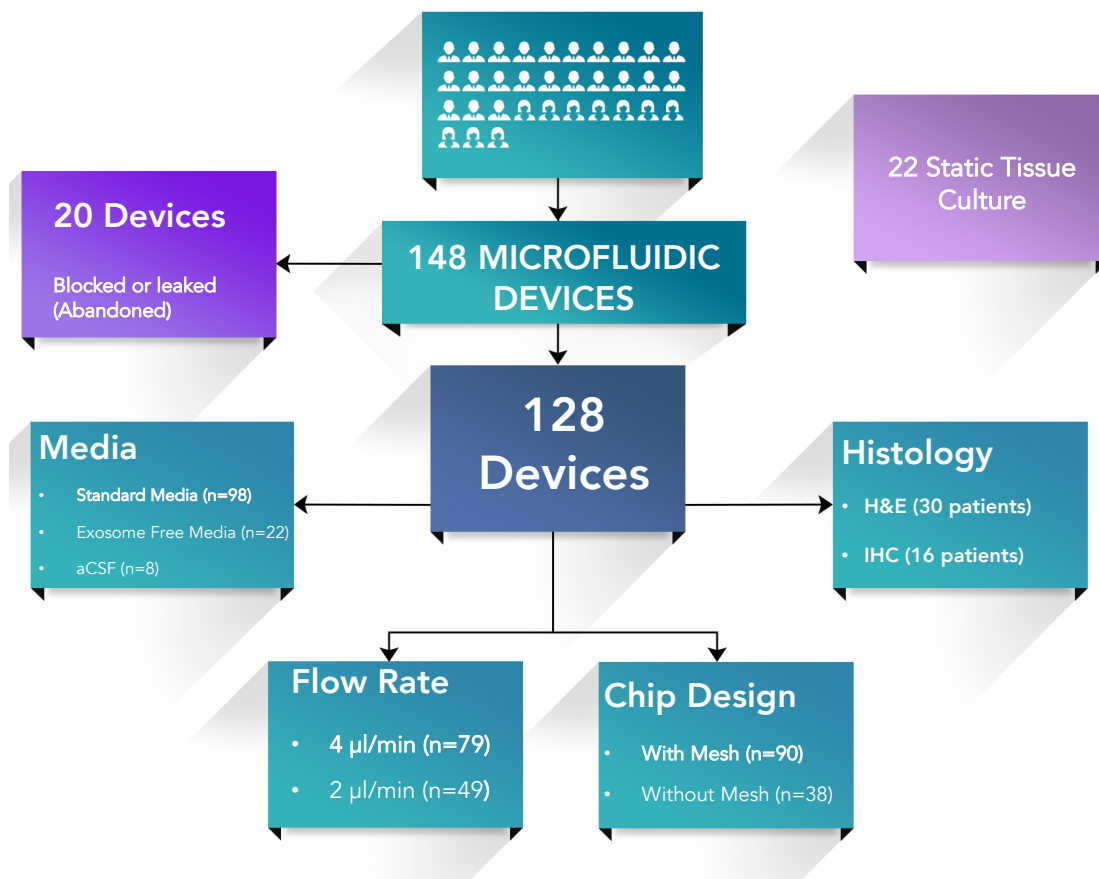


Figure 3.15: Summary of optimisation experiments detailing analysis undertaken and number of devices established.

3.1.6 Discussion

3.1.6.1 Recruitment and Sampling

All patients recruited into the study were managed according to the National Institute of Clinical Excellence (NICE) guidance, with case discussion in a dedicated neuro-oncology multidisciplinary team meeting, pre-operative MRI with and without gadolinium administration, image guided microsurgical resection and post-operative MRI within 72 h of surgery to assess extent of resection.²⁴⁷ For recruitment, pre-operative MR scans were studied for features consistent with a diagnosis of GBM, these included: a heterogeneous mass on T1/T2 images, mass effect from tumour bulk, contrast enhancement on T1 weighted images, peritumoral oedema and central necrosis; all in the absence of a primary systemic cancer.^{248–251} The sensitivity and specificity of pre-operative MR in diagnosing a high-grade glioma (anaplastic and GBM) has previously been reported as 72.5% and 65% respectively,²⁵¹ with a similar margin of error when MR is used to distinguish anaplastic gliomas from GBM.²⁵² As such, errors in diagnoses based on MR are inevitable and though the aim of the study was to examine solely GBM tissue *ex vivo*, 5 of the 33 patients recruited did not have a GBM diagnosis on formal histopathology. Due to the processing time of histological sections and slides, this is only apparent after the patient has been entered into the study and the tissue maintained within the chip. More insidious and difficult to measure is that some of the samples taken from patients, even those with a confirmed diagnosis of GBM, when examined histologically, did not contain representative portions of the GBM tumour. Sampling errors are intrinsic to the method and particularly unavoidable in this setting due to the heterogeneous nature of the tumour itself, therefore, these tumours were included in the analysis. This could explain some of the variation within the viability assays on chip and is likely compounded by the heterogeneity that exists in different tumours. Within the recruited cohort, there were a mixture of patient ages, sex and IDH 1 types and this is likely to translate to mixed GBM phenotype within the cohort; with each of these tumours behaving in a unique manner from the next. As well as tumour heterogeneity, samples obtained were taken during microsurgical resection of the tumour based on the surgeon's knowledge and experience as to what part of the tumour represented the most viable/cellular portion. Despite instructions to provide

non-necrotic tumour and to avoid supplying the study with normal brain tissue, it is difficult for the surgeon to be able to determine with absolute certainty, the microscopic appearance of a tumour at surgery. There was also a wide range of necrosis among tumours sampled, with some of the tumour masses on MR imaging composed of up to 45.5% necrosis, making it more likely that necrotic material could be sampled in these cases.

Non-diagnostic sampling errors, of around 10 %, occur even with stereotactic biopsies, which are calculated to a submillimetre precision level^{253–255} and so it is not surprising that errors in tissue sampling may occur in a study such as this where a 1 – 2 cm tissue section is resected. Evidence suggests that diagnostic yield is increased by the number of samples obtained, as well as the number of sites biopsied.²⁵⁴ The current study, guided by ethical considerations, only obtained a small portion of the gross tumour specimen, from one area of the tumour, after adequate samples had been obtained for clinical diagnosis and molecular marking. As such, tissue maintained in chip, could have included varied amounts of necrotic tissue or only partially invaded brain tissue; the degree in which this occurred is difficult to quantify as only 1 or 2 tissue specimens were processed for histological analysis, with the assumption that those tissues processed were representative of that particular tumour on chip. Indeed, histological analysis did identify at least 5 samples that contained areas not representative of cellular GBM. Regional heterogeneity means that the behaviour of two chips containing tissue from the same patient and even from the same region of the tumour could behave very differently as the tissue behaviour in the chip will be determined by the predominant tissue type within that particular chip. As such, results of individual chip tissue need to be approached with caution and large standard deviations are to be expected, with a lot more weight given to the mean tissue response. Looking forward and beyond this preliminary study, an approach would be to obtain multiple biopsies from different parts of the tumour mass at surgery (including samples from the tumour-brain interface); analysing the samples both on chip and histologically to better understand the relationship between histological findings and tumour behaviour on chip, as well as the behaviour of cells/tissue in various parts of the tumour.

3.1.6.2 Warm Ischaemic Time and the Effect of flow

The length of time in which a tissue remains without perfusion with blood or media is referred to as the warm ischaemic time (WIT).²⁵⁶ The term is commonplace in transplant surgery and highlights that the tissue, while un-perfused is not cooled for cryopreservation. In the current study, there was no correlation between the WIT of the tissue and viability, when assessed with regression analysis. This was despite the fact that there was a statistically significant difference in the viability of tissue processed immediately, and that processed after an hour delay in 3 experimental runs (See Figure 3.7a). Studies looking at the effects of WIT on tissue have found that the length of time without perfusion has an impact on the health of the tissue. Hosgood *et al* found that excised porcine kidneys with a WIT of 15 mins, had significantly better renal function (including creatine clearance, oxygen consumption and renal blood flow) when the tissues were re-perfused, than kidney tissue exposed to 90 or 120 mins of WIT.²⁵⁷ Significantly the group found that the negative effects of warm ischaemic time were most marked in the first hour of reperfusion with particularly higher levels of Neutrophil Gelatinase-Associated Lipocalin, a marker for acute kidney injury, during this time.²⁵⁸ Similarly, longer *ex vivo* WIT has been linked with reduced cell viability and lower engraftment rate of lung tissue xenografts,²⁵⁹ while being shown to have detrimental effects on the histological and morphology of tissue.²⁶⁰ All the papers cited define a critical WIT of 90 – 120 mins and this may explain why there was no significant effect on WIT of GBM tissue as only two samples had a WIT of greater than 90 mins.

By utilising microfluidic principles, the current study perfused tissue with a continuous influx of nutrients as well as removed waste products at a constant rate. Earlier iterations of this device had maintained human tissues successfully with a flow rate of 2 μl per min. A different dual flow device maintained human bowel explants at higher flow rates of 4 μl per min with low levels of LDH release.²⁶¹ Studies on animal brain slices maintained much smaller tissue sections (350 - 500 μm thick) within a wide range of flow rates between 0.3 μl – 17 ml per min.^{158,159,162,163} The rate of perfusion is specific for each device and should be appropriately adjusted depending on the nutrient media used, as well as the tissue

type and thickness. Normal cerebral blood flow is approximately 50 ml per 100 g of tissue per minute but in GBM the cerebral blood flow can range between 39–82 ml/100 g/min.²⁶² This equates to a rate of 4-8 μ l/min per 10 mg of tissue; a rate that was matched during our experiments with flow of media at 4 μ l per min for GBM tissues of an average wet weight of 12.1 mg. With higher flow rates, there is a theoretical risk of increased tissue damage from shear stress¹⁵¹ but in the current study, the flow increment did not have a detrimental effect to the tissue with respect to tissue viability and LDH released. In fact, there was a statistically significant improvement in tissue viability with flow rates of 4 μ l per min compared with 2 μ l per min. The benefits of continuous flow of nutrient media flow over static tissue cultures has been stressed in previous studies. Originally, Reid *et al.* found that electrical activity within hippocampal brain slices from rats failed if the flow underneath the tissue stopped for over a minute.²⁶³ Rambani *et al.* proved that viability of their brain slices was significantly better if the tissue was perfused at 20 μ l per hour compared to un-perfused tissue slices¹⁵⁹ and recently Killian *et al* were able to show that perfusion of brain tissue correlated with an improvement in tissue maintenance as measured by viability of the cells, as well as the thickness of the tissue mantle, which thinned significantly with un-perfused tissue during experimentation.¹⁵⁶ These results were similar to the findings in this study where tissue maintained with flow outperformed static tissue cultures in terms of cell viability, LDH release and morphological appearance. Nonetheless, the results of tissue maintained in static culture and that of tissue left in media for days without any replacement of the media is striking and reinforces the results of previous *h*GBM tissue cultures and highlights the resilience of GBM tissue and cells outside the body; making this tissue an ideal candidate for *ex vivo* studies.

3.1.6.3 Nutrient Media

During the study, three different media solutions were used to maintain the GBM samples, with no significant difference in the viability or LDH released. Studies involved in culturing human brain or GBM tissue have used a variety of nutrient media but have mainly included a balanced salt solution, supplemented with 10-20 % of FBS.^{208,209,264,210,212} These studies all reported adequate viability of the maintained tissues, even with static culture techniques. *h*GBM cell cultures have also

been grown into tumour spheroids or cellular monolayers with media supplemented with FBS.^{265,266} A number of examples, in the literature, of U87 cells cultured using similar nutrient media attest to the benefits of media supplemented with serum.^{98,200,267,268} The literature on the media used for the culture of GBM tissue and glioma cells aligns with the work done on the microfluidic device with acute tissue sections from liver, head and neck cancers and colorectal cancer; all maintained within the device with DMEM media (High Glucose 4.5g/L without L-Glutamine) supplemented with 10% FBS.^{180,218,243,245} As such, the GBM samples in this study were maintained with the same media and supplements as those used on previous microfluidic tissue systems. However, inconsistencies in the results of the first 10 GBM patient samples maintained on chip demanded a review of the nutrient media used, amongst other factors, to improve viability of the GBM specimens.

The historical development of nutrient media used for acute brain tissue slices date back to the works of Nicoll and Alger on interface chambers who cultured rodent brain tissue slices using a balanced salt solution (Earle's Solution).¹⁵⁵ Stoppini *et al.* characterised a nutrient media solution that introduced the addition of HEPES buffer, horses serum and Hank's solution in modified Eagle media for culture of brain slices.¹⁴¹ However the use of serum containing media in brain tissue was called into question as research showed a trend for serum containing media to promote glial proliferation over neuronal growth.²⁶⁹⁻²⁷¹ Most cell types require some serum for optimal growth in culture as the serum contains crucial energy substrates, hormones, growth factors, cytokines, and carrier proteins.^{272,273} With this in mind, Brewer *et al.* developed a serum-free media (Neurobasal), which when supplemented with a medium supplement (B27), contained essential factors for improved neuronal cell growth within organotypic slices. A caveat to this was that the media had a negative effect on the glial cells and glioma cells.²⁷⁴ The group felt that the positive effects of Neurobasal were due to the reduced osmolarity, high glutamine and the elimination of toxic ferrous sulphate. However, Eugène *et al.* found that the Neurobasal/B27 medium performed poorly in the maintenance of *human* temporal lobe tissue and as such, developed a new nutrient media with lower levels of glutamate and an enriched mixture of D-glucose, lactate and pyruvate.²⁷⁵ Schwarz *et al.* showed that human cerebrospinal fluid (CSF) solutions (obtained from patients with normal pressure hydrocephalus) performed better at maintaining human organotypic slices and

increased survival of neurons, intact network and cellular function compared to slices kept in media based culture.²⁷⁶ Importantly, the group also showed that glial cells remained intact when cultured with human CSF. Similar results were found using human CSF solutions on rat hippocampal brain.²⁷⁷ With various recipes of aCSF in existent,²⁷⁸ and various brands commercially available, the use of artificial CSF appears to be an alternative nutrient media for scientist who culture acute thick brain slices.^{151,157,164,279} In the current study, artificial CSF was prepared using a recipe from a reputable lab²²⁰ and the efficacy of this solution, as an alternative nutrient media, was tested in 8 GBM samples and compared against the media containing FBS. Though there was no difference in viability of the matched pair samples, it appears that serum-containing media is as effective as aCSF media solutions in maintaining GBM tissue (*See Table 3.2*).

It is important to note that although the tissue being maintained in the chip originates from the brain, the tumour itself is glial in origin and as such, utilising media that favours neuronal cells over glial cells such as serum-free media is likely to be detrimental to the growth/maintenance of GBM tissue. Interestingly, two groups have successfully maintained *h*GBM tissues in static cultures using medium that did not contain serum, or human/artificial CSF. Instead, the groups utilised media composed of Hank's Balanced Salt Solution supplemented with N-hydroxysuccinimide and L-glutamine.^{213,214} This nutrient media solution offers an alternative solution that can be explored in future research aimed at optimising the maintenance of GBM tissue.

The use of serum containing media, also exposes the GBM tissue to exosomes, that are naturally occurring within serum. Exosomes are vesicles of endocytic origin, released from cells into the extracellular space and are involved in cellular signalling to modulate the extracellular milieu.^{280,281} Though there are wide range of extracellular vesicles, including microsomes and apoptotic bodies, exosomes are usually 40-120 nm in diameter, formed from the inward budding of multivesicular bodies, and contain mRNA, cytoplasmic and membrane proteins.²⁸² Their significance in essential biological processes is becoming more apparent with increasing evidence of their role as “couriers” in delivering protein and RNA messages to cells they come into contact with.²⁸³ Exosomes have been reported to

transmit transcription factors,²⁸⁴ oncogenes,²⁸⁵ growth factors and their receptors,²⁸⁶ mRNA and infectious particles²⁸⁷ into recipient cells and thus can be regarded as multifunctional signalling complexes for controlling fundamental cellular and biological functions. In cancer, exosomes secreted from cancer cells, are involved in reprogramming the environment to favour tumorigenesis and are involved in priming distant tissues for metastatic invasion.^{288,289} In GBM, exosomes have been shown to be involved in immune modulation, metabolic regulation and angiogenesis.²⁸¹ As the scientific community comes to terms with the implications of exosomes, a few groups have begun to explore therapeutic avenues. Exosomes derived from mesenchymal stem cells have been shown to promote recovery of cardiac myocytes after cardiac injury, as well as enhance angiogenesis and reduce the degree of fibrosis.²⁸³ ExoPr0, is an experimental drug that has been shown in pre-clinical studies to significantly reduce proliferation of GBM cell lines.²⁹⁰ The drug company ReNeuron developed a process for purifying exosomes from stem cells and are looking to start phase one clinical trials on the background of successful *in vitro* studies. In order to test the efficacy of the drug ExoPr0 on *h*GBM tissue, the standard media was supplemented with exosome-depleted (instead of FBS), to examine the effects of media without exosomes on the tissue, prior to drug treatment. Previous work has found exosomes within serum to be crucial in the proliferation of cardiac progenitor cells²⁹¹ and skeletal muscle.²⁹² Aswad *et al.* cultured a number of cells, including human U87 glioblastoma, human, HeLa cells and neuroblastoma cells in two different media; one containing 10% (v/v) FBS and the other with 10% (v/v) exosome-depleted FBS. The results showed that, the exosomes were internalised into the cells and (except for U87 cells) promoted growth. Cell lines grown in the presence of exosome-depleted media had significantly reduced growth rates when compared to cells grown in media containing exosomes.²⁹² For an unknown reason, the glioblastoma cell lines were resistant to the negative effects of exosome depletion and growth was comparable to that of U87 cells grown in media containing exosomes. This finding can be extrapolated to support the current study, where there was no difference in the viability of GBM tissue when maintained with exosome free media as compared to normal FBS media.

3.1.6.4 Blockages

To prevent recurrent blockages of the device, the chip was modified by inserting a mesh layer to form a semi-permeable membrane between the tissue and the micro-channels. Such a modification can have a significant effect on the direction of flow within the device. Previously, flow within this device has been characterised with computational studies to show that Reynold numbers are less than 1 with viscous forces dominating over inertial energies, promoting a flow that is laminar.²⁴⁵ As such, the introduction of the mesh layer, has the potential to restrict the nutrient media from perfusing the tissue, or even disrupting the laminar flow and introduced a degree of turbulence. Yet, tissue maintained in the device after the introduction of the mesh was significantly more viable (with Annexin V and PI assays) and released comparable levels of LDH. The tissue mesh also significantly reduced the rate of chip blockage and improved efficiency of the device, with the optimised set-up having only 3 out of 90 device blockages. With a model that allows successful maintenance of GBM without blockages or leakages in 96.6% of cases, the use of the method as a viable pre-clinical model can challenge current options such as patient derived xenografts, which currently have an engraftment rate that can be as low as 22%.²⁹³

Uncertainty arises as to why the tissue viability improved with the mesh as opposed to without and this will require further investigation. One possibility is that the mesh may have acted as a wick, drawing up nutrients down a concentration gradient and improved the tissue perfusion, similarly to the pattern of nutrient supply seen with interface chambers used to maintain brain tissue slices.^{152,154} Flow studies carried out utilising fluorescent labels to assess tissue penetration with and without the mesh were inconclusive (*see Appendix 3*) due to the auto-florescence of the tissue, likely due to lipofuscin,^{294–296} which is associated with autofluorescence of brain tissue within the same spectrum of the fluorescent marker used PKH26. Further studies with appropriate fluorescent markers as well as fluid flow modelling would allow evaluation of the distribution of flow and guide device modifications. Alterations to the direction of flow, from the parallel axis of the tissue to flow that is perpendicular to the tissue has the potential to improve viability of tissue. Vukasinovic *et al.* describe the advantages of forced convection interstitial perfusion for long term

maintenance of tissue slices over superfusion and capillary wicking of tissue placed above a porous membrane.¹⁵⁶ Future experiments could compare forced convection with passive diffusion to better understand the parameters involved in tissue maintenance. Such a modification would require only minor amendments to the basic units of the device and how it is assembled.

4.1 Analysis of GBM Tumours using a Microfluidic Device

4.1.1 Study Results

4.1.1.1 Overview

A total of 36 patients were approached for recruitment over a 21-month period (April 2016 - October 2017). Recruitment was stopped at the 18-month period to allow adequate time for data interpretation and analysis. One patient refused consent into the study and two patients were excluded as they were unable to give informed consent due to reduced cognition. In total 33 patient tumour samples were available for analysis. Sample acquisition was performed by 8 different surgeons and ranged from large 2 cm tissue slices of debulked tumour to biopsies obtained using a kerrison rongeur or a needle biopsy. Tumour samples placed within the MF device were from a cohort summarised in *Table 4.1*. The average age of the group was 59.2 years (+/- 11.7; Range 38-81). Of the 33 patients whose samples were analysed on a chip, 25 had a histological diagnosis of Glioblastoma. A further 3 had mixed features of Glioblastoma and an Anaplastic Astrocytoma. Five patients had a diagnosis that was not GBM, including a *Schwannoma*, a *Gemistocytic Astrocytoma*, an *Anaplastic Oligoastrocytoma* and 2 *Anaplastic Astrocytomas*. Of those that were GBM, all had the IDH 1 wild type gene. MGMT methylation was only tested in 7 patients, out of which, 1 patient was verified as having methylation status. Two patients had a TERT mutation, which is associated with an overall poorer prognosis.²⁹⁷ Within the cohort, a biopsy was performed for 2 of the patients with another 31 patients having a surgical debulking of the tumour. Biopsy was usually performed for cases in which the diagnosis was uncertain or where the tumour was located in an eloquent area that meant surgical debulking carried greater risks than benefits for the patient. *Table 4.1* displays the demographics of the patients included in the study.

<i>Patients Recruited (n = 33)</i>	<i>No.</i>
<i>Age</i>	59.2
<i>Sex (M : F)</i>	2.3 : 1
<i>WHO Grade Tumour</i>	
<i>GBM IDH1 Wild Type</i>	23
<i>GBM IDH Status Unknown</i>	1
<i>Gliosarcoma</i>	1
<i>Anaplastic/GBM IDH1 Mutant</i>	3
<i>Anaplastic Oligoastrocytoma IDH1 Mutant*</i>	1
<i>Schwanomma Grade 1*</i>	1
<i>Anaplastic Astrocytoma IDH1 Wild Type*</i>	2
<i>Gemistocytic Astrocytoma IDH1 Mutant*</i>	1
<i>Primary Tumours</i>	29
<i>Recurrent Tumours</i>	4
<i>Surgical Resection</i>	
<i>Debulking</i>	31
<i>Biopsy</i>	2

Table 4.1: Histological types and demographics of patients included in the study.

** Indicates non-GBM Tumours*

4.1.2 Viability of GBM on Chip

4.1.2.1 Annexin V and Propidium Iodide

Flow cytometry analysis of matched pairs (n = 26; though there were 28 GBM samples, only 26 had matched paired analysis of Annexin V and PI) of fresh and chip tissue samples showed mean viability of **68.9%** (+/- 29.8) and **61.1%** (+/- 28.3), respectively. Though the mean difference between the two groups was less than 8%,

this difference was statistically significant when analysed with a paired t-test; $P = 0.01$ (Figure 4.1).

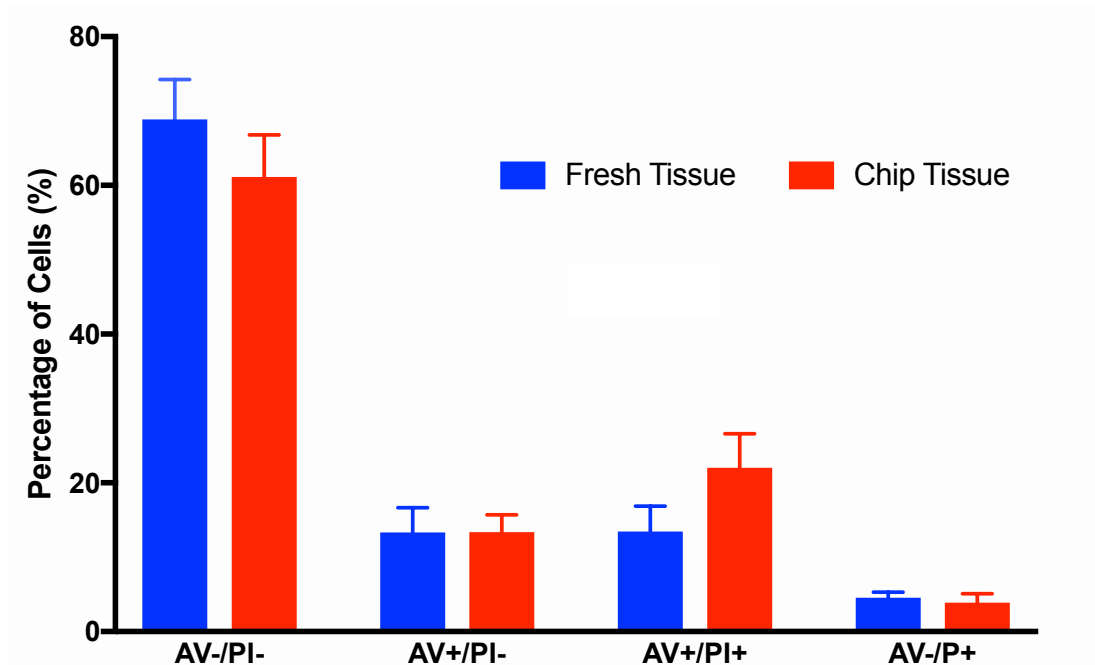


Figure 4.1: Histogram of flow cytometric analysis of Matched Pairs (Fresh Tissue and Chip Tissue), used to quantify healthy cells (AV-/PI-).

Histogram of 26 matched pairs of tissue (Fresh Tissue vs. Chip Tissue) to show the fate of disaggregated cells after Annexin V and PI staining and stratification with the Flow Cytometer. The difference in healthy cells (AV-/PI-) between fresh tissue (68.9%) and chip tissue (61.1%) was statistically significant with a paired t-test; $P = 0.01$.

Stratifying the results according to diagnosis allowed an analysis to see if other tumours within the cohort behaved differently to tissues confirmed to be GBM. This showed that GBM tissue viability ($n = 27$) was greater than lower grade tumours ($n = 5$), with a mean viability of Grade 1-3 tumours at 31.8% (+/- 17.2), compared to GBM tissue which had a mean viability of 60.1% (+/- 28.8). This difference was statistically significant with a P value (t-test) of 0.01 as exemplified in Figure 4.2.

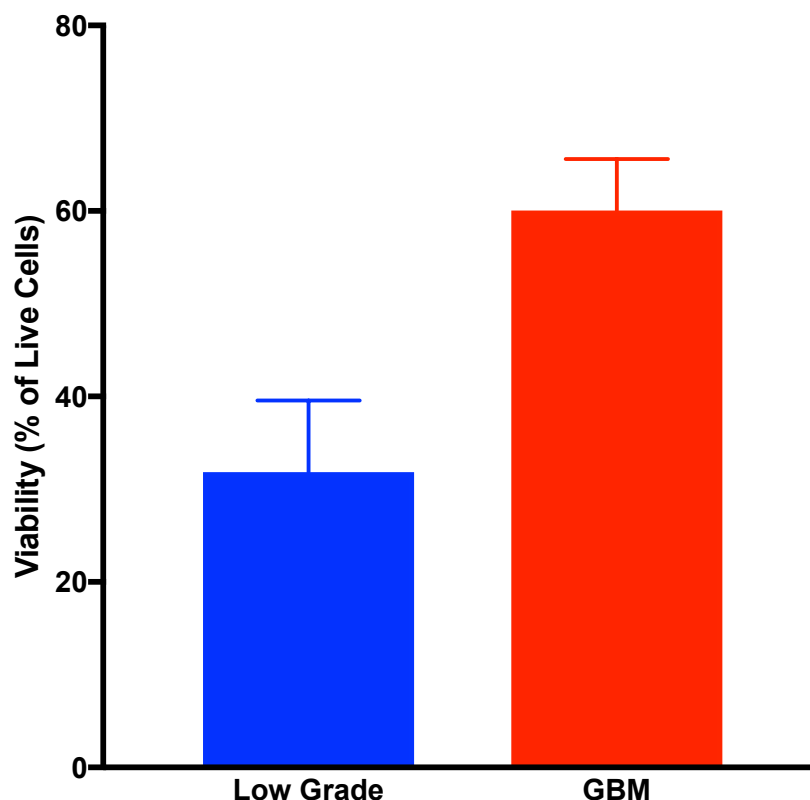


Figure 4.2: Histogram of viability according to tumour grade.

Bar graph comparing the viability (determined by Annexin V and PI) of GBM ($n = 27$) tissues on chip with tumours other than GBM ($n = 5$). $P = 0.01$.

4.1.2.2 Trypan Blue

In parallel to the Annexin V/PI viability assay, trypan blue staining of cells and counting on a haemocytometer allowed visual confirmation of cell viability via dye exclusion. This was performed on the disaggregated cells from fresh tissue and chip tissue ($n = 19$), with 6 fresh tissue and chip tissue matched pairs. The results from the 6 matched pair samples revealed mean cell viability of 73% (+/- 14.2) for fresh tissue and 61% (+/- 26.4) in tissue that had been maintained within the microfluidic device for 72 h. The differences between the two means was not statistically significant ($P = 0.16$; paired t-test – see *Figure 4.3*).

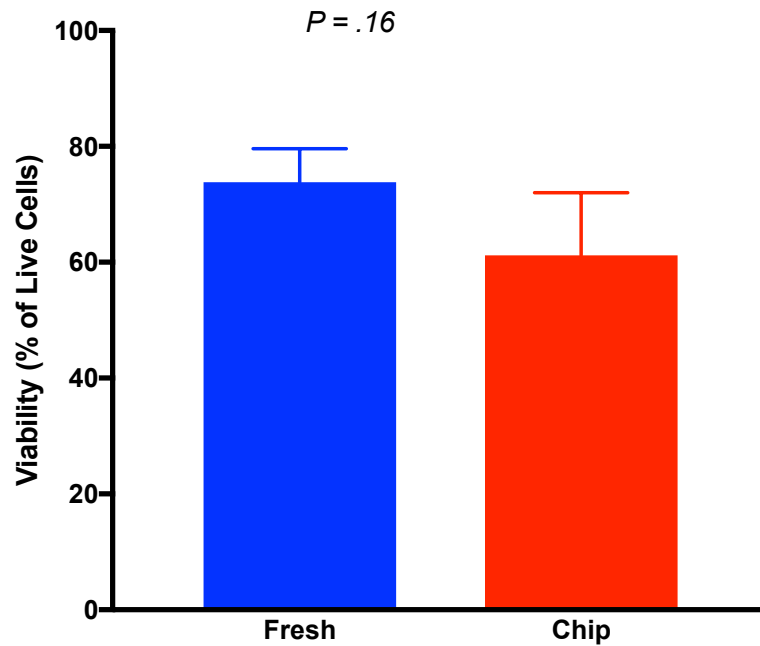


Figure 4.3: Fresh and Chip Tissue viability according to Trypan Blue.

Mean cell viability as measured with trypan blue stained cells from disaggregated fresh tissue (n=6) and chip tissue (n=6); 73 % and 61 %, respectively. *t*-test showed no significant difference; $P = 0.16$.

In total, 19 trypan blue cell viability assays were performed which when compared to the Annexin V/PI assays showed a positive correlation, with an r^2 value of 0.78, suggestive that there is a strong linear relationship between the two methods of assessing viability (see *Figure 4.4*).

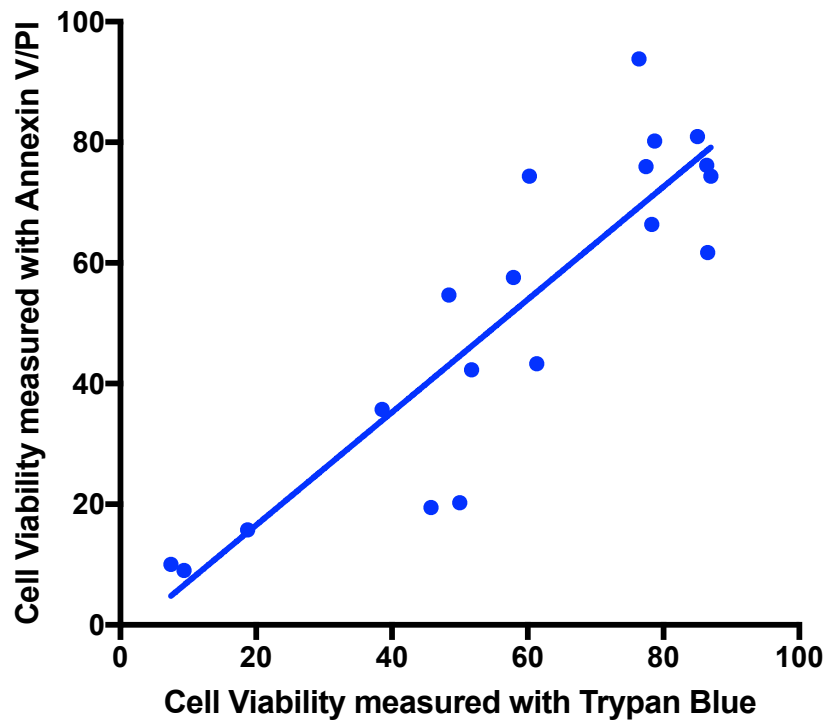


Figure 4.4: Correlation between two viability assays.

Comparing viability according to trypan blue (*x* axis) with viability according to PI/Annexin V (*y* axis). There was a linear relationship between the two tests with an r^2 value of 0.78.

4.1.2.3 LDH Absorbance

4.1.2.3.1 LDH released into effluent

The pattern of LDH release from chip tissue has already been summarised in *section 3.1.2.2*. This is primarily one in which there is an initial peak in LDH absorbance (previously attributed to tissue dissection and handling) followed by a low and steady state of absorbance.¹⁷⁹ *Figure 4.5* summarises the average LDH released at set time points during all experiments and confirms this pattern of LDH release.

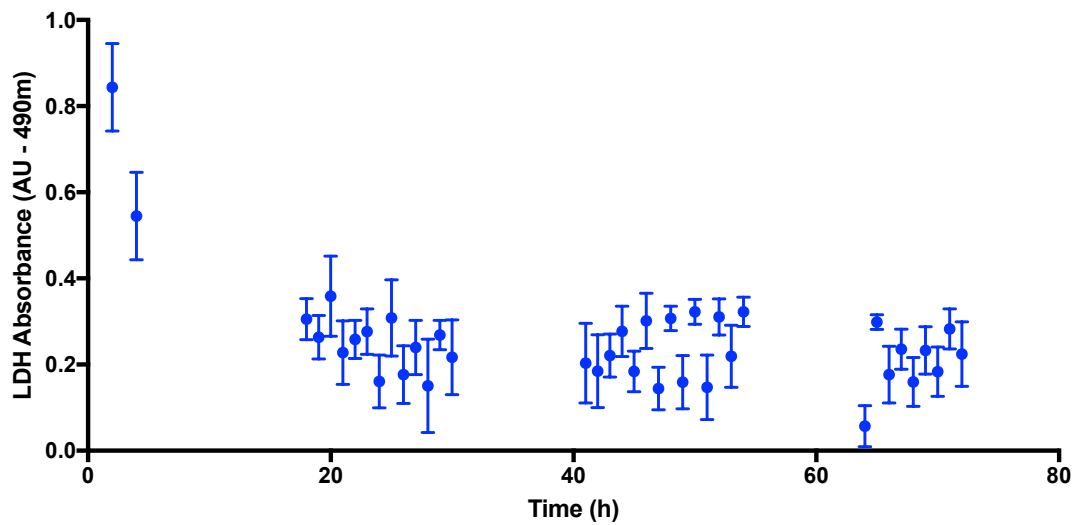


Figure 4.5: Average LDH absorbance over 72 h time period.

Graph displaying the average absorbance values for each time point from all experiments e.g. the average absorbance of all effluent samples collected at 2 h (first value on graph) after the start of the experiments was 0.84 AU. 4 h after the start of the experiments, the average absorbance from the effluents collected was 0.54 AU etc. The graph confirms the trend of an initially high LDH absorbance, followed by a low and stable absorbance value.

4.1.2.3.2 LDH absorbance after infusion with lysis solution

Proof that viable tissue remained at the end of experimentation was achieved by lysing the tissue on chip with the lysis agent and assessing for an increase in LDH absorbance. This was performed on 8 GBM samples run within the microfluidic device; all at the 71st hour. The introduction of the lysis solution usually led to an increase in the LDH released (measured by absorbance), exemplified in the 6th patient, where there was a 4-fold increase in the amount of LDH released after the introduction of the lysis solution (see Figure 4.6a). Analysis of all the effluent samples collected immediately after introduction of the lysis solution revealed on average, a 3-fold increase in LDH (see Figure 4.6b).

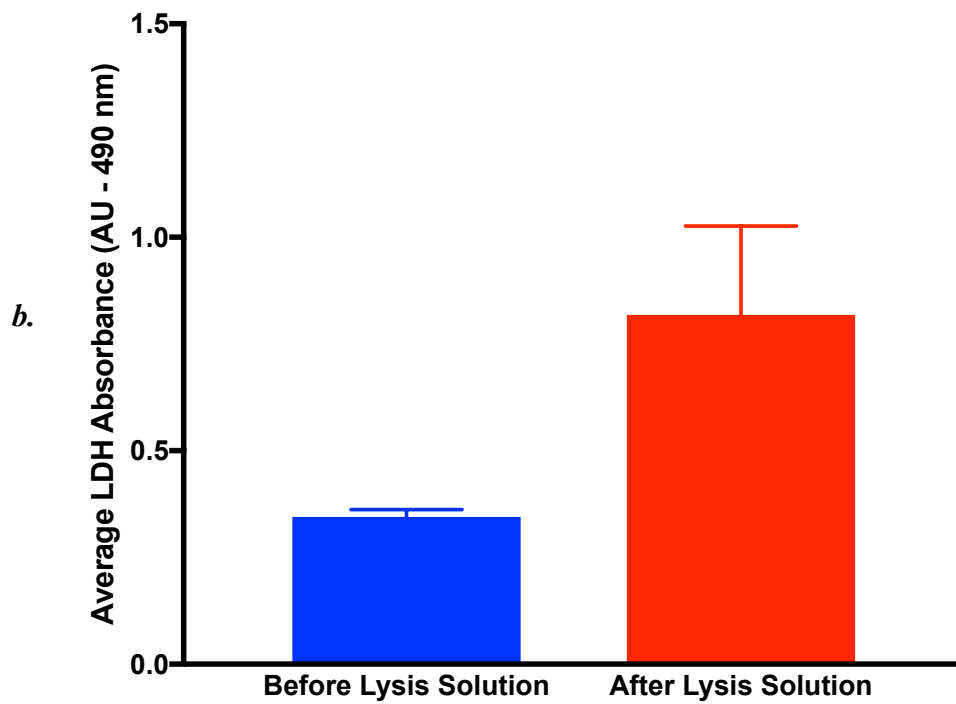
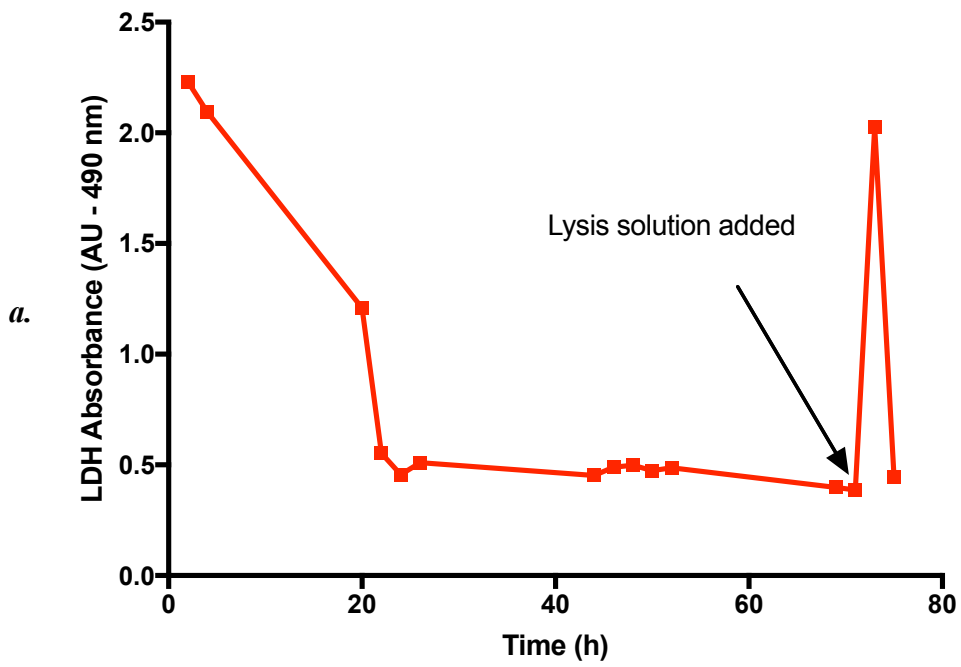


Figure 4.6: Effects of tissue lysis on LDH Absorbance

a. LDH absorbance over time in the 6th patient, where there was a 4-fold increase in LDH absorbance after introduction of the lysis solution. *b.* Mean LDH absorbance an hour prior to, and an hour after the introduction of the lysis solution in 8 experimental runs.

4.1.2.4 H&E

Maintaining tissue within the microfluidic device for 72 hours did not disrupt the tissue architecture when H&E sections were compared to fresh tissue samples. In particular, there was no difference in cellular architecture within peripheral portions of the tissue section compared to the central portion suggestive that there was diffusion of nutrients to the whole specimen within the device. *Figure 4.7* compares fresh tissue with tissue maintained in the device for 72 h.

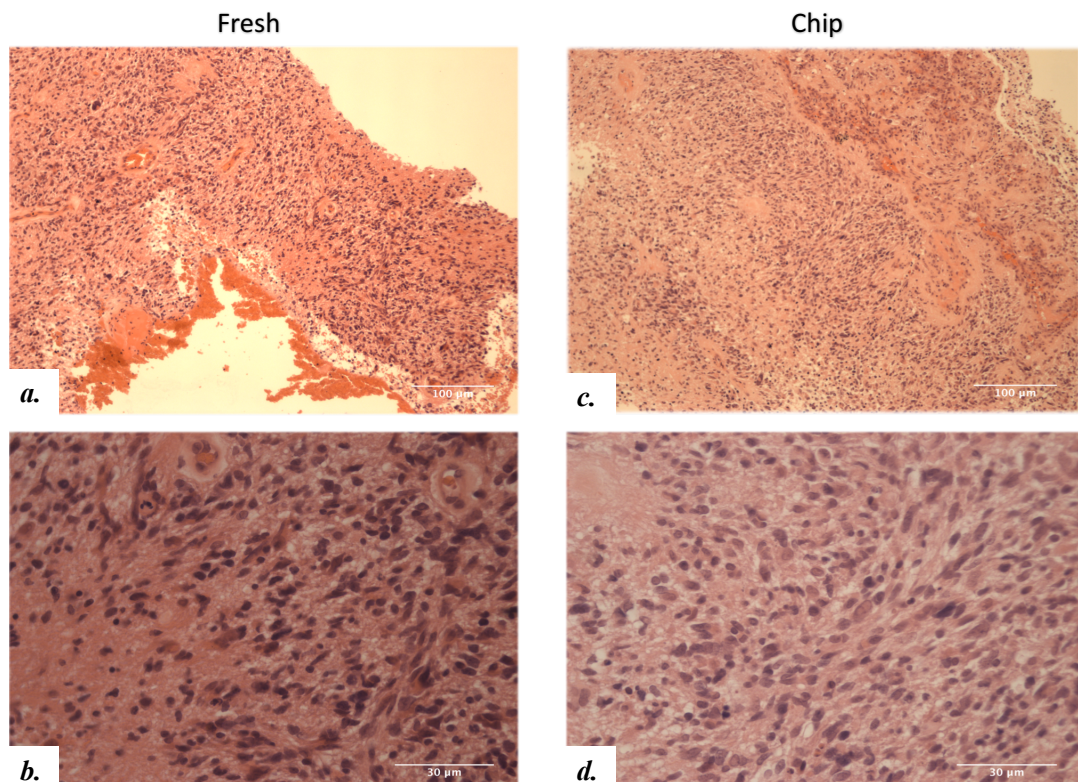


Figure 4.7: Representative images of H&E sections of GBM tissue

- *GBM sections processed immediately from the patient (a. x100 magnification b. x400 magnification)*
- *GBM tissue sections after maintenance within the microfluidic device for 72 h (c. x100 magnification d. x400 magnification).*

4.1.2.4 Immunohistochemistry

Similarly, immunohistochemical markers were relatively well preserved on chip over the 72-h period when compared to fresh tissue. *Figure 4.8* is an example of Ki67 staining of fresh tissue that was maintained for 72 h on chip. Proliferation indices ranged from 0.7 - 41%. The average proliferation index amongst 14 matched pairs (fresh and chip tissue) was 16.6% (+/- 15.5) for fresh tissue compared with 15.9 % (+/- 17.7) for chip tissue. There was no statistical significance between the two means. *Figure 4.9* displays the results in a graph format.

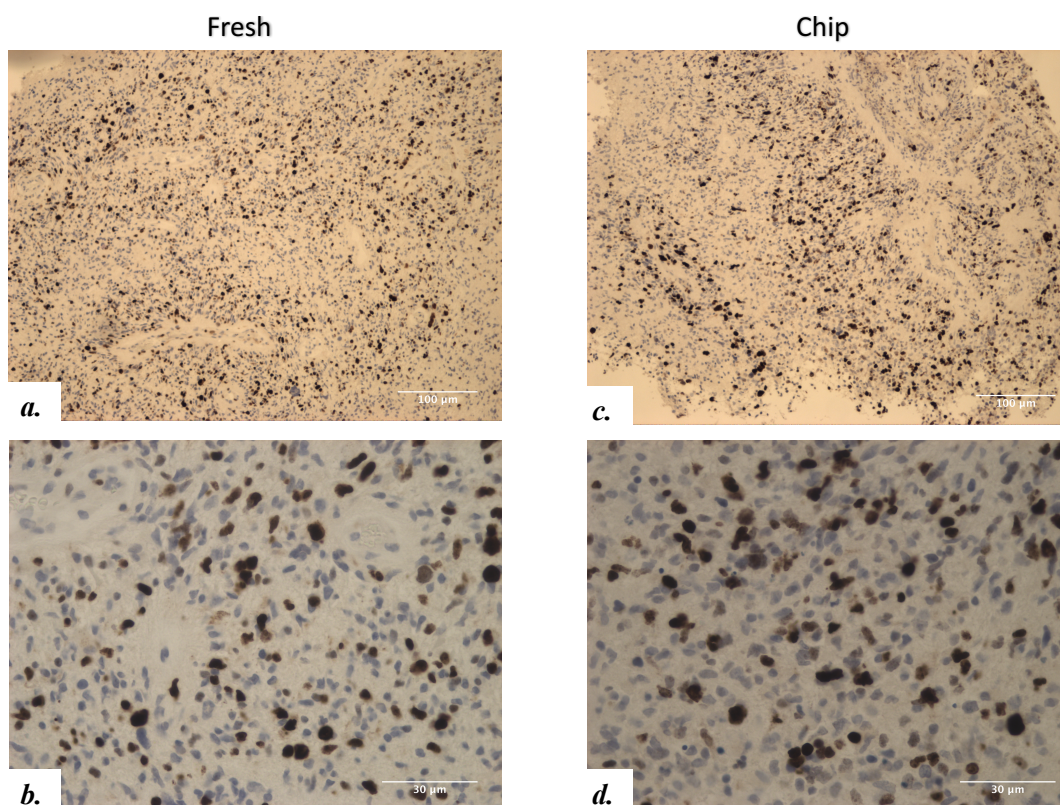


Figure 4.8: Representative IHC of GBM tissue (Ki67; n = 14)

- GBM sections straight from the patient (a. x100 magnification b. x400 magnification)
- GBM tissue sections after maintenance within the microfluidic device for 72 h (c. x100 magnification d. x400 magnification).

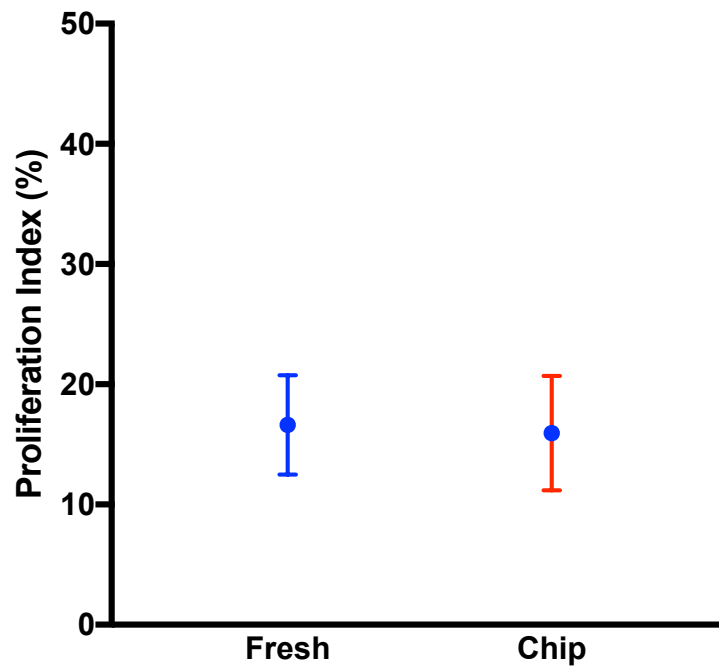


Figure 4.9: Proliferation indices (Ki67 staining) of Fresh Tissue and Chip Tissue

Average proliferation index for Fresh tissue (stained immediately) and Chip tissue (stained after 72 h in the microfluidic device) n = 14 paired tissue samples. P = 0.74

Caspase 3 staining of tissue, (13 matched pairs) did not show any difference between fresh tissue and chip tissue. There was marked nuclear staining of Caspase 3 in fresh tissue and chip tissue with average apoptotic indices of 38.9% (+/- 23.9) and 44.4% (+/-21.3), respectively. This pattern of staining, though described, is not as common as the more cytoplasmic location of Caspase 3.²⁹⁸ There was again, no statistical difference in apoptotic indices (paired t-test; *p* value 0.14). Figure 4.10 & 4.11 summarises these results.

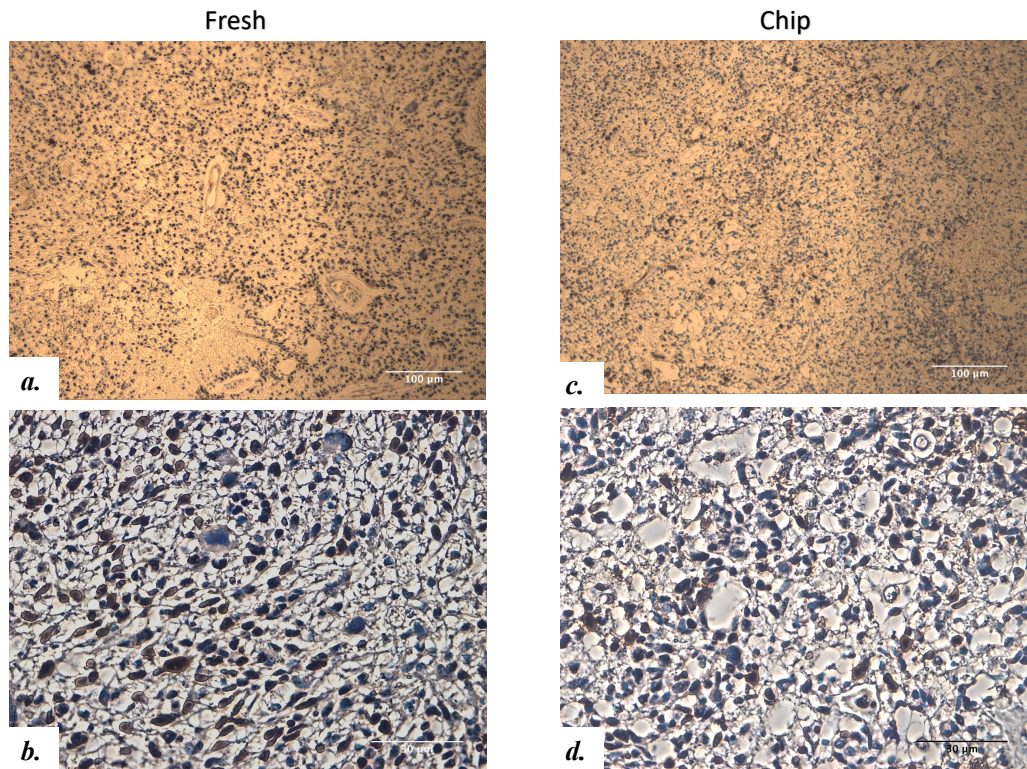


Figure 4.10: Representative IHC of GBM tissue (Caspase 3; n = 13)

- GBM sections straight from the patient (**a.** x100 magnification **b.** x400 magnification)
- GBM tissue sections after maintenance within the microfluidic device for 72 h (**c.** x100 magnification **d.** x400 magnification).

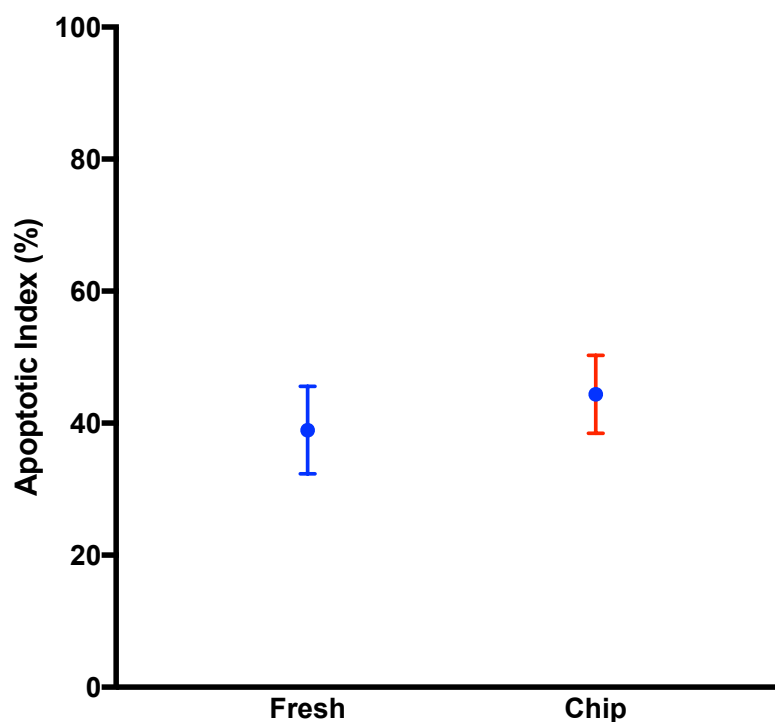


Figure 4.11: Apoptotic indices (Caspase 3 staining) of Fresh Tissue and Chip Tissue.

Average apoptotic index (Caspase 3 staining) for Fresh tissue (stained immediately) and Chip tissue (stained after 72 h in the microfluidic device); $n=13$ paired tissue samples. $P = 0.14$

4.1.3 Drug Treatment

The effect of two drugs on *ex vivo* GBM tissue was assessed. The drugs tested were the alkylating agent TMZ and various concentrations of exosomes in the form of the drug ExoPr0.

TMZ was tested on 6 patient samples. Viability was not affected by the perfusion of the GBM tissue with 100 μM TMZ over 48 h when compared to tissue perfused with the DMSO control or the standard media. Mean viability was 47.2% (+/- 22.5) with TMZ treatment, compared to 53.2 (+/- 25.6) with the control and 42.7% (+/- 26.9) with the standard media. A one-way ANOVA analysis revealed that there was no significant difference between the three mean viabilities; $P = 0.49$. As well as there

being no difference in the viability, there was no difference in histological appearance of the tissue (H&E and IHC – n = 2).

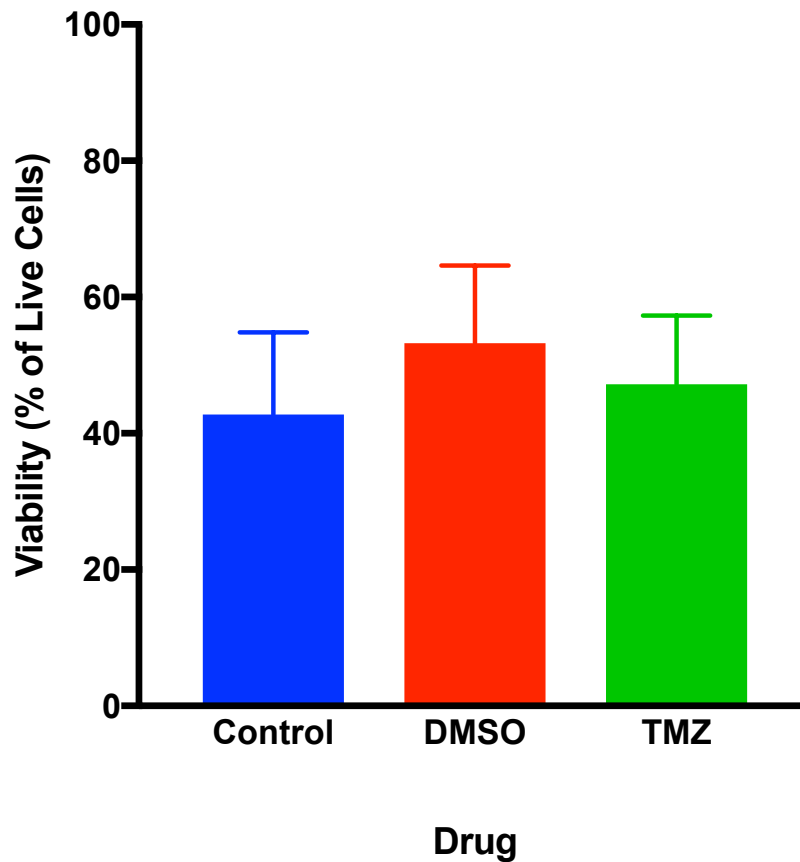


Figure 4.12: Effects of TMZ on GBM on Chip.

Tissue viability of 6 matched samples (with Annexin V and PI assay), perfused with standard media (blue), DMSO (red) and 100 μ M of TMZ (green).

Although there was no difference in the average viability of the tumour samples treated with MGMT, compared to controls, one patient's (16028) tumour appeared to respond to drug treatment with viability in the tumour treated with TMZ at 54.7%, compared to 60.5% with DMSO and 74.4% with standard media alone (see Figure 4.13).

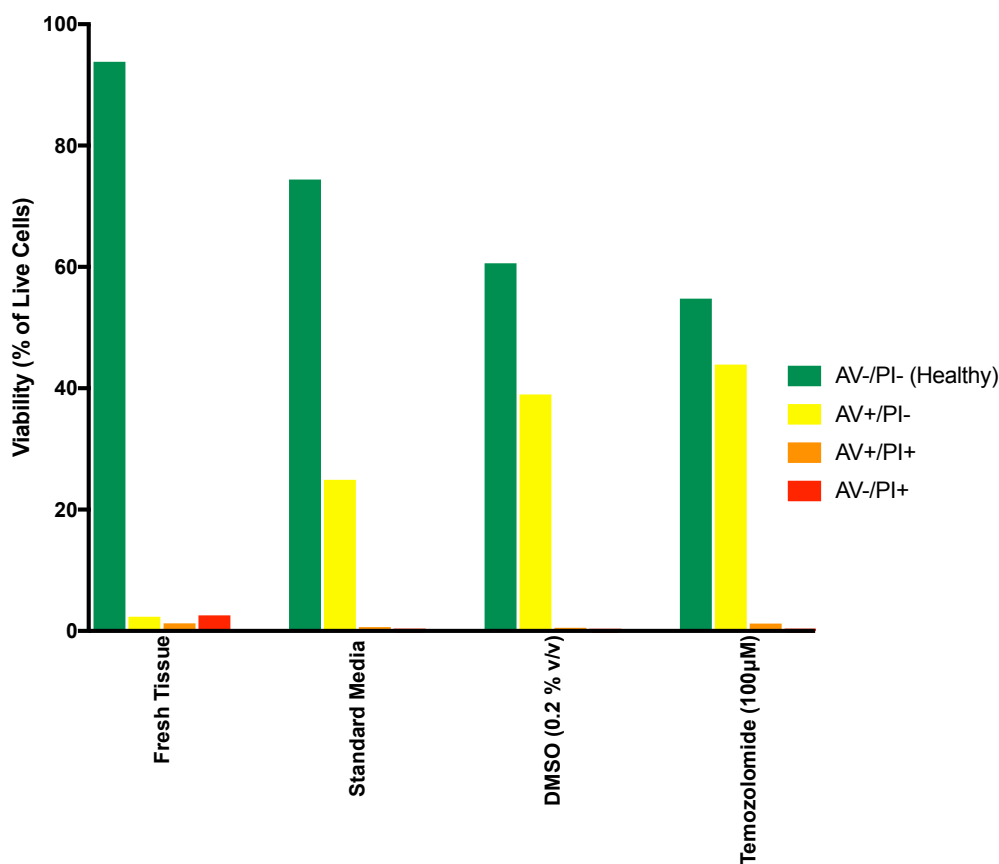


Figure 4.13: The effect of TMZ on GBM from Patient 16028.

Graph displaying the effect of TMZ in the one patient with a clear stepwise reduction in viability (assessed with Annexin V and PI assay) and corresponding increase in apoptosis (AV+/PI-). Note increased apoptosis with DMSO, which is even greater with TMZ (dissolved in DMSO).

Analysis of 6 GBM tissue samples perfused with the experimental drug ExoPr0 were compared to tissue perfused with exosome-depleted media. There was no significant difference in viability specimens were compared, nor when compared to tissue perfused with standard media. One-way ANOVA analysis did not reveal any statistically significant difference in mean viability (see Figure 4.14).

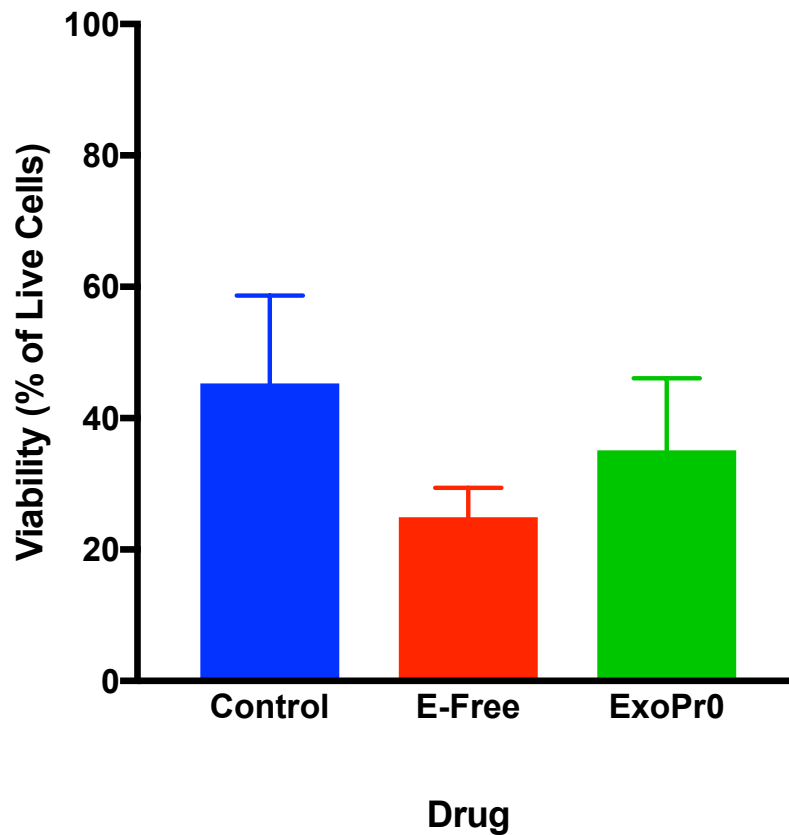


Figure 4.14: Effects of ExoPr0 on GBM on Chip.

Tissue viability of 6 matched samples (viability assessed with Annexin V and PI assay), perfused with standard media (blue), exosome-depleted media (red) and ExoPr0 (green).

Of note, there was no change in the histological appearance of the tissue that was treated with TMZ or ExoPr0 (compared to controls), nor a difference in the proliferation or apoptotic index of the tissue when tested with immunohistochemistry.

4.1.4 Correlation with Clinical Outcomes

Data analysis was completed just under 3 months after the last patient was recruited. At the time of writing, 13 of the 33 patients recruited had lost their lives to their disease. *Figure 4.15* is a Kaplan Meier curve predicting the survival trend for the

study. All the deaths occurred in patients with a Grade 4 Glioma, except one patient who had a histological diagnosis of an Anaplastic Astrocytoma (Grade 3) but with an IDH Wild Type Mutant, which is associated with an aggressive phenotype and poorer prognosis.⁵³ Survival was between 72 and 460 days. There were 5 patients with recurrent disease; one who was having his 3rd operation for GBM and four having surgery for the second time. Of the five recurrent patients, two remained survivors at the time of analysis. Recurrent patients included in the study had their time of survival calculated from their initial operation. All patients recruited in the study only had one operation during the study period.

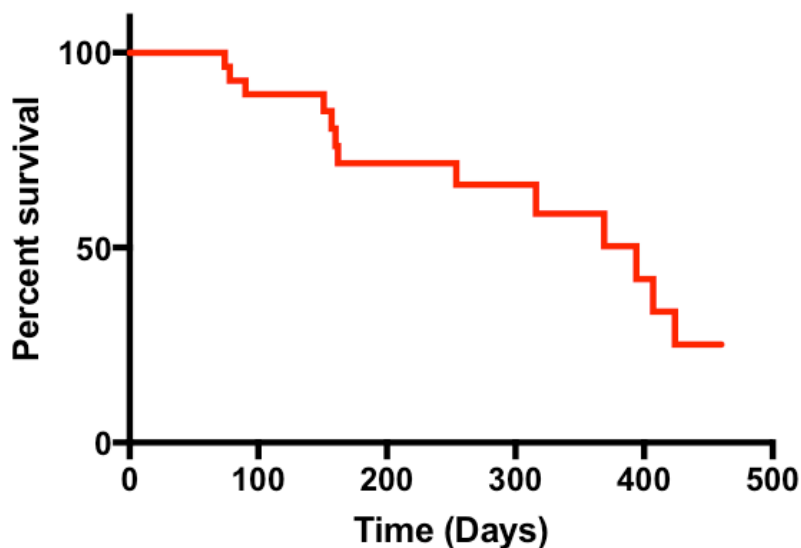


Figure 4.15: Patient Survival.

Kaplan-Meier Analysis of patient survival within the study (cohort size n=28).

The extent of tumour resection, according to post-operative MR scans, was recorded for all the patients as there is clear evidence that this has a significant impact on the prognosis.^{299–304} Of note, two patients had biopsies and five patients had subtotal resections of their tumour (<78%). All of the patients except one received adjuvant therapy; this patient had suffered a significant infarct at the time of surgery and was not deemed fit enough for further therapy. Fifteen patients had standard post-operative therapy in the form of radiotherapy (60 Gy in 30 Fractions) with concomitant TMZ. With standard therapy, TMZ was given daily at 75 mg/m² during radiotherapy (5 days a week), followed by 6 cycles of adjuvant TMZ chemotherapy

at 150–200 mg/m² for 5 days in each 28-day cycle (5/28 d). The remaining 14 had either dose-dense TMZ (smaller, daily doses) or non-TMZ chemotherapy; this occurred mainly with patients who had recurrent tumours. *Table 4.2* summarises the age, extent of resection and adjuvant therapy, as well as performance status of the various GBM patients recruited, at the time of data analysis.

Age	EOR (%)	ChemoRadiotherapy	Post-Op Days	WHO Performance Status
54	>90	40/60 Gy + Temozolomide 40mg	460	5
38	>80	PCV Chemotherapy (Palliative)	316	5
68*	>80	Dose Dense Temozolomide	151	5
65	>80	Standard Therapy	160	5
76	>80	Significant Infarction – Poor Performance Status - Palliation	74	5
69	>80	Standard Therapy (Developed Intracranial Abscess)	369	5
67	100	Standard Therapy	460	0
81	<78	Radiotherapy 40 Gy in 15 Fractions with Adjuvant Temozolomide	90	5
30	<78	Standard Therapy	439	1
70	>90	40 Gy in 15 Fractions with Concomitant Chemotherapy.	254	5
47	>90	Lomustine followed by PCV Chemotherapy. Stable disease. Treated with Avastatin	424	2
65	>80	Dose Dense TMZ	394	5
67	>90	Standard Therapy	319	0
53	Biopsy	Standard Therapy	291	1
51	>90	Standard Therapy	285	0
56	>90	PCV Chemotherapy	407	5
57	100	Standard Therapy	270	0
51	>90	Standard Therapy	242	0
55	>80	Standard Therapy	228	1
68	<78	Dose Dense TMZ	162	5
49	<78	Developed Hydrocephalus - VP Shunt. Adjuvant Chemotherapy for 12 months	157	5
74	>90	Standard Therapy	185	1
64	>90	Standard Therapy	152	0
54	>90	Standard Therapy	144	1
59	>90	Standard Therapy	144	0
42	Biopsy	Dense Dose TMZ	78	5
62	<78	Dose Dense TMZ	123	3
63	>90	Standard Therapy	116	0
65	>90	Standard Therapy	72	1

Key:
EOR = Extent of Resection;
Post-Op Days = Number of days from surgery to the end of the study/death;
TMZ = Temozolomide
WHO Performance Status:
0 – Asymptomatic
1 – Symptomatic and Ambulatory
2 – Symptomatic (<50% in Bed)
3 – Symptomatic (>50% in bed)
4 – Bedbound
5 – Death (patients in italics).

Table 4.2: Extent of tumour resection, adjuvant therapy and performance status of GBM patients recruited into the study.

* Indicates a patient diagnosed with Anaplastic Astrocytoma but with an IDH wild type gene, giving a phenotype very similar to GBM.

When correlating the viability of chip tissue (measured with Annexin V and PI flow cytometry) with patient survival, there was no significant difference in the viability of tissues from survivors when compared to tissues from those who died (non-GBM diagnoses were excluded – see *Figure 4.16*). Viability of tissue from survivors was lower than that of those who died; 54.5% (+/- 28.1) and 66.7% (+/- 30.7), respectively, but there was no statistically significant difference between the two groups.

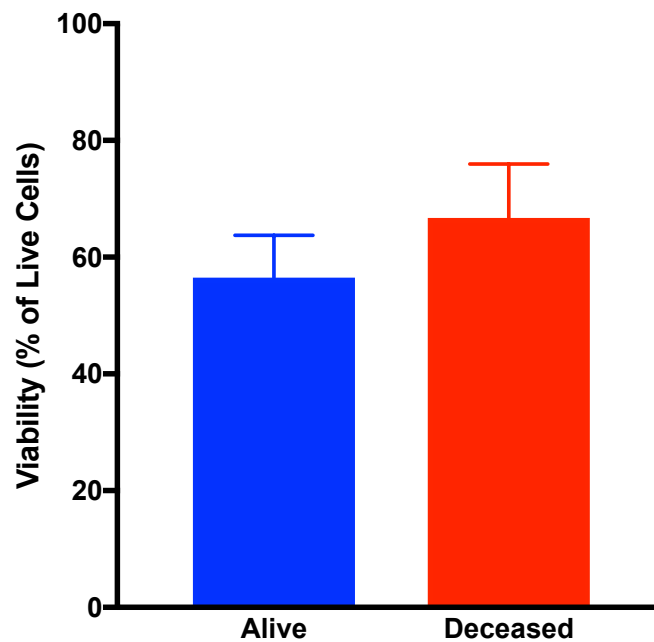


Figure 4.16: Histogram comparing viability of survivors with viability of deceased patients.

Comparison of tissue viability (with Annexin V/PI) with patient outcomes; tissues from patient survivors (n = 15) had reduced viability compared to GBM tissue from patients who did not survive (n = 11) their disease (54.5% vs. 66.7%). There was no statistically significant difference between the groups (unpaired t-test; P = 0.38).

When the number of days survived (from date of surgery) was plotted against viability, there was no correlation between the two parameters. The r^2 value was 0.005, suggestive that there was a non-linear relationship between the two (see *Figure 4.17*).

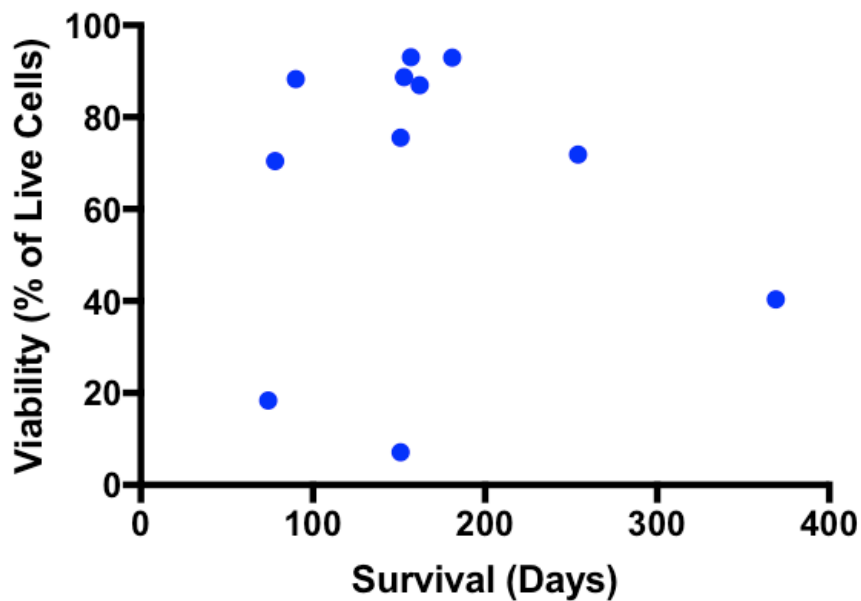


Figure 4.17: Correlation of patient survival with tissue viability.

Graph plot of surviving days versus viability in patients who died during the experimental period.

It should be noted that there was a disparity in confounding factors known to have an impact on patient survival between the two groups, such as age,³⁰⁵ post-operative therapy,³² extent of tumour resection³⁰⁴ and number of previous operations³⁰⁶. In particular, post-operative chemo-radiotherapy appeared to play a role in survival, as only 1 of the 13 (7.7%) patients that died received standard therapy, whereas 14 of 17 (82.4%) that survived received standard therapy. One of the more sensitive markers of GBM prognosis is the extent of tumour resection,²⁹⁹⁻³⁰⁴ and it was possible to stratify the performance of tissue on chip according to the extent of resection. When analysing only patients that had greater than 90% of their tumours resected, there is a trend towards reduced viability in tumours from patients that survived (n = 5), compared to patients that died (n = 5; see *Figure 4.18*).

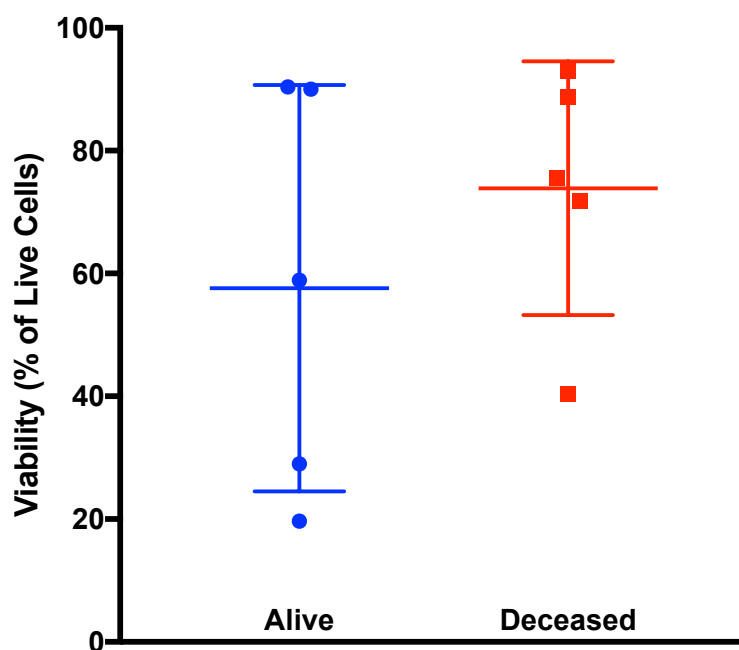


Figure 4.18: Viability in patients with maximal (>90%) resection.

Comparing viability (using Annexin V and PI assay) of tissues in which greater than 90% of the tumour was resected. There was a greater difference observed when the extent of tumour resection was controlled between the two groups with viability 16.3% greater in tumours obtained from deceased patients ($n = 5$) as opposed to survivors ($n = 5$) (Unpaired t-test - $P = 0.38$).

When comparing the performance of recurrent tumours ($n = 4$) with that of primary tumours ($n = 22$), there was a trend towards improved viability (79% +/- 15.3 vs. 57.5% +/- 29.9) as measured with Annexin V/PI flow cytometry. Similarly, IDH Wild Type tumours retained greater viability on chip than the IDH mutant tumours (76.7% +/- 22 vs. 55.7% +/- 13.4). However, there was no statistically significant difference when the groups were compared with a t-test (Figure 4.19).

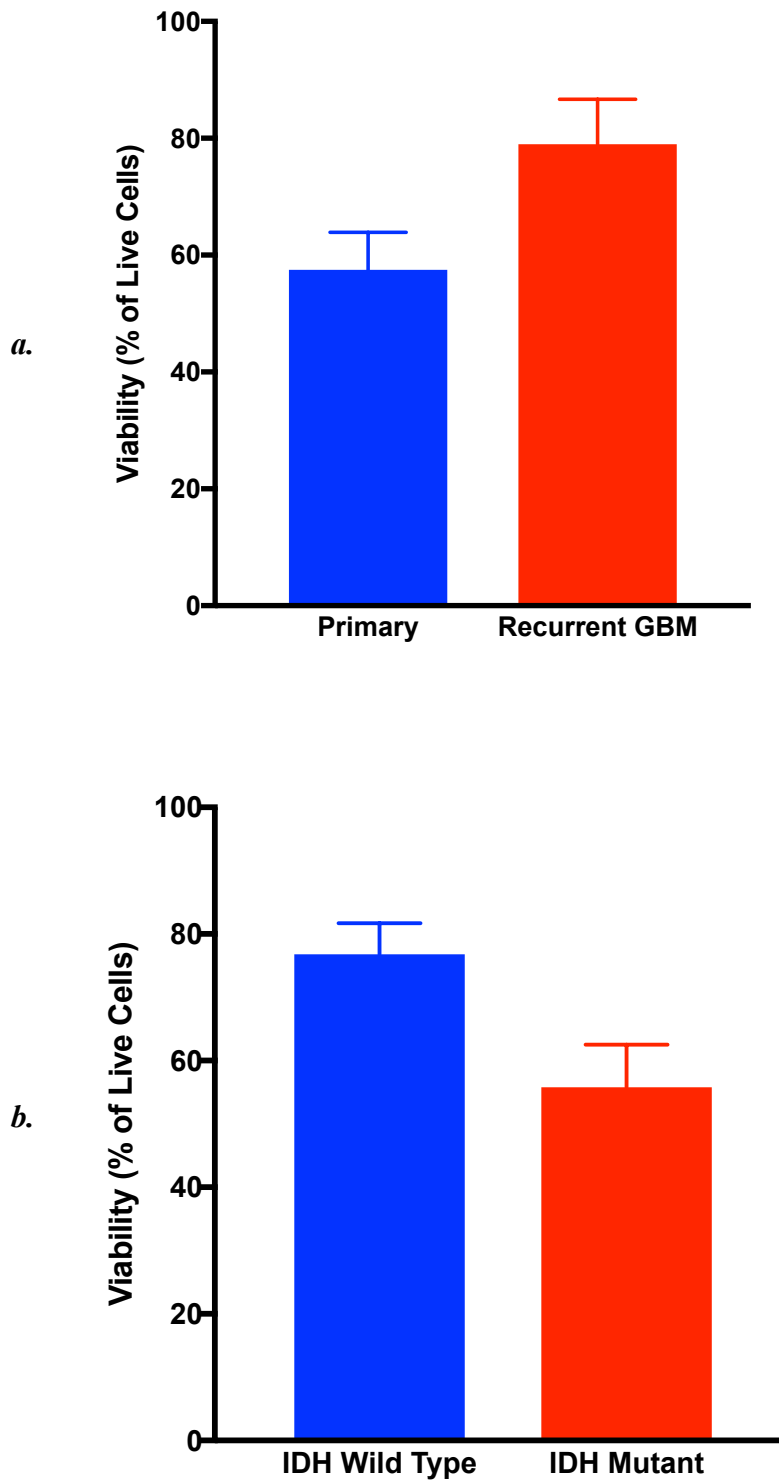


Figure 4.19: Viability of different GBM subtypes.

a. Comparing viability (measured with Annexin V and PI assay) of recurrent tumours ($n = 4$) with that of primary tumours ($n = 22$) – No statistically significant difference (unpaired t -test; $P = 0.017$). **b.** Comparing viability (with Annexin V and PI assay) of IDH wild type ($n = 20$) with IDH mutant tumours ($n = 4$). Results were not significantly different; $P = 0.08$ as analysed with unpaired t -test.

4.1.5 Discussion

4.1.5.1 Overview

The current study maintained 128 GBM tissues from 33 patients within a microfluidic device for 3 days. The bespoke device was made from two layers of glass thermally bonded to incorporate connected micro-channels and a tissue well; facilitating the continuous perfusion of GBM tissue with nutrient media. Cell viability assays, including Annexin V and PI, LDH release, Trypan Blue dye exclusion as well as histological and immunohistochemical analysis confirm that viable tissue was maintained during the assigned time. Results of tissue viability and morphological appearances were comparable to that of tissue that was analysed immediately after excision from the patient. The model was used to test the effects of chemotherapeutic agents on GBM tissue *ex vivo* but failed to demonstrate any cytotoxic effects within 3 days, when compared to controls.

The microfluidic device used in the present study has been established in the maintenance of a variety of tissues including animal liver biopsies,²¹⁸ human colorectal cancer specimens^{243,307} and head and neck cancers.^{179,180,245} Hattersley *et al* kept liver tissue from rats in a viable state within the device for 70 h and showed that tissues retained normal morphology on H&E sections as well as viability, measured with LDH release and urea and albumin synthesis.²⁴⁴ The group expanded on the applications of the device by maintaining head and neck squamous cell carcinomas for 7 days, proving tissue was viable with LDH and a tetrazolium proliferation assay.¹⁷⁹ Similarly, Bower *et al.* found that PI and Trypan Blue staining in head and neck cancer tissues maintained on chip for 48 h, was comparable to tissue that was processed immediately from the patient.²⁴⁵

This is the first time that human glioblastoma tissue has been maintained in any type of microfluidic device. Previous studies focused on maintaining *h*GBM tissue, date back to the 1970s and utilise static culture techniques in culture dishes that required the culture media to be replenished every 1-4 days.^{207-209,308} More recently, a number of groups have maintained *h*GBM tissues on collagen gel matrices²¹² and on membrane culture inserts (Millipore)^{213,214} but none of these experimental models

have applied continuous tissue flow. Compared to previous experiments, the length of tissue culture in the current study is considerably shorter, with only 2 tissue sections cultured for more than 3 days; one for a week and another for 3 weeks. Rubenstein *et al.* were able to culture GBM explants from 5 patients for up to 4 months^{208,264} and showed that tissue architecture and cytological features were conserved. The group also confirmed that DNA synthesis occurred in a small fraction of the glioma cells using pulse labelling with tritiated thymidine (³H-TdR). However, viability, cell death or apoptosis, was not measured to correlate the histological and pulse labelling experiments with cell survival. Ono *et al.* cultured 22 GBM tissues for 7 days and treated the tissues with a variety of chemotherapeutic agents, and though the group were able to assess the inhibitory effects of the drugs, they did not report on the viability of the untreated tissues.²¹² Merz *et al.* maintained 12 GBM tissue for over 2 weeks and though they showed that histological appearances were maintained over that time period, the group did not report on any viability assays, and how these compared to fresh tissue.²¹³ To the author's knowledge, the current study, is not only the largest series of *h*GBM tumours maintained as whole tissue sections, but is also the first time that the combined analysis of histology, immunohistochemistry and cell viability assays have been used to gain a comprehensive understanding of the fate of GBM tissue cultured, *ex vivo*.

4.1.5.2 Annexin V and Propidium Iodide as Biomarkers

The use of annexin V and propidium iodide as markers of viability and cell death was first used to study irradiated lymphocytes where it was found that the method accurately quantified the number of cells in apoptosis and necrosis when compared to DNA-flow cytometry and electrophoresis.²³² Recently Ji *et al.* used flow cytometer analysis with annexin V and propidium iodide assays to study human lung cell adenocarcinomas and validated the method by showing that an upregulation of apoptosis-associated genes such as Caspase 3, 9 and PARP with Western blots correlated with increased levels of apoptosis as measured by annexin V.³⁰⁹ A number of other studies have used the technique in cell viability measurements³¹⁰⁻³¹² and more specifically in glioma cell cultures.³¹³⁻³¹⁵

Recent examples with microfluidic tissue culture include Astolfi *et al.*¹⁸¹ who utilised Annexin V and 7-Aminoactinomycin D (7AAD) for viability of cells dissociated

from tissue, and Bower *et al.*²⁴⁵ used PI to measure viability of individual cells, similarly from disaggregated tissue. Bower found that viability within the microfluidic device was less than 40% but the results were comparable to the fresh tissue from the patient. Astolfi *et al.*, found that tissue maintained within their device had measurable viability above 80%. Despite the different methodologies, (Astolfi used 7 AAD, instead of PI and Bower did not have a marker for apoptosis) the viability results of 61.1%, obtained in the current study, is midway between these two results and more importantly, is not too dissimilar to the viability of fresh tissue, which had a mean of 68.9%.

Confirmation of the accuracy of results obtained with the Annexin V/PI assay was achieved with the positive correlation with the results of the Trypan Blue dye exclusion test. With the trypan blue assay, the dye acts in a very similar manner to PI; unable to penetrate the intracellular compartment of healthy cells, allowing a visual confirmation of the number of viable cells. Unlike the Annexin V/PI assay, however, Trypan Blue will not identify cells in early apoptosis (with intact membranes) and as such may overestimate the viability. Similar to this study, Bower and Astolfi found that flow cytometer results for viability were concordant with microscopic measurements of viability (Bower – Trypan Blue; Astolfi – Fluorescent microscopy with PI for necrosis and CellTracker™ Green CMFDA for live cells) and lend further support to the method as a valid assessment of cell viability.

Of some concern in the accuracy of the Annexin V/PI assay was the fact that on four occasions the viability of the tissue on chip was greater than that of the fresh tissue. There are a variety of explanations for this; the first is that the number of cells left at the end of the microfluidic experiment is not an accurate reflection of the cells that were present at the start of the experiment. There is evidence from previous iterations of this microfluidic device in head and neck cancers, of cells that are washed away off the tissue into the effluent media (with a viability of 72%).¹⁷⁹ As such, the cells that are dissociated for single cell analysis at the end of the experiment represent only the cells that remain within the tissue. The viability of those cells could be greater than that of the original tumour specimen, as it is likely that viable cells are more likely to remain within the tissue bulk as opposed to necrotic cells. The second point to consider is that though the fresh tissue and chip tissue are matched pairs

from the same patient and from the same tumour region, due to regional heterogeneity, different segments of tumour, containing varied amounts of necrotic material may have been maintained on chip. Viability could be significantly different from fresh tissue, as the tissues are quite different. Finally, one must also consider the possibility of tumour proliferation within the GBM tissue as a reason for the higher cell viability in chip tissue compared to fresh tissue, although this has not been examined and there was no clear evidence from the study of cells actively dividing.

The viability as measured by flow cytometric analysis with Annexin V and PI of disaggregated tissue provides a useful measure of viability of cells within the tissue as it accounts for all cells within all tissue layers. The assay however does not specify what cells are being analysed, and though it is possible to differentiate the cells by cell specific markers and cell size, this was not carried out. Further studies to evaluate the cell surface markers and size of the cells analysed will improve the confidence in the method.

4.1.5.3 LDH as a marker of cell death/injury

The use of LDH as a marker of cell death is a well-established scientific method that stems from the stability of the LDH enzyme³¹⁶ and its high intracellular content. Though LDH is replenished intracellularly, there is no cellular re-uptake of extracellular LDH.³¹⁶ As such there is no distortion of the released LDH, and because of the linearity of the assay, it can be used to enumerate cell death from necrosis.³¹⁷ LDH has been used as a biomarker of cell death in the study of neuronal cells and glioma cells alike and has correlated with cellular injury/viability when compared with trypan blue staining of cells.²³⁴

The results in this study were similar to previous reports of tissue maintained on chip;^{180,246,318} with an initially high rate of LDH absorbance in the first 10 h of tissue maintenance that normalised to a low and steady release of LDH for the remainder of the experiment. Previous reports have stated that this initial peak in LDH is likely related to cellular damage from tissue handling and dissection.^{243,244,261} However, since the peak in LDH can last for up to 18 h after commencing tissue perfusion, and

after the tissue was last handled, it is likely that this is not the sole reason for the initial peak in LDH absorbance. The negative effects of *short periods of ischaemia*, though proven not to correlate with GBM viability in these experiments, may explain some of the tissue damage that is seen in the first few hours of perfusion.

Transplantation surgery has dealt with the negative effects of re-perfusing tissue with the term reperfusion injury coined to explain the paradoxical damage that occurs when tissue that has been ischaemic for a period of time is perfused. With complex and interconnected pathways, reperfusion injury is theorised to occur as a result of the generation of mitochondrial reactive oxygen species. This triggers a host of signalling networks that result primarily in vascular endothelial damage but also damage to the parenchyma.³¹⁹⁻³²¹ One of the pathways implicated involves Protein Kinase C, which has been shown to be activated during ischaemic and reperfusion periods within the brain.³²² Bright *et al.* studied the effects of Protein Kinase C (the δ isoform) in instigating reperfusion injury and found that organotypic brain slices that were deprived of oxygen and glucose for 40 mins retained greater viability if treated with a selective inhibitor of δ Protein Kinase C during reperfusion. Particularly the protective effects were only achieved if the inhibitor was given during reperfusion of the tissue, with little effects if given during the ischaemic insult. The protective effect against reperfusion correlated with reduced level of apoptosis and reduced cerebral infarction in live mice when the experiment was carried out *in vivo*. Zhang *et al.*³²³ found supportive evidence with hippocampal neurons which were subjected to 2 hours of oxygen and glucose deprivation, only to find significantly worse viability when the cells were re-perfused, with greater reperfusion time leading to worse viability.

The effects of reperfusion injury are typically worse immediately after reperfusion, as was seen in the study by Hosgood *et al.* who found the highest levels of kidney injury occurred in the first hour after reperfusion of kidney tissue after up to 90 mins of WIT.²⁵⁷ This is a similar trend experienced in the microfluidic tissue culture paradigm, with the highest levels of tissue damage (according to levels of LDH absorbance) observed during the first effluent samples (the first 2 hours). This theory is further supported by the results of the static tissue cultures in which despite there being a more erratic rate of LDH absorbance in static tissue, unlike the tissues

maintained with flow, the peak in LDH absorbance was not in the first 2 h but occurred subsequently suggesting that the high LDH absorbance in this case is more to do with re-perfusion. Though not conclusive, the role of reperfusion injury in early cellular damage in tissues maintained within microfluidic devices offers the possibility for further studies; particularly, the application of techniques that minimise reperfusion injury, including the use of ischaemic preconditioning techniques as well as mediators of oxidative stress.^{319,321,324}

The LDH absorbance curves provided a detailed representation of the pattern of absorbance and this can be extrapolated to represent LDH release over the course of the experiment. Each graph showed how LDH is released (surmised from the absorbance) from individual GBM tissues and the recurrent pattern observed provides robust evidence that low levels of LDH were released from the tissue after an initial surge of LDH at the start of experimentation. This pattern is clearly demonstrated in *Figure 4.5* and the absorbance pattern allows comparison between two representative samples on chip, as well as between chip tissue and static tissue (see *Figure 3.12*). The LDH absorbance graphs, however, do not provide quantitative data that allows comparisons between fresh tissue and chip tissue as it only provides data on what happens to the tissue once within the device. To measure and compare viability with LDH, the amount of LDH released (or maintained within tissues) needs to be quantified. This can be done by measuring the absorbance of known concentrations of LDH to develop a calibration curve for each experiment; interpolation can then be used to determine an LDH concentration / mg of tissue.

For example, each 96 well analysis plate could also contain known concentrations of LDH (ranging from 1 – 0.01 U/ml), and this would be used to generate the calibration curve. *Figure 4.20* is an example of such a graph that plots known concentrations of LDH (x axis) against the recorded absorbance (y axis). The logarithmic equation of the curved trend line is used to calculate the amount of LDH released in the effluent/solution. The background solutions in the assay (e.g. BSA) is subtracted from the average absorbance (of the triplicate samples of each specimen time point at 490 nm and the final figure is substituted into the equation for the amount of LDH released in Units (U) per millilitre of media. This figure is then

divided by the wet weight of the tissue to obtain the units of LDH released per millilitre per gram of tissue.

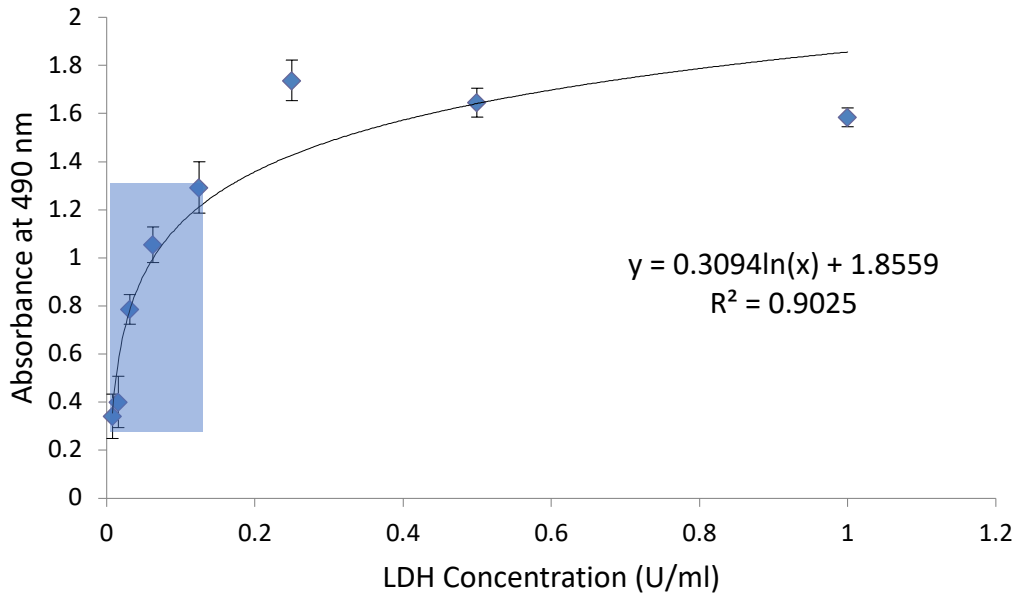


Figure 4.20: LDH Calibration Curve.

Graph plotting known concentrations of LDH against absorbance of the solutions. The trend line of the curved graph is used to produce an equation that can allow calculation of LDH concentrations in the test sample effluents from their absorbance values. NB: Only figures on the linear part of the curve (between 0.34 – 1.2 on the y axis – blue highlight) can reliably be used in conjunction with the equation to calculate LDH concentration.

A worked example to demonstrate how this could be used is shown below, using the Calibration curve in Figure 4.20.

The absorbance figures for the effluent sample collected at 23 h is:

Triplicate samples - 0.471, 0.526 and 0.469. The average is 0.49.

From this figure, the background absorbance (of reagents – BSA and reaction dye) is subtracted:

0.49 – 0.053 = 0.44. Note this value is >0.34 Absorbance units (490nm)

This figure is then substituted into the re-arranged equation to quantify the units of LDH based on the calibration curve $(x - 1.8559)/0.3094$:

$$(0.49 - 1.8559)/0.3094 = -4.56$$

The inverse log (exponent) of this figure gives the units of LDH within the sample:

$$\text{Exp}(-4.56) = 0.010377 \text{ U per ml}$$

This is then divided by the wet weight of the tissue in grams (0.013g for this sample):

$$0.0103/0.013 = 0.79 \text{ Units per ml per gram of tissue}$$

Importantly, using this method, care must be taken to ensure that absorbance values are not used if above or below the linear part of the calibration curve (in *Figure 4.20*, this corresponds to between 0.34 and 1.2 AU – 490 nm on the y axis) as these will result in unreliable calculations. If such values are given the samples will need appropriate dilution and re-assaying to determine accurately the LDH concentration.

Being able to quantify the LDH levels as described above would allow the rate and total amount of LDH released per gram of tissue to be calculated. Furthermore, by culturing dissected tissues for 24 h in a 10% (v/v) LDH lysis solution, majority of the tissue cells could be lysed, forcing the release of all intracellular LDH into solution. The total amount of LDH released from lysed fresh tissue at the start of the experiment could then be compared to the LDH released from lysed chip tissue, at the end of the experiments and used as a marker of how well chip tissue retained LDH throughout the tissue maintenance period. Dawson *et al.* performed similar experiments while maintaining human bowel tissue on a dual flow device and found that after a 72 h period in their device, chip tissue released the equivalent of 80% of what was released from fresh tissue.²⁴⁶ A similar analysis could be incorporated into future research and used as a surrogate marker of viability.

4.1.5.4 Immunohistochemistry

Ki67

Ki67 is a ubiquitous protein that is expressed within the nucleus of cells that are within the active phases of the cell cycle - G1, S, G2 and mitosis.³²⁵ The protein is not present within quiescent or resting cells (Go) and has developed to be a good indicator for active cells, with the potential to proliferate. The exact role of Ki67 in the cell is not fully understood and though it is linked with active phases of the cell cycle. There is no clear evidence that cells that stain for the active protein are destined to replicate.³²⁵

A high Ki67 index has been used often to quantify the proliferative index of tissues, particularly neoplasms. There is evidence to suggest that this correlates with clinical outcome and can predict aggressiveness of a tumour such as it does in breast cancers.²²⁷ This trend is also seen in glial tumours, with GBM having higher Ki67 proliferation indices than grade 2 and 3 gliomas have. Various studies report mean Ki67 indices in GBM of between 15-20%³²⁶⁻³³⁰ which is similar to what was found in the current study where a mean Ki67 proliferation index of 16.6% was observed with fresh GBM tissue. There was only a 1 % difference in the proliferation index between fresh tissue and tissue maintained on chip, suggestive that the GBM tissue were able to maintain their proliferative capacity for at least 3 days within the microfluidic device. The half-life of the Ki67 protein is between 60-90 mins.^{325,331} The staining present in the chip tissue represents cells that are active, even within the last few hours of the experiment. This was in contrast to tissue that was kept within static culture for 1 to 3 days without any replenishing media in which, even after 1 day, the Ki67 index dropped to 0, compared to matched tissue maintained in chip for 3 days that had an index of 4 (see *Figure 3.14*).

Ki67 has previously been used as a marker to assess quality of GBM xenografts and in this instance, has been found to correlate with the proliferation index of the parent tumour.³³² Ki67 was also used to estimate the effect of radiotherapy on GBM explants maintained *ex vivo* and found to reduce significantly in treated samples when compared to untreated samples.²¹³ Results from this study did not identify any appreciable difference in the immunohistochemistry of the tissues treated with TMZ

when compared to the IHC of control tissue. This may be related to the reduced concentration of the drug, or the short length of drug exposure. Further experiments can focus on the effects on Ki67 of varied drug concentrations and length of ‘treatment’.

Caspase 3

Cleaved Caspase 3 is another ubiquitous protein that is synthesised as the inactive form or procaspase.³³³ It is part of a family of proteins that are involved in the initiation (caspase 8, 9 and 10) and execution (caspase 3, 6 and 7) of programmed cell death. Initiator caspases trigger effector caspases, which in turn cleave intracellular substrates and lead to the morphological and biochemical changes unique to apoptosis.³³⁴ Caspase 3 is thought to be the final executioner protein in the apoptotic pathway and is best correlated with apoptosis in humans.³³⁵ Unlike Ki67, its expression is predominantly cytoplasmic, although, on occasions it can be present within the nucleus.³³⁴ Previous Caspase 3 apoptotic index in GBM has been estimated to be at 17.7%,³³⁶ which is considerably lower than in the current study. Other studies have cited apoptotic indices as high as 50% in GBM tissue,³³⁷ and the figure of 38.9% within *fresh tissue* in this study is within the range of results present in the literature. This study’s apoptotic index is also comparable to the estimates of apoptosis measured by the Annexin V and Propidium assay; which showed that a total of 30.7% of the cells were undergoing either early or late apoptosis. Similarly, the apoptotic index of chip tissue of 44.4%, correlated with the total number of cells undergoing apoptosis as quantified by flow cytometry (38.4%).

The slight discrepancy between the immunohistochemistry and flow cytometry results is likely related to the different methods of measuring apoptosis but may also be to do with the fact that the majority of activated caspase 3 staining in this study was intranuclear. Nuclear predominant staining of caspase 3 is uncommon, but known to occur due to nuclear translocation of cleaved caspase 3 substrates.^{334,338} Evidence suggests that the sub-units of the protein initiate nuclear morphological changes essential to apoptosis but there is also another school of thought that highlights a role for caspase 3 distinct from apoptosis. Intranuclear activated caspase 3 has been identified in rat and mice brain within glial cells without any active apoptosis quantified by terminal deoxynucleotidyl transferase-mediated dUTP nick-

end labelling (TUNEL).^{339,340} The exact role of caspase 3 in this setting is still being clarified, although some evidence appear to show that caspase 3 has an active role in the motility of GBM cells in the absence of cellular stress;³³⁹ as cell motility of GBM cells was reduced by inhibition of caspase 3.

Despite the uncertainty of any additional roles activated caspase 3 may have had in the GBM tissue, the immunohistochemical profile was very similar for fresh tissue and tissue maintained on chip for 72 h, with no statistical difference between the two tissue types. It may be that caspase 3 activation is not a major mechanism of cell death in TMZ treatment and thus other immunohistochemical markers could be investigated such as Caspase 9 and Bax²⁹⁸. TUNEL assays have also been used successfully with glioma cells and GBM tissue and this is another viable option for future research into GBM apoptosis on chip.^{341,342}

4.1.5.5 Drugs

TMZ

There was no discernible effect of drug treatment on the GBM tissue despite 48 h of perfusion with TMZ. The viability was unchanged in most samples and in a few instances, even greater in the treatment samples, compared to the control. In one sample TMZ treatment was accompanied by a reduction in viability and an increase in early apoptosis of the cells. This, the anticipated response was, however, only present in one of the tissue samples, and, as such, the mean viability was unchanged. As per the histopathology policy in the Hull and East Yorkshire NHS Trust, MGMT methylation status is only clarified in patients above the age of 70; this translates to 7 patients within the cohort having a diagnosis of their MGMT methylation status. Of the 7 patients, one patient was found to have methylation of their MGMT gene. This patient's tumour (16026) also happened to be treated with TMZ and despite the favourable methylation status, there was no obvious treatment effect with TMZ. The MGMT status of the one patient (16028) whose tumour appeared to respond to TMZ was unfortunately not identified.

Though the lack of a response in GBM tissue within the microfluidic device to TMZ treatment could be interpreted as a failure of the method to predict clinical response,

there is yet to be conclusive evidence that the parent tumours themselves respond significantly to the drug. Though Stupp identified an improvement in survival with Temozolomide, the survival benefit provided by the drug, given with concomitant radiotherapy, was 2.5 months when compared to radiotherapy alone.³² Also it is important to note that TMZ does not significantly prolong the survival of patients without methylation of the MGMT promoter,³⁴³ and research estimates MGMT methylation in GBM at 30-60%.³⁴⁴ As such, there is a chance that the lack of a response to TMZ may be related to the MGMT methylation status of the treated samples making tumours less sensitive to the drug.

The length of exposure to TMZ is also likely to have played a part in the lack of a response. Previous evidence of the treatment effects of TMZ in *h*GBM tissue maintained *ex vivo* has been provided by Merz *et al.*, who identified an increase in PI labelling of GBM tissue cells cultured in TMZ for 72 h and 96 h as compared to controls. This was also associated with an increase in the apoptotic index (measured by caspase 3) of TMZ treated tissue.²¹³ Aspects of the methodology by Merz *et al.* draw comparisons to the current study that may explain the inconsistency in results. The first is the dosage and length of TMZ treatment (50 - 200 μ M for 72 - 96 h) used by Merz *et al.*, which is a higher dose and longer time period than in the current study (100 μ M for 48 h). The second concern is that the tissue and drug incubated by Merz *et al.* was with standard culturing techniques in a culture medium without flow, which meant that the tissue was maintained in a stagnant concentration of TMZ. With microfluidic flow, there is constant delivery and removal of the drug, which means that the concentration around the tissue is always changing. Particularly with a drug like TMZ, which has a relative short half-life,²⁴² after the first few hours, there is a steady decline in the active drug concentration. Previous reports suggest that drug sensitivity measured at tenfold the peak plasma concentration corresponded better with that measured with a nude mouse assay in xenograft tumours.^{345,346} The current study used the approximate peak plasma concentration of TMZ, and though there are reports of similar dosage in pre-clinical trials,^{241,343,347,348} a higher dosage appears appropriate in microfluidic drug testing where the drug is constantly being washed away.

Perhaps most important, though, is the small number of experiments in which TMZ was infused through the microfluidic device. A greater number of tests need to be carried out, with a likely longer duration of treatment, to clarify the drug response on chip.

ExoPr0

The drug ExoPr0 is still in the experimental phase and this was the first time it had been used in the treatment of *h*GBM tissue. There was no difference in viability in tissues treated with ExoPr0 when compared to untreated tissues. This finding is probably in keeping with the limited available data on the effects of ExoPr0 on U87 cells, as the main therapeutic effect is obtained only after 21 days of treatment. Culturing microfluidic devices for 21 days is yet to be tested and the viability of the tissue is likely to be significantly affected for tissues maintained for this length of time. One of the samples was cultured for 21 days using static culture techniques, and this was treated with ExoPr0 for the 21-day duration but unfortunately, the viability of the tissue (as well as the control) was less than 1 %, making it impossible to ascertain any meaningful drug effect.

4.1.5.6 Clinical Correlation

The results of the study show that GBM tissues can be maintained within a microfluidic device for at least 72 h with good viability comparable to fresh tissue. There appears to be a trend towards improved viability in tumours from patients who died from their disease when compared to tumours from survivors. There was, however, no association between the number of days survived and the viability of tumour samples. Further evaluation of clinical parameters identified various uncontrolled variables, such as patient age, IDH status, extent of tumour resection and adjuvant therapy, that determine survival and as such affect the correlation. For example, there was a high proportion of patients who survived more than 250 days that had greater than 90 % of their tumours resected, as well as benefitted from the standard/optimum adjuvant therapy. There is clear evidence that the extent of tumour resection has an independent impact on survival, an effect that is just as significant as treatment with the drug TMZ. Sanai *et al.* showed a survival advantage of 3.5 months in patients who had complete macroscopic resection of their tumour when

compared to patients who had a >78 % resection.³⁰⁰ When the extent of resection was controlled as a variable, it amplified differences between the tumours obtained from patients that survived their disease and tumours from those that did not. Nonetheless, there was no statistically significant difference between the groups.

The lack of a clear clinical correlation between tissue viability on chip and patient survival may be in part to do with the fact that the patient's general health after the tumour has been resected, including their age, performance status, and the extent of tumour debulked; all have an impact on survival. Viability of the tumour *ex vivo*, however, is purely to do with the inherent nature of the disease (which varies with tumour heterogeneity) and the ability of the microfluidic device to maintain GBM tissue. As such, it is unlikely that an accurate prediction of patient survival could be achieved based on the performance of the tissue on chip, as the tumour *ex vivo* doesn't embody any of the patient's risk factors. In simple terms, a patient's survival is determined by the difference between the patient's risk factor profile (that determines how well the patient can defend themselves against the deleterious effects of the tumour) and the inherent tumour biology (which determines the lethal effects of the tumour). Patient survival is probably not the best correlate to tissue viability on chip because survival is so multifactorial.

The performance of the tissue on chip can be used to deduce the aggressiveness of the GBM tissue as well as predict the ease of treating a tumour. When patient risk factors, are controlled for, the performance of the tumour on chip bores out some association with patient survival in terms of viability, despite no statistical significance.

As is the case in GBM, the cohort of GBM diagnoses contains a heterogeneous population and even though genomic profiling was not performed, the different ages and different survival data suggest that the group could be stratified into the four distinct GBM subtypes: Classical, Proneural, Neural and Mesenchymal. The inclusion of 5 recurrent GBM tumours makes it likely that these tumours will display a more mesenchymal phenotype, as glioma stem cells following therapy display phenotypic transition from Proneural to Mesenchymal subtype, leading to disease recurrence and a more aggressive tumour.²⁸¹ The recurrent tumours were more

sustainable and viable tumours on chip than the primary tumours (though this difference did not reach statistical significance). Also, in keeping with the trend that more aggressive tumours were more likely to have better viability is the finding that GBM tumours had higher viabilities than the low grade tumours. There was also improved viability in the IDH wild type tumours, which are known to have a more aggressive phenotype.⁵⁶ Though also not showing a statistical significance, a trend was identified amongst IDH wild type being more viable *ex vivo*. As such, the method was able to predict aggressive tumour phenotypes such as IDH 1 Wild Type and Recurrent tumours in terms of viability. Further experiments with a larger cohort are required to clearly elucidate the associations and clarify the usefulness of the method in predicting the aggressiveness of GBM tumours.

5.1 Conclusion

5.1.1 Discussion of Findings

A diagnosis with Glioblastoma equates to a poor prognosis regardless of treatment. Conventional therapy (surgery, radiotherapy and chemotherapy) affords a modest survival benefit of approximately 12 months compared to patients who are left untreated.^{349,350} To improve the outcome for patients diagnosed with GBM, a more effective pre-clinical model and patient-specific screening methods are required to customise treatment to individual molecular signatures. The aim of this study was to explore the application of a microfluidic device in the maintenance of *h*GBM tissue *ex vivo*; as a simple and cost-effective GBM model that translates the *in vivo* tumour phenotype into a controlled laboratory setting, where treatment modalities can be tested with minimal contamination of tumour behaviour or response.

128 GBM tissue samples (of 10 – 15 mg), were maintained for 3 days using a microfluidic device, made from two pieces of glass, bonded together to contain a network of microchannels; continuously perfused with nutrient media. The device in the current study was a modification of an established design previously used for the maintenance of a variety of tissue types.^{180,244,245} The modification, the addition of a mesh layer between the tissue cavity and the microchannel, prevented chip blockages and ensured the efficacy of the device to 96.6% in supporting the tissue for the prescribed time frame.

Viability assays showed comparable results to tissue taken fresh from the patient. LDH absorbance assays revealed that GBM tissue maintained on chip had an initial surge in LDH release, only to stabilise to low and steady levels throughout the maintenance period. This may be related to a tissue reperfusion injury after a period of warm ischaemia time. Other aspects of the tissue maintained on chip were comparable to the original tissue, including histological and immunohistochemical evaluation. The results of viability assays and histological assessments were in-keeping with previous results of tissue maintenance in microfluidic devices, as well as previous experiments focused on maintaining *h*GBM tissues in static culture paradigms. The effects of fluid flow on GBM tissue viability was also examined

against controlled samples, maintained without microfluidic flow; with continuous tissue perfusion improving viability, reducing the rate of LDH release and preserving the histological appearance of the tissue.

During the study, the effect of 100 μM of Temozolomide was tested on 6 patient samples without an obvious cytotoxic effect on the tissues. There was no obvious correlation between patient survival and tissue viability, but this may be related to the many confounding factors including patient age, extent of resection and adjuvant therapy.

The results obtained from this pilot study add to the ever-increasing knowledge on microfluidic tissue culture and the emerging work on *h*GBM tissue maintenance *ex vivo*; providing a platform for future research on GBM tumour models.

5.1.2 Limitations

A total of 33 patients were recruited for the study and though a reasonable number of tumour samples were available for analyses, the small patient sample size increases the likelihood of a type II statistical error, where the null hypothesis is accepted to be true despite a real difference between variables being present. This is particularly true for the sub-group analyses where differences between patient groups (e.g. alive vs. deceased, IDH subtypes, recurrent vs. primary tumours) showed a trend towards statistical significance. The current study is an observational study, and the power of the study was not quantified; as such, the statistical analysis should be interpreted with caution. However, with the relevant data obtained from this study, a power analysis can now be carried out to provide guidance on sample size and improve confidence in the statistical analysis.

The current life-expectancy of patients treated with a GBM is approximately 15-18 months, and at the time of writing the thesis, half of the patients recruited into the study were still alive. Future analysis of the mortality trend will allow a clearer perspective of the results; the current cohort can be followed up until after the last mortality and the complete data set can be evaluated for any meaningful correlation between tissue performance on chip (viability, LDH release) and length of survival.

The lack of a definite drug response to TMZ, the current drug of choice for GBM, needs further investigation. Though a variety of reasons exist as to why a response was not identified – including drug dosage and length of exposure; a response to treatment is vital if the model is to be applicable to GBM patients. Drug assays to test TMZ activity in the effluent, as well as from the tissue, were not performed and will need to be completed prior to further drug tests to better understand the response of GBM tissue *ex vivo* to TMZ. Experiments were stopped (due to insufficient time) prior to more detailed testing of drug response such as exposing the tumour to different dosages, different cytotoxic agents, and for different lengths of time.

5.1.3 Further Research

Sampling

Sampling errors could be reduced by sampling multiple areas of the tumour and maintaining the tissues concurrently to ascertain global tissue response on chip. This would also average out the discrepancy that occurs from inter-tumour heterogeneity. Samples from at least 3 different regions of the tumour would need to be obtained and at least one 10 – 15 mg piece of tissue from each area sampled should be maintained on chip to obtain an average tumour response/behaviour. Drug response of tumours from different areas of the tumour would allow a practical assessment of the effects of *intra*-tumoral heterogeneity. This could be combined with DNA sequencing and genetic profiling to identify GBM subtype and any reported variations tested *ex vivo*.

Chip Design

The effects of changing the direction of flow within the chip to one that is perpendicular to the tissue is thought to improve viability by enhancing the diffusion of nutrients and this method can easily be adapted to the microfluidic device. Such a modification can also ensure that nutrient media is delivered directly to the tissue before coming into contact with mesh layer. This would optimise the amount of nutrients or drugs that reach the tissue and may improve viability or drug responses. *Figure 5.1b* outlines the design modification which has already been developed.

Other modifications to the device include the use of Millipore inserts as a barrier between the tissue compartment and the microfluidic channel, or the introduction of other media solutions without serum.²¹³ Modifications could easily be carried out and tested to suit the requirement of the model and to improve the quality of the method.

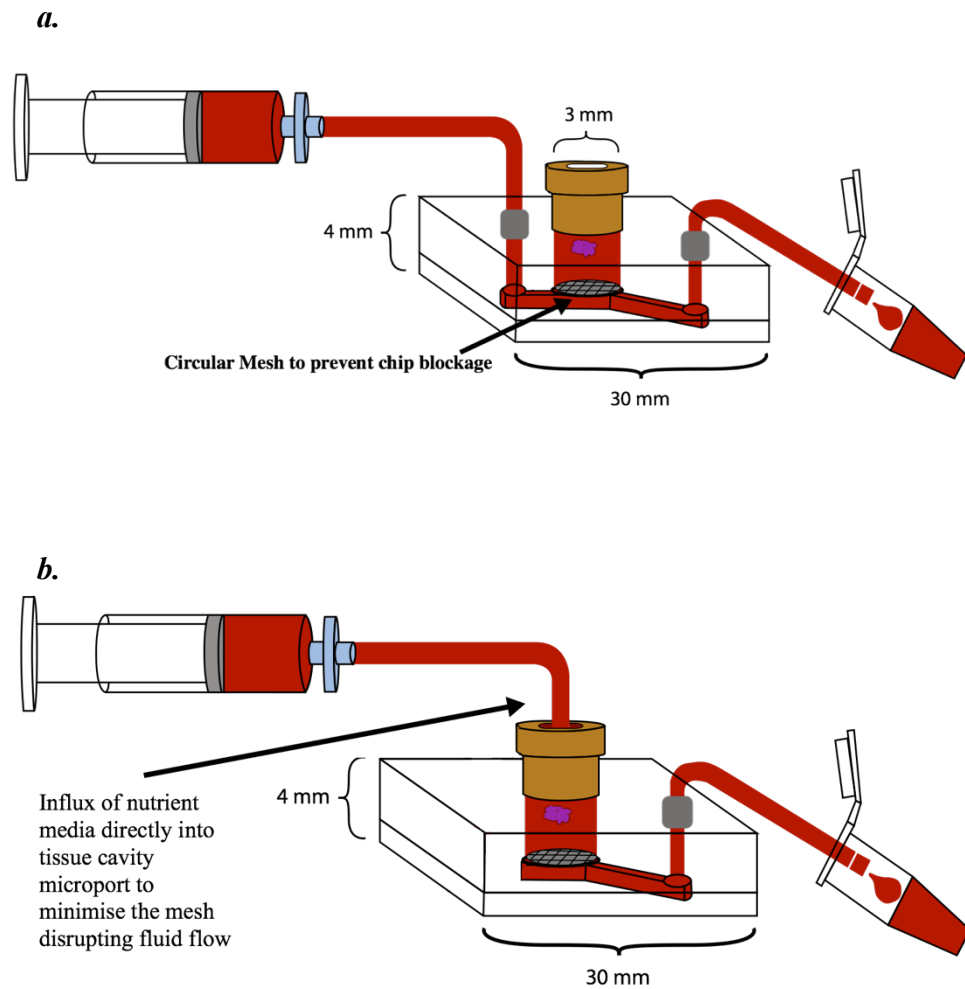


Figure 5.1: Redesigning the chip.

a. Original microfluidic device set up, with inflow of media directly into microchannels. **b.** Proposed set up of microfluidic device, with influx of media directly into the central portion of the microport adaptor, to promote forced convection interstitial perfusion.

Microfluidic Tissue Culture Paradigm

An important aspect of this study that requires further exploration is the length of time the tissue is maintained. Previous groups have maintained tissues in microfluidic devices for as long as 9 days,²¹⁹ and there is evidence of GBM tissues

being maintained in Millipore insets for up to 2 weeks.²¹³ The longer the tissue can be kept viable, the more information can be garnered from the sample. This would also allow more detailed drug testing and could identify factors that impeded a positive drug response in the current study. Exposure to different drug doses, as well as exposing the tissue to drug treatments for longer time-frames would provide a more systematic approach to pre-clinical modelling. Long-term tissue perfusion would not only be more representative of the *in vivo* state, but it would also provide long term stabilisation of the tissue.

As well as testing established and experimental chemotherapeutic drugs, the effect of radiotherapy could be assessed to predict tumour response. Radiotherapy treatment has previously been applied to tissues within a microfluidic device and the same methods could be applied in the study of GBM. Carr *et al.* were able to continue tissue maintenance within their microfluidic device while irradiation of the tissue on chip took place using a 6-MV photon beam from a Varian Linear Accelerator.¹⁸⁰ The group ensured that a uniform dose was delivered to the tissue by keeping the device and tissue within a Perspex phantom. Single doses and fractionated doses of radiotherapy were delivered to head and neck tumours, and the effect on the tissues was assessed. Utilising such a set up would allow the effects of radiotherapy and chemotherapy given concomitantly on GBM tissue explants to be analysed and the tissue response quantified and compared to patients who received the same treatment.

Detailed Cellular and Molecular Analysis

Despite proliferation indices (Ki67 IHC) of the tissue being maintained on chip, there is no definite proof of cellular growth or proliferation. Confirmation of this would strengthen the claim of this technique as an ideal pre-clinical method, since treatment methods (including chemotherapy and radiotherapy) rely particularly on actively dividing cells to have therapeutic efficacy. The proportion of cells involved with mitosis could be quantified by staining of disassociated cells at the end of the experiment with a stain that selects for DNA. Nuclear Propidium Iodide content (after fixing and making cells permeable to PI) could also be used to stratify cells into different stages of the cell cycle and ascertain what proportion of cells are actively dividing – in M phase. Active cellular proliferation can also be clarified with

the aid of Bromodeoxyuridine (BrdU), which can be infused within the nutrient media and the uptake and incorporation of BrDU into the DNA can be used to provide an estimate of cells that have been involved in proliferation. Clarification of cell types could also be achieved by labelling tissues and/or cells with cell markers. In particular, identification of glial cell markers could be used to confirm that the viable cells are indeed glial in origin, as opposed to microglia or other cellular infiltrates. Staining with glioma cell surface markers such as Glial Fibrillary Acidic Protein or Nestin²¹³ could help identify the proportion of viable glioma cells.

5.1.4 Final Comments

This pilot study demonstrates, for the first time, that a microfluidic device can be used to maintain *h*GBM tissue *ex vivo*. Though still in its infancy, the use of microfluidic principles to study whole tissues is improving our understanding of complex diseases. A lot more work is required to better understand the true potential of this type of experimentation in GBM research. More robust analyses of experiments with a larger number of patients will allow a more definitive exploration of the method and its potential as a pre-clinical disease model. A model with the prospect of enabling more detailed inspections of GBMs; more accurate predictions of treatment responses and better outcomes for patients.

References

1. Cancer Research UK. Brain, other CNS and intracranial tumours incidence statistics [Internet]. [cited 2017 Aug 21]. Available from: <http://www.cancerresearchuk.org/health-professional/cancer-statistics/statistics-by-cancer-type/brain-other-cns-and-intracranial-tumours/incidence#heading-Two>
2. Ostrom QT, Bauchet L, Davis FG, Deltour I, Fisher JL, Langer CE, et al. The epidemiology of glioma in adults: a “state of the science” review. *Neuro Oncol* [Internet]. 2014;16(7):896–913. Available from: <http://neuro-oncology.oxfordjournals.org/cgi/doi/10.1093/neuonc/nou087>
3. Wu B, Miao Y, Bai Y, Ye M, Xu Y, Chen H, et al. Subgroup Economic Analysis for Glioblastoma in a Health Resource-Limited Setting. *PLoS One* [Internet]. 2012;7(4):e34588. Available from: <http://dx.plos.org/10.1371/journal.pone.0034588>
4. Aldape KD, Okcu MF, Bondy ML, Wrensch M. Molecular epidemiology of glioblastoma. *Cancer J* [Internet]. 2003;9(2):99. Available from: <http://search.ebscohost.com/login.aspx?direct=true&db=rzh&AN=106103467&site=ehost-live>
5. Ferguson S, Lesniak MS. Percival Bailey and the classification of brain tumors. *Neurosurg Focus*. 2005;18(4):e7.
6. Zong H, Verhaak RG, Canoll P. The Cellular origin for malignant glioma and prospects for clinical advancements. *Expert Rev Mol Diagn*. 2012;12(4):383–94.
7. Louis DN, Perry A, Reifenberger G, von Deimling A, Figarella-Branger D, Cavenee WK, et al. The 2016 World Health Organization Classification of Tumors of the Central Nervous System: a summary. *Acta Neuropathol* [Internet]. 2016;131(6):1–18. Available from: <http://link.springer.com/10.1007/s00401-016-1545-1>
8. Chang K, Creighton CJ, Davis C, Donehower L, Drummond J, Wheeler D, et al. The Cancer Genome Atlas Pan-Cancer analysis project. *Nat Genet* [Internet]. 2013;45(10):1113–20. Available from: <http://www.nature.com/doi/10.1038/ng.2764>
9. Sant M, Minicozzi P, Lagorio S, Børge Johannesen T, Marcos-Gragera R, Francisci S. Survival of European patients with central nervous system tumors. *Int J Cancer*. 2012;131(1):173–85.
10. Bianco J, Bastiancich C, Jankovski A, des Rieux A, Pr at V, Danhier F. On glioblastoma and the search for a cure: where do we stand? *Cell Mol Life Sci* [Internet]. 2017;0(0):1–16. Available from: <http://link.springer.com/10.1007/s00018-017-2483-3>
11. Brodbelt A, Greenberg D, Winters T, Williams M, Vernon S, Collins VP. Glioblastoma in England: 2007-2011. *Eur J Cancer* [Internet]. 2015;51(4):533–42. Available from: <http://dx.doi.org/10.1016/j.ejca.2014.12.014>
12. Arora RS, Alston RD, Eden TOB, Estlin EJ, Moran A, Birch JM. Age-incidence patterns of primary CNS tumors in children, adolescents, and adults in England. *Neuro Oncol* [Internet]. 2009;11(4):403–13. Available from:

- http://neuro-oncology.oxfordjournals.org/content/11/4/403.abstract?ijkey=8aa75ed78816e3d8de5241819c905d46538f26&keytype=tf_ipsecsha
13. Thakkar JP, Dolecek TA, Horbinski C, Ostrom QT, Lightner DD, Barnholtz-Sloan JS, et al. Epidemiologic and molecular prognostic review of glioblastoma. *Cancer Epidemiol Biomarkers Prev.* 2014;23(10):1985–96.
 14. Ohgaki H, Kleihues P. Epidemiology and etiology of gliomas. *Acta Neuropathol.* 2005;109(1):93–108.
 15. Dubrow R, Darefsky AS. Demographic variation in incidence of adult glioma by subtype, United States, 1992-2007. *BMC Cancer* [Internet]. 2011;11(1):325. Available from: <http://www.pubmedcentral.nih.gov/articlerender.fcgi?artid=3163630&tool=pmcentrez&rendertype=abstract>
 16. Porter AB, Lachance DH, Johnson DR. Socioeconomic status and glioblastoma risk: a population-based analysis. *Cancer Causes Control.* 2015;26(2):179–85.
 17. Agnihotri S, Burrell KE, Wolf A, Jalali S, Hawkins C, Rutka JT, et al. Glioblastoma, a brief review of history, molecular genetics, animal models and novel therapeutic strategies. *Arch Immunol Ther Exp (Warsz).* 2013;61(1):25–41.
 18. Alifieris C, Trafalis DT. Glioblastoma Multiforme: Pathogenesis and Treatment. *Pharmacol Ther.* 2015;152:1–20.
 19. Farrell CJ, Plotkin SR. Genetic Causes of Brain Tumors: Neurofibromatosis, Tuberous Sclerosis, von Hippel-Lindau, and Other Syndromes. *Neurol Clin.* 2007;25(4):925–46.
 20. Abd-El-Barr MM, Huang KT, Chi JH. Infiltrating spinal cord astrocytomas: Epidemiology, diagnosis, treatments and future directions. *J Clin Neurosci* [Internet]. 2016;29:15–20. Available from: <http://dx.doi.org/10.1016/j.jocn.2015.10.048>
 21. Simpson JR, Horton J, Scott C, Et A. Influence of location and extend of surgical resection on survival of patients with glioblastoma multiforme: results of three consecutive Radiation Therapy Oncology Group (RTOG) clinical trials. *Int J Radiat Oncol Biol Phys.* 1993;26(December):239–44.
 22. Gopalakrishnan C V., Dhakoji A, Nair S, Menon G, Neelima R. A retrospective study of primary cerebellar glioblastoma multiforme in adults. *J Clin Neurosci* [Internet]. 2012;19(12):1684–8. Available from: <http://dx.doi.org/10.1016/j.jocn.2011.12.035>
 23. Posti JP, Bori M, Kauko T, Sankinen M, Nordberg J, Rahi M, et al. Presenting symptoms of glioma in adults. *Acta Neurol Scand.* 2015;131(2):88–93.
 24. Oliver Tucha, Christian Smely, Michael Preier KWL. Cognitive Deficits before Treatment among Patients with Brain Tumors. *Neurosurgery.* 2000;47(2):324–34.
 25. Klein M, Postma TJ, Taphoorn MJB, Aaronson NK, Vandertop WP, Muller M, et al. The prognostic value of cognitive functioning in the survival of patients with high-grade glioma. *Neurology.* 2003;61:1796–8.
 26. Kerkhof M, Vecht CJ. Seizure characteristics and prognostic factors of gliomas. *Epilepsia.* 2013;54(SUPPL. 9):12–7.
 27. Toledo M, Sarria-Estrada S, Quintana M, Maldonado X, Martinez-Ricarte F, Rodon J, et al. Epileptic features and survival in glioblastomas presenting with seizures. *Epilepsy Res* [Internet]. 2017;130:1–6. Available from:

- <http://www.ncbi.nlm.nih.gov/pubmed/28073027>
<http://www.ncbi.nlm.nih.gov/pubmed/28073027>
28. Berendsen S, Varkila M, Kroonen J, Seute T, Snijders TJ, Kauw F, et al. Prognostic relevance of epilepsy at presentation in glioblastoma patients. *Neuro Oncol.* 2016;18(5):700–6.
 29. Purdy RA, Kirby S. Headaches and brain tumors. *Neurol Clin.* 2004;22(1):39–53.
 30. Goffaux P, Fortin D. Brain tumor headaches: From bedside to bench. *Neurosurgery.* 2010;67(2):459–66.
 31. Guilfoyle MR, Weerakkody RA, Oswal A, Oberg I, Jeffery C, Haynes K, et al. Implementation of neuro-oncology service reconfiguration in accordance with NICE guidance provides enhanced clinical care for patients with glioblastoma multiforme. *Br J Cancer [Internet].* 2011;104(12):1810–5. Available from: <http://www.pubmedcentral.nih.gov/articlerender.fcgi?artid=3111193&tool=pmcentrez&rendertype=abstract>
 32. Stupp R, Mason WP, Bent MJ van den, Weller M, Fisher B, Taphoorn MJB, et al. Radiotherapy plus concomitant and adjuvant temozolomide for glioblastoma. *N Engl J Med.* 2005;352(10):987–96.
 33. Burnet NG, Jefferies SJ, Benson RJ, Hunt DP, Treasure FP. Years of life lost (YLL) from cancer is an important measure of population burden--and should be considered when allocating research funds. *Br J Cancer.* 2005;92(2):241–5.
 34. Chang S, Long SR, Kutikova L, Bowman L, Finley D, Crown WH, et al. Estimating the cost of cancer: Results on the basis of claims data analyses for cancer patients diagnosed with seven types of cancer during 1999 to 2000. *J Clin Oncol.* 2004;22(17):3524–30.
 35. Latif a Z, Signorini D, Gregor a, Whittle IR. The costs of managing patients with malignant glioma at a neuro-oncology clinic. *Br J Neurosurg.* 1998;12(2):118–22.
 36. Patterson H, Brain Tumour Foundation. Nobody can afford a brain tumour..... the financial impact of brain tumors on patients and families: a summary of findings MAY. 2007.
 37. Blomqvist P, Lycke J, Strang P, Törnqvist H, Ekbom a. Brain tumours in Sweden 1996: care and costs. *J Neurol Neurosurg Psychiatry.* 2000;69(6):792–8.
 38. Holland EC. Glioblastoma multiforme: the terminator. *Proc Natl Acad Sci U S A.* 2000;97(12):6242–4.
 39. Masui K, Cloughesy TF, Mischel PS. Molecular pathology in adult high-grade gliomas: From molecular diagnostics to target therapies. *Neuropathol Appl Neurobiol.* 2012;38(3):271–91.
 40. Kenneth Aldape, Gelareh Zadeh, Sheila Mansouri, Guido Reifenberger A von D. Glioblastoma: pathology, molecular mechanisms and markers. *Acta Neuropathol.* 2015;129:829–48.
 41. Thon N, Kreth S, Kreth FW. Personalized treatment strategies in glioblastoma: MGMT promoter methylation status. *Onco Targets Ther.* 2013;6:1363–72.
 42. Sonoda Y, Kumabe T, Watanabe M, Nakazato Y, Inoue T, Kanamori M, et al. Long-term survivors of glioblastoma: Clinical features and molecular analysis. *Acta Neurochir (Wien).* 2009;151(11):1349–58.
 43. Walid MS. Prognostic factors for long-term survival after glioblastoma. *Perm*

- J [Internet]. 2008;12(4):45–8. Available from:
<http://www.pubmedcentral.nih.gov/articlerender.fcgi?artid=3037140&tool=pmcentrez&rendertype=abstract>
44. Greenberg MS. Handbook of Neurosurgery. Seventh. Thieme; 2010.
 45. Prayson RA, Agamanolis DP, Cohen ML, Estes ML, Kleinschmidt-DeMasters BK, Abdul-Karim F, et al. Interobserver reproducibility among neuropathologists and surgical pathologists in fibrillary astrocytoma grading. *J Neurol Sci*. 2000;175(1):33–9.
 46. Aldape K, Simmons ML, Davis RL, Miike R, Wiencke J, Ph D, et al. Discrepancies in Diagnoses of Neuroepithelial Neoplasms: The San Francisco Bay Area Adult Glioma Study. *Cancer*. 2000;88(10):2342–9.
 47. Coons SW, Johnson PC, Scheithauer BW, Yates AJ, Pearl DK. Improving diagnostic accuracy and interobserver concordance in the classification and grading of primary gliomas. *Cancer*. 1997;79(7):1381–93.
 48. Dunn GP, Rinne ML, Wykosky J, Genovese G, Quayle SN, Dunn IF, et al. Emerging insights into the molecular and cellular basis of glioblastoma. 2012;756–84.
 49. Dang L, White DW, Gross S, Bennett BD, Bittinger MA, Driggers EM, et al. Cancer-associated IDH1 mutations produce 2-hydroxyglutarate. *Nature* [Internet]. 2010;465(7300):966–966. Available from:
<http://www.nature.com/doi/10.1038/nature09132>
 50. Verhaak RGW, Hoadley KA, Purdom E, Wang V, Qi Y, Wilkerson MD, et al. Integrated genomic analysis identifies clinically relevant subtypes of glioblastoma characterized by abnormalities in PDGFRA, IDH1, EGFR, and NF1. *Cancer Cell* [Internet]. 2010;17(1):98–110. Available from:
<http://www.pubmedcentral.nih.gov/articlerender.fcgi?artid=2818769&tool=pmcentrez&rendertype=abstract>
 51. Crespo I, Vital AL, Gonzalez-Tablas M, Del Carmen Patino M, Otero A, Lopes MC, et al. Molecular and Genomic Alterations in Glioblastoma Multiforme. *Am J Pathol* [Internet]. 2015;185(7):1820–33. Available from:
<http://www.sciencedirect.com/science/article/pii/S0002944015001972>
 52. Thuy MN, Kam JK, Lee GC, Tao PL, Ling DQ, Cheng M, et al. A novel literature-based approach to identify genetic and molecular predictors of survival in glioblastoma multiforme: Analysis of 14,678 patients using systematic review and meta-analytical tools. *J Clin Neurosci* [Internet]. 2015;22(5):785–99. Available from:
<http://www.ncbi.nlm.nih.gov/pubmed/25698544>
 53. Yan H, Parsons DW, Jin G, McLendon R, Rasheed BA, Yuan W, et al. IDH1 and IDH2 Mutations in Gliomas. *N Engl J Med* [Internet]. 2009;360(8):765–73. Available from: <http://www.nejm.org/doi/abs/10.1056/NEJMoa0808710>
 54. McLendon R, Friedman A, Bigner D, Van Meir EG, Brat DJ, M. Mastrogiannis G, et al. Comprehensive genomic characterization defines human glioblastoma genes and core pathways. *Nature*. 2008;455(7216):1061–8.
 55. Cohen A, Holmen S, Colman H. IDH1 and IDH2 Mutations in Gliomas. *Curr Neurol Neurosci Rep*. 2013;13(5):345.
 56. Sanson M, Marie Y, Paris S, Idhah A, Laffaire J, Ducray F, et al. Isocitrate dehydrogenase 1 codon 132 mutation is an important prognostic biomarker in gliomas. *J Clin Oncol*. 2009;27(25):4150–4.
 57. Thomas J. Lynch, M.D., Daphne W. Bell, Ph.D., Raffaella Sordella, Ph.D.,

- Sarada Gurubhagavatula, M.D., Ross A. Okimoto, B.S., Brian W. Brannigan, B.A., Patricia L. Harris, M.S., Sara M. Haserlat, B.A., Jeffrey G. Supko, Ph.D., Frank G. Haluska, M.D., Ph.D PD, Abstract. Activating Mutations in the Epidermal Growth Factor Receptor Underlying Responsiveness of Non-Small-Cell Lung Cancer to Gefitinib Thomas. *N Engl J Med*. 2014;350(21):2129–39.
58. Kwak EL, Bang Y-J, Camidge DR, Shaw AT, Solomon B, Maki RG, et al. Anaplastic Lymphoma Kinase Inhibition in Non-Small-Cell Lung Cancer. *N Engl J Med*. 2010;363(18):1693–703.
 59. Raizer JJ, Abrey LE, Lassman AB, Chang SM, Lamborn R, Kuhn JG, et al. A phase 2 trial of erlotinib in patients with recurrent malignant gliomas and non progressive glioblastoma multiforme post radiation therapy. *Neuro Oncol*. 2010;12(1):95–103.
 60. Chheda MG, Wen PY, Hochberg FH, Chi AS, Drappatz J, Eichler AF, et al. Vandetanib plus sirolimus in adults with recurrent glioblastoma: results of a phase I and dose expansion cohort study. *J Neurooncol*. 2015;121(3):627–34.
 61. Zorzan M, Giordan E, Redaelli M, Caretta A, Mucignat-Caretta C. Molecular targets in glioblastoma. *Futur Oncol*. 2015;11(9):1407–20.
 62. Dandy WE. Removal of right cerebral hemisphere for certain tumours with hemiplegia: Preliminary Report. *J Am Med Assoc*. 1928;90(11):823–5.
 63. Silbergeld DL, Rostomily RC, Alvord EC. The cause of death in patients with glioblastoma is multifactorial: - Clinical factors and autopsy findings in 117 cases of supratentorial glioblastoma in adults. *J Neurooncol*. 1991;
 64. Facchino S, Abdouh M, Bernier G. Brain cancer stem cells: Current status on glioblastoma multiforme. *Cancers (Basel)*. 2011;3(2):1777–97.
 65. Parker NR, Khong P, Parkinson JF, Howell VM, Wheeler HR. Molecular Heterogeneity in Glioblastoma: Potential Clinical Implications. *Front Oncol* [Internet]. 2015;5(March):1–9. Available from: <http://journal.frontiersin.org/Article/10.3389/fonc.2015.00055/abstract>
 66. Patel AP, Tirosh I, Trombetta JJ, Shalek AK, Gillespie SM, Wakimoto H, et al. Single-cell RNA-seq highlights intratumoral heterogeneity in primary glioblastoma. *Science (80-)*. 2014;344(6190):1396–401.
 67. Baysan M, Woolard K, Cam MC, Zhang W, Song H, Kotliarova S, et al. Detailed Longitudinal Sampling of Glioma Stem Cells In Situ Reveals Chr7 Gain and Chr10 Loss As Repeated Events in Primary Tumor Formation and Recurrence. *Int J Cancer* [Internet]. 2017;2013:2002–13. Available from: <http://doi.wiley.com/10.1002/ijc.30887>
 68. Westphal M, Maire CL, Lamszus K. EGFR as a Target for Glioblastoma Treatment: An Unfulfilled Promise. *CNS Drugs*. 2017;31(9):723–35.
 69. Ding H, Nagy A, Gutmann DH, Guha A, Gurmman D. A review of astrocytoma models. *Neurosurg Focus*. 2000;8(4):1–8.
 70. William D, Mullins CS, Schneider B, Orthmann A, Lamp N, Krohn M, et al. Optimized creation of glioblastoma patient derived xenografts for use in preclinical studies. *J Transl Med* [Internet]. 2017;15(1):27. Available from: <http://www.ncbi.nlm.nih.gov/pubmed/28183348><http://www.pubmedcentral.nih.gov/articlerender.fcgi?artid=PMC5301415>
 71. Laverty H, Benson C, Cartwright E, Cross M, Garland C, Hammond T, et al. How can we improve our understanding of cardiovascular safety liabilities to develop safer medicines? *Br J Pharmacol* [Internet]. 2011;163(4):675–93. Available from: <http://doi.wiley.com/10.1111/j.1476-5381.2011.01255.x>

72. El Meskini R, Iacovelli AJ, Kulaga A, Gumprecht M, Martin PL, Baran M, et al. A preclinical orthotopic model for glioblastoma recapitulates key features of human tumors and demonstrates sensitivity to a combination of MEK and PI3K pathway inhibitors. *Dis Model Mech* [Internet]. 2015;8(1):45–56. Available from: <http://dmm.biologists.org/cgi/doi/10.1242/dmm.018168>
73. Semenkow S, Li S, Kahlert UD, Raabe EH, Xu J, Janowski M, et al. An immunocompetent mouse model of human glioblastoma. 2017;8(37):1–11.
74. Allen DD, Caviedes R, Cárdenas AM, Shimahara T, Segura-Aguilar J, Caviedes P a. Cell lines as in vitro models for drug screening and toxicity studies. *Drug Dev Ind Pharm*. 2005;31(8):757–68.
75. Inamdar NK, Borenstein JT. Microfluidic cell culture models for tissue engineering. *Curr Opin Biotechnol* [Internet]. 2011 Oct [cited 2015 Nov 10];22(5):681–9. Available from: <http://www.sciencedirect.com/science/article/pii/S0958166911006161>
76. A. Dawson, V. Green, R. Bower JG. Microfluidics: The fur-free way towards personalised medicine in cancer therapy. *Drug Target Rev*. 2016;3:12–7.
77. Iom. Conflict of interest in medical research, education, and practice [Internet]. *Conflict of Interest in Medical Research, Education, and Practice*. 2009 [cited 2017 Apr 23]. 440 p. Available from: https://www.ncbi.nlm.nih.gov/books/NBK22942/pdf/Bookshelf_NBK22942.pdf
78. Brannen KC, Chapin RE, Jacobs AC, Green ML. Alternative models of developmental and reproductive toxicity in pharmaceutical risk assessment and the 3Rs. *ILAR J*. 2016;57(2):144–56.
79. Yi Y, Park J, Lim J, Lee CJ, Lee SH. Central Nervous System and its Disease Models on a Chip. *Trends Biotechnol* [Internet]. 2015;33(12):762–76. Available from: <http://dx.doi.org/10.1016/j.tibtech.2015.09.007>
80. Clemence M, Leaman J. Public attitudes to animal research in 2016. *Ipsos MORI | Public attitudes to Anim Res – 2016 Rep* [Internet]. 2016;(July). Available from: <http://www.ipsos-mori.com/terms>.
81. Midasi JA, Grabowski HG, Hansen RW. The Cost of Drug Development. *N Engl J Med*. 2015;372(1):1972.
82. Arrowsmith J. Trial watch: Phase II failures: 2008–2010. *Nat Rev Drug Discov* [Internet]. 2011;10(5):328–9. Available from: <http://www.nature.com/doi/10.1038/nrd3439>
83. Cook D, Brown D, Alexander R, March R, Morgan P, Satterthwaite G, et al. Lessons learned from the fate of AstraZeneca’s drug pipeline: a five-dimensional framework. *Nat Rev Drug Discov* [Internet]. 2014;13(6):419–31. Available from: <http://www.nature.com/doi/10.1038/nrd4309>
84. Ziółkowska K, Kwapiszewski R, Brzózka Z. Microfluidic devices as tools for mimicking the in vivo environment. *New J Chem* [Internet]. 2011;35(5):979. Available from: <http://pubs.rsc.org/en/content/articlehtml/2011/nj/c0nj00709a>
85. Taylor AM, Jeon NL. Micro-scale and microfluidic devices for neurobiology. *Curr Opin Neurobiol* [Internet]. 2010;20(5):640–7. Available from: <http://www.sciencedirect.com/science/article/pii/S0959438810001194>
86. Wei Z, Amponsah PK, Al-Shatti M, Nie Z, Bandyopadhyay BC. Engineering of polarized tubular structures in a microfluidic device to study calcium phosphate stone formation. *Lab Chip* [Internet]. 2012 Oct 21 [cited 2016 Jan 2];12(20):4037–40. Available from: <http://pubs.rsc.org/en/content/articlehtml/2012/lc/c2lc40801e>

87. Yetisen AK, Volpatti LR. Patent protection and licensing in microfluidics. *Lab Chip* [Internet]. 2014;14(13):2217. Available from: <http://xlink.rsc.org/?DOI=c4lc00399c>
88. Kang DK, Monsur Ali M, Zhang K, Pone EJ, Zhao W. Droplet microfluidics for single-molecule and single-cell analysis in cancer research, diagnosis and therapy. *TrAC - Trends Anal Chem* [Internet]. 2014;58:145–53. Available from: <http://dx.doi.org/10.1016/j.trac.2014.03.006>
89. Liong M, Hoang AN, Chung J, Gural N, Ford CB, Min C, et al. Magnetic barcode assay for genetic detection of pathogens. *Nat Commun*. 2013;4.
90. Van Midwoud PM, Groothuis GMM, Merema MT, Verpoorte E. Microfluidic biochip for the perfusion of precision-cut rat liver slices for metabolism and toxicology studies. *Biotechnol Bioeng*. 2010;105(1):184–94.
91. Huang Y, Agrawal B, Sun D, Kuo JS, Williams JC. Microfluidics-based devices: New tools for studying cancer and cancer stem cell migration. *Biomicrofluidics*. 2011;5(1):1–17.
92. Swain JE, Smith GD. Advances in embryo culture platforms: novel approaches to improve preimplantation embryo development through modifications of the microenvironment. *Hum Reprod Update*. 2011;17(4):541–57.
93. Park J, Kim S, Park SI, Choe Y, Li J, Han A. A microchip for quantitative analysis of CNS axon growth under localized biomolecular treatments. *J Neurosci Methods* [Internet]. 2014 Jan 15 [cited 2015 Dec 27];221:166–74. Available from: <http://www.sciencedirect.com/science/article/pii/S0165027013003294>
94. Young EWK. Advances in Microfluidic Cell Culture Systems for Studying Angiogenesis. *J Lab Autom* [Internet]. 2013;(X):2211068213495206-. Available from: <http://jla.sagepub.com/content/early/2013/07/03/2211068213495206.long>
95. Dollé J-P, Morrison B, Schloss RS, Yarmush ML. An organotypic uniaxial strain model using microfluidics. *Lab Chip* [Internet]. 2013;13(3):432–42. Available from: <http://pubs.rsc.org/en/content/articlehtml/2013/lc/c2lc41063j>
96. Huh D, Matthews BD, Mammoto A, Montoya-Zavala M, Hsin HY, Ingber DE. Reconstituting Organ-Level Lung Functions on a Chip. *Science* (80-) [Internet]. 2010;328(5986):1662–8. Available from: <http://www.sciencemag.org/cgi/doi/10.1126/science.1188302>
97. Huang Y, Agrawal B, Clark P a, Williams JC, Kuo JS. Evaluation of cancer stem cell migration using compartmentalizing microfluidic devices and live cell imaging. *J Vis Exp* [Internet]. 2011;(58):e3297. Available from: <http://www.pubmedcentral.nih.gov/articlerender.fcgi?artid=3369664&tool=pmcentrez&rendertype=abstract>
98. Logun MT, Bisel NS, Tanasse EA, Zhao W, Gunasekera B, Mao L, et al. Glioma cell invasion is significantly enhanced in composite hydrogel matrices composed of chondroitin 4- and 4,6-sulfated glycosaminoglycans. *J Mater Chem B* [Internet]. 2016;4:6052–64. Available from: <http://pubs.rsc.org/en/content/articlehtml/2016/tb/c6tb01083k>
99. Ziolkowska K, Stelmachowska A, Kwapiszewski R, Chudy M, Dybko A, Brzozka Z. Long-term three-dimensional cell culture and anticancer drug activity evaluation in a microfluidic chip. *Biosens Bioelectron*. 2013;40(1):68–74.
100. Tanweer F, Green VL, Stafford ND, Greenman J. Application of microfluidic

- systems in management of head and neck squamous cell carcinoma. *Head Neck*. 2013;3(5):756–63.
101. Griep LM, Wolbers F, de Wagenaar B, ter Braak PM, Weksler BB, Romero IA, et al. BBB ON CHIP: microfluidic platform to mechanically and biochemically modulate blood-brain barrier function. *Biomed Microdevices* [Internet]. 2013;15(1):145–50. Available from: <http://link.springer.com/10.1007/s10544-012-9699-7>
 102. Gomez FA. The future of microfluidic point-of-care diagnostic devices. *Bioanalysis*. 2013;5(1):1–3.
 103. Yetisen AK, Akram MS, Lowe CR. Paper-based microfluidic point-of-care diagnostic devices. *Lab Chip*. 2013;13(12):2210–51.
 104. Xu H, Li Z, Yu Y, Sizzdahkhani S, Ho WS, Yin F, et al. A dynamic in vivo-like organotypic blood-brain barrier model to probe metastatic brain tumors. *Sci Rep* [Internet]. 2016;6(May):1–12. Available from: <http://dx.doi.org/10.1038/srep36670>
 105. Wang YI, Abaci HE, Shuler ML. Microfluidic blood–brain barrier model provides in vivo-like barrier properties for drug permeability screening. *Biotechnol Bioeng*. 2017;114(1):184–94.
 106. Shao X, Gao D, Chen Y, Jin F, Jiang U, Liu H. Development of a blood-brain barrier model in a membrane-based microchip for characterization of drug permeability and cytotoxicity for drug screening. *Anal Chim Acta*. 2016;934:186–93.
 107. Terrell-Hall TB, Ammer AG, Griffith JIG, Lockman PR. Permeability across a novel microfluidic blood-tumor barrier model. *Fluids Barriers CNS*. 2017;14(1):1–10.
 108. Adriani G, Ma D, Pavesi A, Kamm RD, Goh ELK. A 3D neurovascular microfluidic model consisting of neurons, astrocytes and cerebral endothelial cells as a blood–brain barrier. *Lab Chip* [Internet]. 2017;17(3):448–59. Available from: <http://xlink.rsc.org/?DOI=C6LC00638H>
 109. Falanga AP, Pitingolo G, Celentano M, Cosentino A, Melone P, Vecchione R, et al. Shuttle-mediated nanoparticle transport across an in vitro brain endothelium under flow conditions. *Biotechnol Bioeng*. 2017;114(5):1087–95.
 110. Shibata K, Terazono H, Hattori A, Yasuda K. Collagen micro-flow channels as an for in vitro blood-brain barrier model. *Jpn J Appl Phys*. 2008;47(6 PART 2):5208–11.
 111. Prabhakarandian B, Shen M-C, Nichols JB, Mills IR, Sidoryk-Wegrzynowicz M, Aschner M, et al. SyM-BBB: a microfluidic blood brain barrier model. *Lab Chip* [Internet]. 2013;13(6):1093. Available from: <http://xlink.rsc.org/?DOI=c2lc41208j>
 112. Booth R, Kim H. Characterization of a microfluidic in vitro model of the blood-brain barrier (μ BBB). *Lab Chip* [Internet]. 2012;12(10):1784. Available from: <http://xlink.rsc.org/?DOI=c2lc40094d>
 113. Brown JA, Pensabene V, Markov DA, Allwardt V, Diana Neely M, Shi M, et al. Recreating blood-brain barrier physiology and structure on chip: A novel neurovascular microfluidic bioreactor. *Biomicrofluidics* [Internet]. 2015;9(5). Available from: <http://dx.doi.org/10.1063/1.4934713>
 114. Walter FR, Valkai S, Kincses A, Petnehazi A, Czeller T, Veszélka S, et al. A versatile lab-on-a-chip tool for modeling biological barriers. *Sensors Actuators, B Chem* [Internet]. 2016;222:1209–19. Available from:

- <http://dx.doi.org/10.1016/j.snb.2015.07.110>
115. Le Gac S, Nordhoff V. Microfluidics for mammalian embryo culture and selection: Where do we stand now? *Mol Hum Reprod.* 2017;23(4):213–26.
 116. Raty S, Walters EM, Davis J, Zeringue H, Beebe DJ, Rodriguez-Zas SL, et al. Embryonic development in the mouse is enhanced via microchannel culture. *Lab Chip.* 2004;4:186–90.
 117. Yang F, Chen Z, Pan J, Li X, Feng J, Yang H. An integrated microfluidic array system for evaluating toxicity and teratogenicity of drugs on embryonic zebrafish developmental dynamics. *Biomicrofluidics.* 2011;5(2):1–13.
 118. Kim HS, Jeong S, Koo C, Han A, Park J. A microchip for high-throughput axon growth drug screening. *Micromachines.* 2016;7(7):1–13.
 119. Kilinc D, Peyrin JM, Soubeyre V, Magnifico S, Saias L, Viovy JL, et al. Wallerian-like degeneration of central neurons after synchronized and geometrically registered mass axotomy in a three-compartmental microfluidic chip. *Neurotox Res.* 2011;19(1):149–61.
 120. Kerman BE, Kim HJ, Padmanabhan K, Mei A, Georges S, Joens MS, et al. In vitro myelin formation using embryonic stem cells. *Development* [Internet]. 2015;142(12):2213–25. Available from: <http://dev.biologists.org/cgi/doi/10.1242/dev.116517>
 121. Li Jeon N, Baskaran H, Dertinger SKW, Whitesides GM, Van de Water L, Toner M. Neutrophil chemotaxis in linear and complex gradients of interleukin-8 formed in a microfabricated device. *Nat Biotechnol.* 2002;20(8):826–30.
 122. Mi S, Du Z, Xu Y, Wu Z, Qian X, Zhang M, et al. Microfluidic co-culture system for cancer migratory analysis and anti-metastatic drugs screening. *Sci Rep* [Internet]. 2016;6:35544. Available from: <http://www.nature.com/articles/srep35544>
 123. Anguiano M, Castilla C, Maška M, Ederra C, Peláez R, Morales X, et al. Characterization of three-dimensional cancer cell migration in mixed collagen-Matrigel scaffolds using microfluidics and image analysis. *PLoS One* [Internet]. 2017;12(2):e0171417. Available from: <http://dx.plos.org/10.1371/journal.pone.0171417>
 124. Gallego-Perez D, Higuera-Castro N, Denning L, DeJesus J, Dahl K, Sarkar A, et al. Microfabricated mimics of in vivo structural cues for the study of guided tumor cell migration. *Lab Chip* [Internet]. 2012;12(21):4424–32. Available from: <http://dx.doi.org/10.1039/C2LC40726D>
<http://pubs.rsc.org/en/content/articlepdf/2012/lc/c2lc40726d>
 125. Blaha L, Zhang C, Cabodi M, Wong JY. A microfluidic platform for modeling metastatic cancer cell matrix invasion A micro fluidic platform for modeling metastatic cancer cell matrix invasion. *Biofabrication.* 2017;9.
 126. Irimia D, Ellett F. Big insights from small volumes : deciphering complex leukocyte behaviors using microfluidics. *J Leukoc Biol.* 2016;100(August):0–0.
 127. Low LA, Tagle DA. Tissue chips – innovative tools for drug development and disease modeling. *Lab Chip* [Internet]. 2017;17:3026–36. Available from: <http://xlink.rsc.org/?DOI=C7LC00462A>
 128. Grosberg A, Alford PW, McCain ML, Parker KK. Ensembles of engineered cardiac tissues for physiological and pharmacological study: Heart on a chip. *Lab Chip.* 2011;11(24):4165.

129. Verneti LA, Senutovitch N, Boltz R, DeBiasio R, Ying Shun T, Gough A, et al. A human liver microphysiology platform for investigating physiology, drug safety, and disease models. *Exp Biol Med* (Maywood) [Internet]. 2016;241(1):101–14. Available from: <http://www.pubmedcentral.nih.gov/articlerender.fcgi?artid=4723301&tool=pmcentrez&rendertype=abstract>
130. Rigat-Brugarolas LG, Elizalde-Torrent A, Bernabeu M, De Niz M, Martin-Jaular L, Fernandez-Becerra C, et al. A functional microengineered model of the human splenon-on-a-chip. *Lab Chip* [Internet]. 2014;14(10):1715. Available from: <http://www.ncbi.nlm.nih.gov/pubmed/24663955%5Cnhttp://xlink.rsc.org/?DOI=c3lc51449h>
131. Yasotharan S, Pinto S, Sled JG, Bolz S-S, Günther A. Artery-on-a-chip platform for automated, multimodal assessment of cerebral blood vessel structure and function. *Lab Chip* [Internet]. 2015;15(12):2660–9. Available from: <http://pubs.rsc.org/en/content/articlelanding/2015/lc/c5lc00021a%5Cnhttp://moscow.sci-hub.cc/15289c41e4a2296dff60224b8213c8c9/yasotharan2015.pdf>
132. Hasan A, Paul A, Memic A, Khademhosseini A. A multilayered microfluidic blood vessel-like structure. *Biomed Microdevices* [Internet]. 2015;17(5):88. Available from: <http://link.springer.com/10.1007/s10544-015-9993-2>
133. Perestrelo AR, Águas ACP, Rainer A, Forte G. Microfluidic organ/body-on-a-chip devices at the convergence of biology and microengineering. *Sensors* (Switzerland). 2015;15(12):31142–70.
134. Maschmeyer I, Lorenz AK, Schimek K, Hasenberg T, Ramme AP, Hübner J, et al. A four-organ-chip for interconnected long-term co-culture of human intestine, liver, skin and kidney equivalents. *Lab Chip* [Internet]. 2015;15(12):2688–99. Available from: <http://pubs.rsc.org.globalproxy.cvt.dk/en/content/articlehtml/2015/lc/c5lc00392j>
135. Wikswo JP, Curtis EL, Eagleton ZE, Evans BC, Kole A, Hofmeister LH, et al. Scaling and systems biology for integrating multiple organs-on-a-chip. *Lab Chip* [Internet]. 2013;13(18):3496–511. Available from: <http://pubs.rsc.org/en/content/articlehtml/2013/lc/c3lc50243k>
136. Booth R, Kim H. Characterization of a microfluidic in vitro model of the blood-brain barrier (μ BBB). *Lab Chip* [Internet]. 2012;12(10):1784. Available from: <http://xlink.rsc.org/?DOI=c2lc40094d>
137. Verneti L, Gough A, Baetz N, Blutt S, Broughman JR, Brown JA, et al. Functional Coupling of Human Microphysiology Systems: Intestine, Liver, Kidney Proximal Tubule, Blood-Brain Barrier and Skeletal Muscle. *Sci Rep* [Internet]. 2017;7(February):42296. Available from: <http://www.nature.com/articles/srep42296>
138. Emulate. Emulate Bio [Internet]. [cited 2017 Nov 10]. Available from: <https://emulatebio.com/about/>
139. Anderson ILK, College C. The perfusion of surviving organs. *J Physiol*. 1903;29(3):266–75.
140. Fell HB. The Application of Tissue Culture In Vitro To Embryology. *J R Microsc Soc*. 1940;
141. Stoppini L, Buchs P-A, Muller D. A simple method for organotypic cultures of nervous tissue. *J Neurosci Methods* [Internet]. 1991;37(2):173–82.

Available from:

<http://linkinghub.elsevier.com/retrieve/pii/016502709190128M>

142. Röller M, Owen SP, Heidelberger C. Studies on the Organ Culture of Human Tumors on the Organ Culture of Human. 1966;26(April):626–37.
143. Guerrero RR, Rounds DE, Booher J. An Improved Organ Culture Method for Adult Mammalian Lung. *In Vitro*. 1977;13(8):517–24.
144. Komeya M, Kimura H, Nakamura H, Yokonishi T, Sato T, Kojima K, et al. Long-term ex vivo maintenance of testis tissues producing fertile sperm in a microfluidic device. *Sci Rep* [Internet]. 2016;6(1):21472. Available from: <http://www.nature.com/articles/srep21472>
145. Yarnell M, Ambrose EJ, Shepley K, Tchao R. Drug Assays on Organ Cultures of Biopsies from Human Tumours. *BMJ*. 1964;2(August):490–1.
146. Masters JRW, Krishnaswamy A, Rigby CC, O'Donoghue EPN. An approach to prediction of tumour response. *Br J Cancer*. 1980;41:199–202.
147. Howdle PD. Organ culture of gastrointestinal mucosa - a technique for the study of the human gastrointestinal tract. *Postgrad Med J*. 1984;(60):645–52.
148. Arsenault P, Menard D. Influence of hydrocortisone on human fetal small intestine in organ culture. *J Pediatr Gastroenterol Nutr* [Internet]. 1985;4(6):893–901. Available from: <http://www.ncbi.nlm.nih.gov/pubmed/4067777>
149. Shamir ER, Ewald AJ. Three-dimensional organotypic culture: experimental models of mammalian biology and disease. *Nat Rev Mol Cell Biol* [Internet]. 2014;15(10):647–64. Available from: <http://www.nature.com/doifinder/10.1038/nrm3873>
150. Jain V, Langham MC, Wehrli FW. MRI estimation of global brain oxygen consumption rate. *J Cereb Blood Flow Metab* [Internet]. 2010;30(9):1598–607. Available from: <http://dx.doi.org/10.1038/jcbfm.2010.49>
151. Huang Y, Williams JC, Johnson SM. Brain slice on a chip: opportunities and challenges of applying microfluidic technology to intact tissues. *Lab Chip* [Internet]. 2012;12(12):2103–17. Available from: <http://www.ncbi.nlm.nih.gov/pubmed/22534786>
152. Haas HL, Schaerer B, Vosmansky M. A simple perfusion chamber for the study of nervous tissue slices in vitro. *J Neurosci Methods*. 1979;1(4):323–5.
153. Reynaud J., Martini F, Chatel C, Buclin M, Raggenbass M, Puizillout J-J. A new interface chamber for the study of mammalian nervous tissue slices. *J Neurosci Methods*. 1995;58:203–8.
154. Passeraub P, Almeida A, Thakor N. Design, microfabrication and analysis of a microfluidic chamber for the perfusion of brain tissue slices. *Biomed Microdevices* [Internet]. 2003;5(2):147–55. Available from: <http://www.springerlink.com/index/k26hv43718tr31u1.pdf%5Cnhttp://link.springer.com/article/10.1023/A:1024547413721>
155. Nicoll RA, Alger BE. A simple chamber for recording from submerged brain slices. *J Neurosci Methods*. 1981;4(2):153–6.
156. Killian NJ, Vernekar VN, Potter SM, Vukasinovic J. A device for long-term perfusion, imaging, and electrical interfacing of brain tissue in vitro. *Front Neurosci*. 2016;10(MAR):1–14.
157. Hajos N, Mody I. Establishing a physiological environment for visualized in vitro brain slice recordings by increasing oxygen supply and modifying aCSF content. *J Neurosci Methods* [Internet]. 2009;183(2):107–13. Available from: <http://dx.doi.org/10.1016/j.jneumeth.2009.06.005>

158. Choi Y, McClain MA, LaPlaca MC, Frazier AB, Allen MG. Three dimensional MEMS microfluidic perfusion system for thick brain slice cultures. *Biomed Microdevices*. 2007;9(1):7–13.
159. Rambani K, Vukasinovic J, Glezer A, Potter SM. Culturing thick brain slices: An interstitial 3D microperfusion system for enhanced viability. *J Neurosci Methods*. 2009;180(2):243–54.
160. Blake AJ, Rodgers FC, Bassuener A, Hippensteel JA, Pearce TM, Pearce TR, et al. A microfluidic brain slice perfusion chamber for multisite recording using penetrating electrodes. *J Neurosci Methods* [Internet]. 2010 May 30 [cited 2016 Mar 8];189(1):5–13. Available from: <http://www.sciencedirect.com/science/article/pii/S0165027010001111>
161. Tang YT, Kim J, Lopez-Valdes H, Brennan KC, Ju YS. Development and characterization of a microfluidic chamber incorporating fluid ports with active suction for localized chemical stimulation of brain slices. *Lab Chip*. 2011;11:2247–54.
162. Hill MRH, Greenfield SA. The membrane chamber: A new type of in vitro recording chamber. *J Neurosci Methods* [Internet]. 2011;195(1):15–23. Available from: <http://dx.doi.org/10.1016/j.jneumeth.2010.10.024>
163. Blake A, Pearce TM, Rao NS, Johnson SM, Williams JC. Multilayer PDMS microfluidic chamber for controlling brain slice microenvironment. *Lab Chip*. 2007;7(7):842–9.
164. Mauleon G, Fall CP, Eddington DT. Precise spatial and temporal control of oxygen within in vitro brain slices via microfluidic gas channels. *PLoS One* [Internet]. 2012;7(8):e43309. Available from: <http://www.pubmedcentral.nih.gov/articlerender.fcgi?artid=3419219&tool=pmcentrez&rendertype=abstract>
165. Sun M, Kaplan S V, Gehringer RC, Limbocker R a, Johnson M a. Localized drug application and sub-second voltammetric dopamine release measurements in a brain slice perfusion device. *Anal Chem* [Internet]. 2014;86(9):4151–6. Available from: <http://www.ncbi.nlm.nih.gov/pubmed/24734992>
166. Gahwiler B. Organotypic monolayer cultures of nervous tissue. *J Neurosci Met*. 1981;4:329–42.
167. Hoffer B, Seiger A, Ljungberg T, Olson L. Electrophysiological and cytological studies of homografts in the anterior chamber of the eye: Maturation of the cerebellar cortex in oculo. *Brain Res*. 1974;79:165–84.
168. Humpel C. Organotypic brain slice cultures: A review. *Neuroscience* [Internet]. 2015;305:86–98. Available from: <http://dx.doi.org/10.1016/j.neuroscience.2015.07.086>
169. Berdichevsky Y, Staley KJ, Yarmush ML. Building and manipulating neural pathways with microfluidics. *Lab Chip* [Internet]. 2010;10(8):999–1004. Available from: <http://www.pubmedcentral.nih.gov/articlerender.fcgi?artid=3137909&tool=pmcentrez&rendertype=abstract>
170. Dollé J-P, Morrison B, Schloss RS, Yarmush ML. An organotypic uniaxial strain model using microfluidics. *Lab Chip* [Internet]. 2013 Feb 7 [cited 2016 Mar 8];13(3):432–42. Available from: <http://pubs.rsc.org/en/content/articlehtml/2013/lc/c2lc41063j>
171. Caicedo H, Vignes M, Brugg B. Microfluidic Culture Chamber for the Long-Term Perfusion and Precise Chemical Stimulation of Organotypic Brain

- Tissue. 14Th Int Conf Miniaturized Syst Fr Chem Life Sci [Internet]. 2010;(October):1835–7. Available from: http://www.rsc.org/binaries/LOC/2010/PDFs/Papers/625_0125.pdf
172. Liu J, Pan L, Cheng X, Berdichevsky Y. Perfused drop microfluidic device for brain slice culture-based drug discovery. *Biomed Microdevices* [Internet]. 2016;18(3). Available from: <http://dx.doi.org/10.1007/s10544-016-0073-z>
 173. Mohammed JS, Caicedo HH, Fall CP, Eddington DT. Microfluidic add-on for standard electrophysiology chambers. *Lab Chip* [Internet]. 2008;8(7):1048. Available from: <http://xlink.rsc.org/?DOI=b802037j>
 174. Caicedo HH, Hernandez M, Fall CP, Eddington DT. Multiphysics simulation of a microfluidic perfusion chamber for brain slice physiology. *Biomed Microdevices*. 2010;12(5):761–7.
 175. Queval A, Ghattamaneni NR, Perrault CM, Gill R, Mirzaei M, McKinney RA, et al. Chamber and microfluidic probe for microperfusion of organotypic brain slices. *Lab Chip* [Internet]. 2010;10(3):326–34. Available from: <http://pubs.rsc.org/en/content/articlelanding/2010/lc/b916669f%5Cnhttp://pubs.rsc.org/EN/content/articlelanding/2010/lc/b916669f#!divAbstract>
 176. Beraki S, Litrus L, Soriano L, Monbureau M, To LK, Braithwaite SP, et al. A Pharmacological Screening Approach for Discovery of Neuroprotective Compounds in Ischemic Stroke. *PLoS One*. 2013;8(7):1–13.
 177. Noraberg J, Kristensen BW, Zimmer J. Markers for neuronal degeneration in organotypic slice cultures. *Brain Res Brain Res Protoc* [Internet]. 1999;3(3):278–90. Available from: <http://www.ncbi.nlm.nih.gov/pubmed/9974143>
 178. van Midwoud PM, Merema MT, Verpoorte E, Groothuis GMM. Microfluidics enables small-scale tissue-based drug metabolism studies with scarce human tissue. *J Lab Autom* [Internet]. 2011 Dec 1 [cited 2015 Dec 8];16(6):468–76. Available from: <http://jla.sagepub.com/cgi/content/long/16/6/468>
 179. Hattersley SM, Sylvester DC, Dyer CE, Stafford ND, Haswell SJ, Greenman J. A microfluidic system for testing the responses of head and neck squamous cell carcinoma tissue biopsies to treatment with chemotherapy drugs. *Ann Biomed Eng* [Internet]. 2012;40(6):1277–88. Available from: <http://www.ncbi.nlm.nih.gov/pubmed/21997391>
 180. Carr SD, Green VL, Stafford ND, Greenman J. Analysis of radiation-induced cell death in head and neck squamous cell carcinoma and rat liver maintained in microfluidic devices. *Otolaryngol Head Neck Surg* [Internet]. 2014;150(1):73–80. Available from: <http://www.ncbi.nlm.nih.gov/pubmed/24098006>
 181. Astolfi M, Péant B, Lateef MA, Rousset N, Kendall-Dupont J, Carmona E, et al. Micro-dissected tumor tissues on chip: an ex vivo method for drug testing and personalized therapy. *Lab Chip* [Internet]. 2015;16(2):312–25. Available from: <http://pubs.rsc.org/en/content/articlehtml/2016/lc/c5lc01108f>
 182. Cheah L-T, Dou Y-H, Seymour A-ML, Dyer CE, Haswell SJ, Wadhawan JD, et al. Microfluidic perfusion system for maintaining viable heart tissue with real-time electrochemical monitoring of reactive oxygen species. *Lab Chip* [Internet]. 2010;10(20):2720. Available from: <http://xlink.rsc.org/?DOI=c004910g>
 183. Dawson A, Dyer C, Macfie J, Davies J, Karsai L, Greenman J, et al. A microfluidic chip based model for the study of full thickness human intestinal

- tissue using dual flow. *Biomicrofluidics* [Internet]. 2016;10(064101):0–10. Available from: <http://dx.doi.org/10.1063/1.4964813> <http://scitation.aip.org/content/aip/journal/bmf/10/6?ver=pdfcov>
184. Zambon A, Zoso A, Gagliano O, Magrofuoco E, Fadini GP, Avogaro A, et al. High Temporal Resolution Detection of Patient-Specific Glucose Uptake from Human ex Vivo Adipose Tissue On-Chip. *Anal Chem*. 2015;87(13):6535–43.
 185. Changa TC, Mikheevb AM, Huynha W, Jr. RJM, Rostomily RC, Folch A. Parallel Microfluidic Chemosensitivity Testing on Individual Slice Cultures. *Lab Chip*. 2014;14(23):4540–51.
 186. Kuntaegowdanahalli SS, Bhagat AAS, Kumar G, Papautsky I. Inertial microfluidics for continuous particle separation in spiral microchannels. *Lab Chip*. 2009;9(2):2973–80.
 187. Pedron S, Becka E, Harley BA. Spatially graded hydrogel platform as a 3D engineered tumor microenvironment. *Adv Mater*. 2015;27(9):1567–72.
 188. Ayuso JM, Monge R, Martínez-González A, Virumbrales-Muñoz M, Llamazares GA, Berganzo J, et al. Glioblastoma on a microfluidic chip: Generating pseudopalisades and enhancing aggressiveness through blood vessel obstruction events. *Neuro Oncol* [Internet]. 2017;19(January):now230. Available from: <http://neuro-oncology.oxfordjournals.org/lookup/doi/10.1093/neuonc/now230>
 189. Gallego-Perez D, Higuera-Castro N, Denning L, DeJesus J, Dahl K, Sarkar A, et al. Microfabricated mimics of in vivo structural cues for the study of guided tumor cell migration. *Lab Chip*. 2012;12(21):4424–32.
 190. Able R a., Ngnabeuye C, Beck C, Holland EC, Vazquez M. Low concentration microenvironments enhance the migration of neonatal cells of glial lineage. *Cell Mol Bioeng*. 2012;5(2):128–42.
 191. Wan Y, Tamuly D, Allen PB, Kim YT, Bachoo R, Ellington AD, et al. Proliferation and migration of tumor cells in tapered channels. *Biomed Microdevices*. 2013;15(4):635–43.
 192. Liu W, Sun P, Yang L, Wang J, Li L, Wang J. Assay of glioma cell responses to an anticancer drug in a cell-based microfluidic device. *Microfluid Nanofluidics*. 2010;9(4–5):717–25.
 193. Liu W, Xu J, Li T, Zhao L, Ma C, Shen S, et al. Monitoring Tumor Response to Anticancer Drugs Using Stable Three-Dimensional Culture in a Recyclable Microfluidic Platform. *Anal Chem*. 2015;87(19):9752–60.
 194. Pang L, Liu W, Tian C, Xu J, Li T, Chen S, et al. Construction of single-cell arrays and assay of cell drug-resistance in an integrated microfluidics. *Lab Chip* [Internet]. 2016;15:473–83. Available from: <http://pubs.rsc.org/en/Content/ArticleLanding/2016/LC/C6LC01000H>
 195. Wang J, Hwang K, Braas D, Dooraghi A, Nathanson D, Campbell DO, et al. Fast Metabolic Response to Drug Intervention Through Analysis on a Miniaturized, Highly Integrated Molecular Imaging System. *J Nucl Med* [Internet]. 2013;54(10):1820–4. Available from: <http://jnm.snmjournals.org/cgi/doi/10.2967/jnumed.112.118497>
 196. Shin YS, Kim J, Johnson D, Dooraghi AA, Mai WX, Ta L, et al. Quantitative assessments of glycolysis from single cells. *Technol (Singap World Sci)*. 2015;3(4):172–8.
 197. Fan Y, Nguyen DT, Akay Y, Xu F, Akay M. Engineering a Brain Cancer Chip for High-throughput Drug Screening. *Sci Rep* [Internet]. 2016;6:25062.

Available from:

<http://www.ncbi.nlm.nih.gov/pubmed/27151082>
<http://www.pubmedcentral.nih.gov/articlerender.fcgi?artid=PMC4858657>

198. Pohlmann ES, Patel K, Guo S, Dukes MJ, Sheng Z, Kelly DF. Real-Time Visualization of Nanoparticles Interacting with Glioblastoma Stem Cells. *Nano Lett.* 2015;15(4):2329–35.
199. Shao H, Chung J, Lee K, Balaj L, Min C, Carter BS, et al. Chip-based analysis of exosomal mRNA mediating drug resistance in glioblastoma. *Nat Commun* [Internet]. 2015;6(May):6999. Available from: <http://www.nature.com.proxy.findit.dtu.dk/ncomms/2015/150511/ncomms7999/full/ncomms7999.html>
<http://www.nature.com/doi/finder/10.1038/ncomms7999>
200. Wei W, Shi Q, Remale F, Qin L, Shackelford DB, Shin YS, et al. Hypoxia induces a phase transition within a kinase signaling network in cancer cells. *Proc Natl Acad Sci* [Internet]. 2013;110(15):E1352–60. Available from: <http://www.pnas.org/cgi/doi/10.1073/pnas.1303060110>
201. Aibaidula A, Zhao W, Wu J, Chen H, Shi Z, Lu-lu Zheng, et al. Microfluidics for rapid detection of isocitrate dehydrogenase 1 mutation for intraoperative application. *J Neurosurg* [Internet]. 2015;124(6):1–8. Available from: <http://www.ncbi.nlm.nih.gov/entrez/dispmim.cgi?id=147700>
202. Shimizu F, Hovinga KE, Metzner M, Soulet D, Tabar V. Organotypic explant culture of glioblastoma multiforme and subsequent single-cell suspension. *Curr Protoc Stem Cell Biol.* 2011;(SUPPL.19):1–9.
203. Able RA, Ngnabeuye C, Beck C, Holland EC, Vazquez M. Low concentration microenvironments enhance the migration of neonatal cells of glial lineage. *Cell Mol Bioeng.* 2012;5(2):128–42.
204. Mongersun A, Smeenk I, Pratz G, Asuri P, Abbyad P. Droplet Microfluidic Platform for the Determination of Single-Cell Lactate Release. *Anal Chem.* 2016;88(6):3257–63.
205. Han J, Jun Y, Kim SH, Hoang H-H, Jung Y, Kim S, et al. Rapid emergence and mechanisms of resistance by U87 glioblastoma cells to doxorubicin in an in vitro tumor microfluidic ecology. *Proc Natl Acad Sci* [Internet]. 2016;113(50):14283–8. Available from: <http://www.pnas.org/lookup/doi/10.1073/pnas.1614898113>
206. Gu R, Zhang X, Zhang G, Tao T, Yu H, Liu L, et al. Probing the Bidirectional Interaction Between Microglia and Gliomas in a Tumor Microenvironment on a Microdevice. *Neurochem Res.* 2017;42(5):1478–87.
207. Holmström T, Saksela E. Growth of Human Brain Tumour Explants in Matrix Cultures in Different Human Sera. *Acta Pathol Microbiol Scand Sect A Pathol.* 1971;79 A(4):399–406.
208. Rubinstein LJ, Herman MM. In Vitro Characteristics of Human Glioblastomas Maintained in Organ Culture Systems. *Am J Pathol.* 1973;71(April).
209. Sipe JC, Herman MM, Rubinstein LJ. Electron microscopic observations on human glioblastomas and astrocytomas maintained in organ culture systems. *Am J Pathol* [Internet]. 1973;73(3):589–606. Available from: http://www.ncbi.nlm.nih.gov/entrez/query.fcgi?cmd=Retrieve&db=PubMed&dopt=Citation&list_uids=4358392
210. Saez RJ, Campbell RJ, Laws Jr. ER. Chemotherapeutic trials on human malignant astrocytomas in organ culture. *J Neurosurg.* 1977;46(3):320–7.

211. Yuki K, Uozumi T, Kodama Y, Kurisu K, Mikami T. In vitro chemosensitivity test of human brain tumors using a three-dimensional organ culture with a collagen gel matrix. *J Neurooncol* [Internet]. 1994;21(3):225–32. Available from: <http://www.ncbi.nlm.nih.gov/pubmed/7699417>
212. Ono A, Kanno H, Hayashi A, Nishimura S, Kyuma Y, Sato H, et al. Collagen gel matrix assay as an in vitro chemosensitivity test for malignant astrocytic tumors. *Int J Clin Oncol*. 2007;12(2):125–30.
213. Merz F, Gaunitz F, Dehghani F, Renner C, Meixensberger J, Gutenberg A, et al. Organotypic slice cultures of human glioblastoma reveal different susceptibility to treatments Results : Summary : Outlook : 2013;49(6):8352.
214. Bayin NS, Ma L, Thomas C, Baitalmal R, Sure A, Fansiwala K, et al. Patient-Specific Screening Using High-Grade Glioma Explants to Determine Potential Radiosensitization by a TGF- β Small Molecule Inhibitor. *Neoplasia (United States)* [Internet]. 2016;18(12):795–805. Available from: <http://dx.doi.org/10.1016/j.neo.2016.08.008>
215. Malaney P, Nicosia S V., Dave V. One mouse, one patient paradigm: New avatars of personalized cancer therapy. *Cancer Lett* [Internet]. 2014;344(1):1–12. Available from: <http://dx.doi.org/10.1016/j.canlet.2013.10.010>
216. Louvel G, Metellus P, Noel G, Peeters S, Guyotat J, Duntze J, et al. Delaying standard combined chemoradiotherapy after surgical resection does not impact survival in newly diagnosed glioblastoma patients. *Radiother Oncol* [Internet]. 2016;118(1):9–15. Available from: <http://linkinghub.elsevier.com/retrieve/pii/S0167814016000037>
217. McCreedy T. Rapid prototyping of glass and PDMS microstructures for micro total analytical systems and micro chemical reactors by microfabrication in the general laboratory. *Anal Chim Acta*. 2001;427(1):39–43.
218. Hattersley SM, Greenman J, Haswell SJ. Study of ethanol induced toxicity in liver explants using microfluidic devices. *Biomed Microdevices*. 2011;13(6):1005–14.
219. Sylvester DC, Hattersley SM, Stafford ND, Haswell SJ, Greenman J. Development of Microfluidic-based Analytical Methodology for Studying the Effects of Chemotherapy Agents on Cancer Tissue. *Curr Anal Chem*. 2013;9(1):2–8.
220. Artificial cerebrospinal fluid (ACSF). *Cold Spring Harb Protoc* [Internet]. 2011 Sep 1;2011(9):pdb.rec065730. Available from: <http://cshprotocols.cshlp.org/content/2011/9/pdb.rec065730.short>
221. Cardiff RD, Miller CH, Munn RJ. Manual hematoxylin and eosin staining of mouse tissue sections. *Cold Spring Harb Protoc*. 2014;2014(6):655–8.
222. Alturkistani HA, Tashkandi FM, Mohammedsaleh ZM. Histological Stains: A Literature Review and Case Study. *Glob J Health Sci* [Internet]. 2015;8(3):72. Available from: <http://www.ccsenet.org/journal/index.php/gjhs/article/view/48521>
223. Chan JKC. The wonderful colors of the hematoxylin-eosin stain in diagnostic surgical pathology. *Int J Surg Pathol*. 2014;22(1):12–32.
224. Thermo Fisher Scientific. Overview of Immunohistochemistry [Internet]. [cited 2017 Oct 12]. Available from: <https://www.thermofisher.com/uk/en/home/life-science/protein-biology/protein-biology-learning-center/protein-biology-resource-library/pierce-protein-methods/overview-immunohistochemistry.html>
225. Thermo Fisher Scientific. Avidin-Biotin Interaction [Internet]. [cited 2017 Oct

- 12]. Available from: <https://www.thermofisher.com/uk/en/home/life-science/protein-biology/protein-biology-learning-center/protein-biology-resource-library/pierce-protein-methods/avidin-biotin-interaction.html>
226. Suvarna KS, Layton C, Bancroft JD. *Bancroft's Theory and Practice of Histological Techniques*, 7th Edition. 2012. 654 p.
 227. Fulawka L, Halon A. Proliferation Index Evaluation in Breast Cancer Using ImageJ and ImmunoRatio Applications. *Anticancer Res* [Internet]. 2016;36(8):3965–72. Available from: <http://www.ncbi.nlm.nih.gov/pubmed/27466501>
 228. Tuominen VJ, Ruotoistenmäki S, Viitanen A, Jumppanen M, Isola J. ImmunoRatio: a publicly available web application for quantitative image analysis of estrogen receptor (ER), progesterone receptor (PR), and Ki-67. *Breast Cancer Res* [Internet]. 2010;12(4):R56. Available from: <http://www.pubmedcentral.nih.gov/articlerender.fcgi?artid=2949645&tool=pmcentrez&rendertype=abstract%5Cnhttp://www.ncbi.nlm.nih.gov/pubmed/20663194%5Cnhttp://www.pubmedcentral.nih.gov/articlerender.fcgi?artid=PMC2949645>
 229. Parwani A V, Almeida JS, Iriabho EE, Gorrepati VL, Wilkinson SR, Grüneberg A, et al. ImageJS: Personalized, participated, pervasive, and reproducible image bioinformatics in the web browser. *J Pathol Inf* [Internet]. 2012;3. Available from: <http://www.jpathinformatics.org/text.asp?2012/3/1/25/98813>
 230. BD Biosciences. *Introduction to Flow Cytometry: A Learning Guide*. Vols. 11-11032–0. 2000. p. 1–54.
 231. Mariño G, Kroemer G. Mechanisms of apoptotic phosphatidylserine exposure. *Cell Res*. 2013;23(11):1247–8.
 232. Vermes I, Haanen C, Steffens-Nakken H, Reutelingsperger C. A novel assay for apoptosis. Flow cytometric detection of phosphatidylserine expression on early apoptotic cells using fluorescein labelled Annexin V. *J Immunol Methods* [Internet]. 1995;184(1):39–51. Available from: <http://www.ncbi.nlm.nih.gov/pubmed/7622868>
 233. Fotakis G, Timbrell JA. In vitro cytotoxicity assays: Comparison of LDH, neutral red, MTT and protein assay in hepatoma cell lines following exposure to cadmium chloride. *Toxicol Lett*. 2006;160(2):171–7.
 234. Lobner D. Comparison of the LDH and MTT assays for quantifying cell death: Validity for neuronal apoptosis? *J Neurosci Methods*. 2000;96(2):147–52.
 235. Roche Diagnostics. *LDH Cytotoxicity Detection Kit*. Vol. 25, In Vitro. 2007. p. 712252.
 236. Altman SA, Randers L, Rao G. Comparison of Trypan Blue Dye Exclusion and Fluorometric Assays for Mammalian Cell Viability Determinations. *Biotechnol Prog*. 1993;9(6):671–4.
 237. Hornicek FJ, Malinin GI. Viability, methods of assessing leukocyte. In: *Encyclopedia of Immunology*. 1998. p. 2474–5.
 238. Hirst TC, Vesterinen HM, Sena ES, Egan KJ, MacLeod MR, Whittle IR. Systematic review and meta-analysis of temozolomide in animal models of glioma: Was clinical efficacy predicted. *Br J Cancer* [Internet]. 2013;108(1):64–71. Available from: <http://dx.doi.org/10.1038/bjc.2012.504>
 239. Portnow J, Badie B, Chen M, Liu A, Blanchard S, Synold TW. The neuropharmacokinetics of temozolomide in patients with resectable brain

- tumors: Potential implications for the current approach to chemoradiation. *Clin Cancer Res*. 2009;15(22):7092–8.
240. Ostermann S, Csajka C, Buclin T, Leyvraz S, Lejeune F, Decosterd LA, et al. Plasma and cerebrospinal fluid population pharmacokinetics of temozolomide in malignant glioma patients. *Clin Cancer Res* [Internet]. 2004;10(11):3728–36. Available from: <http://www.ncbi.nlm.nih.gov/pubmed/15173079>
 241. Shen W, Hu J-A, Zheng J-S. Mechanism of temozolomide-induced antitumour effects on glioma cells. *J Int Med Res* [Internet]. 2014;42(1):164–72. Available from: <http://imr.sagepub.com/lookup/doi/10.1177/0300060513501753>
 242. Baker SD, Wirth M, Statkevich P, Reidenberg P, Alton K, Sartorius SE, et al. Absorption, metabolism, and excretion of ¹⁴C-temozolomide following oral administration to patients with advanced cancer. *Clin Cancer Res*. 1999;5(2):309–17.
 243. Webster A, Dyer CE, Haswell SJ, Greenman J. A microfluidic device for tissue biopsy culture and interrogation. *Anal Methods* [Internet]. 2010;2(8):1005. Available from: <http://pubs.rsc.org/en/content/articlehtml/2010/ay/c0ay00293c>
 244. Hattersley SM, Dyer CE, Greenman J, Haswell SJ. Development of a microfluidic device for the maintenance and interrogation of viable tissue biopsies. *Lab Chip*. 2008;8(11):1842–6.
 245. Bower R, Green VL, Kuvshinova E, Kuvshinov D, Karsai L, Crank ST, et al. Maintenance of head and neck tumor on- chip: gateway to personalized treatment? *Aim: Futur Sci OA*. 2017;3(2).
 246. Dawson A, Dyer C, Macfie J, Davies J, Karsai L, Greenman J, et al. A microfluidic chip based model for the study of full thickness human intestinal tissue using dual flow. *Biomicrofluidics* [Internet]. 2016;10(6). Available from: <http://dx.doi.org/10.1063/1.4964813>
 247. National Institute for Health and Clinical Excellence. Improving Outcomes for People with Brain and Other CNS Tumours [Internet]. NICE; 2006. 185 p. Available from: http://www.mccn.nhs.uk/userfiles/documents/CSG_brain_manual.pdf
 248. Lasocki A, Tsui A, Tacey MA, Drummond KJ, Field KM, Gaillard F. MRI grading versus histology: Predicting survival of world health organization grade II-IV astrocytomas. *Am J Neuroradiol*. 2015;36(1):77–83.
 249. Bendini M, Marton E, Feletti A, Rossi S, Curtolo S, Inches I, et al. Primary and metastatic intraaxial brain tumors: Prospective comparison of multivoxel 2D chemical-shift imaging (CSI) proton MR spectroscopy, perfusion MRI, and histopathological findings in a group of 159 patients. *Acta Neurochir (Wien)*. 2011;153(2):403–12.
 250. Marcus HJ, Williams S, Hughes-Hallett A, Camp SJ, Nandi D, Thorne L. Predicting surgical outcome in patients with glioblastoma multiforme using pre-operative magnetic resonance imaging: development and preliminary validation of a grading system. *Neurosurg Rev*. 2017;40(4):621–31.
 251. Law M, Yang S, Wang H, Babb JS, Johnson G, Cha S, et al. Glioma grading: sensitivity, specificity, and predictive values of perfusion MR imaging and proton MR spectroscopic imaging compared with conventional MR imaging. *AJNR Am J Neuroradiol* [Internet]. 2003;24(10):1989–98. Available from: <papers3://publication/uuid/C58DFDF1-444E-440B-BD8E-55C3C32585DE>
 252. Dean BL, Drayer BP, Bird CR, Flom RA, Hodak JA, Coons SW, et al.

- Gliomas: classification with MR imaging. *Radiology* [Internet]. 1990;174(2):411–5. Available from: <http://pubs.rsna.org/doi/10.1148/radiology.174.2.2153310>
253. Jain D, Sharma MC, Sarkar C, Deb P, Gupta D, Mahapatra AK. Correlation of diagnostic yield of stereotactic brain biopsy with number of biopsy bits and site of the lesion. *Brain Tumor Pathol.* 2006;23(2):71–5.
 254. Woodworth GF, McGirt MJ, Samdani A, Garonzik I, Olivi A, Weingart JD. Frameless image-guided stereotactic brain biopsy procedure: diagnostic yield, surgical morbidity, and comparison with the frame-based technique. *J Neurosurg* [Internet]. 2006;104(2):233–7. Available from: <http://thejns.org/doi/10.3171/jns.2006.104.2.233>
 255. Chandrasoma PT, Smith MM, Apuzzo MLJ. Stereotactic biopsy in the diagnosis of brain masses: Comparison of results of biopsy and resected surgical specimen. *Neurosurgery.* 1989;24(2):160–5.
 256. Piazza O, Romano R, Cotena S, Santaniello W, De Robertis E. Maximum tolerable warm ischaemia time in transplantation from non-heart-beating-donors. *Trends Anaesth Crit Care* [Internet]. 2013;3(2):72–6. Available from: <http://dx.doi.org/10.1016/j.tacc.2013.01.002>
 257. Hosgood SA, Shah K, Patel M, Nicholson ML. The effect of prolonged of warm ischaemic injury on renal function in an experimental ex vivo normothermic perfusion system. *J Transl Med.* 2015;13(1):1–6.
 258. Devarajan P. Neutrophil gelatinase-associated lipocalin (NGAL) A new marker of kidney disease. *Scand J Clin Lab Invest Suppl* 2008; 241 89–94. 2008;38(1):46–54.
 259. Guerrera F, Tabbo F, Bessone L, Maletta F, Gaudiano M, Ercole E, et al. The influence of tissue ischemia time on RNA integrity and patient-derived xenografts (PDX) engraftment rate in a non-small cell lung cancer (NSCLC) Biobank. *PLoS One.* 2016;11(1):1–15.
 260. Annaratone L, Marchiò C, Russo R, Ciardo L, Rondon-Lagos SM, Goia M, et al. A Collection of Primary Tissue Cultures of Tumors from Vacuum Packed and Cooled Surgical Specimens: A Feasibility Study. *PLoS One.* 2013;8(9):1–9.
 261. Dawson A, Dyer C, Macfie J, Davies J, Karsai L, Greenman J, et al. A microfluidic chip based model for the study of full thickness human intestinal tissue using dual flow. *Biomicrofluidics* [Internet]. 2016;10(6). Available from: <http://dx.doi.org/10.1063/1.4964813>
 262. Kim C, Kim HS, Shim WH, Choi CG, Kim SJ, Kim JH. Recurrent Glioblastoma: Combination of High Cerebral Blood Flow with MGMT Promoter Methylation Is Associated with Benefit from Low-Dose Temozolomide Rechallenge at First Recurrence. *Radiology* [Internet]. 2016;000(0):152152. Available from: <http://pubs.rsna.org/doi/10.1148/radiol.2016152152>
 263. Reid KH, Schurr A, Tseng MT, Edmonds Jr. HL. Resistance to hypoxia in the rat hippocampal slice. *Brain Res* [Internet]. 1984;302(2):387–91. Available from: <http://www.ncbi.nlm.nih.gov/htbin-post/Entrez/query?db=m&form=6&dopt=r&uid=6329464>
 264. Hess JR, Michaud J, Sobel RA, Herman MM, Rubinstein LJ. The kinetics of human glioblastomas maintained in an organ culture system - An in vitro autoradiographic study. *Acta Neuropathol.* 1983;61(1):1–9.
 265. Bjerkvig R, Tønnesen a, Laerum OD, Backlund EO. Multicellular tumor

- spheroids from human gliomas maintained in organ culture. *J Neurosurg*. 1990;72(Table 1):463–75.
266. Jung HW, Berens ME, Krouwer HG, Rosenblum ML. A three-dimensional micro-organ culture system optimized for in vitro growth of human malignant brain tumors. *Neurosurgery* [Internet]. 1991;29(3):390–8. Available from: <http://www.ncbi.nlm.nih.gov/pubmed/1922706>
 267. Islam M, Sajid A, Mahmood MAI, Bellah MM, Allen PB, Kim Y-T, et al. Nanotextured polymer substrates show enhanced cancer cell isolation and cell culture. *Nanotechnology* [Internet]. 2015;26(22):225101. Available from: <http://stacks.iop.org/0957-4484/26/i=22/a=225101?key=crossref.eb40b87f627aae10dd0c1be9e18d7abf>
 268. Yu S, Ping Y, Yi L, Zhou Z, Chen J, Yao X, et al. Isolation and characterization of cancer stem cells from a human glioblastoma cell line U87. *Cancer Lett* [Internet]. 2008;265(1):124–34. Available from: <http://linkinghub.elsevier.com/retrieve/pii/S0304383508000955>
 269. Romijn HJ. Development and advantages of serum-free, chemically defined nutrient media for culturing of nerve tissue. *Biol Cell* [Internet]. 1988;63(3):263–8. Available from: <http://www.ncbi.nlm.nih.gov/pubmed/3066424>
 270. Roth S, Zhang SJ, Chiu J, Wirth EK, Schweizer U. Development of a serum-free supplement for primary neuron culture reveals the interplay of selenium and vitamin E in neuronal survival. *J Trace Elem Med Biol* [Internet]. 2010;24(2):130–7. Available from: <http://dx.doi.org/10.1016/j.jtemb.2010.01.007>
 271. Chen Y, Stevens B, Chang J, Milbrandt J, Barres B a, Hell JW. NS21: Re-defined and Modified Supplement B27 for Neuronal Cultures. *J Neurosci*. 2009;171(2):239–47.
 272. Eitan E, Zhang S, Witwer KW, Mattson MP. Extracellular vesicle-depleted fetal bovine and human sera have reduced capacity to support cell growth. *J Extracell Vesicles*. 2015;4(2015):1–10.
 273. Thomas MG, Marwood RM, Parsons AE, Parsons RB. The effect of foetal bovine serum supplementation upon the lactate dehydrogenase cytotoxicity assay: Important considerations for in vitro toxicity analysis. *Toxicol Vitr* [Internet]. 2015;30(1):300–8. Available from: <http://dx.doi.org/10.1016/j.tiv.2015.10.007>
 274. Brewer Torricelli, J. R., Evege, E. K., Price, P. J. GJ. Optimized Survival of Hippocampal-Neurons in B27-Supplemented Neurobasal(Tm), a New Serum-Free Medium Combination. *J Neurosci Res*. 1993;35(5):567–76.
 275. Eugène E, Cluzeaud F, Cifuentes-Diaz C, Fricker D, Le Duigou C, Clemenceau S, et al. An organotypic brain slice preparation from adult patients with temporal lobe epilepsy. *J Neurosci Methods*. 2014;235:234–44.
 276. Schwarz N, Hedrich UBS, Schwarz H, Harshad PA, Dammeier N, Auffenberg E, et al. Human Cerebrospinal fluid promotes long-term neuronal viability and network function in human neocortical organotypic brain slice cultures. *Sci Rep*. 2017;7(1):1–12.
 277. Perez-Alcazar M, Culley G, Lyckenvik T, Mobarrez K, Bjorefeldt A, Wasling P, et al. Human Cerebrospinal Fluid Promotes Neuronal Viability and Activity of Hippocampal Neuronal Circuits In Vitro. *Front Cell Neurosci* [Internet]. 2016;10(March):1–11. Available from: <http://journal.frontiersin.org/Article/10.3389/fncel.2016.00054/abstract>

278. An JH, Su Y, Radman T, Bikson M. Effects of glucose and glutamine concentration in the formulation of the artificial cerebrospinal fluid (ACSF). *2008;1218:77–86.*
279. Liu J, Saponjian Y, Mahoney MM, Staley KJ, Berdichevsky Y. Epileptogenesis in organotypic hippocampal cultures has limited dependence on culture medium composition. *PLoS One.* 2017;12(2):1–25.
280. Valadi H, Ekström K, Sjöstrand ABM, Lee JJ, Lötvall JO. Exosome-mediated transfer of mRNAs and microRNAs is a novel mechanism of genetic exchange between cells Hadi. *Nat Cell Biol.* 2007;9(6):654–9.
281. Mondal A, Kumari Singh D, Panda S, Shiras A. Extracellular Vesicles As Modulators of Tumor Microenvironment and Disease Progression in Glioma. *Front Oncol [Internet].* 2017;7(July):1–8. Available from: <http://journal.frontiersin.org/article/10.3389/fonc.2017.00144/full>
282. El Andaloussi S, Mäger I, Breakefield XO, Wood MJA. Extracellular vesicles: Biology and emerging therapeutic opportunities. *Nat Rev Drug Discov [Internet].* 2013;12(5):347–57. Available from: <http://dx.doi.org/10.1038/nrd3978>
283. Merino-González C, Zuñiga FA, Escudero C, Ormazabal V, Reyes C, Nova-Lamperti E, et al. Mesenchymal stem cell-derived extracellular vesicles promote angiogenesis: Potencial clinical application. *Front Physiol.* 2016;7(FEB):1–9.
284. Ung TH, Madsen HJ, Hellwinkel JE, Lencioni AM, Graner MW. Exosome proteomics reveals transcriptional regulator proteins with potential to mediate downstream pathways. *Cancer Sci.* 2014;105(11):1384–92.
285. Kharaziha P, Ceder S, Li Q, Panaretakis T. Tumor cell-derived exosomes: A message in a bottle. *Biochim Biophys Acta - Rev Cancer [Internet].* 2012;1826(1):103–11. Available from: <http://dx.doi.org/10.1016/j.bbcan.2012.03.006>
286. Al-Nedawi K, Meehan B, Rak J. Microvesicles: Messengers and mediators of tumor progression. *Cell Cycle.* 2009;8(13):2014–8.
287. Narayanan A, Iordanskiy S, Das R, Van Duyne R, Santos S, Jaworski E, et al. Exosomes derived from HIV-1-infected cells contain trans-activation response element RNA. *J Biol Chem.* 2013;288(27):20014–33.
288. Harris DA, Patel SH, Gucek M, Hendrix A, Westbroek W, Taraska JW. Exosomes released from breast cancer carcinomas stimulate cell movement. *PLoS One.* 2015;10(3):1–18.
289. Maji, Sayantan; Chaudhary, Pankaj; Akopova, Irina; Nguyen, Phung M; Hare, Richard J; Gryczynski, Ignacy; Vishwanatha J. Exosomal Annexin A2 Promotes Angiogenesis and Breast Cancer Metastasis Sayantan. *Mol Cancer Res.* 2017;15(1):93–105.
290. Hellebø O, Officer CE, Howell J, Officer CM, Hunt M, Officer CF. Interim results for the six months ended 30 September 2016. 2016;(December).
291. Angelini F, Ionta V, Rossi F, Miraldi F, Messina E, Giacomello A. Foetal bovine serum-derived exosomes affect yield and phenotype of human cardiac progenitor cell culture. *BioImpacts [Internet].* 2016;6(1):15–24. Available from: <http://dx.doi.org/10.15171/bi.2016.03>
292. Aswad H, Jalabert A, Rome S. Depleting extracellular vesicles from fetal bovine serum alters proliferation and differentiation of skeletal muscle cells in vitro. *BMC Biotechnol [Internet].* 2016;16(1):1–12. Available from: <http://dx.doi.org/10.1186/s12896-016-0262-0>

293. William D, Mullins CS, Schneider B, Orthmann A, Lamp N, Krohn M, et al. Optimized creation of glioblastoma patient derived xenografts for use in preclinical studies. *J Transl Med.* 2017;15(1):1–11.
294. Schnell SA, Staines WA, Wessendorf MW. Reduction of lipofuscin-like autofluorescence in fluorescently labeled tissue. *J Histochem Cytochem* [Internet]. 1999;47(6):719–30. Available from: <http://www.ncbi.nlm.nih.gov/pubmed/10330448>
295. Dowson JH, Harris SJ. Quantitative studies of the autofluorescence derived from neuronal lipofuscin. *J Microsc.* 1981;123(3):249–58.
296. Goyal VK. Lipofuscin Pigment Accumulation in Human Brain During Aging. *Exp Gerontol* [Internet]. 1983;17:481–7. Available from: <http://www.ncbi.nlm.nih.gov/pubmed/10330448>
297. Labussiere M, Di Stefano AL, Gleize V, Boisselier B, Giry M, Mangesius S, et al. TERT promoter mutations in gliomas, genetic associations and clinico-pathological correlations. *Br J Cancer.* 2014;111(10):2024–32.
298. Zarnescu O, Brehar FM, Chivu M, Ciurea AV. Immunohistochemical localization of caspase-3, caspase-9 and Bax in U87 glioblastoma xenografts. *J Mol Histol.* 2008;39(6):561–9.
299. Almenawer SA, Badhiwala JH, Alhazzani W, Greenspoon J, Farrokhyar F, Yarascavitch B, et al. Biopsy versus partial versus gross total resection in older patients with high-grade glioma: A systematic review and meta-analysis. *Neuro Oncol.* 2015;17(6):868–81.
300. Sanai N, Polley M-Y, McDermott MW, Parsa AT, Berger MS. An extent of resection threshold for newly diagnosed glioblastomas. *J Neurosurg* [Internet]. 2011;115(1):3–8. Available from: <http://thejns.org/doi/10.3171/2011.2.JNS10998>
301. Yong RL, Lonser RR. Surgery for glioblastoma multiforme: striking a balance. *World Neurosurg.* 2011;76(6):528–30.
302. Yan J-L, van der Hoorn A, Larkin TJ, Boonzaier NR, Matys T, Price SJ. Extent of resection of peritumoral diffusion tensor imaging-detected abnormality as a predictor of survival in adult glioblastoma patients. *J Neurosurg* [Internet]. 2016;1–8. Available from: <http://www.ncbi.nlm.nih.gov/pubmed/27058207>
303. Hervey-Jumper SL, Berger MS. Maximizing safe resection of low- and high-grade glioma. *J Neurooncol.* 2016;130(2):269–82.
304. Li YM, Suki D, Hess K, Sawaya R. The influence of maximum safe resection of glioblastoma on survival in 1229 patients: Can we do better than gross-total resection? *J Neurosurg* [Internet]. 2016;124(4):977–88. Available from: <http://thejns.org/doi/10.3171/2015.5.JNS142087>
305. Davis FG, Freels S, Grutsch J, Barlas S, Brem S. Survival rates in patients with primary malignant brain tumors stratified by patient age and tumor histological type: an analysis based on Surveillance, Epidemiology, and End Results (SEER) data, 1973-1991. *J Neurosurg.* 1998;88(1):1–10.
306. van Linde ME, Brahm CG, de Witt Hamer PC, Reijneveld JC, Bruynzeel AME, Vandertop WP, et al. Treatment outcome of patients with recurrent glioblastoma multiforme: a retrospective multicenter analysis. *J Neurooncol.* 2017;135(1):183–92.
307. Patel R, Green V, Hunter I, Greenman J. Apoptosis in rectal cancer biopsies following irradiation in a microfluidic device: a predictor of response? *Br J Surg.* 2014;101(Supplement 4):12–12.

308. Lyser KM. Organ culture of human nervous system tumors. *In Vitro*. 1976;12(1):48–56.
309. Fan H, Zhang K, Shan L, Kuang F, Chen K, Zhu K, et al. Reactive astrocytes undergo M1 microglia/macrophages-induced necroptosis in spinal cord injury. *Mol Neurodegener* [Internet]. 2016;11(1):14. Available from: <http://www.molecularneurodegeneration.com/content/11/1/14>
310. Li Y, Wang F, Wang H. Cell death along single microfluidic channel after freeze-thaw treatments. *Biomicrofluidics*. 2010;4(1):1–10.
311. Zhao X, Chen Q, Liu W, Li Y, Tang H, Liu X, et al. Codelivery of doxorubicin and curcumin with lipid nanoparticles results in improved efficacy of chemotherapy in liver cancer. *Int J Nanomedicine*. 2014;10:257–70.
312. Caviglia C, Zór K, Montini L, Tilli V, Canepa S, Melander F, et al. Impedimetric toxicity assay in microfluidics using free and liposome-encapsulated anticancer drugs. *Anal Chem*. 2015;87(4):2204–12.
313. Fan H, Yuan R, Cheng S, Xiong K, Zhu X, Zhang Y. Overexpressed miR-183 promoted glioblastoma radioresistance via down-regulating LRIG1. *Biomed Pharmacother* [Internet]. 2018;97(1):1554–63. Available from: <https://doi.org/10.1016/j.biopha.2017.11.050>
314. Rachlin K, Moore DH, Yount G. Infrasonic sensitizes human glioblastoma cells to cisplatin-induced apoptosis. *Integr Cancer Ther*. 2013;12(6):517–27.
315. Yu HP, Qi ST, Feng WF, Zhang GZ, Zhang HP, Tian JJ. Interference of Notch 2 inhibits the progression of gliomas and induces cell apoptosis by induction of the cell cycle at the G0/G1 phase. *Mol Med Rep*. 2015;11(1):734–8.
316. Koh JY, Choi DW. Quantitative determination of glutamate mediated cortical neuronal injury in cell culture by lactate dehydrogenase efflux assay. *J Neurosci Methods*. 1987;20(1):83–90.
317. Chan FK-M, Moriwaki K, Rosa MJ De. Detection of Necrosis by Release of Lactate Dehydrogenase (LDH) Activity. *Methods Mol Biol* [Internet]. 2013;979:65–70. Available from: <http://link.springer.com/10.1007/978-1-62703-290-2>
318. Tanweer F, Green VL, Stafford ND, Greenman J. Application of microfluidic systems in management of head and neck squamous cell carcinoma. *Head Neck*. 2013;35(5):756–63.
319. Carden DL, Granger DN. Pathophysiology of ischaemia-reperfusion injury. *J Pathol*. 2000;190(3):255–66.
320. Chouchani ET, Pell VR, Gaude E, Aksentijević D, Sundier SY, Robb EL, et al. Ischaemic accumulation of succinate controls reperfusion injury through mitochondrial ROS. *Nature*. 2014;515(7527):431–5.
321. Eltzschig HK, Eckle T. Ischemia and reperfusion—from mechanism to translation. *Nat Med* [Internet]. 2011;17(11):1391–401. Available from: <http://dx.doi.org/10.1038/nm.2507>
322. Bright R, Raval AP, Dembner JM, Perez-Pinzon MA, Steinberg GK, Yenari MA, et al. Protein Kinase C Mediates Cerebral Reperfusion Injury In Vivo. *J Neurosci* [Internet]. 2004;24(31):6880–8. Available from: <http://www.jneurosci.org/cgi/doi/10.1523/JNEUROSCI.4474-03.2004>
323. Zhang W, Qian CY, Li SQ. Protective effect of SGK1 in rat hippocampal neurons subjected to ischemia reperfusion. *Cell Physiol Biochem*. 2014;34(2):299–312.

324. Kalogeris T, Baines CP, Krenz M, Korthuis RJ. Cell Biology of Ischemia/Reperfusion Injury. Vol. 298, *Int Rev Cell Mol Biol*. 2012. 229-317 p.
325. Scholzen T, Gerdes J. The Ki-67 protein: from the known and the unknown. *J Cell Physiol*. 2000;182(3):311–22.
326. Abacioglu U, Gucluer B, Cetin I, Akgun Z, Tezcanli E, Sengoz M, et al. Ki67 Proliferation index as a marker for clinical Radioresponse in Glioblastoma Multiforme. *IJ Radiat Oncol*. 2005;63(2):S258.
327. Darweesh MF, Abdel-Salam LO, Sherif Negm M. Evaluation of the Proliferation Marker Ki-67 in Glioblastoma and its Correlation with the Histopathological Findings. *Acad J Cancer Res [Internet]*. 2016;9(2):13–8. Available from: [https://www.idosi.org/ajcr/9\(2\)16/1.pdf](https://www.idosi.org/ajcr/9(2)16/1.pdf)
328. Stoyanov GS, Dzhenkov DL, Kitanova M, Donev IS, Ghenev P. Correlation Between Ki-67 Index, World Health Organization Grade and Patient Survival in Glial Tumors With Astrocytic Differentiation. *Cureus [Internet]*. 2017;79(6). Available from: <http://www.cureus.com/articles/7619-correlation-between-ki-67-index-world-health-organization-grade-and-patient-survival-in-glial-tumors-with-astrocytic-differentiation>
329. Paldor I, Pearce FC, Drummond KJ, Kaye AH. Frontal glioblastoma multiforme may be biologically distinct from non-frontal and multilobar tumors. *J Clin Neurosci [Internet]*. 2016;34:128–32. Available from: <http://dx.doi.org/10.1016/j.jocn.2016.05.017>
330. Chiesa-Vottero AG, Rybicki LA, Prayson RA. Comparison of Proliferation Indices in Glioblastoma Multiforme by Whole Tissue Section vs Tissue Microarray. *Am J Clin Pathol*. 2003;120(6):902–8.
331. Li LT, Jiang G, Chen Q, Zheng JN. Predict Ki67 is a promising molecular target in the diagnosis of cancer (Review). *Mol Med Rep*. 2015;11(3):1566–72.
332. Joo KM, Kim J, Jin J, Kim M, Seol HJ, Muradov J, et al. Patient-Specific Orthotopic Glioblastoma Xenograft Models Recapitulate the Histopathology and Biology of Human Glioblastomas In Situ. *Cell Rep [Internet]*. 2013;3(1):260–73. Available from: <http://dx.doi.org/10.1016/j.celrep.2012.12.013>
333. Li Y, Plagemann A, Davidowa H. Distribution of activated caspase-3 in relation with apoptosis in human malignant gliomas. *Neurosci Lett*. 2001;300(1):37–40.
334. Kamada S, Kikkawa U, Tsujimoto Y, Hunter T. Nuclear translocation of caspase-3 is dependent on its proteolytic activation and recognition of a substrate-like protein(s). *J Biol Chem*. 2005;280(2):857–60.
335. Krajewska M, Wang H, Krajewski S, Reed JC. Immunohistochemical Analysis of in Vivo Patterns of Expression of CPP32 (Caspase-3), a Cell Death Protease Analysis of in Vivo Patterns of Expression. *Cancer Res*. 1997;57:1605–13.
336. Tirapelli LF, Bolini PHNA, Tirapelli DPDC, Peria FM, Becker ANP, Saggiaro FP, et al. Caspase-3 and Bcl-2 expression in glioblastoma: an immunohistochemical study. *Arq Neuropsiquiatr*. 2010;68(December 2009):603–7.
337. Bodey B, Bodey V, Siegel SE, Nasir A, Coppola D, Hakam A, et al. Immunocytochemical detection of members of the caspase cascade of apoptosis in high-grade astrocytomas. *In Vivo (Brooklyn)*. 2004;18(5):593–

- 602.
338. Luo M, Lu Z, Sun H, Yuan K, Zhang Q, Meng S, et al. Nuclear entry of active caspase-3 is facilitated by its p3-recognition-based specific cleavage activity. *Cell Res* [Internet]. 2010;20(2):211–22. Available from: <http://dx.doi.org/10.1038/cr.2010.9>
 339. Gdynia G, Grund K, Eckert A, Bock BC, Funke B, Macher-Goeppinger S, et al. Basal Caspase Activity Promotes Migration and Invasiveness in Glioblastoma Cells. *Mol Cancer Res* [Internet]. 2007;5(12):1232–40. Available from: <http://mcr.aacrjournals.org/cgi/doi/10.1158/1541-7786.MCR-07-0343>
 340. Noyan-Ashraf MH, Brandizzi F, Juurlink BHJ. Constitutive nuclear localization of activated caspase 3 in subpopulations of the astroglial family of cells. *Glia*. 2005;49(4):588–93.
 341. Chu S-H, Feng D-F, Ma Y-B, Li Z-Q. Hydroxyapatite nanoparticles inhibit the growth of human glioma cells in vitro and in vivo. *Int J Nanomedicine* [Internet]. 2012;3659. Available from: <http://www.dovepress.com/hydroxyapatite-nanoparticles-inhibit-the-growth-of-human-glioma-cells--peer-reviewed-article-IJN>
 342. Ramezani S, Vousooghi N, Ramezani Kapourchali F, Joghataei MT. Perifosine enhances bevacizumab-induced apoptosis and therapeutic efficacy by targeting PI3K/AKT pathway in a glioblastoma heterotopic model. *Apoptosis*. 2017;22(8):1025–34.
 343. Beier D, Schriefer B, Brawanski K, Hau P, Weis J, Schulz JB, et al. Efficacy of clinically relevant temozolomide dosing schemes in glioblastoma cancer stem cell lines. *J Neurooncol*. 2012;109(1):45–52.
 344. Weller M, Stupp R, Reifenberger G, Brandes AA, Van Den Bent MJ, Wick W, et al. MGMT promoter methylation in malignant gliomas: Ready for personalized medicine? *Nat Rev Neurol*. 2010;6(1):39–51.
 345. Tanaka M, Obata T, Sasaki T. Evaluation of antitumour effects of docetaxel (Taxotere®) on human gastric cancers in vitro and in vivo. *Eur J Cancer*. 1996;32(2):226–30.
 346. Koshida K, Egawa M, Imao T, Mizokami A, Namiki M, Endo Y, et al. In vitro chemosensitivity test for human genito-urinary tumors using collagen gel matrix. *Int J Urol* [Internet]. 2005;12(1):67–72. Available from: <http://www.ncbi.nlm.nih.gov/pubmed/15661056>
 347. Park I, Bok R, Ozawa T, Phillips JJ, James CD, Vigneron DB, et al. Detection of early response to temozolomide treatment in brain tumors using hyperpolarized ¹³C MR metabolic imaging. *J Magn Reson Imaging*. 2011;33(6):1284–90.
 348. Newlands ES, Stevens MF, Wedge SR, Wheelhouse RT, Brock C. Temozolomide: a review of its discovery, chemical properties, pre-clinical development and clinical trials. *Cancer Treat Rev*. 1997;23(0305–7372 SB–M SB–X):35–61.
 349. Delgado-López PD, Corrales-García EM. Survival in glioblastoma: a review on the impact of treatment modalities. *Clin Transl Oncol*. 2016;18(11):1062–71.
 350. Coffey RJ, Lunsford LD, Taylor FH. Survival after stereotactic biopsy of malignant gliomas. *Neurosurgery*. 1988;22(3):465–73.

Appendix

Appendix I: Participant Information Sheet.....	182
Appendix II: Consent Form.....	185
Appendix III: Fluorescent imaging of tissue perfused with PKH26 labelled ExoPr0 and tissue perfused with standard media with no fluorescent label.....	186

Research Participant Information Sheet

Application of microfluidics system for evaluating the biology of Brain Tumour tissues and testing their response to treatment

Invitation

We would like to invite you to take part in a research study. Before you decide, you need to understand why the research is being undertaken and what would be required of you. Please take the time to read the following information carefully. Talk to others about the study if you wish; ask us if there is anything that is not clear or if you would like more information.

Purpose of the study

The ultimate aim is to develop a system that could be used to understand why and how certain treatments work on one individual and not on others, and in doing so, help us to personalise treatments in the future. This study forms the basis of a Medical Doctorate project. The University of Hull has developed a method to keep a small piece of tissue functioning for a number of days out of the body on a miniaturised analysis device (often referred to as a 'Lab on a Chip'). We investigate the effects of treatments (e.g. chemotherapy and radiotherapy) on this tissue to give us better information as to how these treatments work on tissues within the body.

Why have I been chosen?

We are inviting you to take part in the study as you are undergoing a procedure that will involve the removal of a brain tumour, or you are having the removal of small pieces of tissue (a diagnostic biopsy) for diagnostic purposes.

Do I have to take part?

It is your decision whether you wish to take part. We will describe the study and go through this information sheet with you. You can keep this information sheet and use it to help you decide. If you decide to be a part of the study, we will ask you to sign a consent form to show you have agreed to take part.

Am I free to withdraw at any time?

You are free to withdraw at any time without giving a reason for your withdrawal. This will not affect the standard of care you receive. However, samples already collected before your withdrawal will continue to be stored and any information gained from these may be used in the study. We would not access any information about your clinical progress.

What will happen to me if I take part?

If you agree to take part in the study and if you're undergoing tumour resection, a small (2 cubic millimetres) sample of tissue will be taken from the specimen removed. If you're undergoing a diagnostic biopsy, a small part (2 cubic millimetres) of the sample tissue (surplus tissue) will be used if available. Once your samples are taken they will only be identifiable by a number; non-clinical laboratory staff will not have any access to your personal details. Information regarding your response to treatment and outcome (if applicable) will be accessed by the clinical staff involved with your treatment and possibly communicated with the research staff. You will not be contacted by the research team after today.

Expenses and payment

You should not incur any expenses during participation. There will not be any financial benefit if this research leads to the development of a new treatment or test.

What are the possible risks of taking part?

There are no risks to you or your treatment if you take part.

What are the benefits of taking part?

There will be no direct benefit to you for taking part, but the information we obtain by studying your sample will potentially help the development of treatments for other patients in the future.

What do I do if I have a complaint?

Any complaint about the way you have been dealt with during the study can be addressed to **Mr. Achawal, Consultant Neurosurgeon on (01482) 605338**. Alternatively, you can contact the patient advice and liaison service (PALS) on (01482) 623065.

Will my role in the study be kept confidential?

Yes. We will follow best ethical and legal practice and all information about you will be handled in confidence. Your sample will be identifiable by a number that can only be linked back to personal details via your clinical team e.g. Mr. Achawal.

What will happen to the samples I give?

The samples will be taken to the research laboratory at the University of Hull where we will investigate the effect of treatments (chemotherapy and/or radiotherapy) on them. Following completion of the study, excess samples will remain stored in liquid nitrogen, securely and anonymously for possible use in

future research. In this instance, new research ethical approval will be sought prior to commencing a study.

What will happen to the results of the research study?

The results of the study may be published in a scientific journal. At no time will you be identifiable to the reader. No feedback will be given to you unless specifically requested, in which instance the research team will be happy to discuss the general findings.

Who is organising and funding the research?

The University of Hull will be organising and conducting research in their laboratories. A joint University of Hull / Hull Neurosurgery Department research account is held at the University of Hull and this will be used to fund the research.

Who has reviewed the study?

To protect your interests, all research in the NHS is reviewed and authorised by an independent group of people called a Research Ethics Committee. This study has been reviewed and authorised by the Hull and East Riding Local Research Ethics Committee.

Further information

If you require any further information on the research, advice on whether to take part, or if you're at all unhappy, please contact Mr. Achawal on (01482) 605338. Thank you for taking time to read this information sheet.

Consent

If you decide to take part in this study, we will provide you with a copy of the information sheet and ask you to sign a Consent Form.

Centre Number:
Study Number:
Patient Identification Number:

CONSENT FORM

Application of microfluidics system for evaluating the biology of Brain Tumour tissues and testing their response to treatment

- I confirm that I have read and understood the information sheet dated 30.09.16 (version 2.2) for the above study. I have had the opportunity to consider the information, ask questions and have had these answered satisfactorily.
- I understand my participation is voluntary and that I am free to withdraw at any time without giving a reason, without my medical care or legal rights being affected. If I do withdraw, samples already obtained may still be used.
- I understand that I am under no obligation to take part and that, in agreeing to take part, I am free to change my mind at any time.
- I understand that I will not benefit financially if this research leads to the development of a new treatment or test.
- I give permission for a sample of tissue taken during my operation/diagnostic biopsy to be used for this research.
- I agree that any samples not used in this study may be stored and used in future research of a similar nature pending ethical approval.
- I understand that these samples will be stored anonymously, and I consent to the information derived from them to be analysed.
- I understand that relevant sections of my medical notes and data collected during the study may be looked at by individuals from the University of Hull, from regulatory authorities or from the NHS trust, where it is relevant to me taking part in this research. I give permission for these individuals to have access to my records.
- I hereby freely give my consent to take part in this study.

Name of Volunteer

Date

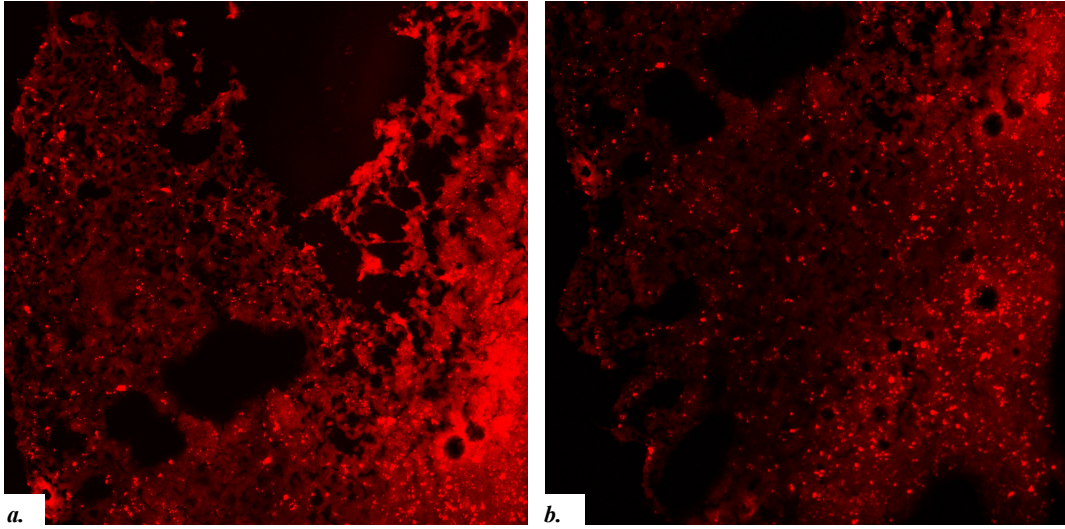
Signature

Consented by

Date

Signature

Appendix III



Appendix 3: Fluorescent imaging of tissue perfused with (a) PKH26 labelled ExoPr0 and (b) tissue perfused with standard media with no fluorescent label. Evidence of auto-fluorescence in tissue without exposure to PKH26 likely due to lipofuscin present in CNS tissue.

List of Abbreviations

5-FU	Fluoroucail
7AAD	7-Aminoactinomycin D
aCSF	Artificial Cerebrospinal Fluid
BBB	Blood Brain Barrier
BTSC	Brain Tumour Stem Cell
BSA	Bovine Serum Albumin
CYP7A1	cytochrome P450 7A1
CDDP	<i>cis</i> -diamminedichloridoplatinum (Cisplatin)
CSF	Cerebrospinal Fluid
CNS	Central Nervous System
DAB	3,3' Diaminobenzidine
DMEM	Dulbecco's Modified Eagle Media
DNA	Deoxyribonucleic Acid
DOX	Doxorubicin
ECM	Extracellular Matrix
EGFR	Epidermal Growth Factor Receptor
ETFE	Ethylene Tetrafluoroethylene
FACS	Fluorescence Activated Cell Sorting
FEP	Fluorinated Ethylene-Propylene
FITC	Fluorescein Isothiocyanate
FSC	Forward-Scattered Light
GBM	Glioblastoma
GFP	Green Florescent Protein
H&E	Haematoxylin and Eosin
<i>h</i> GBM	Human GBM Tissue
HNSCC	Head and Neck Squamous Cell Carcinomas
HRP	Horseradish Peroxidase
IDH1	Isocitrate Dehydrogenase Type 1
IHC	Immunohistochemistry
IRT	Irinotecan Hydrochloride
LDH	Lactate Dehydrogenase

MRI	Magnetic Resonance Imaging
MF	Microfluidic(s)
MTIC	(5-(3-methyl-(triazen-1-yl) imidazole-4-carboxamide
MTT	3-[4,5-dimethylthiazol-2-yl]-2,5-diphenyl-tetrazolium bromide
MGMT	O ⁶ -Methylguanine-DNA Methyltransferase
NSCLC	Non-Small-Cell Lung Cancer
PBS	Phosphate Buffered Saline
PCLS	Precision Cut Liver Slices
PCR	Polymerase Chain Reaction
PDMS	Polydimethylsiloxane
PDX	Patient Derived Xenografts
PEEK	Polyether Ether Ketone
PI	Propidium Iodide
PMT	Photo-Multiplier Tubes
PS	Phosphatidylserine
QALY	Quality Adjusted Life Years
RTK	Receptor Tyrosine Kinase
SSC	Side-Scattered Light
TCGA	The Cancer Genome Atlas
TMZ	Temozolomide
TUNEL	Terminal deoxynucleotidyl transferase-mediated dUTP Nick- End Labelling (TUNEL)
U	Units
UV	Ultraviolet
WHO	World Health Organisation
WIT	Warm Ischaemic Time
WST-1	Water Soluble Tetrazolium-1

Nomenclature

Fresh Tissue = GBM tissue processed immediately from the patient (on average 69 min after sample acquisition).

Chip Tissue = GBM Tissue processed after maintaining in the microfluidic device for 72 h

Static Tissue = GBM Tissue processed after maintaining in media without microfluidic flow

Matched Pairs = Analysis carried out on the same patient tumour but with different conditions e.g. **Patient No. 3: Fresh Tissue vs. Chip Tissue** or **Patient No 3: aCSF vs. Standard Media**